RL-TR-95-48
Final Technical Report
March 1995

RADAR RESOURCE SHARING STUDY

Integrated Sensors, Inc.

Ronald Gouse - Integrated Sensors, Inc.
John Clancy - DSA

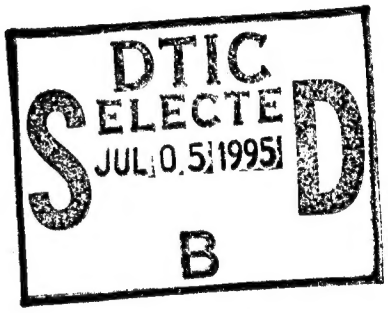

APPROVED FOR PUBLIC RELEASE; DISTRIBUTION UNLIMITED.

Rome Laboratory
Air Force Materiel Command
Griffiss Air Force Base, New York

AD-A295941

ERRATA

RL-TR-95-48
FINAL TECHNICAL REPORT Dated:March 1995

Title: RADAR RESOURCE SHARING STUDY

Please add the following author to the cover and to SF form 298
Block 6:
Dr. Anastasios P. Goutzoulis, Westinghouse Electric Corp.

ROME LABORATORY
AIR FORCE MATERIAL COMMAND
GRIFFISS AIR FORCE BASE, NEW YORK

This report has been reviewed by the Rome Laboratory Public Affairs Office (PA) and is releasable to the National Technical Information Service (NTIS). At NTIS it will be releasable to the general public, including foreign nations.

RL-TR-95-48 has been reviewed and is approved for publication.

APPROVED: Douglas G. Wynne

DOUGLAS G. WYNNE
Project Engineer

FOR THE COMMANDER: Donald W. Hanson

DONALD W. HANSON
Director of Surveillance & Photonics

If your address has changed or if you wish to be removed from the Rome Laboratory mailing list, or if the addressee is no longer employed by your organization, please notify RL (OCSM) Griffiss AFB NY 13441. This will assist us in maintaining a current mailing list.

Do not return copies of this report unless contractual obligations or notices on a specific document require that it be returned.

REPORT DOCUMENTATION PAGE

Form Approved
OMB No. 0704-0188

1. AGENCY USE ONLY (Leave Blank)	2. REPORT DATE	3. REPORT TYPE AND DATES COVERED
	March 1995	Final Sep 92 - Dec 94

4. TITLE AND SUBTITLE
RADAR RESOURCE SHARING STUDY

5. FUNDING NUMBERS
C - F30602-92-C-0061
PE - 62702F
PR - 4506
TA - 16
WU - 1F

6. AUTHOR(S)
Ronald Gouse - Integrated Sensors, Inc.
John Clancy - DSA*

7. PERFORMING ORGANIZATION NAME(S) AND ADDRESS(ES)
Integrated Sensors, Inc.
502 Court Street, Suite 210
Utica, NY 13502

8. PERFORMING ORGANIZATION REPORT NUMBER
ISI94-001

9. SPONSORING/MONITORING AGENCY NAME(S) AND ADDRESS(ES)
Rome Laboratory (OCSM)
26 Electronic Pky
Griffiss AFB NY 13441-4514

10. SPONSORING/MONITORING AGENCY REPORT NUMBER
RL-TR-95-48

11. SUPPLEMENTARY NOTES
Rome Laboratory Project Engineer: Douglas G. Wynne (OCSM) 315 330-4483
*Subcontractors on this effort are Westinghouse Company and (see reverse)

12a. DISTRIBUTION/AVAILABILITY STATEMENT
Approved for public release; distribution unlimited.

12b. DISTRIBUTION CODE

13. ABSTRACT (Maximum 200 words)

The Radar Resource Sharing Study was undertaken to evaluate the relative advantages of three candidate technologies for implementing a shared beamformer for a dual band (S and UHF) airborne surveillance radar. The beamformer was required to interface with the two active array apertures and perform the signal combining and distribution functions necessary to produce the receive and transmit beams required for each band. The objective was to compare the three approaches in terms of size, weight, power consumption and hardware sharing, based on 1997 technology projections. The candidate beamformer technologies investigated were Conventional, Digital and Optical beamformers. In the digital and optical cases, technology limitations precluded accomplishing all of the required beamformer functions. Therefore, hybrid approaches which employed each of these technologies to the maximum practical extent were devised. The study commenced in September 1992 and was conducted primarily on the basis of beamformer requirements for monostatic operation. Later the scope was expanded to consider a bistatic receive implementation having significantly different beam requirements.

14. SUBJECT TERMS
RF Beamforming, Optical Beamforming, Digital Beamforming, Dual Frequency Radar, Monostatic Radar, Bistatic Radar

15. NUMBER OF PAGES
170

16. PRICE CODE

17. SECURITY CLASSIFICATION OF REPORT	18. SECURITY CLASSIFICATION OF THIS PAGE	19. SECURITY CLASSIFICATION OF ABSTRACT	20. LIMITATION OF ABSTRACT
UNCLASSIFIED	UNCLASSIFIED	UNCLASSIFIED	U/L

11. (Cont'd)

Decision Science Applications, Inc.

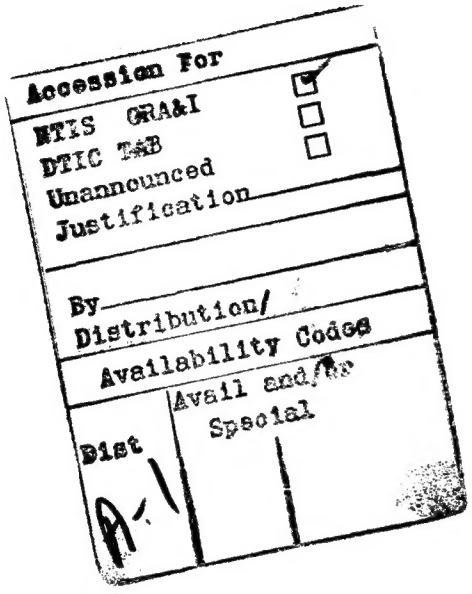

TABLE OF CONTENTS

APPENDICES

1.0 INTRODUCTION

1.1 Objectives

The Radar Resource Sharing Study was undertaken to evaluate the relative advantages of three candidate technologies for implementing a shared beamformer for a dual band (S and UHF) airborne surveillance radar. As shown in Figure 1.1, the beamformer would interface with the two active array apertures and perform the signal combining and distribution functions necessary to produce the receive and transmit beams required for each band.

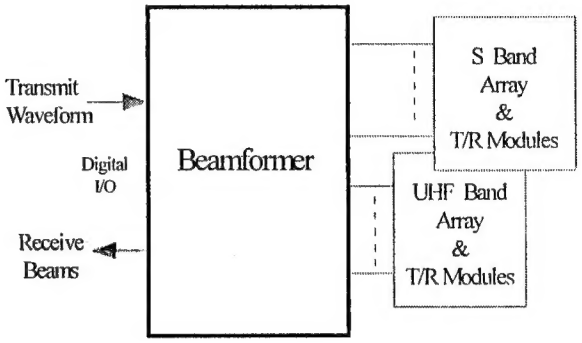

Figure 1-1 Beamformer Function

The objective was to compare the three approaches in terms of size, weight, power consumption and hardware sharing, based on 1997 technology projections.

The candidate beamformer technologies are,

Conventional, defined as a constrained feed type of beamformer in which the signal combining and dividing manifolds are comprised entirely of conventional microwave components such as coax cables, stripline or printed circuits, etc.,

Digital, in which the signals would ideally be converted at the T/R module interface (RF to digital on receive and digital to RF on transmit) with all beamformer functions being performed on the digitized elemental components, a and,

Optical, in which the signals would be converted between optical and electrical at both beamformer interfaces, with all signal combining and dividing manifolds being implemented in fiber optic lines.

In the digital and optical cases, technology limitations precluded accomplishing all of the required beamformer functions. Therefore, hybrid approaches which employed each of these technologies to the maximum practical extent were devised.

The study commenced in September 1992 and was conducted primarily on the basis of beamformer requirements for ***monostatic*** operation. Later the scope was expanded to consider a ***bistatic receive*** implementation having significantly different beam requirements.

Overall technical direction and system design, as well as detailed definition of the conventional beamformers was the responsibility of Integrated Sensors Inc. Westinghouse Corp. shared the system design work and was responsible for the digital and optical beamformer designs. Decision Science Applications, Inc. conducted performance and sensitivity trade-off analyses to quantify the relative advantages of the three beamformer technologies with respect to sharing and radar performance.

1.2 Technical Approach

Figure 1-2 shows the procedure followed for both monostatic and bistatic applications.

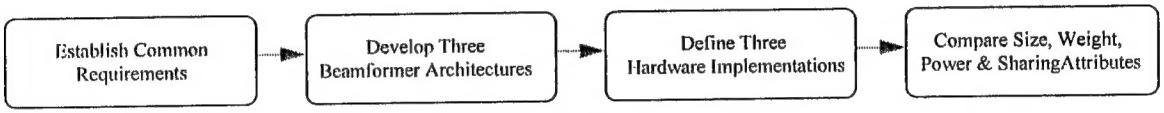

Figure 1-2 Basic Study Procedure

Step 1 - Establish Requirements

To standardize the comparisons, we established a common set of performance and interface requirements to be imposed on each of the three beamformer designs, regardless of the technology type. These requirements were derived from the general guidelines given in the statement of work, augmented by sufficient mode analysis to estimate other parameters critical to the beamformer designs. For example, dynamic range, sidelobe suppression and stability are basically determined by the subclutter visibility needed to detect small, low flying, targets from an airborne surveillance platform. These clutter levels were calculated and the medium prf S-band mode turned out to be the design driver, requiring 13 Bit A/D converters, rms sidelobes lower than minus 20dBi, and LO phase noise approaching -150 dBc/Hz. Detailed discussion of these and other parameter derivations and specifications are provided in Section 2.

Figures 1-3 summarizes the functional and interface requirements imposed on the monostatic beamformer. On transmit, this beamformer accepts transmit commands in

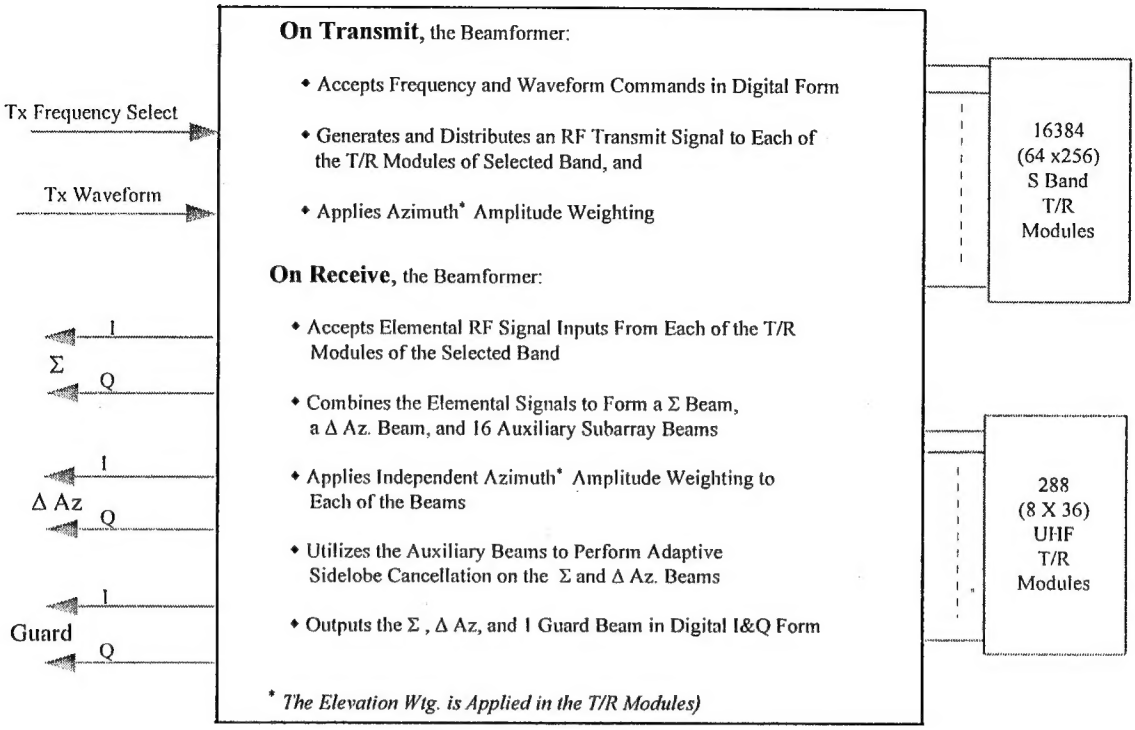

Figure 1-3 Monostatic Beamformer Functions and Interfaces

digital form, converts the signal to RF and distributes amplitude weighted signal components to the T/R modules. On receive, the process is reversed; the elemental signals from the T/R modules are combined to form independently weighted Σ and Δ beams. In addition, the beamformer performs adaptive sidelobe cancellation of CW interference and produces a guard beam for use in rejecting sidelobe pulse interference.

Figure 1-4 shows the functions and interfaces of the bistatic receive beamformer. Obviously, no transmit beams are required. On receive, the functions are significantly different for the two bands. The UHF receive beams are the same as for the monostatic case. For S-band however, the high prf used by the non-collocated transmitter requires an efficient bistatic receiver to collect reflected energy from many directions at the same time, hence the need for multiple simutaneous beams. A cluster of 40 contiguous azimuth beams was assumed as a typical requirement.

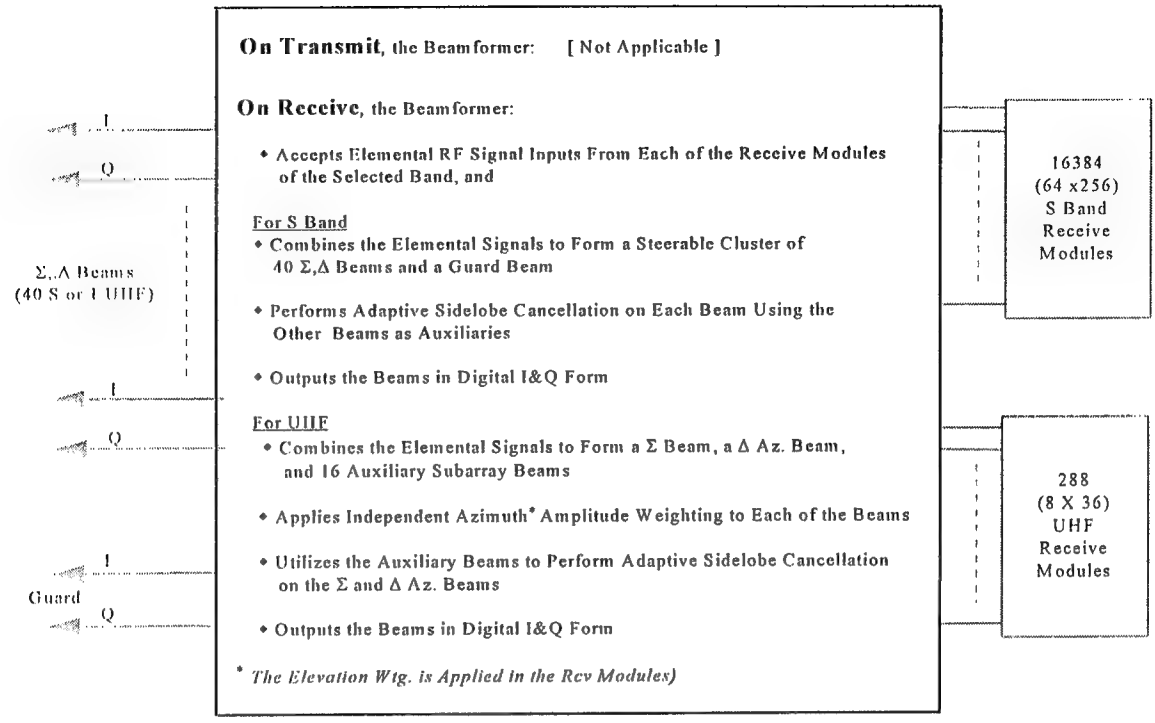

Figure 1-4 Bistatic Receive Beamformer Functions and Interfaces

Step 2 - Develop Beamformer Architectures

Based on the above requirements, monostatic and bistatic architectures were developed for each of the three technology types. This was an iterative process; as the initial concepts were reduced to detailed implementations, the architectures were refined. The final forms are described here.

Conventional Technology

Figure 1-5 shows the conventional technology configurations. For the monostatic configuration of Figure 1.5(a), a sequential manifold organization is employed, e.g. for S-band receive, each column of 64 is combined in an elevation feed manifold and then the

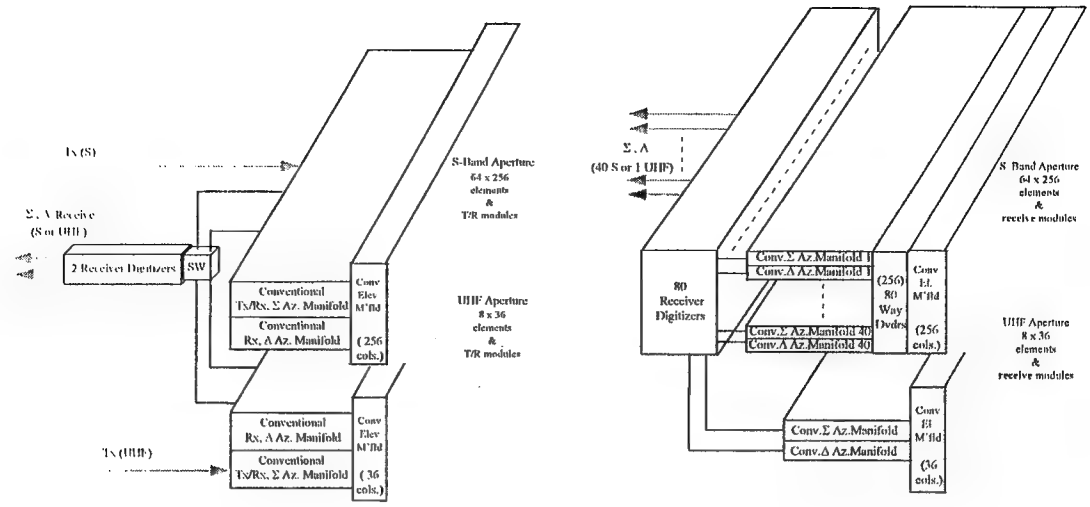

(a) Monostatic **(b) Bistatic Receive**

Figure 1.5 Conventional Beamformer Architectures

256 column outputs are combined in an azimuth feed. Separate Σ azimuth and Δ azimuth manifolds are required to allow different amplitude weightings, Taylor and Bayliss. The azimuth and elevation manifolds are also used for transmit. A functionally similar set of manifolds is Σ used for UHF, and the S and UHF manifolds time share the two receiver channels. (The auxiliary channel manifolds and receivers are omitted from the diagram for simplicity.)

The bistatic receive architecture of Figure 1.5(b) is similar except that for S-band the azimuth manifolds and receivers are duplicated 40 times, once for each beam.

Digital Technology

Figure 1-6 illustrates the digital technology beamformers. Because of the 1997 technology limitation, the 'digital' implementations are actually hybrids that contain both digital and conventional technologies.

For the monostatic configuration shown in Figure 1-6(a), each band retains a conventional elevation manifold which is used for both receive and transmit. This keeps the number of receive channels to a reasonable 256. On receive, the column outputs for the selected band are digitized and the azimuth combining and weighting is performed digitally. Although the receiver and beamforming hardware is time shared by the two bands, its magnitude is clearly driven by the S-band requirement. On transmit, each band has totally conventional beamforming.

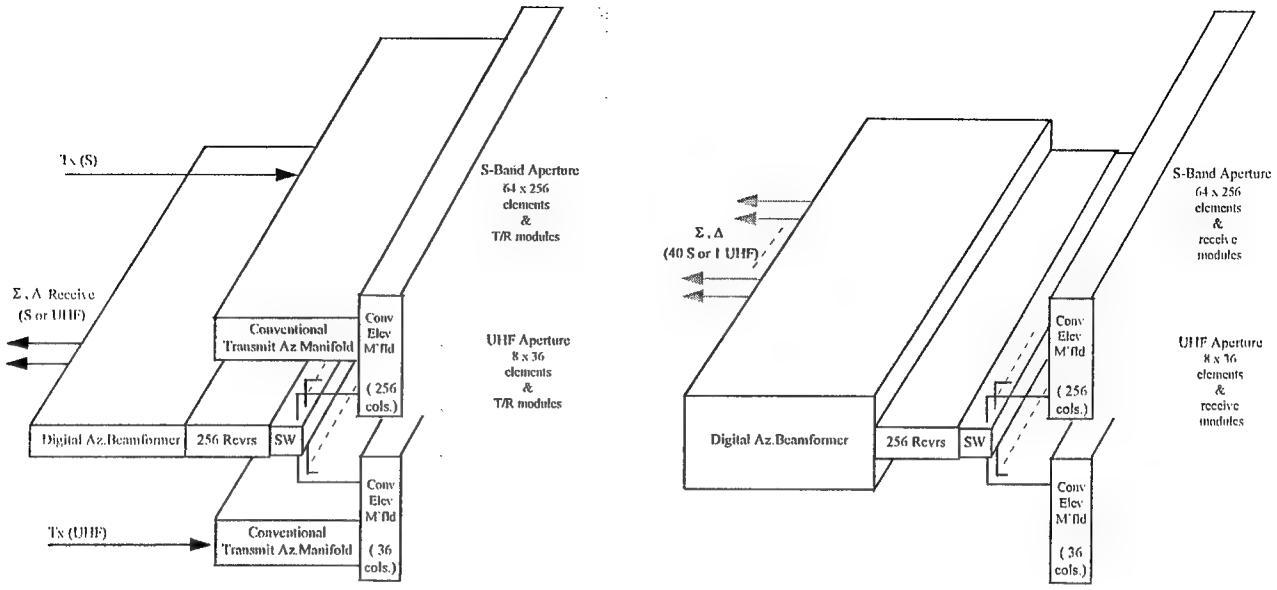

(a) Monostatic **(b) Bistatic Receive**

Figure 1-6 Digital Beamformer Architectures

As shown in the bistatic receive configuration of Figure 1-6(b), digital technology is a better fit because the conventional transmit azimuth manifolds are not required. The 256 column outputs are combined and weighted digitally, but in this case up to 40 simultaneous azimuth beams are required. Thus there is considerably more digital beamforming hardware required in the bistatic system.

Optical Technology

Figure 1-7 illustrates the optical technology architectures. As in the digital case, the proportion of optical technology in these implementations is constrained by 1997 technology availability.

The monostatic configuration is shown in Figure 1-7(a). Note that separate elevation manifolds are required for transmit and receive because optical manifolds are not bidirectional. On transmit, the optical distribution networks are relativelely efficient so both the azimuth and

the elevation transmit manifolds can be implemented optically in both bands. On receive however, low loss optical combining for S-band is limited to combiners of no more than 16 to 1.

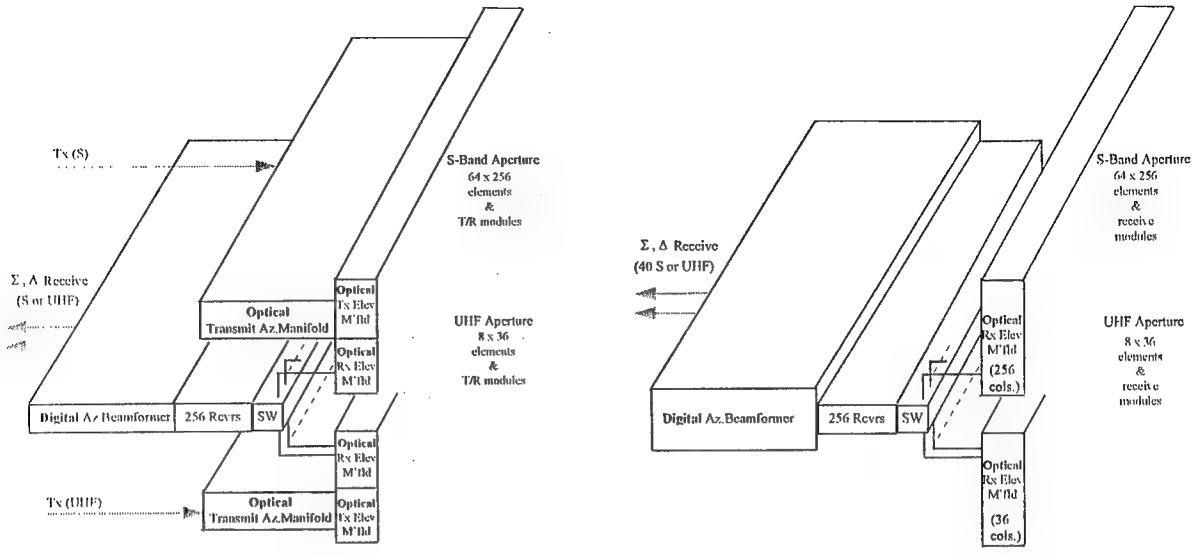

(a) Monostatic **(b) Bistatic Receive**

Figure 1.7 Optical Beamformer Architectures

Therefore, the optical technology cannot be extended beyond the elevation manifolds; in fact, even those must be partially conventional to achieve the required 64 to1. As a result the azimuth receive combining must be performed with either conventional or digital technology, and digital was arbitrarily selected for the baseline configuration

The bistatic receive configuration shown in Figure 1-7(b) is essentially the same as the digital version of Figure 1-6(b). The only difference is that an optical rather than a conventional elevation manifold is employed.

After preliminary analysis showed the baseline optical approach (i.e. an optical-digital combination) to have exceptionally high power consumption, an alternate optical approach which combined optical and conventional technologies was considered for the monostatic configuration only. This alternate architecture is shown in Figure 1-8.

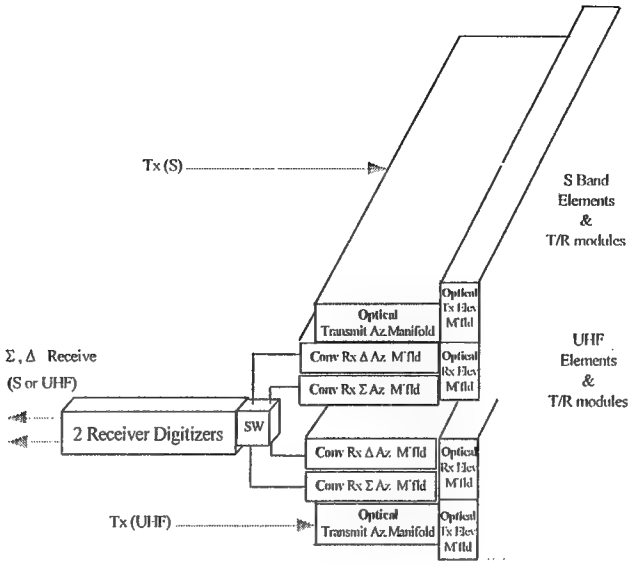

Figure 1-8 Optical/Conventional Monostatic Architecture

Step 3 - Define Hardware Implementations

To create the data base required for the comparative evaluation, detailed hardware implementations were derived for each of the beamformer architectures described above. This entailed the development of designs for each of the required manifolds and RF, digital, and optical circuits in sufficient detail to derive good estimates for size, weight, and power consumption.

Figure 1.9 illustrates the procedure. Part (a) is an overall diagram of the conventional monostatic beamformer showing each of the functional blocks to be defined in detail. The S-band elevation and Δ azimuth manifold which are shaded in (a), are shown detailed in (b), and the 4 to 1 combiner which is circled in (b) is detailed in (c). In this manner all of the basic component assemblies, for all of the beamformer implementations, were defined in sufficient detail to derive their weight, volume, and power consumption. These component estimates were then accumulated in spreadsheet form for side by side comparison of the three technology types.

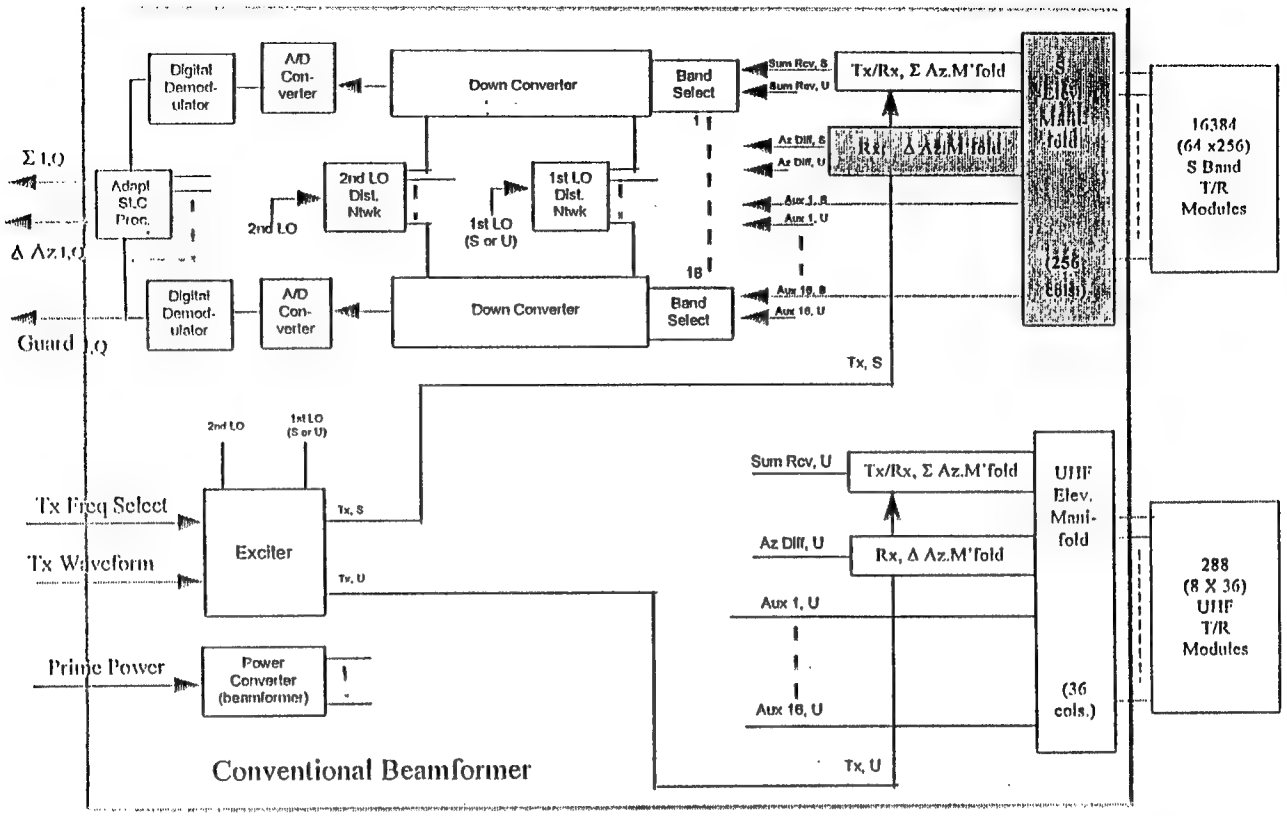

(a) Overall Block Diagram

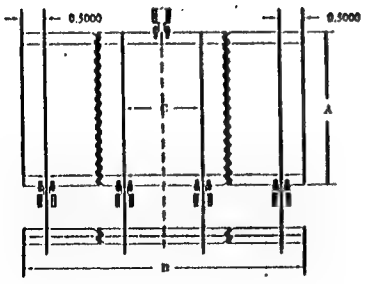

(c) 1:4 Stripline Power Divider

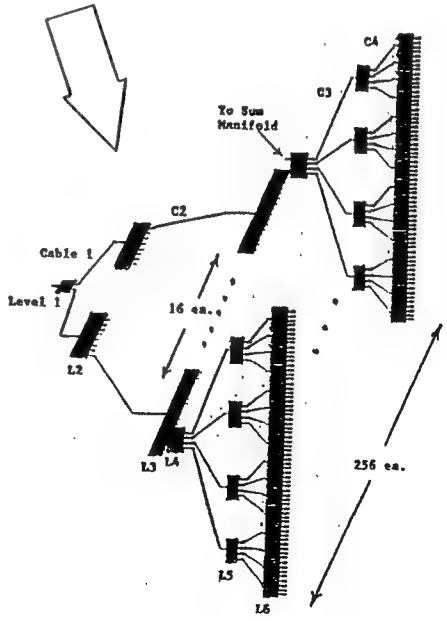

(c) S-Band Δ Az. Manifold

Figure 1-9 Hardware Definition Process

Figure 1.10 is an example spreadsheet which compares the three technologies in terms of weight, for the monostatic system. The upper and lower halves of the table apply to the S and UHF bands, respectively. The shaded sections identify those components that are contained within the beamformer itself, however, the spreadsheet also includes the other aperture components such as T/R modules, radiating elements, etc. The double outlined boxes identify items that are shared by the two bands; these are therefore included in the S band totals only. In the UHF section, these shared items are accumulated in a separate column with their values reduced if necessary to reflect the proportion used for UHF. The UHF totals then represent the *additional* weight required to add the UHF band. At the bottom are the combined dual band totals. For example, for the conventional technology the dual band beamformer weighs 1654 pounds, of which 91 pounds or 6% is shared; and the total aperture weighs 9769 pounds, of which 933 pounds or 10% is shared.

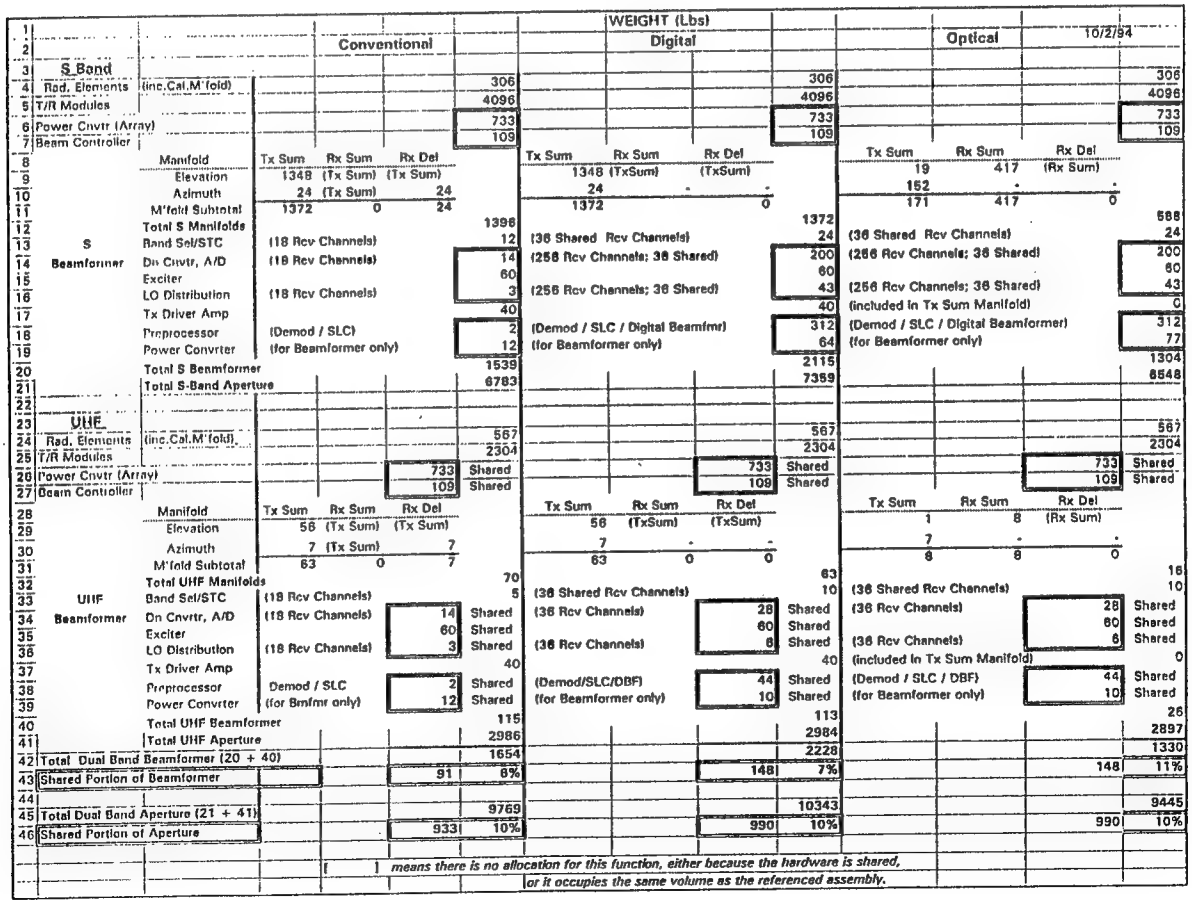

			WEIGHT (Lbs)											
			Conventional				Digital				Optical			10/2/94
S Band														
Rad. Elements	(inc.Cal.M'fold)					306				306				306
T/R Modules						4096				4096				4096
Power Cnvtr (Array)						733				733				733
Beam Controller						109				109				109
	Manifold	Tx Sum	Rx Sum	Rx Del			Tx Sum	Rx Sum	Rx Del		Tx Sum	Rx Sum	Rx Del	
	Elevation	1348	(Tx Sum)	(Tx Sum)			1348	(TxSum)	(TxSum)		19	417	(Rx Sum)	
	Azimuth	24	(Tx Sum)	24			24	-	-		152	-	-	
	M'fold Subtotal	1372	0	24			1372		0		171	417	0	
	Total S Manifolds					1396				1372				588
S	Band Sel/STC	(18 Rcv Channels)				12	(36 Shared Rcv Channels)			24	(36 Shared Rcv Channels)			24
Beamformer	Dn Cnvtr, A/D	(18 Rcv Channels)				14	(256 Rcv Channels; 36 Shared)			200	(256 Rcv Channels; 36 Shared)			200
	Exciter					60				60				60
	LO Distribution	(18 Rcv Channels)				3	(256 Rcv Channels; 36 Shared)			43	(256 Rcv Channels; 36 Shared)			43
	Tx Driver Amp					40				40	(included in Tx Sum Manifold)			0
	Preprocessor	(Demod / SLC)				2	(Demod / SLC / Digital Beamfmr)			312	(Demod / SLC / Digital Beamformer)			312
	Power Convrter	(for Beamformer only)				12	(for Beamformer only)			64	(for Beamformer only)			77
	Total S Beamformer					1539				2115				1304
	Total S-Band Aperture					6783				7359				6548
UHF														
Rad. Elements	(inc.Cal.M'fold)					567				567				567
T/R Modules						2304				2304				2304
Power Cnvtr (Array)				733	Shared				733	Shared			733	Shared
Beam Controller				109	Shared				109	Shared			109	Shared
	Manifold	Tx Sum	Rx Sum	Rx Del			Tx Sum	Rx Sum	Rx Del		Tx Sum	Rx Sum	Rx Del	
	Elevation	56	(Tx Sum)	(Tx Sum)			56	(TxSum)	(TxSum)		1	8	(Rx Sum)	
	Azimuth	7	(Tx Sum)	7			7	-	-		7	-	-	
	M'fold Subtotal	63	0	7			63	0	0		8	8	0	
	Total UHF Manifolds					70				63				16
UHF	Band Sel/STC	(18 Rcv Channels)				5	(36 Shared Rcv Channels)			10	(36 Shared Rcv Channels)			10
Beamformer	Dn Cnvtr, A/D	(18 Rcv Channels)		14	Shared		(36 Rcv Channels)		28	Shared	(36 Rcv Channels)		28	Shared
	Exciter			60	Shared				60	Shared			60	Shared
	LO Distribution	(18 Rcv Channels)		3	Shared		(36 Rcv Channels)		6	Shared	(36 Rcv Channels)		6	Shared
	Tx Driver Amp					40				40	(included in Tx Sum Manifold)			0
	Preprocessor	Demod / SLC		2	Shared		(Demod/SLC/DBF)		44	Shared	(Demod / SLC / DBF)		44	Shared
	Power Convrter	(for Bmfmr only)		12	Shared		(for Beamformer only)		10	Shared	(for Beamformer only)		10	Shared
	Total UHF Beamformer					115				113				26
	Total UHF Aperture					2986				2984				2897
Total Dual Band Beamformer (20 + 40)						1654				2228				1330
Shared Portion of Beamformer				91	6%				148	7%			148	11%
Total Dual Band Aperture (21 + 41)						9769				10343				9445
Shared Portion of Aperture				933	10%				990	10%			990	10%

[ ] means there is no allocation for this function, either because the hardware is shared, or it occupies the same volume as the referenced assembly.

Figure 1.10 Example Spreadsheet for Monostatic Weight

1.3 Results

1.3.1 Weight, Volume and Power Consumption - Monostatic Beamformers

Figure 1-11 summarizes the comparative weight, volume and power consumption results for the monostatic beamformers. Included are the three original technologies, **Conventional**, **'Digital'** and **'Optical'**, plus a fourth type called **Optical/Conventional**, which has a different technology mix than the baseline **'Optical'**.

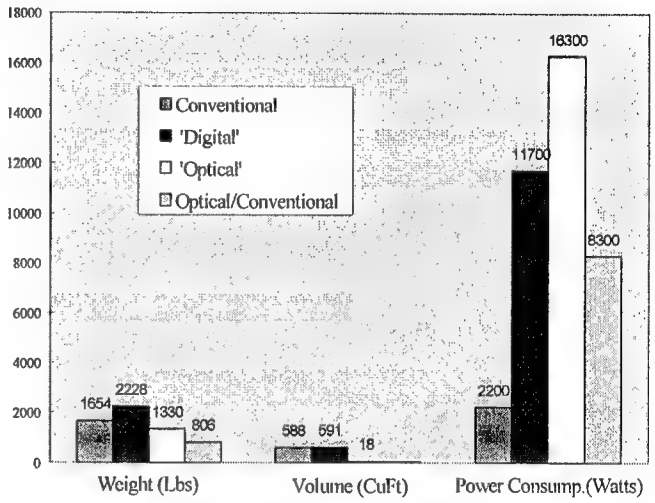

Figure 1-11 Monostatic Beamformer Weight, Volume and Power Consumption

In terms of weight, all four implementations are of the same order of magnitude. **'Digital'** is the heaviest at 2228 lbs due mainly to the weight of its many receivers and digital beamforming circuit boards.

'Optical' at 1330 lbs derives its weight advantage over **'Digital'** by replacing conventional elevation manifold components with optical components; however it still retains the heavy digital azimuth combiner manifold with its large number of receivers and digital boards.

The **Optical/Conventional**, which combines optical elevation manifolds with conventional azimuth manifolds, yields the lightest beamformer at 806 lbs.

Although these weight differences appear substantial, they are relatively insignificant from an overall system standpoint. From line 45 of Figure 1-10, we can see that the total dual band *aperture* weight is about 10,000 lbs; and if we assume that the aperture is only one half of the total system, then the total system weight would be 20,000 lbs. From that perspective, the weight differences among the four beamformer types are less than four percent of the total system weight.

The volume differences are more significant. The **Conventional** and **'Digital'** are roughly equal at about 600 cubic feet, but the **'Optical'** technology yields an impressively compact design at only 18 cubic feet. There is some concern that this size reduction may not be

totally realizable because the **'Optical'** implementation's high power consumption may cause a heat dissapation problem. Nevertheless, the **'Optical'** technology offers great miniaturation potential.

In the area of power consumption, the **Conventional** technology is clearly superior. The reason is that the other technologies must sustain the inefficiencies of converting RF signals into digital or optical form during the beamforming process. These conversions generally require additional power consuming components. Furthermore, although cost estimates were not derived in this study, the added complexity of the **'Digital'** and **'Optical'** beamformers portends a cost disadvantage as well.

1.3.2 Weight, Volume and Power Consumption - Bistatic Beamformers

Figure 1-12 summarizes the weight, volume and power consumption results for the bistatic **Conventional**, **'Digital'**, and **'Optical'** beamformers (note that a logarithmic scale is used in Figure 1-12).

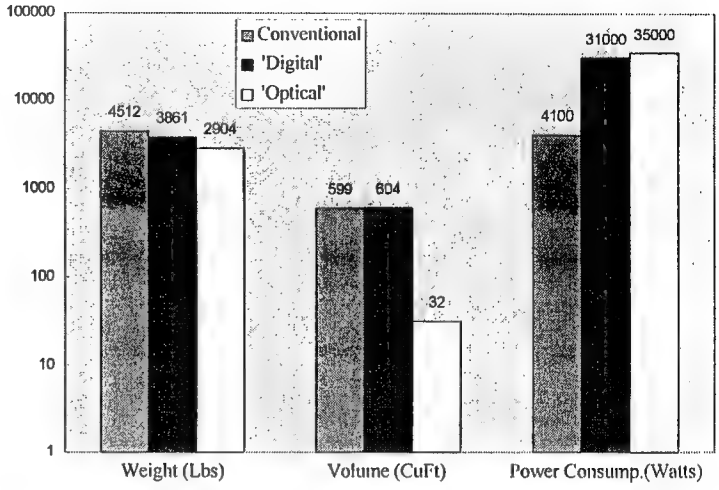

Figure 1-12 Bistatic Beamformer Weight,Volume and Power Consumption

In terms of weight, the three technologies are of the same order of magnitude, just like the monostatic case, but the advantage has shifted away from the Conventional. This is due primarily to the number of simultaneous S-band beams needed for the bistatic system. Conventional is now heaviest, and it would become increasingly so if the number of simultaneous S-band beams were increased beyond the assumed forty. The reason for this is that the conventional azimuth manifolds must be duplicated to produce each additional azimuth beam, while on the other hand, the digital azimuth beamforming hardware used in both the 'Digital' and 'Optical' implementations does not grow linearly with the number of beams.

In terms of volume, the tremendous size advantage of the **'Optical'** approach for bistatic is comparable to the monostatic case.

And in the power consumption area, the much greater efficiency of **Conventional** is again clearly indicated.

1.3.3 Dual Band Sharing

The proportion of hardware that can be shared in a dual band (S and UHF) beamformer is small, regardless of the technology type. Figure 1-13 illustrates the impact of sharing in terms of the weight parameter, for the three technology types. In all cases the amount of beamformer weight that is saved by sharing is less than eleven percent.

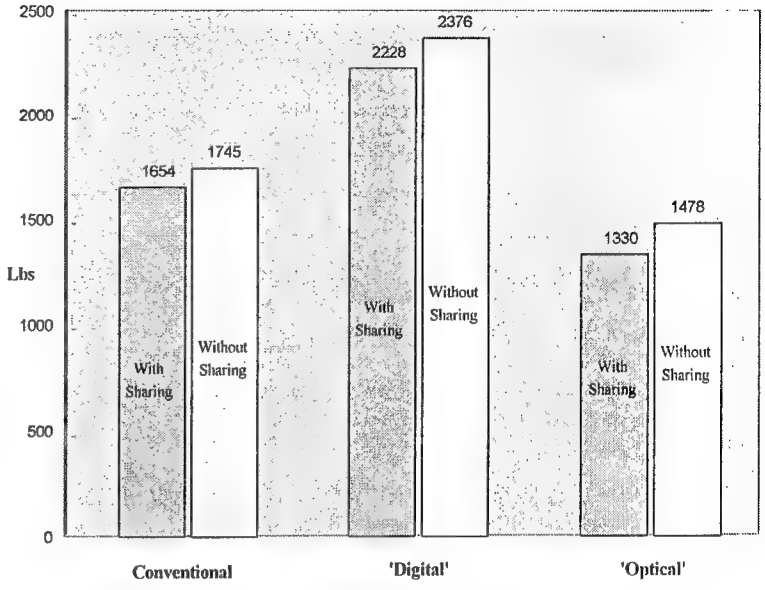

Figure 1-13 Impact of Sharing On Dual Band Beamformer Weight

There are two main reasons for this: (1) All three implementations utilize a substantial amount of RF devices which cannot span the multi-octave frequency range from UHF to S-band. For example, the conventional elevation manifolds which are used in both the **'Digital'** and **'Optical'** beamformers are not sharable. (2) The IF and digital circuitry, which is sharable, is dominated by S-band requirements. For example, the **'Digital'** and **'Optical'** beamformers require 256 receivers for S-band but only 36 of them are needed for UHF. Thus only 14% of those receivers are shared.

2.0 REQUIREMENTS

2.1 Monostatic Radar Sidelobe Requirements

The sidelobe requirements for the beamformer were established after an examination of the original SOW guidelines and from an analysis of sub clutter requirements for the monostatic radar, which is the primary driver for the antenna sidelobes. The sidelobe requirements listed in Table 2.1-1, were selected after performing an analysis of radar performance in urban clutter using deterministic ultra low sidelobe antenna patterns in a sidelooking radar installation. The urban clutter model was selected as it is most stressing for radar operations.

	S Band		**UHF**	
	Baseline	SOW	Baseline	SOW
Antenna Size	64 rows 256 columns	64 256	8 rows 36 columns	8 36
Transmit				
azimuth taper	35 dB Taylor	uniform	30 dB Taylor	uniform
elevation taper	uniform	uniform	uniform	uniform
intercardinal sidelobes	- 20 dBi	not specified	- 20 dBi	not specified
Receive				
azimuth taper	35 dB Taylor	60 dB	30 dB Taylor	45 dB
elevation taper	25 dB Taylor	45 dB	25 dB Taylor	30 dB
intercardinal sidelobes	- 20 dBi	not specified	- 20 dBi	not specified

Table 2.1-1 Monostatic Radar Sidelobe Requirements

The reallocation of parameters between transmit and receive was done to satisfy the beamformer architectures and technology options described in section 1, while retaining the essential two way pattern requirements for target detection in clutter. In particular the intercardinal specifications which were not included in the SOW guidelines, were analyzed and determined to be critical. In the following section, the process which was used to analyze the radar performance is summarized.

2.1.1 Analysis Of Monostatic S Band Sidelobe Requirements

In order to derive a complete and consistent set of specifications for both the transmit and receive beamformers, a parametric analysis of radar performance in clutter was performed

versus sidelobe specifications for transmit and receive ultra low sidelobe antenna (ULSA) patterns. The analysis which focused on the stressing S Band specifications, involved a two step process. In step one, a model of ULSA patterns was developed to calculate and visualize ULSA patterns with various elevation and azimuth tapers and with random excitation errors. In step two, the array parameters were used in the Bistatic Radar Software (BRADS) analysis package to calculate the radar performance in clutter. BRADS is a computer program developed by Rome Labs for the analysis of both monostatic and bistatic radar systems. It includes provisions to model the radar transmit and receive parameters including ULSA antenna patterns, waveform and processing functions. In addition the radar antenna array orientation with respect to the platform velocity vector is modeled as part of the BRADS setup. The analysis package contains various clutter and target models for calculation of signals from various types of clutter background and target types.

Step 1 The beamformer architectures discussed in section 1, show an ULSA array with column beamformers followed by azimuth feeds. This beamformer architecture results in an array with separable array excitations. Patterns for arrays with separable excitations were calculated for different tapers and random errors. The details of the model are contained in Appendix B. An example ULSA pattern is shown in Figure 2.1-1.

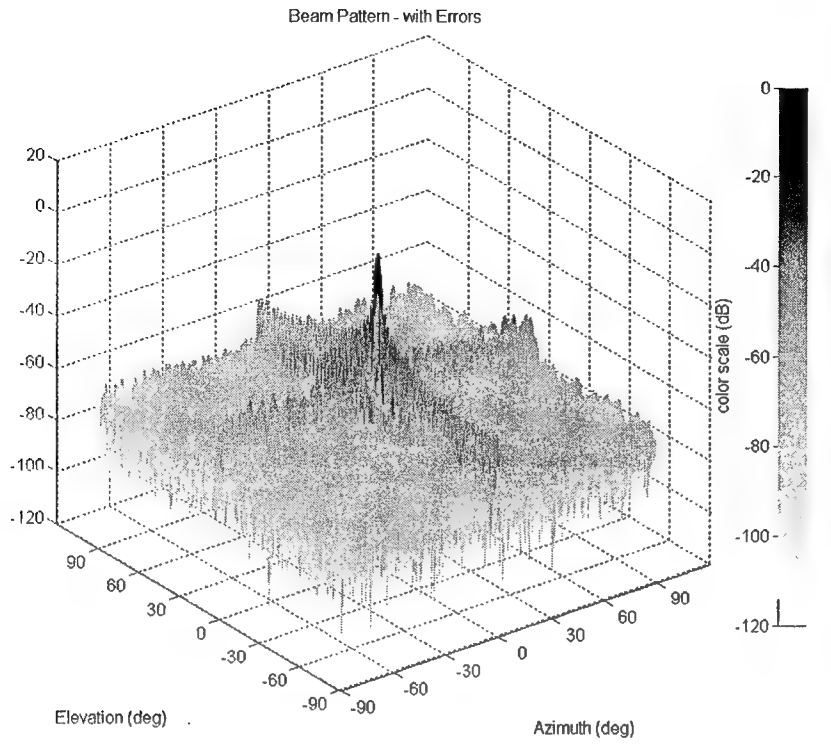

Figure 2.1-1 Antenna Pattern for S Band Array with Separable Excitation and Random Errors

The two dimensional array pattern in Figure 2.1-1 illustrates the characteristics of the ULSA patterns analyzed in this report. It shows ridges of high sidelobes along the elevation and azimuth principal planes set by the respective tapers used in the column and azimuth feeds of the beamformer. The far out or intercardinal sidelobes, shown in this plot, are set by random errors in the array, which are caused by both errors in beamformer excitation, plus those caused by random T/R module and element pattern errors. The effect that these sidelobe regions have on the sub clutter visibility of the radar depends on the array/platform geometry of the airborne radar, the clutter model, and the radar waveform parameters. In order to evaluate these effects, the ULSA antenna parameters were used in the BRADS radar simulation program in step 2 of the analysis procedure.

Step 2 An analysis of radar performance in clutter was performed for various elevation and azimuth tapers for both the transmit and receive antennas. The intercardinal sidelobes were varied and the performance in clutter evaluated. Figure 2.1-2 is a plot of clutter to noise (C/N)

for the S Band monostatic radar with the baseline array parameters listed in Table 2.1-1. The clutter was calculated in range/doppler bins at a range of 200 nmi.

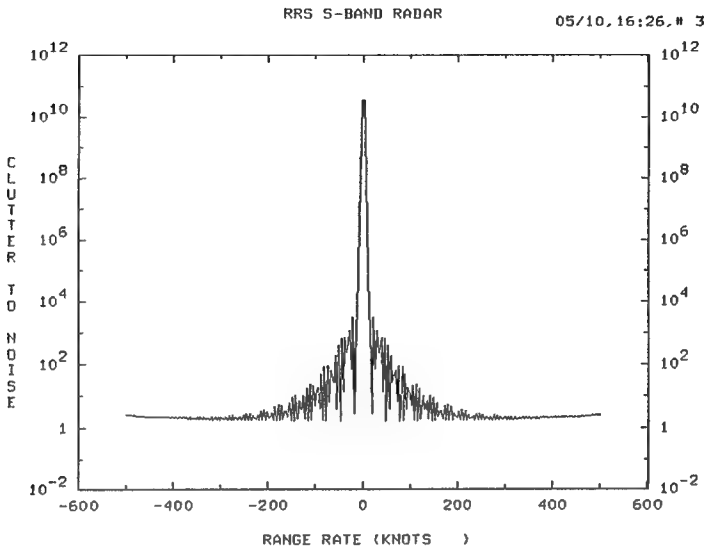

Figure 2.1-2 Clutter to Noise versus Doppler for Baseline S Band Beamformer Parameters
transmit tapers - (az = 35 dB Taylor, el = uniform, IC = -20 dBi)
receive tapers -- (az = 35 dB Taylor, el = 25 dB Taylor, IC = -20 dBi)

The C/N plot shows that an acceptable performance was achieved for range rates greater than 200 knots. For rates less that 200 knots the C/N is seen to increase and effectively degrade the detection of targets. To investigate the source of this effect, the ULSA antenna parameters were individually changed and their effect on performance evaluated.

To investigate the effect of elevation tapers on the performance of the radar in clutter, the elevation taper of the receive beamformer was increased 10 dB, to a 35 dB Taylor taper. The transmit beam taper was not changed. The resultant effect on the received clutter spectrum is shown in Figure 2.1-3.

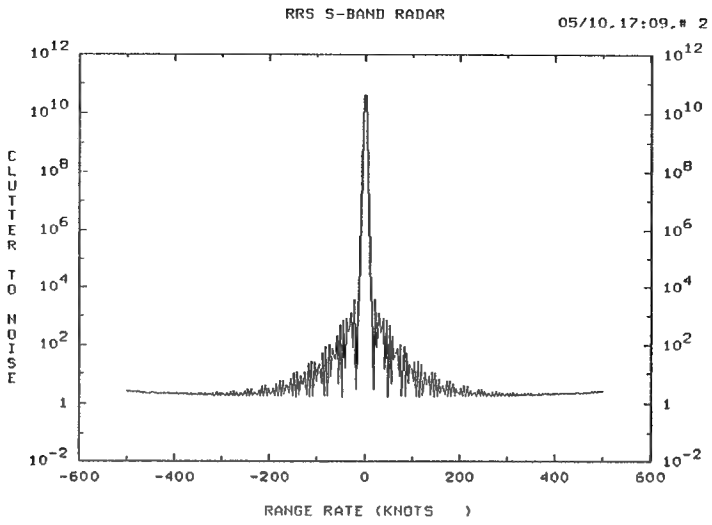

Figure 2.1-3 Clutter to Noise versus Doppler for S Band Beamformer with Increased Elevation Taper on the Receive Antenna
receive tapers -- (az = 35 dB Taylor, *el = 35 dB Taylor*, IC = -20 dBi)

The clutter to noise spectrum is identical with that produced by the baseline receive antenna pattern. The 10 dB increase in elevation taper did not change the C/N plot from that shown in Figure 2.1-2, for the baseline beamformer parameters. This insensitivity to elevation taper is characteristic of sidelooking airborne radars. Thus there is no reason to select heavier tapers than specified in the baseline parameters.

Next the effect of azimuth tapers was evaluated by modifying the azimuth tapers of the baseline parameters. Both the transmit and receive antennas tapers were increased 10 dB, to a 45 dB Taylor weight The elevation taper was reduced back to the baseline taper. The resultant clutter plot is shown in Figure 2.1-4.

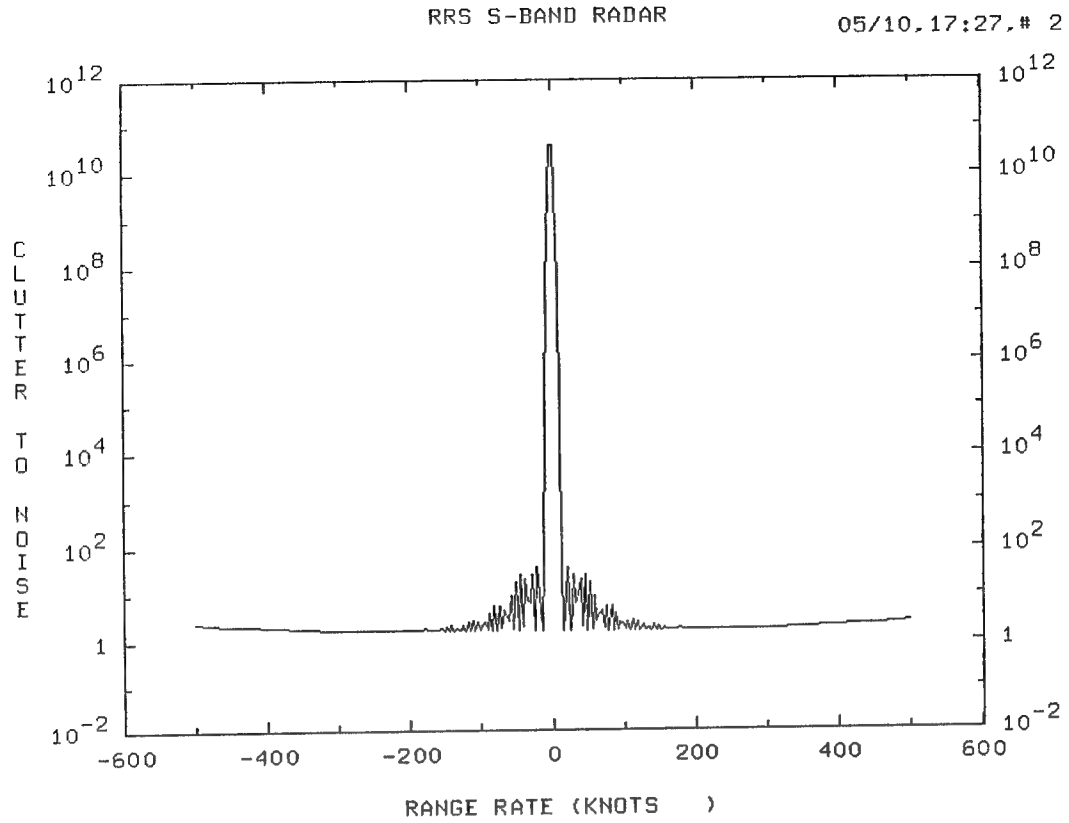

Figure 2-4 Clutter to Noise versus Doppler for S Band Beamformer with Increased Azimuth Taper on Transmit and Receive Antennas
transmit tapers (*az = 45 dB Taylor*, el = uniform, IC = -20 dBi)
receive tapers (*az = 45 dB Taylor*, el = 25 dB Taylor, IC = -20 dBi)

The increase in the azimuth taper shows improved clutter to noise performance for all range rates with acceptable performance being reached above 100 knots. Specification of the azimuth sidelobes is thus seen to be set by the required minimum discernible velocity (mdv) for the target of interest. Since this is not a major technology driver the baseline specification was not changed, with the realization that they could readily be set to meet the required mdv.

Next, the intercardinal sidelobes of the baseline parameters were changed. The intercardinal sidelobes of both the transmit and receive beams were degraded to -10 dBi, and the resultant clutter to noise plots are shown in Figure 2.1-5.

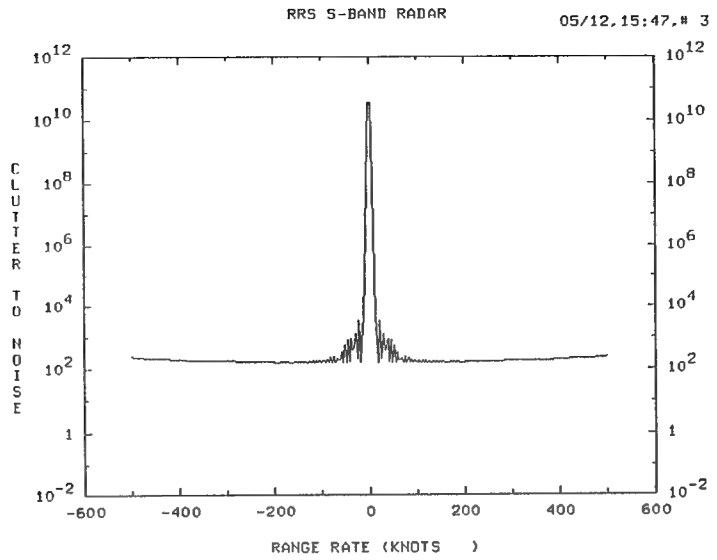

Figure 2.1-5 Clutter to Noise versus Doppler for S Band Beamformer with degraded Intercardinal Sidelobes on Transmit and Receive
transmit tapers (az = 35 dB Taylor, el = uniform, *IC = -10 dBi)*
receive tapers (az = 35 dB Taylor, el = 25 dB Taylor, *IC = -10 dBi)*

The clutter to noise ratio in this plot is seen to increase at all range rates. The radar would be clutter limited at all range rates and thus the performance of the radar with the increased intercardinal sidelobe is unacceptable. The intercardinal sidelobe specification is seen to be critical for acceptable radar performance. Finally the effect of crab angle was analyzed. In Figure 2.1-6, the clutter spectrum is shown for the baseline array with a 10 degree crab angle between the antenna axis and the velocity vector.

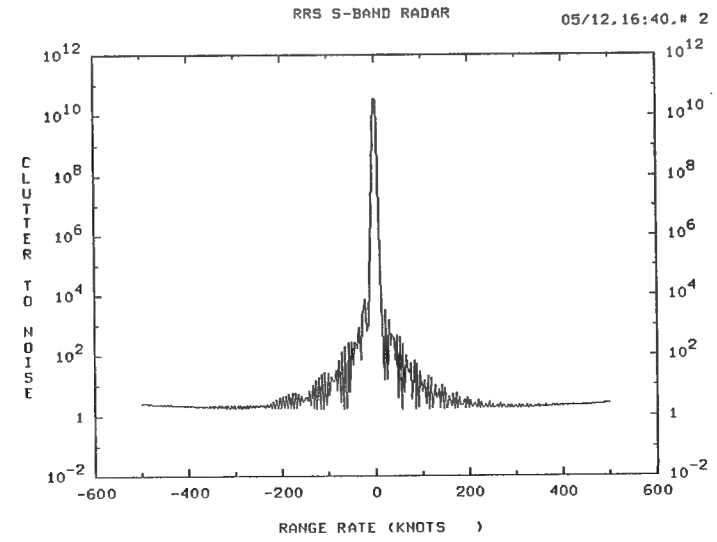

Figure 2.1-6 Clutter to Noise versus Doppler for S Band Beamformer with Baseline Parameters and a 10 Degree Crab Angle

The clutter spectrum plot for the 10 degree crab angle is seen to be unchanged from that shown in Figure 2.1-2 for the case of no crab angle.

2.1.2 Summary Of The S Band Monostatic Radar Antenna Sidelobe Requirements

The beamformer requirements for the S Band monostatic radar were evaluated, based on a parametric analysis of radar performance in clutter using ULSA beam patterns with various beamformer tapers and intercardinal sidelobe specifications. The S Band beamformer requirements were the most stressing and the analysis was performed to verify the adequacy of the baseline parameters used throughout the technology evaluations. The following is a summary of the observations derived from this analysis.

Elevation Sidelobe Specification

Little effect was noted in the clutter spectrums as the elevation taper was varied. This is due to the fact that the radar being analyzed is a side looking radar. In this geometry the range ambiguities of the radar yield clutter returns with the same Doppler as that of the main beam. The effect also remained the same as crab angles up to 10 degrees were analyzed

Azimuth Sidelobe Specification

The effect of azimuth taper is important for determining the minimum discernible velocity. The higher levels of clutter seen in the C/N plots near the mainlobe are a function of the azimuth taper, and thus determine the minimum discernible velocity of the radar. For the RRSS baseline the azimuth tapers were retained on both transmit and receive since it was not a major technology driver, although it is recognized that adjustments may be necessary once the target type and radar minimum discernible velocity are specified .

Intercardinal Sidelobe Specification

The intercardinal region specifications are key in achieving a generally acceptable level of performance in clutter. Both the transmit and receive antennas need to have antenna intercardinal levels of at least -20 dBi to achieve acceptable C/N performance.

2.1.3 Analysis Of Monostatic UHF Band Sidelobe Requirements

The UHF radar was analyzed with the BRADS simulator using a similar approach as that for the S Band radar. In step one, the UHF antenna sidelobes were analyzed for various beamformer tapers and random errors. The results are contained in Appendix B. Next the effect of various sidelobe levels on radar performance in clutter was then analyzed. Acceptable performance was achieved when the sidelobe clutter level was below noise for target range rates of interest. It did not consider target RCS effects which would be different at UHF for many targets of interest. Therefore no attempt was made in this analysis to tailor the UHF radar design for a specific target.

Figure 2.1-7 is a plot of the clutter spectrum for the UHF radar in a range bin located 150 nmi from the radar. The baseline UHF antenna/beamformer parameters listed in Table 2.1-1 were used in the BRADS simulator for the urban clutter model..

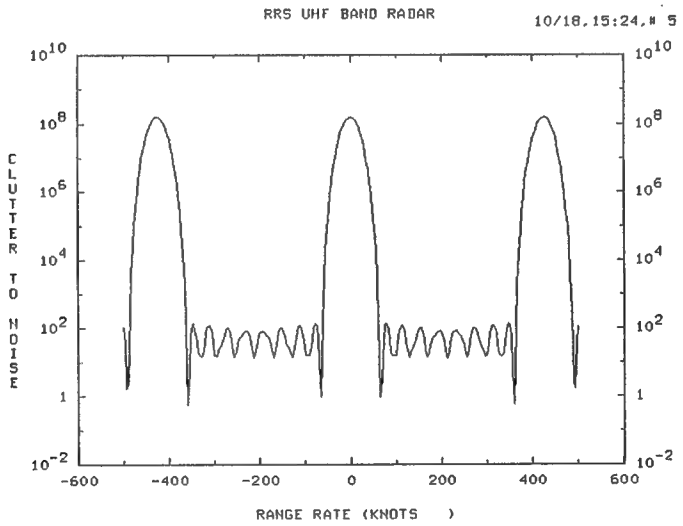

Figure 2.1-7 Clutter Spectrum for UHF Radar with Baseline Parameters

From the plot it is clear that the radar is limited at all target velocities. The effect of the low prf used in the UHF radar, is seen as multiple peaks in the clutter spectrum.. High clutter to noise levels are also noted at other range rates, in between the prf lines, which is unacceptable for target detection. The azimuth sidelobes of both antennas were then changed. The transmit taper was increased 5 dB to a 35 dB Taylor taper, and the receive azimuth taper was increased 15 dB to a 45 dB Taylor taper. The resultant clutter plot is shown in Figure 2.1-8.

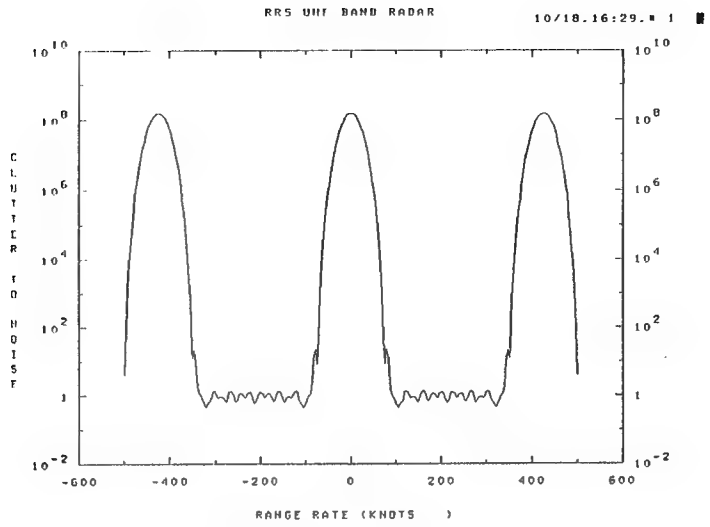

Figure 2.1-8 Clutter Spectrum for UHF Radar with Improved Azimuth Sidelobes

The spectral plot with the improved antenna azimuth sidelobes is acceptable for all target velocities between the prf lines. Based on this analysis it is clear that the UHF antenna needs to have low intercardinal sidelobes and also along the azimuth principal plane.

2.2 RECEIVE DYNAMIC RANGE

The dynamic range requirements may be driven by either clutter or jamming. The requirements differ with frequency band and architecture. Dynamic range requirements are presented for both formed beam (conventional beamformer) and column (digital and optical beamformers) architectures. These two architectures are shown in Figures 2.2-1 and 2.2-2. Both architectures have a T/R module per element. The formed beam architecture collects the signals from each element by means of elevation and azimuth manifolds to form the Σ, Δ, and Guard beams for both the S-band and UHF radars. A common set of receive channels is shared between the S-band and UHF radars. The column architecture collects the receive signals in column combiners and employs one receive channel per column. The A/D outputs are processed in a digital beamformer to form the Σ, Δ, and Guard beams.. Thirty-six of the receive channels are shared between the UHF and S-band radars. The remainder are used for S-Band only.

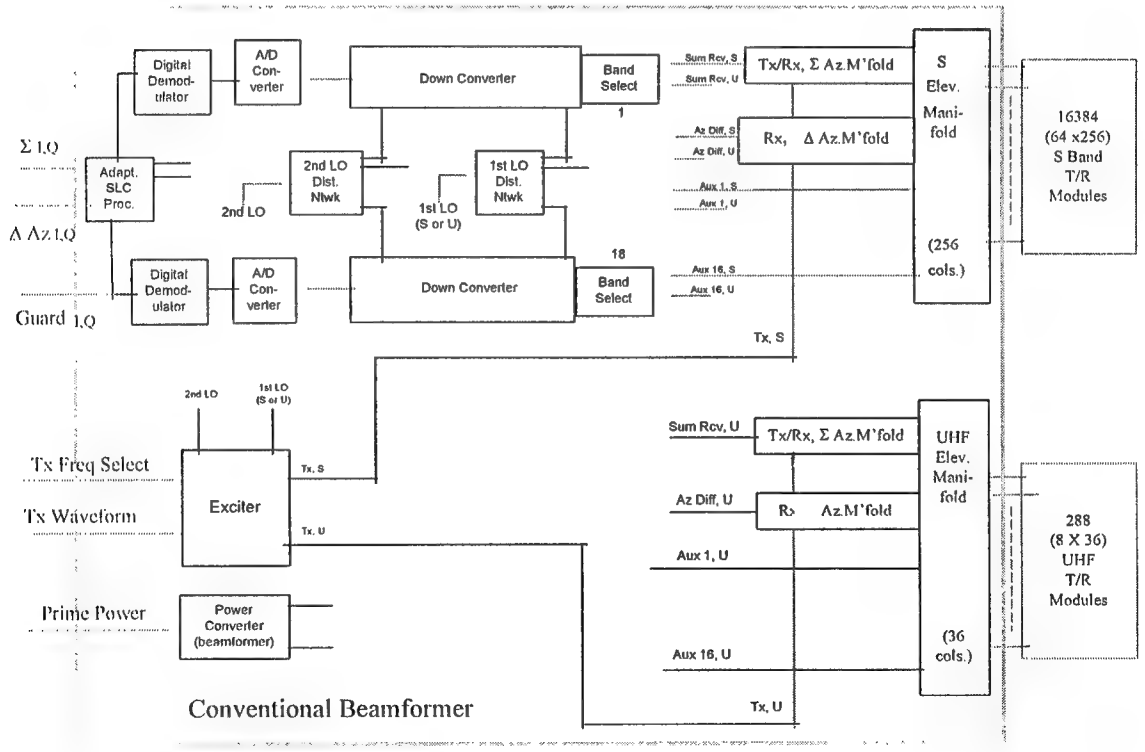

Figure 2.2-1 Conventional Beamformer

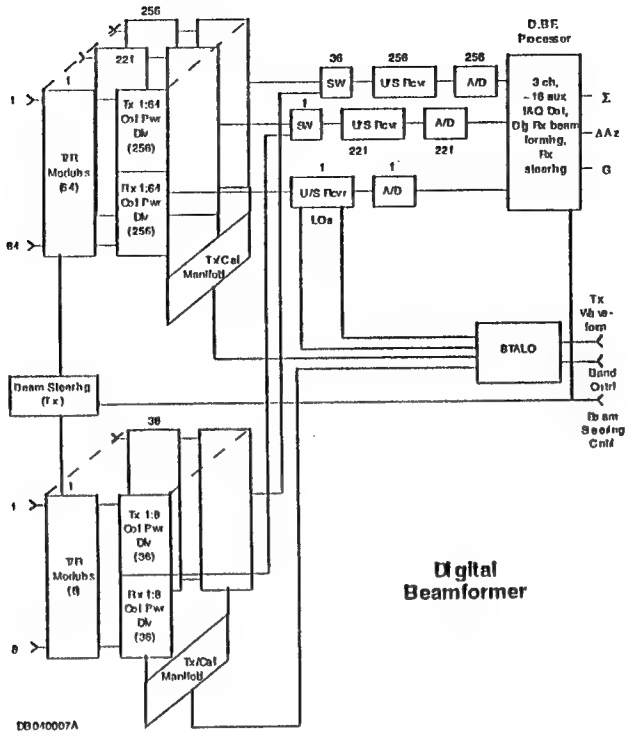

Figure 2.2-2 Digital Beamformer

The formed beam architecture coherently sums the signals from all elements and, therefore, requires greater A/D dynamic range against clutter than the column architecture. The required A/D dynamic range, when operating agains sidelobe jammers, is higher for the column architecture. This is because the azimuth sidelobes of the formed beam are far lower than the azimuth sidelobes (azimuth element pattern) of a column.

The parameters used to calculate the required dynamic range are shown in Table 2.2-1. No losses were used in the calculation to insure that the results provide a conservative estimate of dynamic range. The clutter program used to compute the C/N assumed a gaussian beam pointed at the horizon.

Table 2.2-1 Parameters for Dynamic Range Calculation

Parameter	UHF	S-Band	Comments
Radiated Power (Peak)	54.5 dBw	54.5 dBw	100 W/Ft^2 Avg Pwr
Gain (Antenna)			
XMIT	28.4	45.3	No Taper
RCV	26.3	42.3	Taper Loss
Beamwidth			
AZ XMIT	3.2°	0.5°	No Taper
EL XMIT	14.5°	2.1°	No Taper
AZ REC	4.7°	0.7°	Taper
EL REC	18.1°	2.6°	Taper
Bandwidth	5 Mhz	5 MHz	
Wavelength	.59 M (435 MHz)	0.9M (3250 MHz)	
PRF	349 Hz	10 Khz	UHF Unamb ~ 1.1 RH S-Band Max Spec
XMIT Pulse	287 μSec	10μSec	
Υ	-8 dB	-8 dB	Mountain Clutter
Losses	0	0	
H	30,000 Ft	30,000 Ft	Given Platform Altitude
Noise Figure	3 dB	3 dB	
KTB	-204	-204	

A scenario of 10 sidelobe jammers at a range of 100 nm, radiating ERP of 30 dBw for UHF and 36 dBw for S-band was used to determine the jammer-to-noise ratio (J/N) which must be accommodated. These ERP values were chosen because they are believed to be obtainable today. It was assumed that the jammers radiate their total ERP in the radar's 5 Mhz bandwidth. The receive gain used in the J/N equation,

$$\frac{J}{N} = \frac{ERP \bullet G \bullet \lambda^2}{(4\pi R)^2 \bullet KTB \bullet NF}$$

was -18 dBi (S-band) and -19 dBi (UHF) for the formed beam sidelobe gain and 23 dBi (S-band), 14 dBi (UHF) for the column gain. The values for KTB and λ were given in Table 2.2-1.

The azimuth positioning of the sidelobe jammers in the case of the column architecture is unimportant since the azimuth pattern is the element pattern. This is the stressing architecture as can be seen by the difference between formed beam sidelobe gain and column gain. Consequently the ERP used was 10 times the single jammer ERP. This approach gives a J/N for

the formed beam which is higher than would actually be encountered because many of the jammers would be in azimuth sidelobes which are lower than the peak value which was used in the calculation.

Table 2.2-2 shows the results of the dynamic range calculations for both formed beam and column architectures. In the formed beam case, C/N is the stressing parameter with UHF requiring 18.5 dB more dynamic range than S-band. The UHF operates with a low PRF and STC can be employed to reduce the A/D dynamic range to the S-band value. The S-band value is, therefore, used to determine the A/D dynamic range requirements.

STC can also be used to reduce the UHF dynamic range required against clutter when the column architecture is employed. The STC is not effective against sidelobe jamming and, therefore, the column architecture dB dynamic range requirement is the 56.1 dB. The selected dynamic range values for both the formed beam and column architectures are shaded in the table. It should be noted that these J/N calculations were made using azimuth receive sidelobe levels which are lower than those which were finally selected. However, these changes would affect only the 'formed' beam J/N numbers and would not increase them enough to exceed the 'column' values.

Table 2.2-2

	UHF (dB)		S-Band (dB)	
	Formed	Column	Formed	Column
C/N	80.3	66.6	61.8	40.7
J/N	25	56.1	15	54.8

The reason the C/N is much larger for UHF is the large UHF elevation composite beamwidth which results in nearer range clutter and larger grazing angle.

The number of A/D bits which are required is computed using the equation

$$\#\,BITS = \frac{(C/N \text{ or } J/N) + Overhead}{6}$$

where J/N or C/N are the shaded values from Table 2.2-2. The overhead is:

3.0 dB noise
4.8 dB peak clutter or jamming
6.0 dB sign
13.8 dB

Using the overhead and the shaded values result in the formed beam architecture requiring a 13 bit A/D and the column architecture requiring a 12 bit A/D. However, for the purpose of this study, it was assumed that 13 bit would be used for both architectures.

2.3 Local Oscillator Stability

The system stability requirements are divided into two parts, broadband and discrete. The broadband stability (dBc/Hz) is computed as C/N + 4.8 dB + 10 dB + 67 dB. The 4.8 dB accounts for clutter peaks, and the 67 dB is the bandwidth. It is desired to keep the broadband noise to 10 dB below thermal noise to minimize its impact on system performance (.4 dB), so 10 dB margin is included in the equation.

The equation to determine discretes (dBc) is C/N + 4.8 dB (peak) + 10 LOG (PRF • CPI). The 10 LOG (PRF • CPI) term accounts for the coherent integration of the discrete instabilities.

Twenty-five (25) ms was chosen as a reasonable CPI length for the S-band and radar with the beam pointing to broadside (maximum clutter). The UHF beamwidth is much broader and consequently longer dwell times can be employed. The length of the CPI is constrained, however, by fly through considerations (both range and velocity). Consequently, the UHF CPI was limited to 120 ms.

The S-band calculations used C/N values of 61.8 dB for the formed beam architecture and 40.7 dB for the column architecture. The corresponding UHF values are 61.8 dB and 56.1 dB respectively. The UHF C/N values reflect the effect of STC (see Table 2.2-2).

After the system stability requirements have been calculated, stability requirements must be allocated to the affected sub-systems. The STALO is the stressing sub-system and is allocated 1/2 of the system stability requirement. The system and STALO requirements are summarized in Table 2.3-1.

Table 2.3-1 Stability Requirements

S-Band				
	Broadband		Discrete	
Architecture	System	STALO	System	STALO
Formed Beam	143.6	146.6	100.6	103.6
Column	122.5	122.5	79.5	82.5

UHF				
	Broadband		Discrete	
Architecture	System	STALO	System	STALO
Formed Beam	143.6	146.6	92.8	95.8
Column	137.9	140.9	87.1	90.1

2.4 Calibration Techniques

Numerous calibration methods have been investigated in other studies by Westinghouse. The techniques applicable to this program that have been considered are:

1. Cooperative far field source from ground, airplane or satellite.
2. Clutter source.
3. Near field source by scanning the focused antenna.
4. Near field source viewing one element at a time.
5. Mutual coupling method.
6. Signal injection at each radiating element.

Depending on the accuracy of calibration required, several techniques are suitable only as a trigger to activate more accurate methods.

2.4.1 Cooperative Far Field Source

On the ground, calibration by means of a ground based far field source is akin to replication of the antenna range tests performed during manufacture. As such, this technique could be effective as a preflight verification of radar performance if a dedicated highly controlled site could be obtained. It is unlikely however that this much control of the site could be obtained at most places where operation would be required. An advantage of all of the far field techniques is that the weight of the calibration transmitter and antenna are removed from the ariframe. However, a very serious problem arises in the effects of secondary reflections. On an antenna range secondary reflectors in the azimuth and elevation planes are eliminated or controlled. In order to achieve a meaningful ground based calibration, the aircraft would need to be positioned where it would not be affected by other reflecting objects such as other parked or

moving aircraft, hangers or vehicular traffic. This implies that an exclusive area be set aside for ground calibration, and that the aircraft be parked very nearly identically each time before the calibration run. This technique would verify operation only on the ground. There would be no way of checking for system degradation after takeoff.

The only advantage in using a cooperating escort aircraft for antenna calibration would be that the hardware and associated weight of the calibration transmitter would be removed from the aircraft. It does remove the limited range restriction of the ground based source; however, using an escort aircraft as a transmitter source for calibration presents several problems. The most serious of these would be performing highly precise angle measurements in two coordinates to locate the source transmitter simultaneously with reading one calibration point. In addition, there is the considerable logistics problem and expense of maintaining a dedicated aircraft to support the mission.

Satellite source calibration eliminates the problem of ground and other reflections. But, it has other problems. The position of the satellite is governed by its orbital dynamics, thus calibration sessions would be driven by the availability of the satellite rather than by mission requirements. This technique is not known to have been attempted with airborne antennas, nor for the purpose of achieving ultra low sidelobes. It is not considered to be feasible, and is not recommended for further consideration.

2.4.2 Calibration Against Clutter

Antenna calibration through the use of the radar's own clutter return signal may be possible in a limited way. By monitoring the clutter level it is possible to determine that a degradation in antenna performance, such as an increase in sidelobe levels has occurred. The increase in the radar clutter return level above a predetermined threshold would cause a warning to be given to the operator, who would initiate the calibration sequence. Since neither the phase nor the amplitude of the clutter return signal can be controlled, there is no way of using the clutter return, except as an indicator of system performance.

2.4.3 Near Field Scanning Method

Near field source calibration by scanning the focused array entails turning on the full array and scanning its beam past a fixed calibration antenna fixed on the wing. As the beam is scanned, a set of data is collected and stored. An onboard computer program then transforms

this near field pattern into a far field pattern while correcting for amplitude, phase and polarization errors of the source. The corrected far field pattern is then transformed into a phase and amplitude distribution. The processing necessary to perform the transformations is quite extensive, but finally the resulting corrected pattern can be compared to the stored 'standard' pattern taken at the time of manufacture and examined for variations. This method has a further application as a ground check whereby a boresighted source is placed on a stand in front of the radar antenna. A focused scan may be produced to show, for example, that a newly produced antenna has not been degraded in placing it in the airplane.

2.4.4 Near Field Calibration of One Element at a Time

Near field source calibration by viewing one element is similar to the method described in the previous paragraph except that all elements are turned off but the one in question. All elements would be cycled and examined individually. The main disadvantage of this technique is that it will consume a lot of measurement time since each element would be measured several times. This should not present a problem. It is envisioned that the calibration would be performed while time sharing with radar operation over many scans, or perhaps one face of the radar would be in standby/calibration while the other face would be in operation. This technique is feasible and although not recommended in this report, it is a very viable alternative.

2.4.5 Mutual Coupling Calibration

Mutual coupling calibration involves illuminating individual elements from either adjacent or nearby elements of the array. This technique seems attractive at first. Aside from the controls needed to switch the various elements on and off, and the necessary and complex software, there is little additional hardware required. However, the results of tests at Westinghouse indicate that the mutual coupling path is not stable at small coupling values. This method requires further study to determine its viability.

2.4.6 Calibration by Signal Injection at Each Element

Signal injection from a dedicated divider network to each radiator, as a means of calibration, can be considered as a proven solution to the problem. A Westinghouse IR&D program, Multirole Electrically Scanned Array (MESA) program has successfully implemented this technique. In order to implement this method, a separate calibration power divider and switching network would be installed to feed each of the elements. In this way, each element

could be calibrated singly in sequence and restored to close to its original factory calibration. Because the signal is injected by a non-directional coupler within the radiating element, the error caused by the variability of the element VSWR is taken into account. The major problem with this technique is the increase in system complexity and the decrease in reliability due to the additional hardware and switching. Associated with this option would be an increase in system weight.

Injector manifolds have been considered as equal power division corporate feeds and as traveling wave dividers. The traveling wave divider can be made more precise than corporate dividers at low coupling values, and in addition take less critical space by placing the transmission line in each elevation column at the side of the radiating elements. At each element a non-directional coupling is made of about -45 dB. Thus each element receives identical amplitude signals of closely controlled phase. Placing the non-directional injection port in the radiating element allows the calibration to include the possible variability of the mutual coupling with scan. The phase has a carefully controlled progression simulating a far field phase front from about 45^0, depending upon the design of the injector line velocity. The azimuth plane is then similarly fed with a traveling wave line. This provides a known constant amplitude phase front against which the antenna is calibrated. Calibration may proceed one element at a time, comparing the existing amplitude and phase with that of the antenna on the measurement range, or it may proceed with all elements activated normally, deriving element errors from an FFT. The signal injection method utilizing a traveling wave divider is recommended. The configuration is shown in Figure 2.4-1

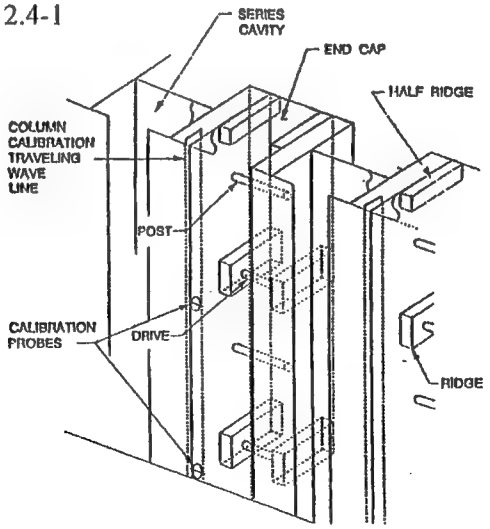

Figure 2.4-1 Injection Calibration Scheme

2.4.7 Conclusion

The simplest method is the clutter method, but it is only useful as a trigger to activate more accurate calibration methods. Further study is required before the mutual coupling or wing mounted source methods can be recommended. As a result, the injection method is recommended, as it is the most accurate and has been proven in actual hardware (MESA, JSTARS). The additional weight can be minimized and the advantage of this system in accuracy make it the preferred method.

2.5 Beamformer Specifications

Table 2.5-1 gives the specifications that were established early in the program to guide the beamformer implementation studies. Many of the requirements were suggested in the initial statement of work. Others, particularly the antenna pattern, dynamic range, and stability characteristics were derived based upon an assumed set of operational requirements such as detection ranges, target cross-sections, clutter models, etc..

Table 2.5-1 Dual Band Beamformer Specifications

Transmit Mode		
	S-Band	UHF
Digital Control Inputs		
Frequency Control	TTL, 10 Bits (9 Freq., 1 Band)	
Waveform Select	TTL, 4 Bits	
RF Signal Outputs		
Number	16384	288
Frequency (Ghz)	3.0 - 3.5	.42 - .45
Max. Pulse Power (watts)	.013	.75
Max. Duty Factor	.15	.15
Max. Pulse Width (μs)	50	300
Max. PRF (hz)	10000	600
Sidelobe Amplitude Wtg.		
Azimuth	Taylor 35 dB	Taylor 30 dB
Elevation	Uniform	Uniform
RMS Sidelobe Level	-25 dBi	-20 dBi
Receive Mode		
RF Signal Inputs		
Number	16384	288
Frequency (Ghz)	3.0 - 3.5	.42 - .45
Max. Pulse Power (dBm)	-60	-15
Signal Outputs		

Format (all beams)	13 Bits I&Q, Conv.	Same
	12 Bits I&Q, Dig. or Opt.	Same
Σ Beam Amplitude Wtg. - Az.	Taylor 35dB	Taylor 30dB
- Elev.	Uniform*	Uniform*
Δ Az Beam Ampl. Wtg. - Az.	Bayliss 35dB	Bayliss 30dB
- Elev.	Uniform*	Uniform*
RMS Sidelobe Level	-25 dBi	-20 dBi
Guard Beam		
Gain	10 dBi	4 dBi
Beamwidth	120^0 Az. X 30^0 El.	120^0 Az. X 30^0 El.
Maximum Noise Figure	8 dB	6 dB
Bandwidth	1 or 5 Mhz, Selectable	Same
Stalo		
Stability		
Short Term Stability: Conv.	<147 dBc/hz	<147 dBc/hz
Dig or Opt.	<126 dBc/Hz	<141 dBc/hz
	@ f_{offset}= 250 Khz	@ f_{offset}= 250 Khz
Discrete Spurious: Conv.	< 104 dBc	< 96 dBc
	< 83 dBc	< 90 dBc
Long Term	850 ppm	850 ppm
Frequency Step Size	1 Mhz	1 Mhz
Switching Speed	1 μsec	50 μsec
* *Elevation Weighting in T/R Modules*		

3.0 BEAMFORMER IMPLEMENTATION

3.1 Conventional Beamformer

The S-Band and UHF conventional beamformers are composed of manifolds, exciter, RF drives, LO distribution, receivers (band select/STC's, down converter, and A/D converter), preprocessor (demodulator, sidelobe canceller), and beamformer power converter.

The S-band conventional beamformer contains two separate manifolds. One manifold functions as the receive difference channel feed and the other as a shared transmit/receive sum network. The manifolds together weigh approximately 1,400 lb. and have approximately 10 dB of insertion loss. A single RF source is used instead of a distributed gain approach since the single source configuration allows full sharing of the sum manifold for transmit and receive. The source provides about 150 W average power and about 1 kW peak power in order to ensure +3.0 dBm average power to the T/R modules in the center of the array.

The UHF conventional beamformer also contains two separate manifolds. As with the S-band beamformer, one manifold functions as the receive difference channel feed, and the other acts as a shared transmit/receive sum network. The UHF manifolds together weigh approximately 70 lb. and have approximately 3.6 dB insertion loss. A single RF source is selected instead of a distributed gain approach since, as with the S-band beamformer, the single source configuration allows full sharing of the sum manifold for transmit and receive. The RF source provides about 36 W average power and about 240 W peak power in order to ensure +20 dBm average power to the T/R modules in the center of the array.

The hardware implementation incorporates coax, stripline and microstrip transmission media, and is derived on the basis of minimizing weight, and unique parts count. The following subsections present a detailed discussion of the manifold configuration and hardware issues, and the other beamformer constituents (receivers, exciters, etc.).

3.1.1 Manifold Configuration

A corporate feed network configuration was selected for the conventional beamformer S-band and UHF manifolds. It utilizes lightweight, low loss stripline and microstrip components and coaxial cables. It also offers the potential for excellent channel amplitude and phase matching control.

The original design for the manifolds was based upon an "interleaved az/el" configuration (Figures 3-1 and 3-2), and included waveguide in the early stages of power division to minimize losses and heat build up. It also included amplifiers in an azimuth divide

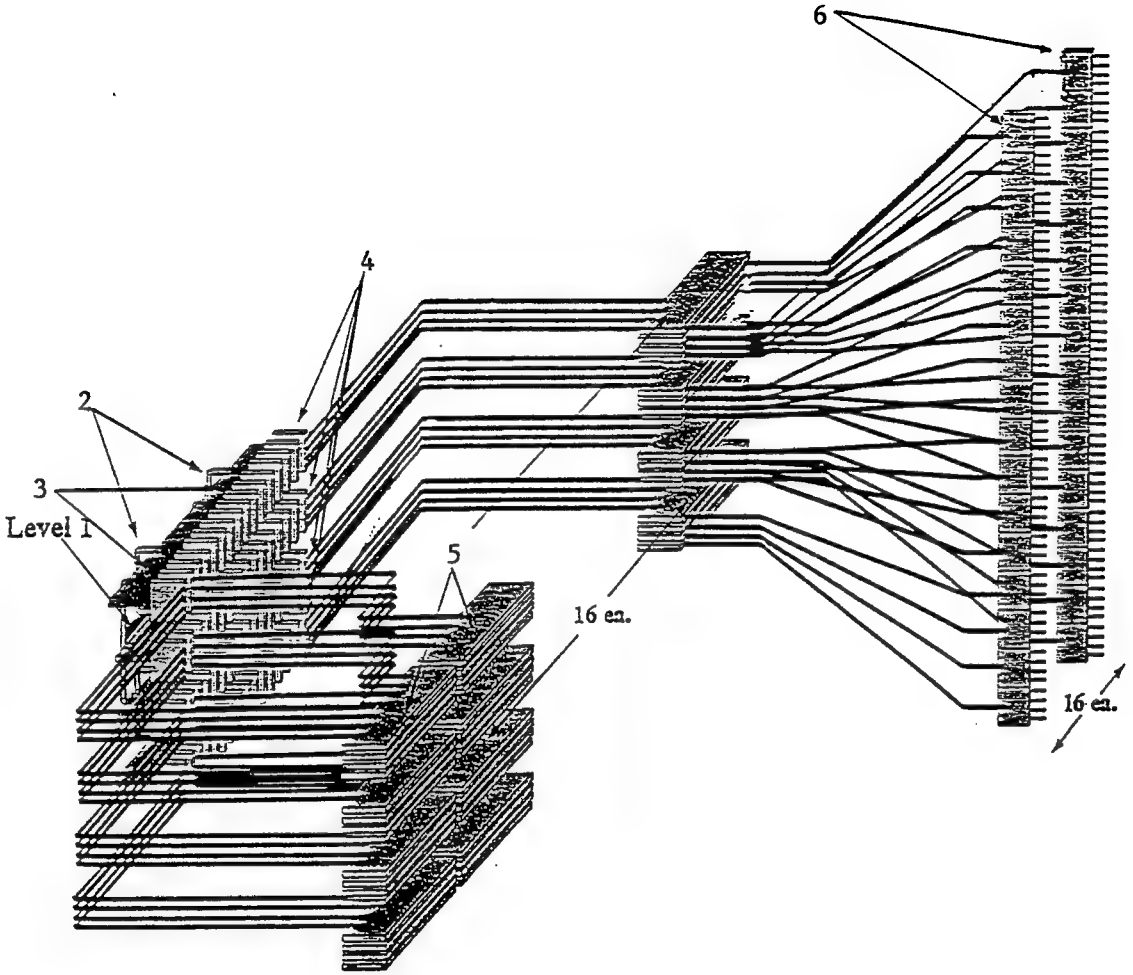

Figure 3-1. S-Band Interleaved Az/El Combiner Network

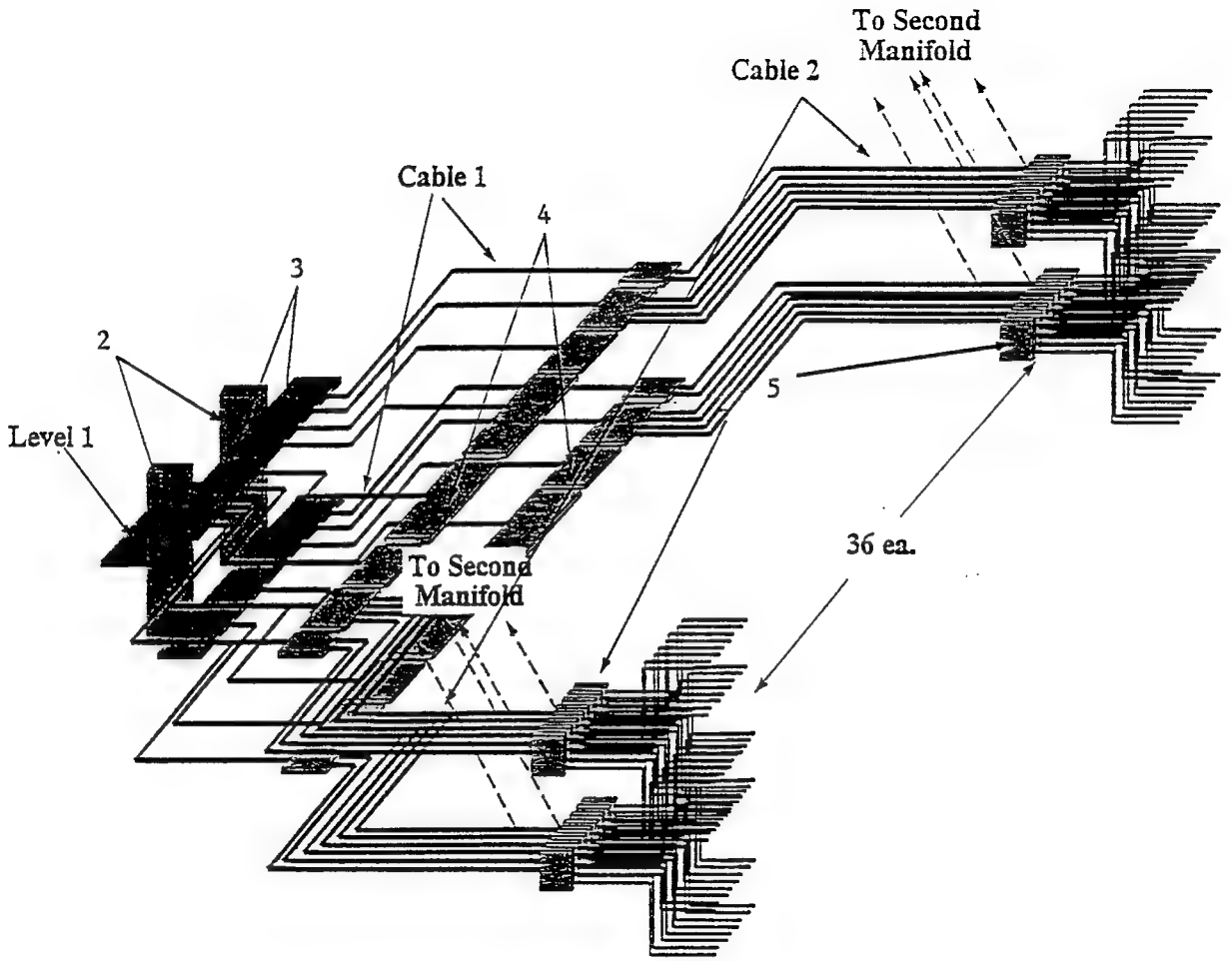

Figure 3-2. UHF Interleaved AzEl Combiner Network

level in order to achieve the desired low sidelobe weighting. One advantage of the interleaved az/el configuration was low far sidelobes arising from channel mismatch associated with amplitude and phase errors.

The interleaved az/el configuration was dropped in favor of the "sequential az/el" configuration (Figures 3-3 and 3-4). The principal reason for the revision was the potential for greater component sharing between the difference receive and sum receive/transmit manifolds. Also, the azimuth divide level, wherein expensive channel matching control elements would be located (Level 3 for S-band and Level 4 for UHF) contained far fewer components than contained in the corresponding levels of the interleaved configuration [Level 5 (formerly denoted "Az Level 3") for S-Band and Level 4 (formerly denoted "Az Level 3") for UHF].

Further simplification of the conventional beamformer was obtained by modifying the transmit beam azimuth weighting to coincide with that of the receive sum beam. Since the transmit and receive sum beams share the same manifold, this modification allowed the weighting to be implemented by unequal power division dividers in the azimuth divide levels rather than by amplification. Channel amplitude matching then would be effected by adjustable attenuators since the amounts of attenuation required would be minimal.

A final alteration was the replacement of waveguide in the first two divide levels of the interleaved az/el configuration with stripline dividers and coaxial cables in the corresponding levels of the sequential az/el configuration. The RF drive power requirements were determined to be low enough to justify the lighter weight components (Section 3.1.5).

The far sidelobe levels of the sequential az/el configuration would be higher along a narrow ridge in the azimuth plane. This sidelobe region, however, was shown by simulation to not appreciably affect radar performance. A detailed discussion of the dependence of average sidelobe level on beamformer errors in a corporate feed array is given in Appendix A. The further from the array face that independent errors originate in the corporate feed, the greater the extent of spatial correlation of the corresponding errors in the aperture. This correlation introduces higher sidelobes concentrated about broadside. Figures 3-5 and 3-6 show the average sidelobe level distribution throughout the radiation sphere for the sequential az/el S-band and UHF configurations, respectively. The coordinates are in units of beamwidth. The average sidelobe levels indicated are only those associated with beamformer errors. Sidelobe levels in dBi (s_{iso}) and in dB with respect to the directive gain (S_r) are shown. Independent amplitude and phase errors of identical statistical distributions occurring at each power division level in each

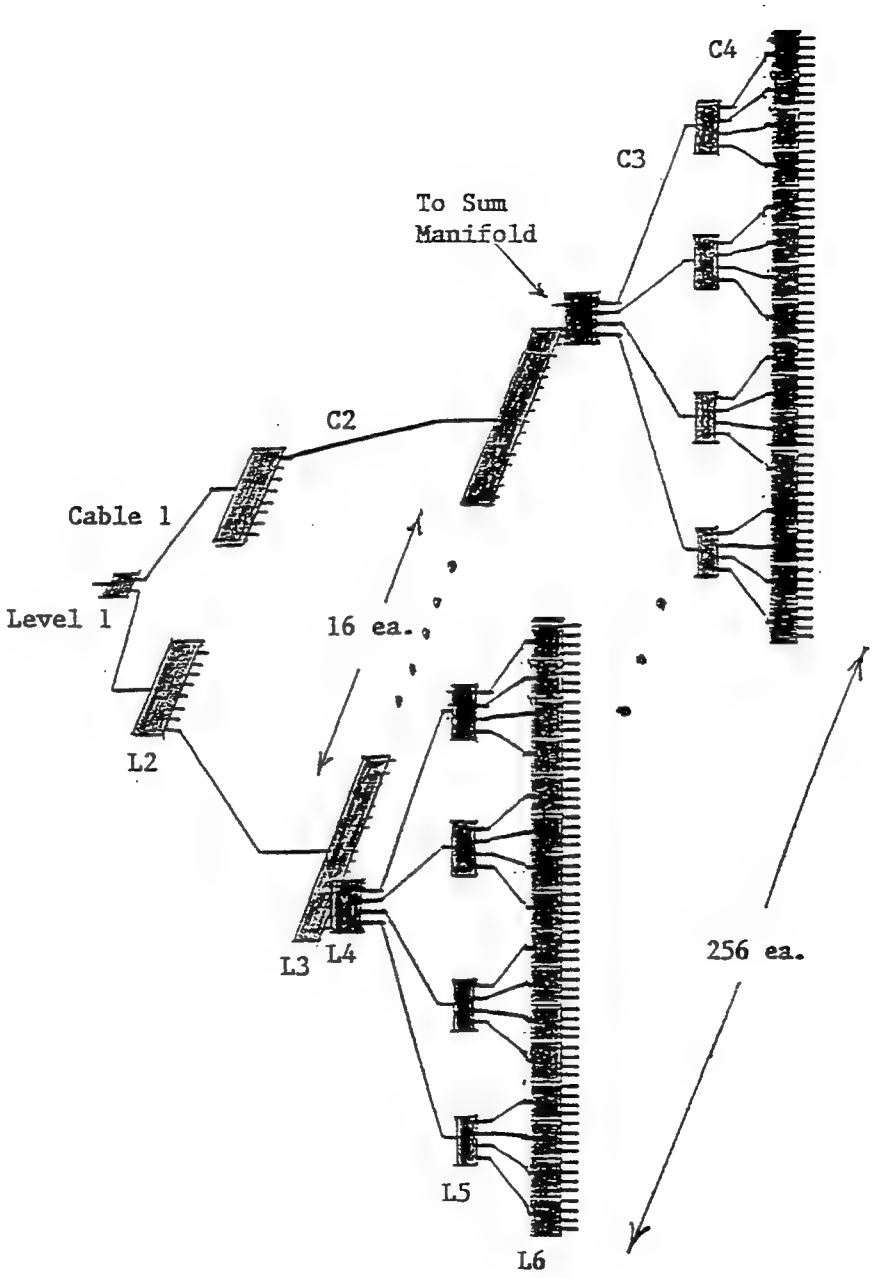

Figure 3-3. S-Band Sequential Az/El Combiner Network

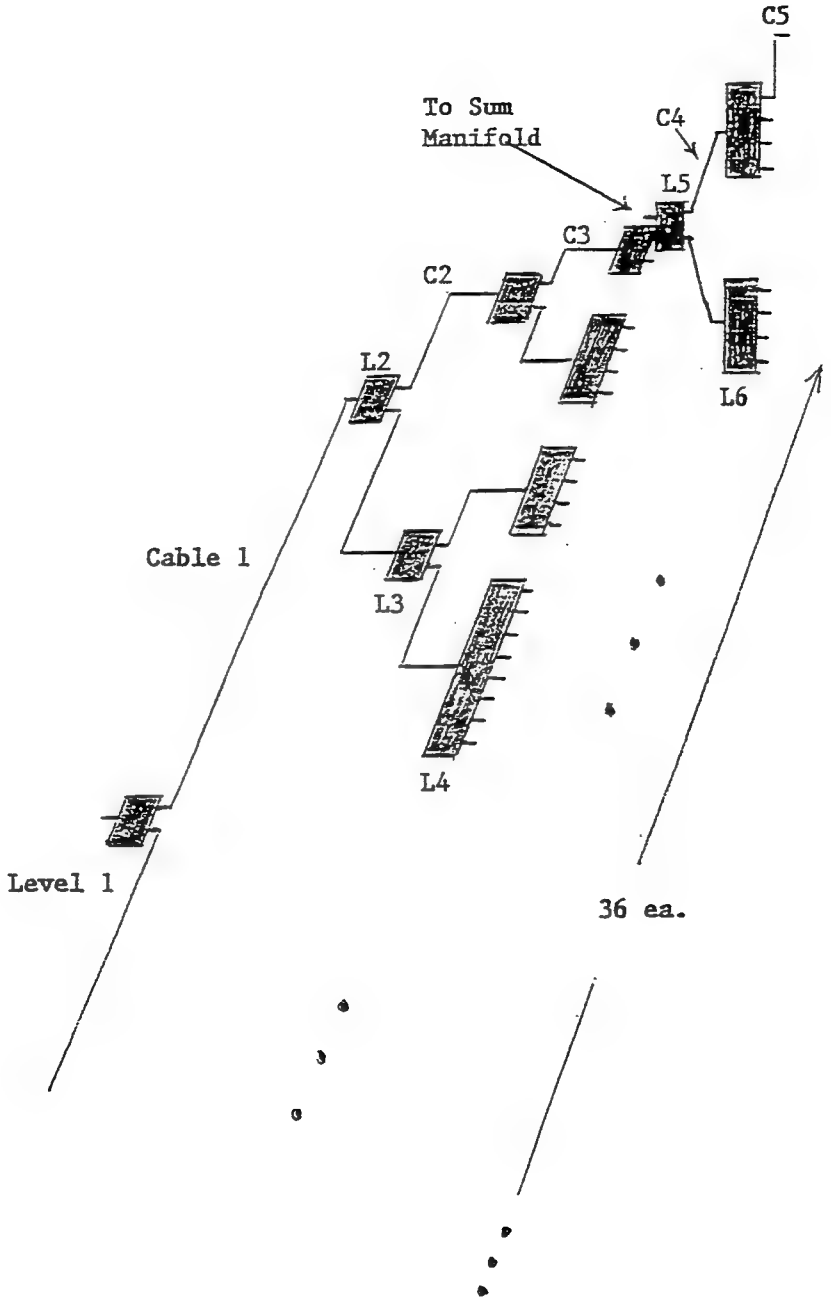

Figure 3-4. UHF Sequential Az/El Combiner Network

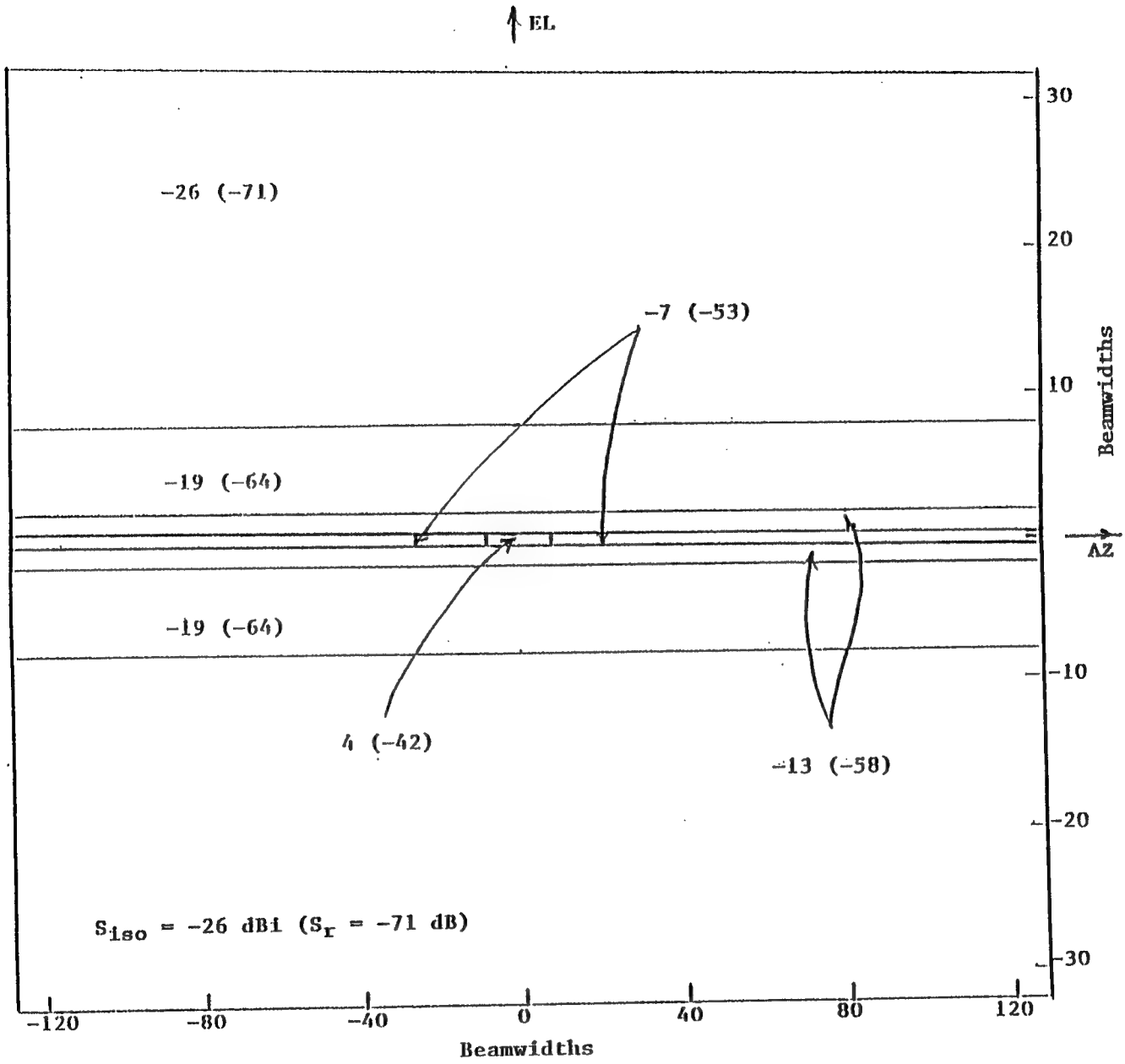

Figure 3-5. Average Sidelobe Error Due to Random Errors in Sequential Az/El S-Band Combiner

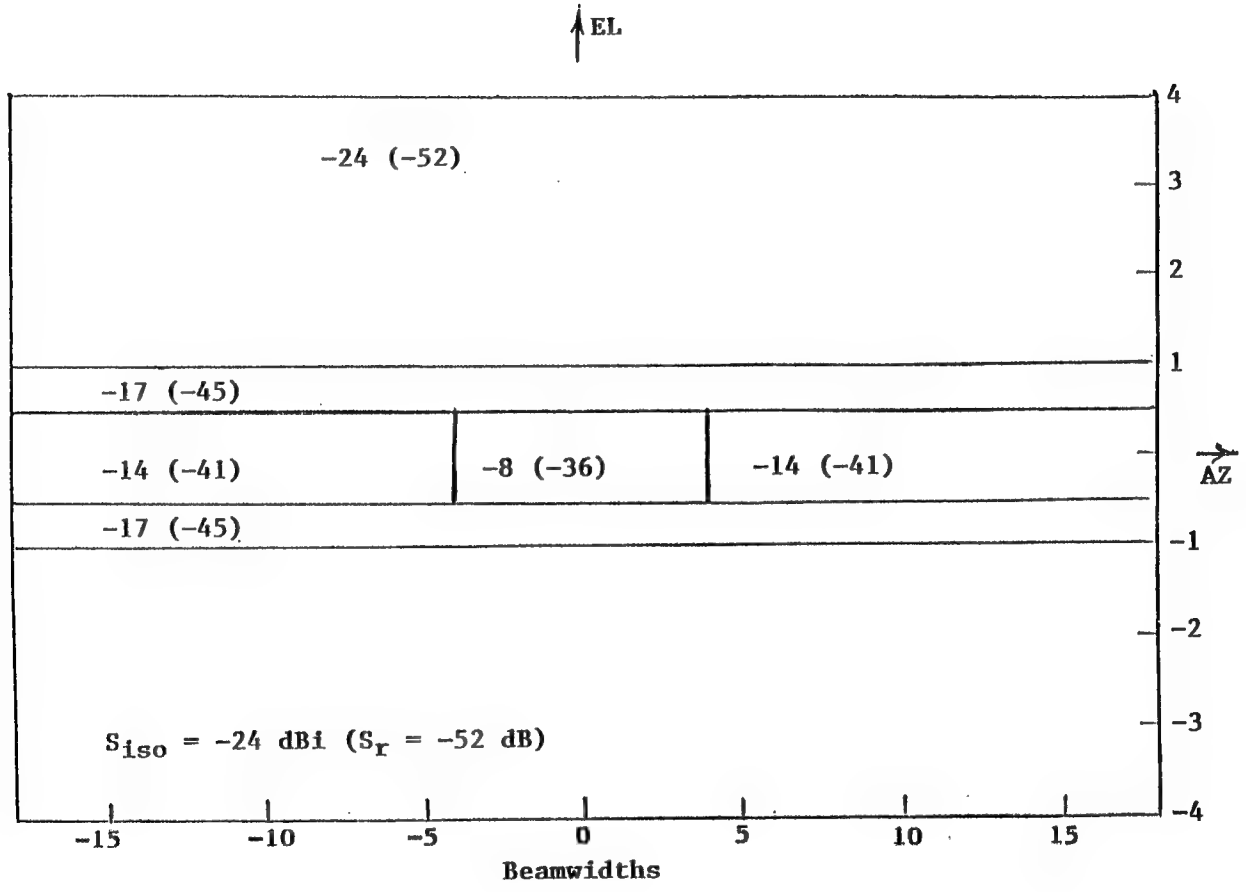

Figure 3-6. Sequential Az/El Combiner (UHF) Average Sidelobe Levels

channel were assumed in obtaining these results. The error variances associated with amplitude and phase errors at each level were obtained by specifying reasonable total channel error variances, shown in Figure 3-7, and by dividing these variances by the number of levels (six). Four contributions to the total channel error variances (σ^2) are phase shifter quantization ($\sigma^2_{\phi,q}$), attenuator quantization ($\sigma^2_{a,q}$), residual phase ($\sigma_\phi{}^2$) and residual amplitude ($\sigma_a{}^2$). Residual errors are those remaining after channel matching. The phase error variances are in units of square radians and the amplitude error variances are in units of square fractional amplitude error; i.e., if the zero error channel complex excitation is denoted a exp(jϕ), the corresponding excitation with error is denoted $a(1+\epsilon_a)$ exp $(j(\phi+\epsilon_\phi))$ where ϵ_a = fractional amplitude error and ϵ_ϕ= radian phase error. It can be shown that the error variance that is associated with average sidelobe levels is the sum of the amplitude and phase error variances. The average sidelobe level also depends on aperture efficiency, η. η = .67 for the S-band system (35 dB Taylor weighting in both planes), and η = .72 (30 dB Taylor weighting in both planes) for the UHF system.

The total channel residual errors shown in Figure 3-7 correspond to one percent of a wavelength phase error and one percent of a fractional amplitude error. Such error bounds are nearly within the realm of today's technology at UHF and microwave frequencies.

3.1.2 Manifold Components

The number of separate component enclosures within a manifold was kept to a minimum to keep down overall system weight. Some case sizes, however, were large enough to allow direct interconnection of all of an adjacent level's components. This reduced the number of cables needed for interconnection and therefore eliminated extra interfaces which are normally sources of system failure or degradation.

3.1.2.1 S-Band

Consider first the S-band manifolds (Figure 3-3). Wherever practical, interconnection is arranged to maximize the amount of hardware that is shared between the receive difference and transmit/receive sum manifolds. All but one of the power dividers are designed in stripline which provides more compact, lighter weight configurations than does microstrip. The Level 3 power divider is chosen to be microstrip to allow easy integration of the amplitude and phase control circuits necessary for calibration.

The first level azimuth feed of each manifold is a 2:1 stripline Wilkinson power combiner. Typical construction is shown in Figure 3-8. The following dimensions are assumed for this divider:

$$\sigma^2 = \sigma_{\phi,q}^2 + \sigma_{a,q}^2 + \sigma_{\phi}^2 + \sigma_{a}^2$$

Total	Phase Shifter Quantization	Attentuator Quantization	Residual Phase	Residual Amplitude

		S-Band	**UHF**
	$\sigma_{\phi,q}^2$	8.0×10^{-4} (6 Bits)	3.2×10^{-3} (5 Bits)
	$\sigma_{a,q}^2$	1.3×10^{-6} (8 Bits, .01 dB)	2.0×10^{-5} (6 Bits, .04 dB)
	σ_{ϕ}^2	3.9×10^{-3} (.01 λ)	3.9×10^{-3} (.01 λ)
	σ_{a}^2	1.0×10^{-4} (1%, .09 dB)	1.0×10^{-4} (1%, .09 dB)
	σ^2	4.8×10^{-3}	7.2×10^{-3}
Error Per Level	$\sigma^2 / 6$	8.0×10^{-4}	1.2×10^{-3}

Figure 3-7. Element Excitation Errors

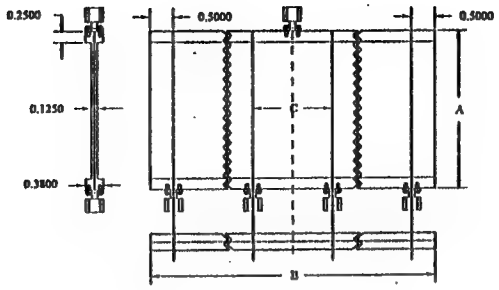

Figure 3-8. Stripline Case Outline (Dimensions in Inches)

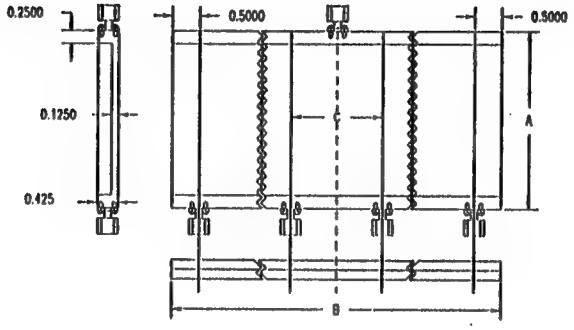

Figure 3-9. Microstrip Case Outline (Dimensions in Inches)

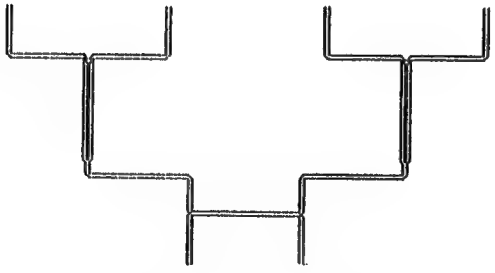

Figure 3-10. Sum/Diff Manifold Divider Circuit

A = 1.9 in

B = 1.4 in

C = 0.5 in

The purpose of the two Cable 1 cables in each of the two manifolds is to fan out roughly 1.2 inch on either side to align with the center of each half of the azimuth axis. The cables are composed of 0.141 inch semirigid coax which offers moderate loss.

There are two, Level 2 8:1 combiners in each of the two manifolds. They are unequal split stripline in-phase power combiner circuits with isolation resistors (Wilkinson type) fabricated as a laminated circuit assembly so that compression screws are not necessary. They are housed in a channelized case with SMA connectors. Typical construction is as shown in Figure 3-8. The following dimensions are assumed for this divider:

A = 3.5 in

B = 4.5 in

C = 0.5 in

The purpose of the Cable 2 cables in each of the two manifolds is to fan out each Level 3 combiner so that it can be centered behind the 16 columns which it feeds. This places the greatest length (heaviest) of cable at this level rather than at the Cable 3 level since there are fewer cables required here (16 vs. 1024). Each of the 16 cables is approximately 120 inches of 0.141 inch semirigid coax which offers moderate loss in a lightweight and compact form.

There are 16, 16:1 combiners in each of the two manifolds. They are microstrip unequal split in-phase Wilkinson power combiners with drop-in phase and amplitude control circuits in hermetic packages. They are housed in a channelized case with a cover and SMA connectors. Typical construction is as shown in Figure 3-9. The following dimensions are assumed for this divider:

A = 8.0 in

B = 8.5 in

C = 0.5 in

There are 256, 4:1 combiners in Level 4. Each combiner is a 2:1 stripline Wilkinson power combiner in tandem with a 3 dB broadside directional coupler. The entire circuit is fabricated as a laminated assembly so that compression screws are not necessary. Each combiner is housed in a channelized case with SMA connectors. Typical construction is as shown in Figure 3-8. The following dimensions are assumed for this divider:

A = 2.7 in
B = 2.5 in
C = 0.5 in

A conceptual sketch of the circuit is shown in Figure 3-10. As indicated, both outputs are provided from a single circuit. One output is connected to the transmit/sum receive manifold and the other to the difference manifold. Levels 3 and 4 are connected without cabling. Low insertion force ONP connectors at these junctions ensure low loss and easy accessibility.

The purpose of the Cable 3 cables is to fan out each Level 5 combiner to equal spacing along the elevation axis. There are 1,024 of these cables, each approximately 50 in. They are composed of 0.141 inch semirigid coax which offers moderate loss in a lightweight and compact form.

Level 5 is composed of 1024, 4:1 combiners. They also are stripline Wilkinson combiners fabricated as laminated circuit assembly so that compression screws are not necessary. They are housed in channelized case with SMA connectors. Typical construction is as shown in Figure 3-8. The following dimensions are assumed for this divider:

A = 2.7 in
B = 2.5 in
C = 0.5 in

Several of these combiners may be replaced with Level 4 type combiners in order to feed auxiliary channels for elevation nulling.

The purpose of the Cable 4 cables is to fan out each Level 6 combiner so that it can be properly located with respect to the four elements which it feeds. These 4096 cables are

fabricated in approximately 17 inch lengths of 0.141 inch coax cable to maintain moderate losses and weight.

There are 4096, Level 6 4:1 combiners. Each is a stripline Wilkinson combiner fabricated as a laminated circuit assembly so that compression screws are not necessary. Each is housed in a channelized case with SMA connectors. Typical construction is as shown in Figure 3-8. Connector spacing is matched to the T/R module spacing (interelement spacing). The following dimensions are assumed for this divider:

A = 2.7 in

B = 6.8 in

C = 1.7 in

3.1.2.2 UHF

The UHF manifold components are described here with reference to Figure 3-4. All but the Level 4 power dividers are designed in stripline which provides for more compact and lighter weight configurations than does microstrip. The Level 4 power dividers are assumed to be microstrip to allow easy integration of the amplitude and phase control circuits necessary to provide calibration capability.

Levels 1, 2, and 3 in each manifold has seven 2:1 unequal split (except for Level 1) stripline Wilkinson power combiners, one in Level 1, two in Level 2, and four in Level 3. Each divider is fabricated as a laminated circuit assembly and is housed in a channelized case with SMA connectors. Typical construction is shown in Figure 3-8. The following dimensions are assumed for this divider:

A = 2.0 in

B = 5.0 in

C = 0.5 in

There are 72, 4:1 equal split combiners in Level 6. Each is a Wilkinson power combiner fabricated as a laminated circuit assembly and is housed in a channelized case with SMA connectors. Typical construction is shown in Figure 3-8. The following dimensions are assumed for this divider:

A = 4.0 in

B = 5.0 in

C = 0.5 in

There are two sets of three different sized combiners in Level 4 of each of the two manifolds. Each set is composed of one 2:1, two 4:1, and one 8:1 dividers. Each divider is a microstrip unequal split in-phase Wilkinson power combiner with a drop-in phase and amplitude control circuit in a hermetic package. Each divider is housed in a channelized case with a cover and SMA connectors. Typical construction is as shown in Figure 3-9. The following dimensions are assumed for each set:

A = 15 in

B = 25 in

C = .5 in

Note that the B dimension does not include the considerable spacing between components within a set that is necessary to minimize cable lengths.

There are 36, 2:1 "hybrid" Wilkinson power combiners in Level 5. The combiner sum port connects to the difference manifold and the combiner difference port connects to the sum receive/transmit manifold. The device is also fabricated as a laminated circuit assembly so that compression screws are not necessary. Levels 4 and 5 are connected without cabling. Low insertion force ONP connectors at these junctions ensure low loss and easy accessibility. Typical construction is as shown in Figures 3-8 and 3-10. The following dimensions are assumed for this divider:

A = 2.0 in.

B = 5.0 in.

C = 0.5 in.

The purpose of the two Cable 1 cables in each of the two manifolds is to fan out roughly 120 inches on either side to align with the center of each half of the azimuth axis. The cables are composed of 0.141 inch semirigid coax which features moderate loss.

The purpose of the four Cable 2 cables in each of the two manifolds is to center the Level 3 combiners in azimuth. Each cable is approximately 65 inches of 0.141 semirigid coax.

The purpose of the eight Cable 3 cables in each of the two manifolds is to center the Level 4 combiners in azimuth. Each cable is approximately 35 inches of 0.141 semirigid coax.

The purpose of the 72 Cable 4 cables is to fan out each Level 6 combiner (two per column) to center in each half of the elevation plane. Each cable is approximately 35 inches of 0.141 semirigid coax.

The purpose of the Cable 5 cables is to connect Level 6 combiners to each of the T/R modules. Each of these 288 cables is approximately 1.7 inches of 0.141 coax.

3.1.3 Manifold Weight

The manifold weight calculations were determined for both 6061 aluminum alloy and Aluminum/Silicon Carbide, a common matrix metal in use for T/R modules today. The weight budgets do not account for calibration networks, built in test circuits or cooling manifolds. The following values for key parameters were assumed:

Aluminum density = 0.098 lb/in^3
matrix metal density = 0.078 lb/in^3
0.141 cable weight = 0.04 oz/in
SMA connector weight = 0.25 oz/pair

A manifold weight breakdown is given in Table 3-1a for S-Band and in Table 3-1b for UHF. The individual combiner weights are given for aluminum alloy construction and for the lighter, more expensive matrix metal construction. The weights per level are for matrix metal construction only. The weights per level corresponding to components that are shared between manifolds within a band are indicated by the notation "shared" so that these elements could easily be excluded in arriving at manifold weight totals. The totals are 1,396 lb for S-Band and 70 lb for UHF. The grand total manifold weight, therefore, is 1,466 lb.

TABLE 3-1a

S-BAND MANIFOLD WEIGHT/VOLUME

Component	Type	Per Component			Quantity		Per Level				
		Wg(oz)[1]		Vol.(cu. in)	Diff.Manif	Sum Manif.	Wg(lbs)		Vol. (cu.ft)[2]		
							Diff	Sum	Diff	Sum	
Level 1	2:1 Strine	2.0	1.6	1.01	1	1	≈0	≈0	Shared with UHF		
Level 2	8:1 Strine	4.8	3.84	5.99	2	2	≈0	≈0	Shared with UHF		AZ
Level 3	16:1 μstr	20.	16.	28.9	16	16	16	16	Shared with UHF		
Level 4	4:1 Strine	2.0	1.6	2.57	256	Shared	26	Shared	Shared with UHF		
Level 5	4:1 Strine	2.0	1.6	2.57	1,024	Shared	102	Shared	55	Shared	EL
Level 6	4:1 Strine	3.7	2.96	4.6	4,096	Shared	758	Shared	74	Shared	
Cable 1	120" Coax	5.3		1.87	2	2	1	1	Shared with UHF		AZ
Cable 2	120" Coax	5.3		1.87	16	16	5	5	Shared with UHF		
Cable 3	50" Coax	2.5		.78	1,024	Shared	160	Shared	157	Shared	EL
Cable 4	17" Coax	1.18		.27	4,096	Shared	302	Shared	291	Shared	
Connector	Low Insertion Force	.1		≈0	256	256	2	2	Shared with UHF		AZ
TOTAL S-BAND MANIFOLDS							1,396		577		

NOTES:

(1) With connector; 1st Number - 6061 Alum. Alloy, 2nd Number - Matrix Metal; .141 Cable = .04 oz/in; SMA Connector = .25 oz/pair

(2) Includes space between components (See Figure 3-11)

TABLE 3-1b

UHF MANIFOLD WEIGHT/VOLUME

Component	Type	Per Component			Quantity		Per Level				
		Wg(oz)[1]		Vol.(cu. in)	Diff.Manif	Sum Manif.	Wg(lbs)		Vol. (cu.ft)[2]		
							Diff	Sum	Diff	Sum	
Level 1	2:1 Strine	3	2.4	3.8	1	1	≈0	≈0	≈0	≈0	
Level 2	2:1 Strine	3	2.4	3.8	2	2	≈0	≈0	.1	.1	AZ
Level 3	2:1 Strine	3	2.4	3.8	4	4	1	1	.2	.2	
Level 4	2:1(1), 4:1(2) 8:1(1) μstr	30	2.4	159	2	2	3	3	3.0	3.0	
Level 5	2:1 Strine	3	2.4	3.8	36	Shared	5	Shared	2.5	Shared	EL
Level 6	4:1 Strine	5.8	4.64	7.6	72	Shared	21	Shared	Shared with S		
Cable 1	120" Coax	5.3		1.87	2	2	1	1	0	0	
Cable 2	65" Coax	3.1		1.01	4	4	1	1	0	0	AZ
Cable 3	35" Coax	1.9		.55	8	8	1	1	0	0	
Cable 4	35" Coax	1.9		.55	72	Shared	9	Shared	Shared with S		EL
Cable 5	17" Coax	1.18		27	288	Shared	21	Shared	Shared with S		
Connector	Low Insertion Force	.1		≈0	36	36	≈0	≈0	≈0	≈0	AZ
TOTAL UHF MANIFOLDS							70.		9.1		

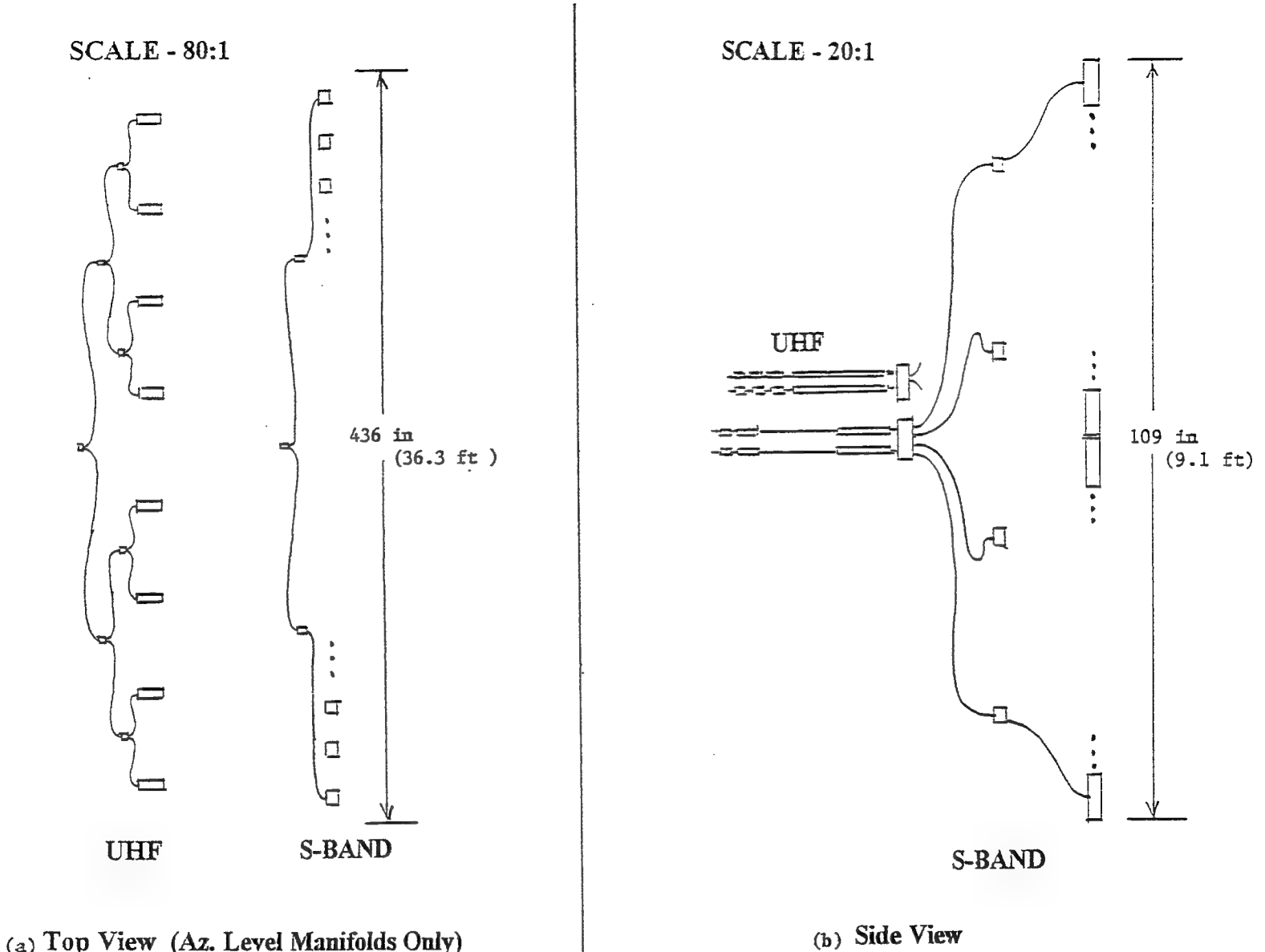

Figure 3-11. Conventional Beamformer Manifolds

3.1.4 Manifold Volume

A volume assessment of the manifolds was determined by estimating the enveloping volume required to house all S-band and UHF manifolds. Scale sketches of top (azimuth plane) and side (elevation plane) views of the manifolds are shown in Figure 3-11. The UHF elevation level division sections will fit within the volume occupied by the S-band elevation level division sections (Figure 3-11b). The S-band azimuth level division sections will fit within the volume occupied by the UHF azimuth level division sections (Figure 3-11a). Of course, the transmit/receive sum and receive difference manifolds share the same elevation level division sections.

The individual component volumes are listed in Table 3-1. The volumes occupied by each level are identified in Table 3-1 also. The latter are the enveloping volumes, including space between components. They were obtained from Figure 3-11. Shared volumes are so indicated. The grand totals of manifold volumes, taking into account sharing, are 577 cu ft for S-band and 9.1 for UHF. The grand total occupancy volume is approximately 586 cu ft.

3.1.5 RF Drive

Consideration was given to incorporating distributed gain in the form of transmit amplifiers at some appropriate point in the transmit sum beam manifold. The amplifier circuits would have been full T/R modules with the phase control and receive LNA circuits removed. This approach would have allowed the use of a low-power RF source at the transmit input, and would have provided graceful degradation since the drive signal would not be completely lost as a result of a single component failure. This design, however, would call for an additional set of feed components to handle the receive sum beam formation forward of the amplifier insertion point. In addition, an extra set of interconnect cabling would be necessary to ensure easy access to all amplifier modules for maintainability. For these reasons, as well as others concerning cooling, amplifier efficiency, and power dissipation in the remaining transmit feed output levels, a single source approach has been taken.

The required transmit manifold RF drive power was determined from the specified T/R module input power adjusted to allow for power dissipation in the manifold and reduced in accordance with the azimuth amplitude taper. The 35 dB sidelobe Taylor amplitude taper for the

S-band system is achieved with 45 percent of the power required for a uniform taper, assuming that the center column is excited for peak module power in both cases. The drive power is reduced to 45 percent of the uniform value by virtue of the unequal power divide implementation of the manifold. If the taper were to be achieved with attenuators, the "45 percent power" would increase manifold dissipation. In either case, the total power radiated will be 45 percent of that for uniform excitation, and since the aperture efficiency associated with the taper is 0.82, the effective radiated power (ERP) is reduced from that of uniform weighting by 37 percent (4.3 dB). The constraint on maximum module input power and the perceived need for low sidelobes on transmit is the reason for accdepting the 4.3 dB reduction in ERP.

The sidelobe taper for the UHF system is less severe than that for the S-band system. A 30 dB sidelobe Taylor weighting yields a power reduction that is 48 percent of that of uniform and an azimuth plane aperture efficiency of .85. The ERP then is reduced to 41 percent of that of uniform weighting (3.93 dB).

The factors entering the computation of drive power are given in Table 3-2. The factors include single channel manifold loss (10.1 dB for S-band), and (3.6 dB for UHF), the number of elements (channels), the aforementioned adjustments for azimuth taper and the maximum T/R module peak input power. The RF drive peak power requirements are less than 1 kW for S-band and less than .25kW for UHF. These power levels would not cause voltage breakdown or excessive heating problems in the first level stripline dividers.

A TWT amplifier was selected for providing the S-band drive power because of the relatively high average power requirement (about 150 W). The S-band amplifier sizing was based upon the Keltec Model SA-600-200. The DC power, weight, and volume are estimated at 1300 W (about 10 percent overall efficiency), 40 lb, and 0.5 cu ft. These estimates include the possible presence of a small driver amplifier that may be required in addition to the TWT in order to realize the necessary 60 dB gain (S-band exciter output is 0 dBm.)

The UHF T/R module power amplifier was used as a basis in sizing the UHF band RF drive power. The DC power, weight, and volume are estimated at 106 W (35 percent efficiency), 8 lb, and 0.1 cu ft. These estimates include the presence of a small driver emplifier in order to achieve the necessary 52 dB gain (the UHF exciter output power is 2 dBm.)

TABLE 3-2

RF DRIVE POWER COMPUTATION

	S-BAND	UHF
Level 1 Loss Factor	0.6 dB	0.25 dB
Level 2 Loss Factor	0.7 dB	0.25 dB
Level 3 Loss Factor	0.9 dB	0.25 dB
Level 4 Loss Factor	0.6 dB	0.45 dB
Level 5 Loss Factor	0.6 dB	0.25 dB
Level 6 Loss Factor	0.6 dB	0.3 dB
Cable 1 Loss Factor [1]	2.27 dB	0.772 dB
Cable 2 Loss Factor [1]	2.27 dB	0.436 dB
Cable 3 Loss Factor [1]	1.008 dB	0.253 dB
Cable 4 Loss Factor [1]	0.414 dB	0.253 dB
Cable 5 Loss Factor [2]		0.143 dB
Connector Loss Factor [2]	0.112 dB	0.02 dB
Subtotal	10.07 dB	3.63 dB
No. of Elem.	+42.14 dB (16,384)	+24.59 dB (288)
Azimuth Taper	-3.47 dB (45%)	-3.19 dB (48%)
Subtotal	48.74 dB	25.03 dB
T/R Module Peak Power	-18.06 dBW (.013 W)	-1.25 dBW (.75W)
RF Drive Power (Peak)	29.88 dBW (973 W)	23.78 dBW (239 W)

[1] 0.141 Cable Loss = 0.017 dB/in (Precision Tube AA50141)

[2] SMA Connector Loss = 0.03 $\sqrt{f}$; f = frrequency in GHz

3.1.6 Channel Matching

Amplitude and phase adjustors in all channels are necessary to allow the periodic correction that is essential to maintaining low sidelobe performance. It is anticipated that the T/R module phase shifters and attenuators will be used to match the elevation manifold and the transmit/receive sum azimuth manifold. Only the azimuth manifold of the difference beam requires separate adjustment. This adjustment will be accomplished by actuating a slight amount of adjustable attenuation and phase shift included in each channel of the S-band Level 3 combiners (Level 4 in the UHF beamformer). This adjustment is shown in Figure 3-12 for S-band. A similar assignment applies to UHF. Only one set of adjustors is required per band. Since the nominal weighting is achieved by unequal divide combiners, variable resistors should be adequate to provide the small amount of amplitude correction. Small, light weight digital phase shifters are recommended for phase correction. The resistors and phase shifters could be imbedded in the appropriate power combiners in the difference beam azimuth manifold.

3.1.7 Auxiliary Channels

The 16 subarrays which form the adaptive nulling auxiliary array are formed by combining the outputs from some of the difference receive ports of the Level 6 combiners. Each of these subarrays is one element wide by 16 elements high (1 by 4 in the UHF beamformer). The subarrays are distributed throughout the array. The unequal power division that is used to obtain azimuth low sidelobe weighting occurs at lower levels of power division (closer to the receiver) and thus does not impact the auxiliary array amplitude. Elevation taper, however, is imparted by the T/R modules and thus will affect the levels and distributions of the auxiliary arrays and must be considered in the selection of the arrays.

3.1.8 Receivers

There are 18 identical receivers required for the conventional beamformer. These correspond to the sum and azimuth difference beams and the 16 auxiliaries required for sidelobe cancelling. A block diagram for one of these receivers is shown in Figure 3-13. The S-band and UHF systems share the same receiver after the first amplifiers, A1 and A2. An IF frequency was selected that would meet three criteria: (1) the LO's for both the UHF and the S-band radars could be generated from one source, (2) no intermodulation products from the receive and LO

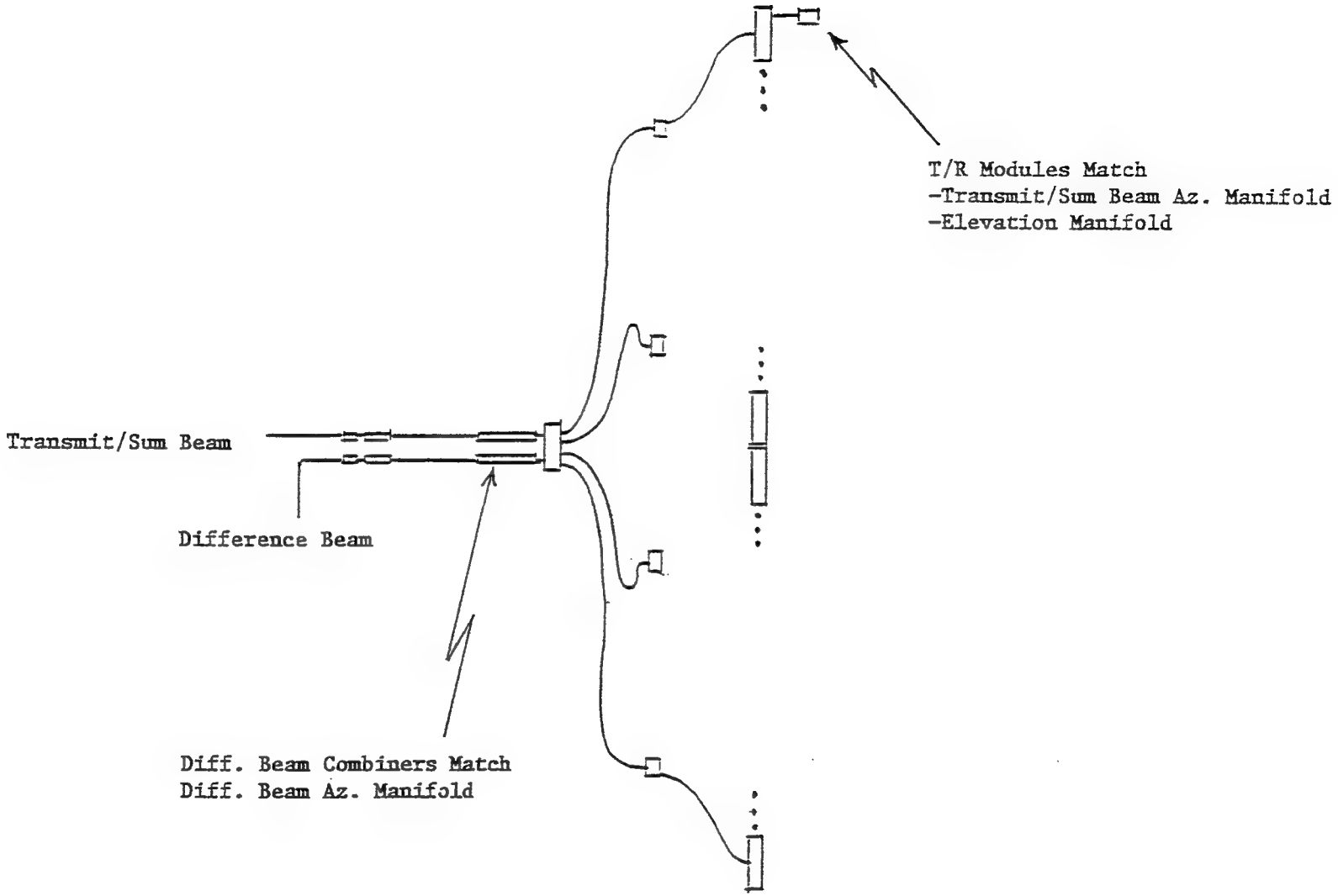

Figure 3-12. S-Band Channel Matching Elements

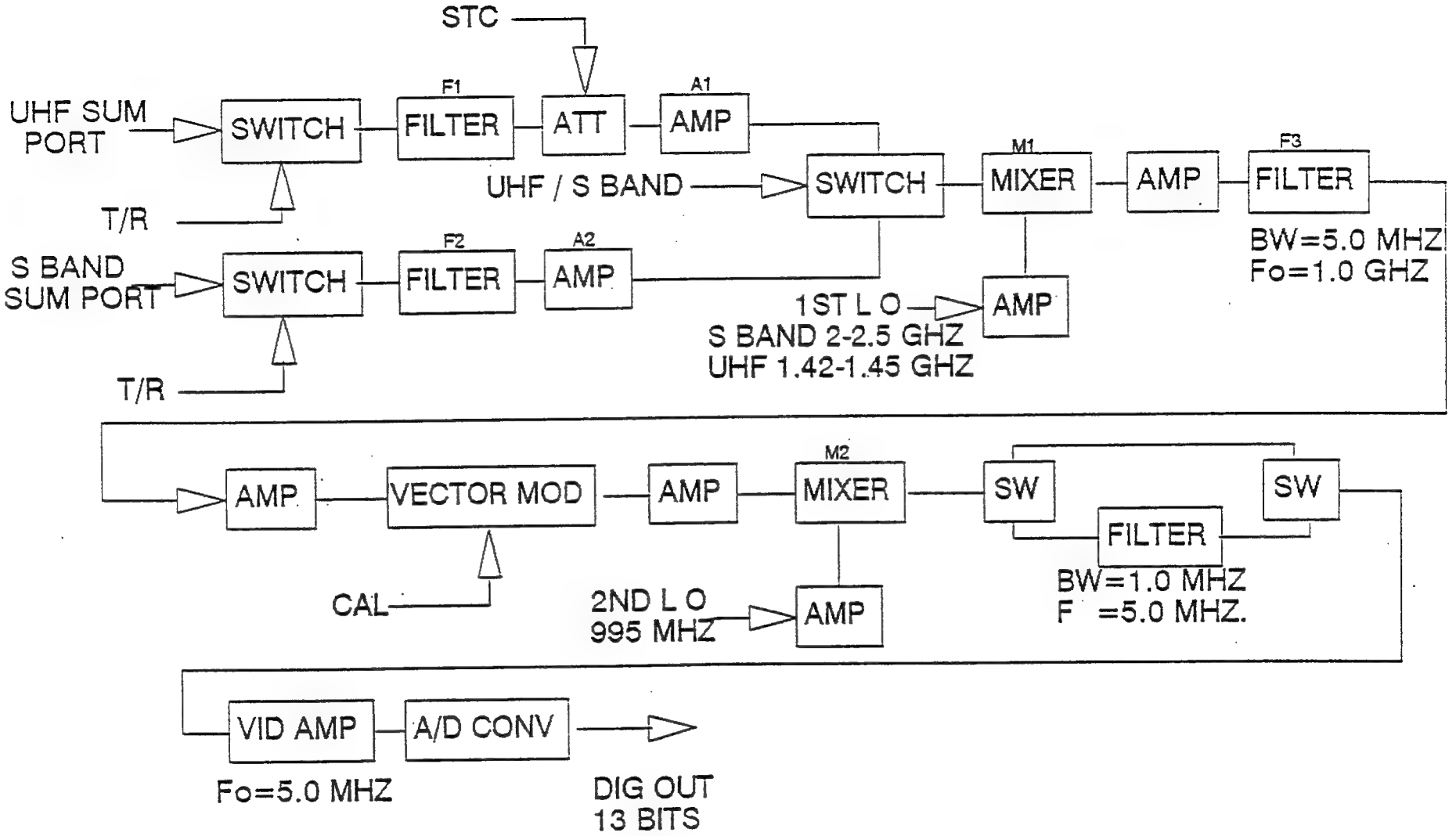

Figure 3-13. UHF/S-Band Receiver Block Diagram

signals would occur in the IF passband, and (3) components are readily available. A 1.0 Ghz IF frequency meets these requirements.

Detailed information on each of the devices shown in Figure 3-13, including gain, noise figure, compression point, etc. is given in the charts of Tables 3-3 and 3-4. Other information such as cumulative noise figure, noise output power, and peak clutter power at the output of each stage is given for the 5.0 Mhz bandwidth only. The information on the first line of Table 3-3 and Table 3-4 (SUM PORT OUTPUT) includes the effects of the T/R Modules and the manifold on the noise figure, gain, and clutter signal levels.

Also given in Tables 3-3 and 3-4 are the maximum and minimum gains for each device as well as the maximum and minimum total gains. This information is required to determine the attenuator range for receiver gain matching.

The system noise figure is about 3.5 dB for S-band and about 3.1 dB for UHF. The higher noise figure for S-band is due to 10 dB less gain in the T/R module circuit and more beamforming loss.

The switches at the inputs are used to provide an additional 60 dB of isolation during transmit for receiver protection and to avoid saturation to allow a fast recovery time. Filters F1 and F2 were selected to give 44 dB and 37 dB rejection at the image frequencies for the UHF and S-band systems respectively. This rejection is in addition to any image rejection provided by the T/R module. Since UHF estimated clutter to noise ratio of 80 dB exceeds the dynamic range of the 13 bit A/D converter, approximately 20 dB of STC (Sensitivity Time Control) is required.

The common mixer for both bands down converts the S-band signal and up converts the UHF signal to the common 1.0 Ghz IF. Since the LO is below the receive signal for S-band and above the receive signal for UHF, the frequency time relationships are reversed for any LFM (linear frequency modulation) waveforms. This reversal can be accommodated either in signal processing or waveform generation. Two receiver bandwidths of 1.0 MHz and 5.0 MHz are available to accommodate a range of transmit pulsewidths. A SAW device was selected for the 5 Mhz filter because of its superior in band channel to channel matching. The 1.0 MHz filter is an LC filter placed after the second down conversion and is switched in and out as required. Alternatively, this filter could be implemented digitally.

Table 3-3 S-Band Receiver Performance Spreadsheet

DEVICE	VENDOR	MODEL	GAIN(dB)	CUM GAI dB	SIG.OUT dBm	COMP PT 1dB[dBm]	N.F. dB.	CUM N.F. dB	B.W. (MHZ)	NOI OUT dBm	C/N [PK] dB	GAIN MIN dB	SIG.OUT MIN.[dBm]	GAIN MAX dB.	SIG.OUT MAX[dBm]
SUM PORT OUTPUT			10.5	10.5	-26.9		3.2	3.2	1000.0	-70.3	43.4		-28.9		-25.0
SWITCH	TRIANGL	QB-54-HAD	- 0.8	9.7	-27.7	MAX 10W	0.8	3.2	1000.0	-71.1	43.4	-0.5	-29.4	-0.5	-25.5
FILTER	K&L	LFV20-3250/500-O/O	- 0.5	9.2	-28.2		0.5	3.3	500.0	-74.5	46.3	-0.3	-29.7	-0.3	-25.8
AMPLIFIER	AVANTEK	PPA-4213	27.0	36.2	-1.2	13.0	2.1	3.4	500.0	-47.4	46.2	26.5	-3.2	31.0	5.2
UHF AND S BAND RECEIVERS ARE COMMON BELOW THIS POINT															
SWITCH [SPDT]	AVANTEK	PPA-4213	-1.6	34.6	-2.8	17.0	1.6	3.4	100.0	-56.0	53.2	-1.4	-4.6	-1.0	4.2
MIXER [.01-3.4GHZ]	WJ	M8T	-7.0	27.6	-9.8	7.0	8.0	3.4	100.0	-63.0	53.2	-8.0	-12.6	-6.0	-1.8
AMPLIFIER	WJ	A28	20.5	48.1	10.7	13.0	6.0	3.4	100.0	-42.5	53.2	18.0	5.4	22.0	20.2
SAW FILT [MARK S	SAWTEK		-15.0	33.1	-4.3	[IN] 20	15.0	3.4	5.0	-70.5	66.2	-16.0	-10.6	-14.0	6.2
AMPLIFIER	WJ	A28	10.0	43.1	5.7	13.5	3.9	3.4	5.0	-60.5	66.2	9.5	-1.1	11.0	17.2
VECT MOD	OLEKTRO	P-CPM-550-4	-16.0	27.1	-10.3	12.0	16.0	3.4	5.0	-76.5	66.2	-15.0	-16.1	-15.0	2.2
AMPLIFIER	WJ	A28	10.0	37.1	-0.3	13.5	3.9	3.4	5.0	-66.5	66.2	9.5	-6.6	-11.0	13.2
MIXER	WJ	M8T [LO = 10]	-6.0	31.1	-6.3	7.0	6.0	3.4	5.0	-72.5	66.2	-7.0	-13.9	6.0	7.2
SWITCH	SILICONIX		-0.3	30.8	-6.6		0.3	3.4	5.0	-72.8	66.2	-0.3	-13.9	-0.3	6.9
BP FILTER	K&L	LB20	0.0	30.8	-6.6		0.0	3.4	5.0	-72.8	66.2	0.0	-13.9	0.0	6.9
SWITCH	SILICONIX		-0.3	30.5	-6.9		0.3	3.5	5.0	-73.1	66.2	-0.3	-14.2	-0.3	6.6
VID AMP [RL + 100]	TELE/PHI	[1437]	25.0	55.5	18.1	30.0	1.0	3.5	5.0	-48.1	66.2	25.0	10.8	25.0	31.6
A/D CONVERTER	WEST. DEVELOPMENT				MAX IN+19										
LO AMP [2ND LO]	WJ	WJ A26	20.5		10.0	12.5						18.5		22.0	
LO AMP [1ST LO]	AVANTEK	PPA-4132	22.0		10.0	16.0						19.0		24.0	

Table 3-4 UHF Receiver Performance Spreadsheet

DEVICE	VENDOR	MODEL	GAIN(dB)	CUM GAI STC(dB)	SIG.OUT STC(dBm) [PK CLUTT]	COMP PT 1dB[dBm]	GAIN (dB) NO STC	CUM GAI NO STC [dBm]	NF(MAX) dB.	CUM N.F. dB	B.W. [MHZ]	NOI OUT NO STC [dBm]	GAIN MIN dB	SIG. OUT. MIN. [dBm]	GAIN MAX dB	SIG.OUT MAX [dBm]
SUM PORT OUTPUT			24.0	24.0	5.1		24.0	24.0	3.0	3.0	100.0	-67.0		2.1		8.1
SWITCH	TRIANGL	QN16	-0.4	23.7	4.8	MAX 10W	-0.4	23.7	0.4	3.0	100.0	-67.3	-0.4	1.8	-0.4	7.8
FILTER	K&L	K&L 2ML1	-0.3	23.4	4.5		-0.3	23.4	0.3	3.0	100.0	-67.6	-0.3	1.5	0.2	8.0
STC ATT	AVANTEK	UTF/PPF-	-21.0	2.3	-16.6		-2.5	20.9	2.5	3.0	100.0	-70.1	-20.0	-18.6	-20.0	-12.1
AMPLIFIER	ANZAC	AM-/AMC-	12.5	14.8	-4.1	18.0	12.5	33.4	4.0	3.0	100.0	-57.6	12.5	-6.1	15.0	2.9
UHF AND S BAND RECEIVERS ARE COMMON BELOW THIS POINT																
SWITCH [SPDT]	WJ	MS254	-1.6	13.2	-5.7	17.0	-1.6	31.7	1.6	3.0	100.0	-59.2	-1.4	-7.5	-1.0	1.9
MIXER [.1-3.4GHZ]	WJ	WJ-M4TH	-8.5	4.7	-14.2	[IN] 17	-8.5	23.2	8.5	3.0	100.0	-67.7	-8.0	-15.5	-8.0	-4.1
AMPLIFIER	AVANTEK	AWT-4532	21.0	25.8	6.9	12.0	21.0	44.2	3.8	3.1	100.0	-46.7	18.0	2.5	22.0	18.0
SAW FILT [MARK S	SAWTEK		-15.0	10.8	-8.2	[IN] 20	-15.0	29.2	15.0	3.1	5.0	-74.7	-16.0	-13.5	-14.0	3.9
AMPLIFIER	WJ	A28	10.0	20.8	1.8	13.5	10.0	39.2	3.9	3.1	5.0	-67.7	9.5	-4.0	11.0	15.0
VECT MOD	OLEKTRO	P-CPM-55	-12.0	8.8	-10.2	12.0	-12.0	27.2	13.0	3.1	5.0	-76.7	-15.0	-19.0	-15.0	-0.1
AMPLIFIER	WJ	A28	10.0	18.8	-0.2	13.5	10.0	37.2	3.9	3.1	5.0	-66.7	9.5	-9.5	11.0	11.0
MIXER	WJ	P M8T	-6.0	12.8	-6.2	7.0	-6.0	31.2	0.3	3.1	5.0	-72.7	-7.0	-16.5	-6.0	5.0
SWITCH	SILICONIX		-0.3	12.5	-6.5		-0.3	30.9	0.0	3.1	5.0	-73.0	-0.3	-16.8	-0.3	4.7
BP FILTER	K&L	LB20	0.0	12.5	-6.5		0.0	30.9	0.3	3.1	5.0	-73.0	0.0	-16.8	0.0	4.7
	SILICONIX		-0.3	12.2	-6.8		-0.3	30.6		3.1	5.0	-73.3	-0.3	-17.1	-0.3	4.4
VID AMP [RL = 100]	TELE/PHI	[1437]	25.0	37.2	18.3	30.0	25.0	55.6		3.1	5.0	-48.3	26.0	8.9	26.0	30.4
A/D CONVERTER	WEST. DEVELOPMENT				MAX IN+19											
LO AMP [2ND LO]	WJ	WJ A26	20.5		10.0	12.5							18.5		22.0	
LO AMP [1ST LO]	AVANTEK	PPA-4132	22.0		10.0	16.0							19.0		24.0	

The vector modulator provides both amplitude and phase control for receiver matching of the 18 receivers during calibration. During calibration it is used to set the noise level of the sum channel equal to 2 LSB's of the A/D converter. The sum channel is used as a reference for matching the other receivers.

The signal is down converted to 5.0 Mhz before A/D conversion. A/D conversion prior to I and Q generation eliminates the difficult I and Q matching requirements at video frequencies and only requires one A/D converter per channel instead of two. It does, however, require A/D conversion at four times the rate that I and Q conversion requires. Thirteen bit A/D converters at 20 Mhz rates are realizable with today's technology.

A 20 dB gain amplifier is provided for each LO input signal to recover signal lost in the 18:1 power division required to apply the LO to the 18 receivers. The advantage of applying amplification after the division is reduced leakage of the LO into the IF.

3.1.9 Exciter*

The goal in the design of the exciter was to maximize the sharing between the S Band and UHF systems. The following assumptions were made:

1) A 10 Mhz reference signal would be provided and all output signals would be coherent with this,
2) 1.0 Mhz frequency steps for both S Band and UHF, and
3) Frequency switching time of 50 microseconds.

A receiver first IF frequency of 1.0 Ghz was selected to allow the same frequency synthesizer to be used for both bands and to avoid generating intermodulation products between the transmit and receive signals within the IF passband.

A PLL (phase locked loop) synthesizer was chosen over a direct synthesizer for the following reasons:

*The exciter design described here was not used in the final weight, volume, power estimates. A faster switching, direct synthesizer design provided by Westinghouse was used. However, the comparative discussion is of interest, and it remains a viable alternate.

1) The PLL filtering required to reduce the input reference sidebands is at baseband and is simpler to implement than the bandpass filters required with direct synthesis, and

2) The PLL is smaller and requires less DC power than does direct synthesis when a large number of frequency steps are required (500 for S-band).

The disadvantage of the PLL is that the time required to change frequencies is greater than for direct synthesis. A block diagram of the exciter is given in Figure 3-14.

The system (single side band) phase noise for both the UHF and S-band systems is given in Figure 3-15. This data is worst case and is the sum of the phase noise for the transmit, first LO and second LO signals. The low phase noise at offset frequencies under about 1.0 kHz is dominated by the 10 MHz reference input. Consequently the transmit, first LO and second LO phase noises are coherent at these frequencies. This coherence results in lower system phase noise than that shown in Figure 3-15 for short ranges and low offset frequencies. The exact reduction is undetermined at this time. Noise at offset frequencies between 10 Khz and 100 Khz is dominated by the phase detector. Phase noise from the reference signal and the phase detector that exceeds 300 Khz is outside the loop bandwidth and does not appear in the output thus leaving only VCO (voltage controlled oscillator) noise. Figure 3-15 also shows typical phase noise for a good 10 Mhz crystal oscillator. This data was used in designing the exciter.

A comparison between the PLL and an ideal direct frequency synthesizer using the same reference signal and producing one transmit frequency and both LO's is given in Figure 3-16. The phase noise is slightly lower for the direct synthesizer at frequencies from 10 Hz to 1.0 KHz and approximately 10 dB lower from 10 KHz to 300 KHz. Above 300 KHz, the PLL has lower phase noise.

A description of the implementation of the exciter functions follows. Figure 3-17 shows a detailed block diagram of the LO synthesizer which is part of the exciter. To generate the second LO of 995 Mhz the 10 MHz input is divided by two producing a 5 Mhz reference for the 2nd LO phase detector. The VCO output is mixed with a 1.0 Ghz reference and the 5 Mhz difference output is used for the other phase detector input. The detector output error voltage is amplified, low pass filtered, and applied to the VCO control to maintain the output at 99.5 times the 10 MHz reference input (995 Mhz).

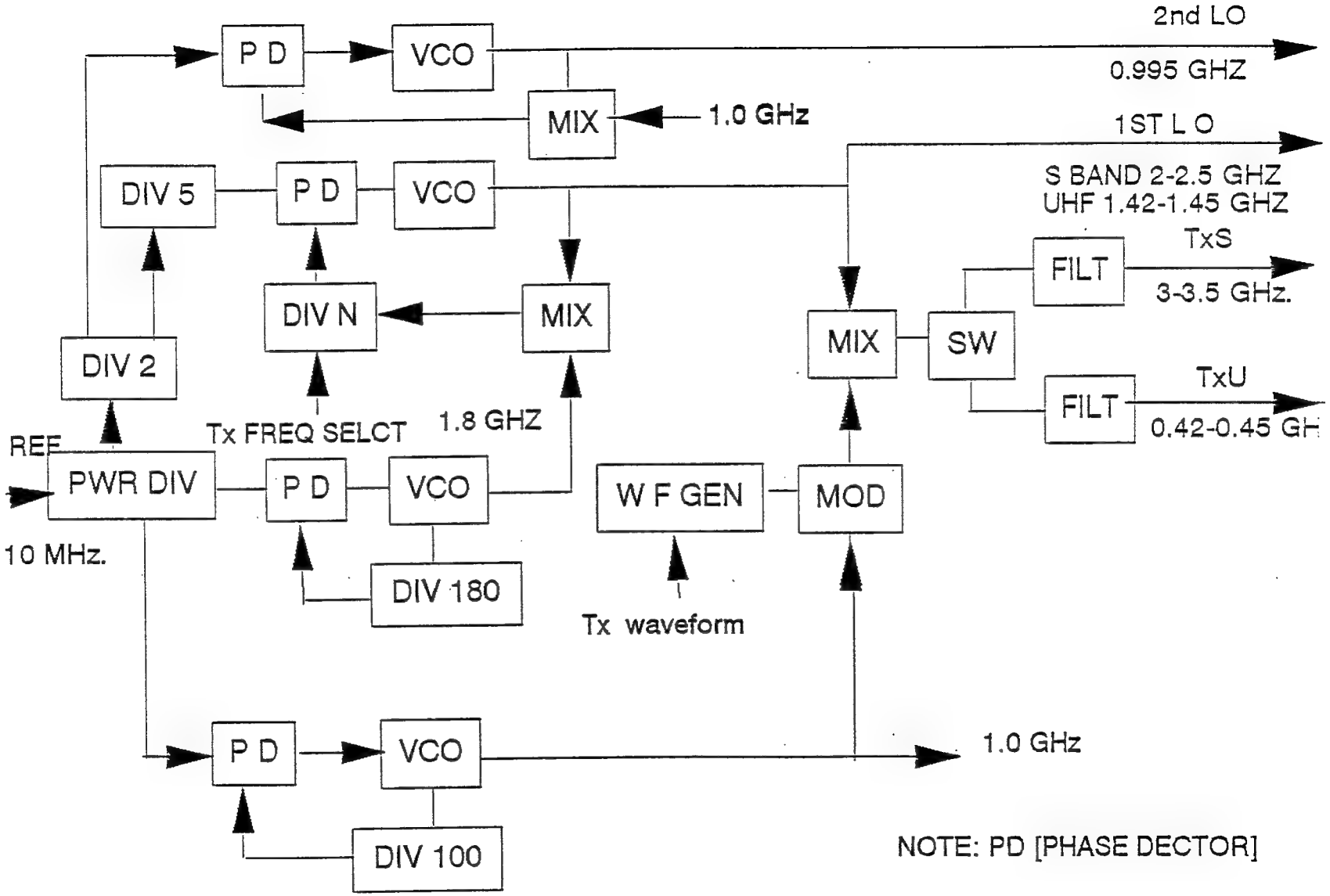

Figure 3-14. Exciter

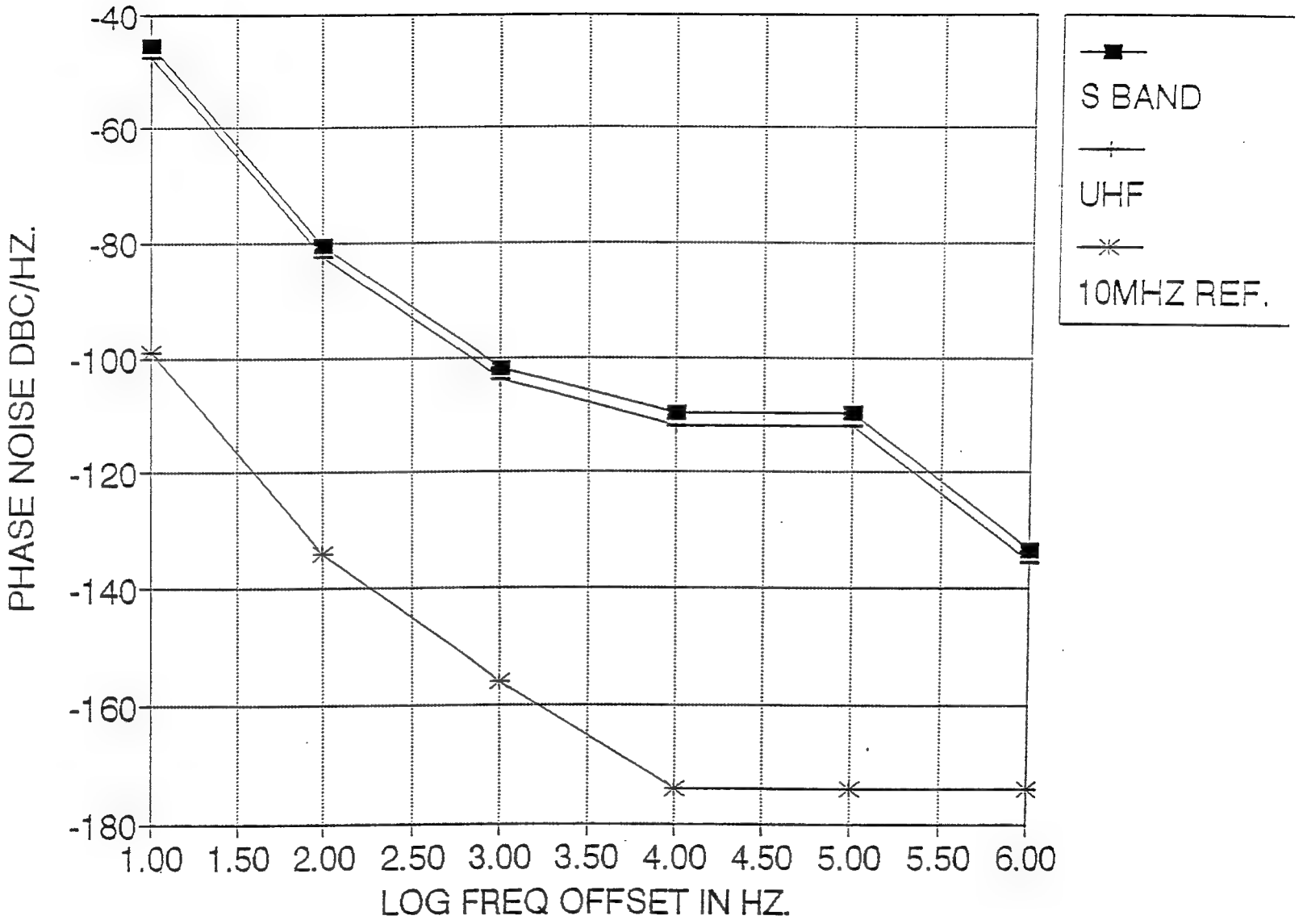

Figure 3-15. SSB Phase Noise

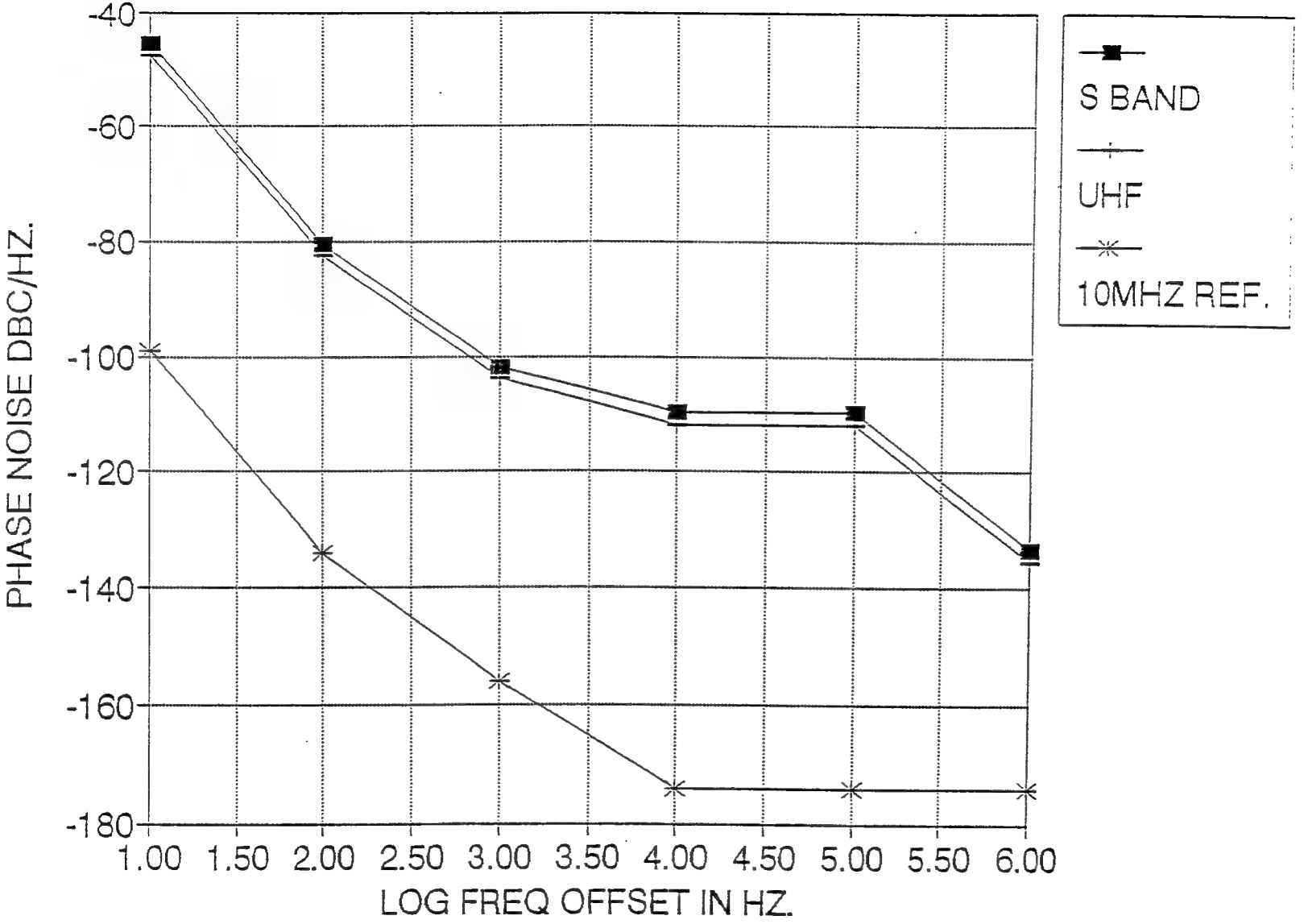

Figure 3-15. SSB Phase Noise

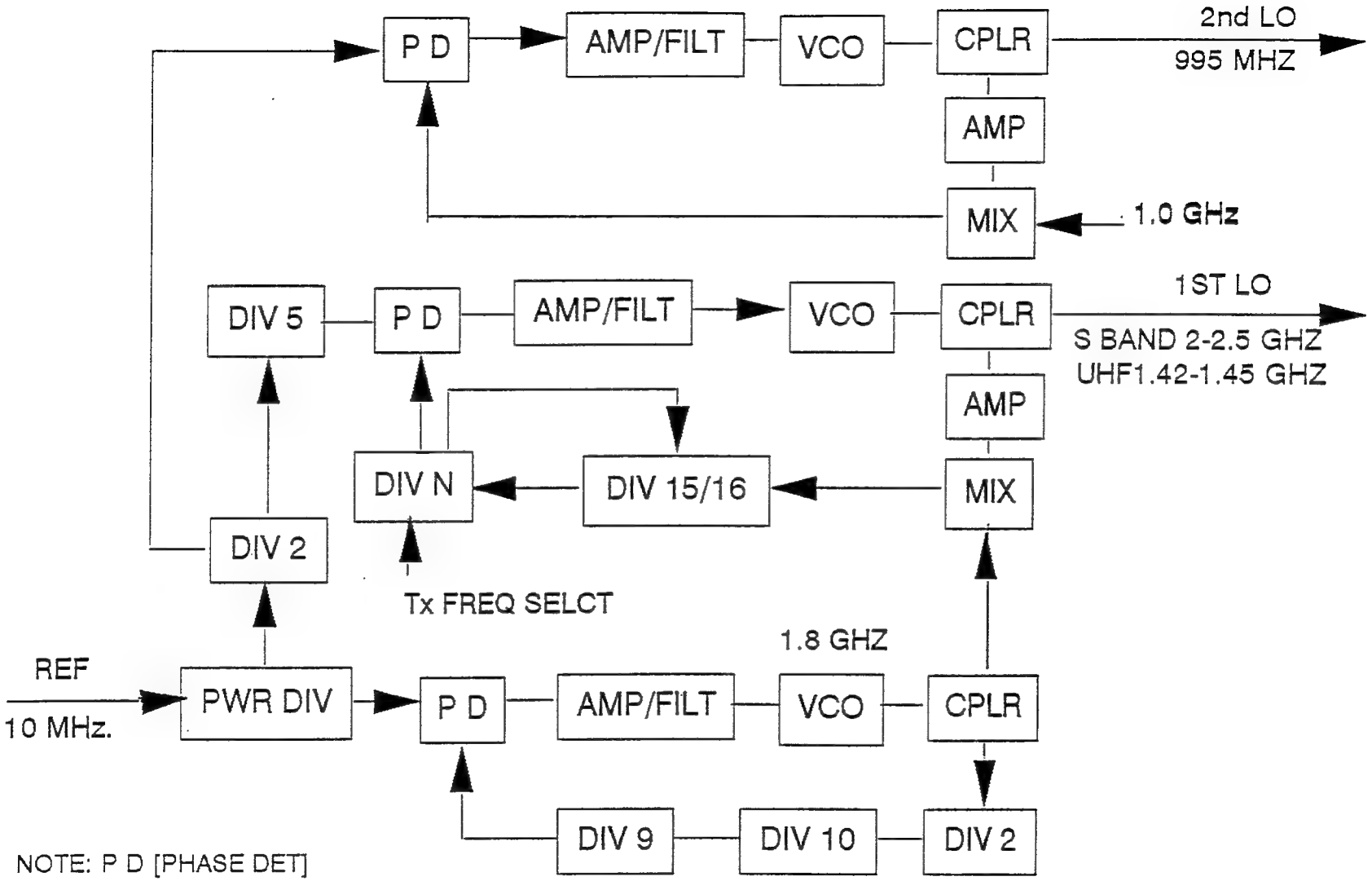

Figure 3-17. LO Synthesizer

The 1.0 MHz reference for the first LO synthesizer phase detector is obtained by dividing the 5 MHz signal by 5. The first LO VCO output is down converted, using a 1.8 GHz signal, to a maximum frequency of 700 MHz to get within the operating range of the digital dividers. The LO ouput frequency is set by changing the variable divider with the transmit frequency select command. A "UHF/S" command is also sent to the VCO which limits its frequency range to the desired band. The 1.8 GHz signal required for down conversion is also generated by a PPL in a similar manner as shown in Figure 3-17.

A block diagram of the modulator and transmit drive section of the exciter is given in Figure 3-18. Digital synthesis of the transmit waveforms allows flexibility. The digital waveforms are converted to analog signals that are used to modulate the 1.0 GHz signal that, in turn, is mixed with the first LO signal. A switch selects the mixer sum frequency output for S-band transmit, and the mixer difference frequency output for UHF transmit. These signals are gated and limited to maintain a constant amplitude. The gating is used to keep all spurious signals out of the transmit amplifier chain except during the transmit interval. An additional PLL is used to generate the 1.0 GHz modulator source.

3.1.10 LO Distribution

The Local Oscillator (LO) signals generated in the exciter are distributed to the 18 receivers as shown in Figure 3-19. The first and second LO's require the same power levels, and the same configuration is used by both. The amplification provided by the 18 receiver amplifiers could have been provided at the input to the power divider but it is desirable to maintain signals at lower levels to reduce the leakage of spurious signals into the receiver.

3.1.11 Preprocessor

The preprocessor is composed of the demodulator and sidelobe canceller. The demodulator is used to glean the complex (I/Q) modulation from the sampled waveform. The sidelobe canceller assumes a straight forward implementation of the Sample Matrix Inversion algorithm.

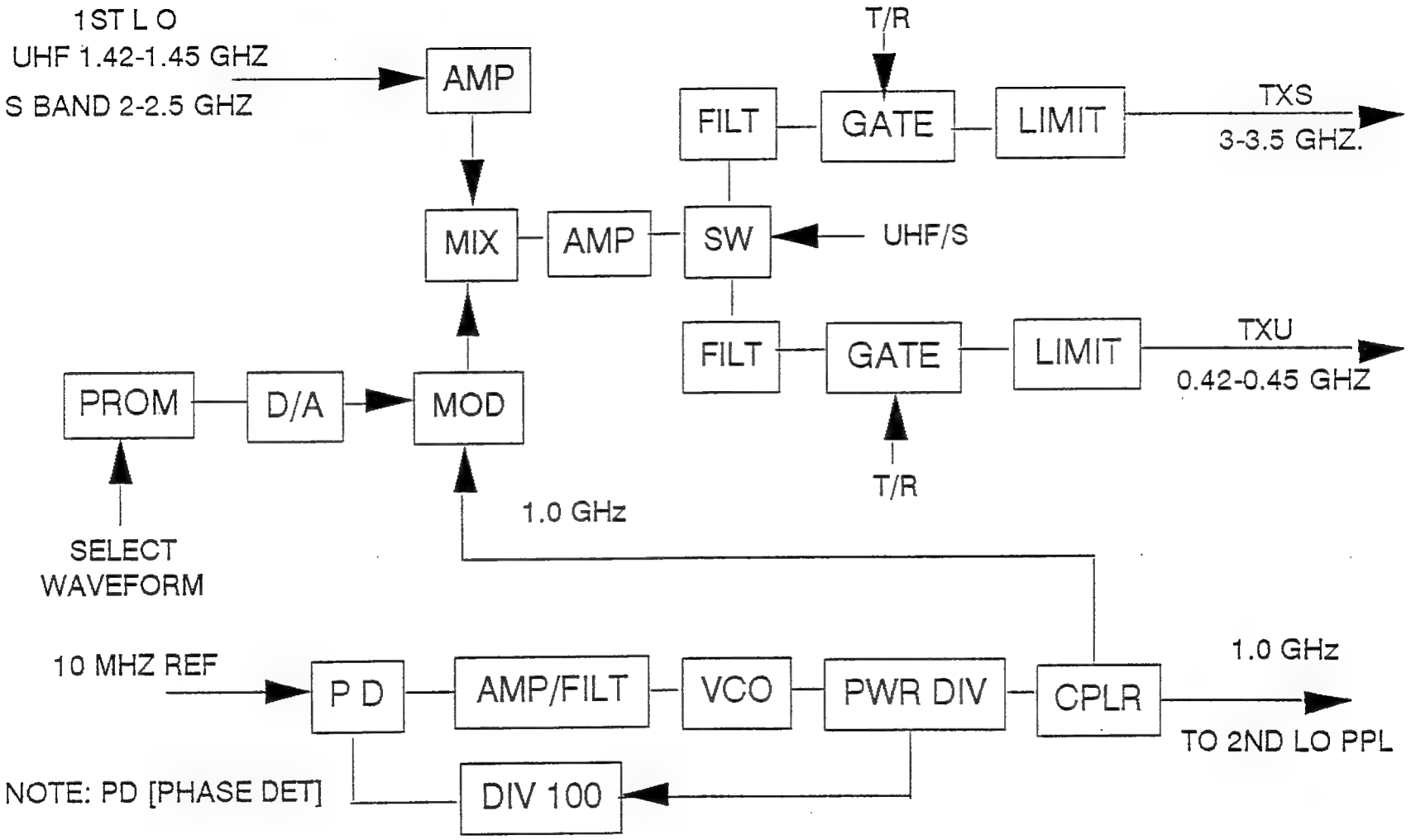

Figure 3-18. Modulator/Transmit Drive

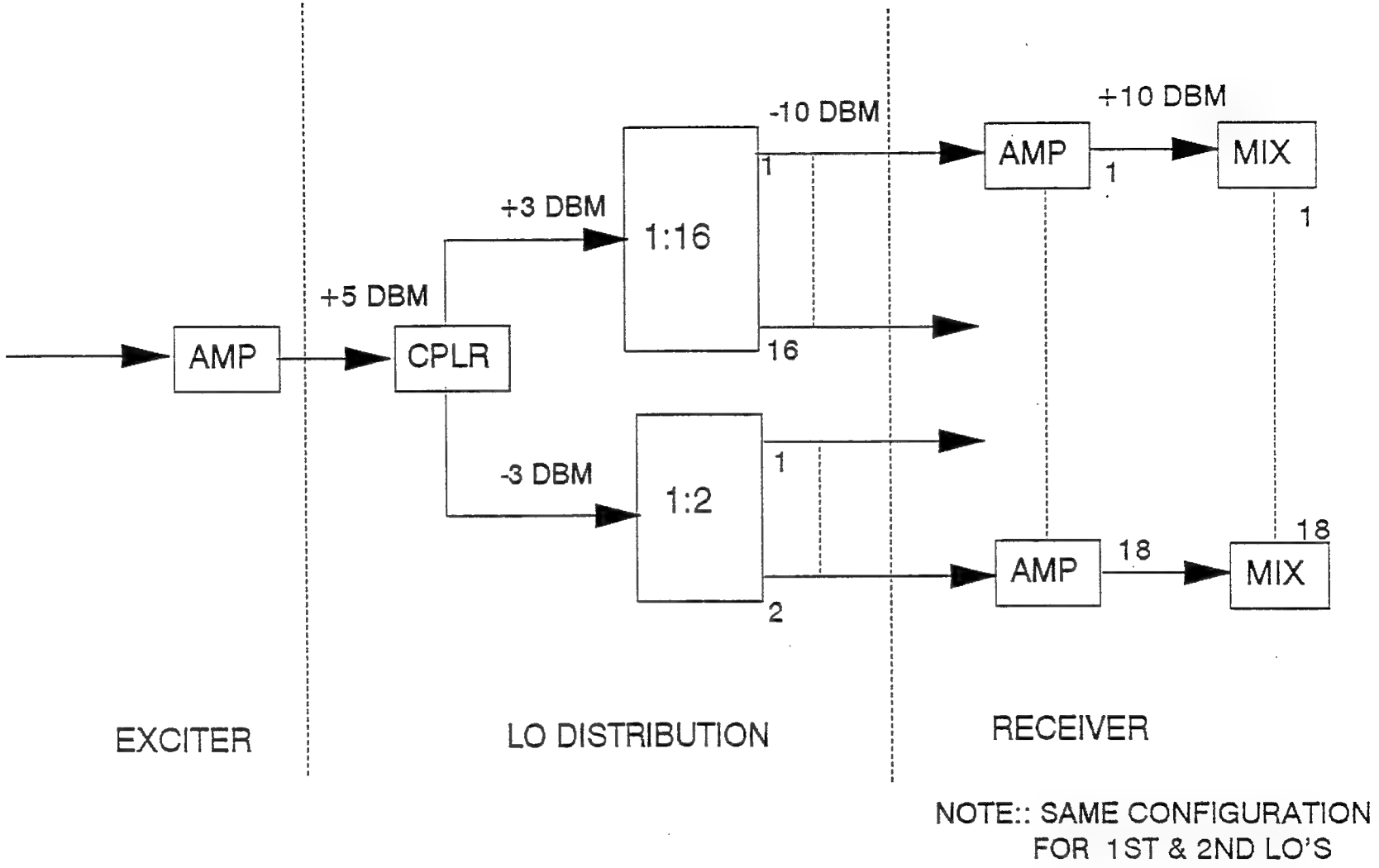

Figure 3-19. LO Distribution

3.1.1.2 Isolation

Receiver saturation occurs at about -20 dBm. The 60 dBm S-band RF drive then would imply the need for 80 dB of isolation between the transmit and sum receive beam ports because the corresponding azimuth combining manifolds are shared (as well as the elevation combining manifolds).

A 20 dB isolation low loss coaxial circulator separating the transmit and sum receive ports and a 60 dB isolation switch at the input to the receiver would satisfy this requirement if the switch can accommodate 10 W at microsecond rates. The switch requirements at the input to the difference beam receiver is less demanding because of at least 13 dB of total loss in the azimuth transmit manifold and azimuth difference beam manifold. A 47 dB isolation switch with less than .5 W power handling would be adequate. The Level 4 combiners (Section 3.1.2.1) contain directional couplers with about 20 dB of isolation between the receive difference port and transmit port.

A 60 dB isolation, 10 kW switch has been identified (Section 3.1.8). If the switch requirements should prove to be substantially more demanding, however, it is recommended that a separate azimuth combining manifold be used for transmit, with less than three percent increase in manifold weight and volume. The additional manifold would allow different aperture weighting, in azimuth, between sum receive and transmit. A less severe amplitude taper on transmit, however, would imply up to 3 dB more drive power to optimally excite the T/R modules. This, in turn, would further stress the isolation circuitry.

The S-band isolation implementation is shown in Figure 3-20. The UHF Band system isolation requirements mirror those for S-band. The RF drive power is 6 dB less, however.

It is important to note that these designs avoid the need for distributed amplification in the manifolds thus considerably simplifying the overall implementation (Section 3.1.6). The azimuth weighting is achieved by unequal divide combiners. Only the receive difference beam azimuth combining manifold contains amplitude and phase control elements for channel matching (transmit and receive sum beam channel matching is achieved via the T/R modules) and this can be implemented by light weight, small variable resistors and digital phase shifters.

The coaxial circulators are sized to fit within .1 cu ft and to weigh under .5 lb. Isolation (20 dB) and power handling (1 kW peak, 150 W average) are not expected to be a problem.

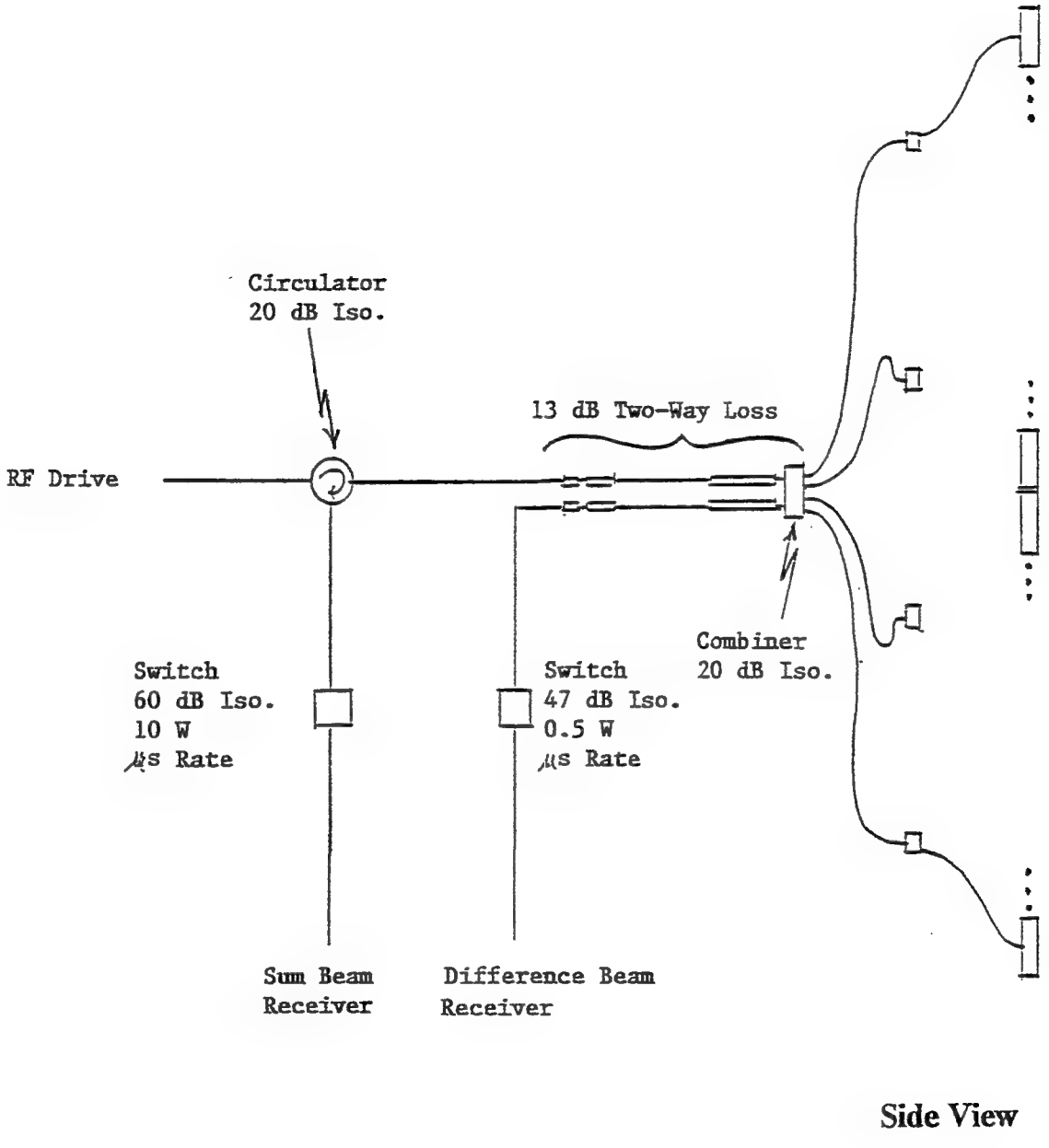

Figure 3-20. S-Band Isolation Implementation

3.2 Digital Beamformer

3.2.1 Introduction and Design Process

As with the conventional beamformer, the digital beamformer design began with the radar concept and a baseline design described below.

The digital beamformer for the dual frequency radar follows closely the block diagram introduced in Figure 2.2-2 and shown in Figure 3.2-1.

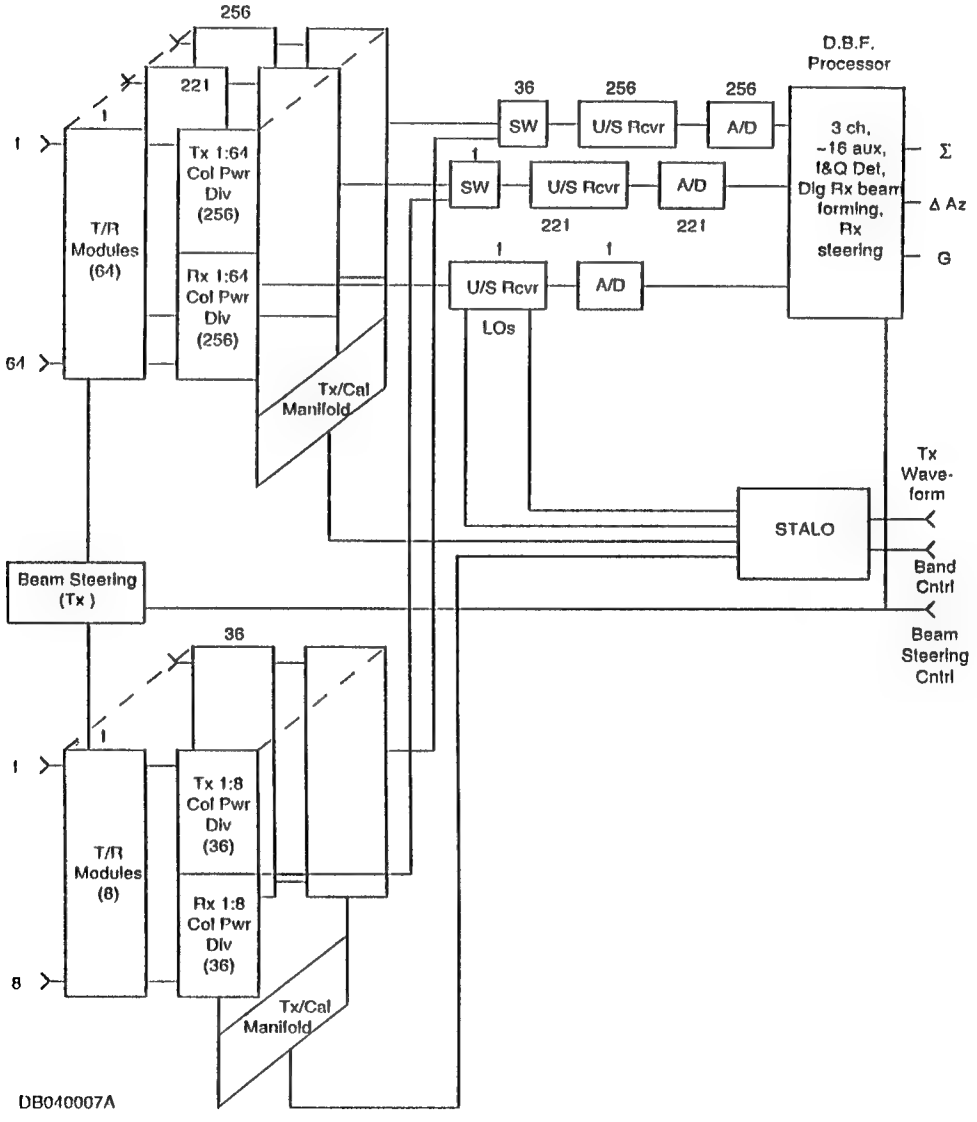

Figure 3.2-1 Digital Beamformer

Each of the radiating elements is fed to/from a separate T/R module. A hybrid design results for the S-band part of the array as these modules in turn are combined in column manifolds to reduce the huge number of degrees of freedom (64 x 256 = 16384) to a manageable level of 256. The UHF array is also reduced from 288 (8 x 36) elements to 36 column ports.

The transmit path is fed through separate azimuth manifolds, one each for S-band and UHF. The RF drive originates at the STALO (or exciter, as the STALO is sometimes called), modulated by the radar synchronizer.

The receive path follows from the column manifolds and the transmit/receive switches. Band-select/Sensitivity-time-control (STC) units select the band of operation and in the UHF band provide STC attenuation. This design is common with the conventional beamformer of Section 3.1. Judicious design has allowed the same IFs to be shared between the two bands.

The receiver outputs from the A/D converters feed the preprocessing sections of the adaptive beamforming, adaptive nulling processor. One of the first functions is digital I/Q formation which halves the number of A/D converters over analog I/Q architectures, while reducing the I/Q images to insignificance. Next, channel to channel equalization is performed to balance the frequency dependent variances from channel to channel. These variances should be minimized to maximize the degrees of freedom in the adaptive beamformer. (Non-equalized channels take away degrees of freedom best used to form adaptive nulls and low sidelobe beams.) This is followed by signal processing that first calculates, then applies adaptive weights to the multiple beams. In this manner, the beams are digitally formed with the desired taper weighting, desired sidelobe levels, and the desired jammer nulling. Three standard beams: Sum, delta azimuth, and guard are output to the radar processor.

There were several assumptions and/or ground rules followed in arriving at the digital beamformer design.

- Keeping the hardware per channel to a minimum - there are 256 channels required.
- Meeting all performance requirements, including the extremely low phase noise and discrete spurious in the exciter and high dynamic range in the receive chain (low IMD and HD)
- Using as much common hardware between S-band an UHF as possible (consistent with minimization of hardware per channel).
- Reducing the digital beamformer processor to a realizable throughput machine - keep the number of beams to be formed low (3 main and 16 aux beams is reasonable)

- Presenting a common interface to the other elements of the radar for comparison purposes.

3.2.2 Digital Beamformer Design

The main features of the design shown in Figure 3.2-1 are listed below.

The S-band calculations used C/N values of 61.8 dB for the formed beam architecture and 40.7 dB for the column architecture. The corresponding UHF values are 61.8 dB and 56.1 dB respectively. The UHF C/N values reflect the effect of STC (see Table 2.2-2).

1. The S-band and UHF corporate feed networks interface the antennas and T/R modules to the receivers and exciter - these must be unique manifolds.
   - Column manifolding reduces the large number of individual elements to a more manageable number and is still system worthy with full azimuth adaptability - 256 columns for S-band, 36 for UHF.
   - A single transmit feed port on a transmit manifold provides drive to the transmit modules.
   - A separate calibration feed port allows calibration of the receive chain elements.
2. Thirty-six band select assemblies bring together the S-band and UHF columns to shared receive channels - the remaining S-band channels are unique and do not need band select.
   - Sensitivity time control is used for the UHF only to help reduce the overall UHF dynamic range.
3. The IF receivers are of one common design, being used for both bands (but never simultaneously)
4. The A/D converters sample the final IF (offset baseband) of 5 MHz with 13 bits at 20 MHz sample rate
   - The real sample technique cuts the number of A/D's in half.
5. The DBF processor combines the 256 (36 for UHF) column information into 3 main and 16 aux beams for adaptive sidelobe cancellation and outputs Sum, Delta azimuth, an Guard beams.
6. The exciter takes a stable reference signal and control information and generates all required local oscillator signals, transmit drive, calibration, and clocks required by the receiver and antenna electronics
   - Suitable transmit waveforms are digitally generated and modulate the transmit carrier.
   - Multiple transmit frequencies are provided by a programmable frequency generator.

The design of the digital beamformer logically begins with the S-band corporate feed manifold (Figure 3.2-2). We have elected to share the elevation column manifold between

transmit and receive to minimize manifolding. The transmit manifolds are all analog at this time due to power and control considerations. The azimuth feed is divided 1:256, while common column feeds are divided 1:64. Manifolding is made largely with air dielectric stripline at S-band and UHF as well. Independent traveling wave lines for calibration of transmit and receive weighting are used to best balance and distribute the critical calibration signal to all modules equally. The UHF corporate feed manifold (Figure 3.2-3) also shares an elevation column manifold between transmit and receive to minimize manifolding. Here the transmit azimuth feed is divided 1:36, with a common column feed division of 1:8.

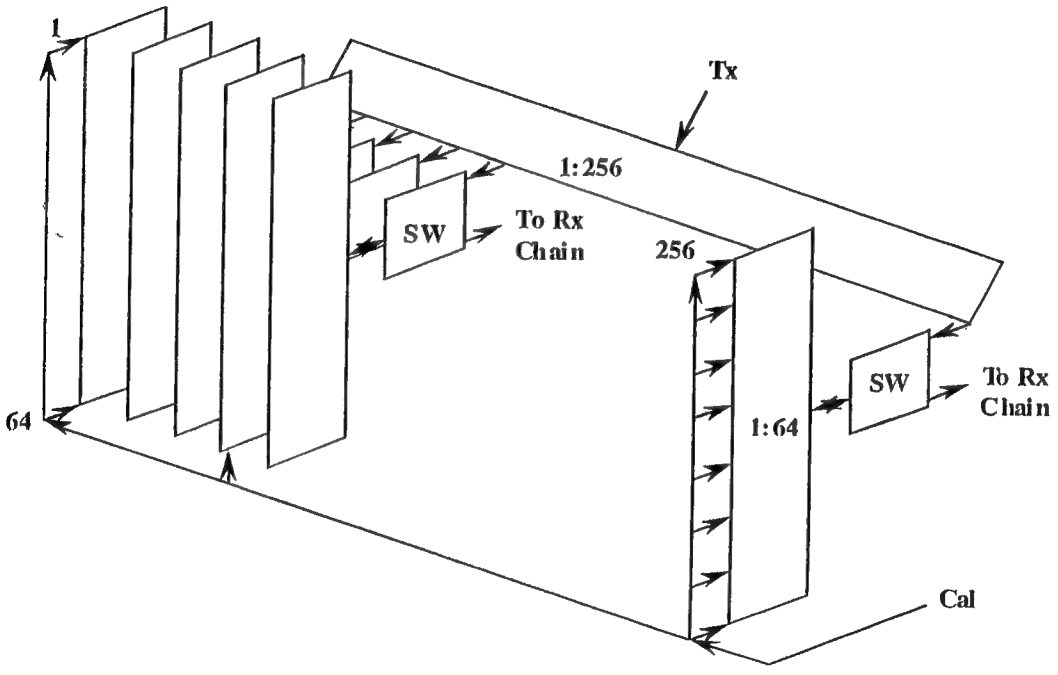

Figure 3.2-2 S-Band Corporate Feed Manifold

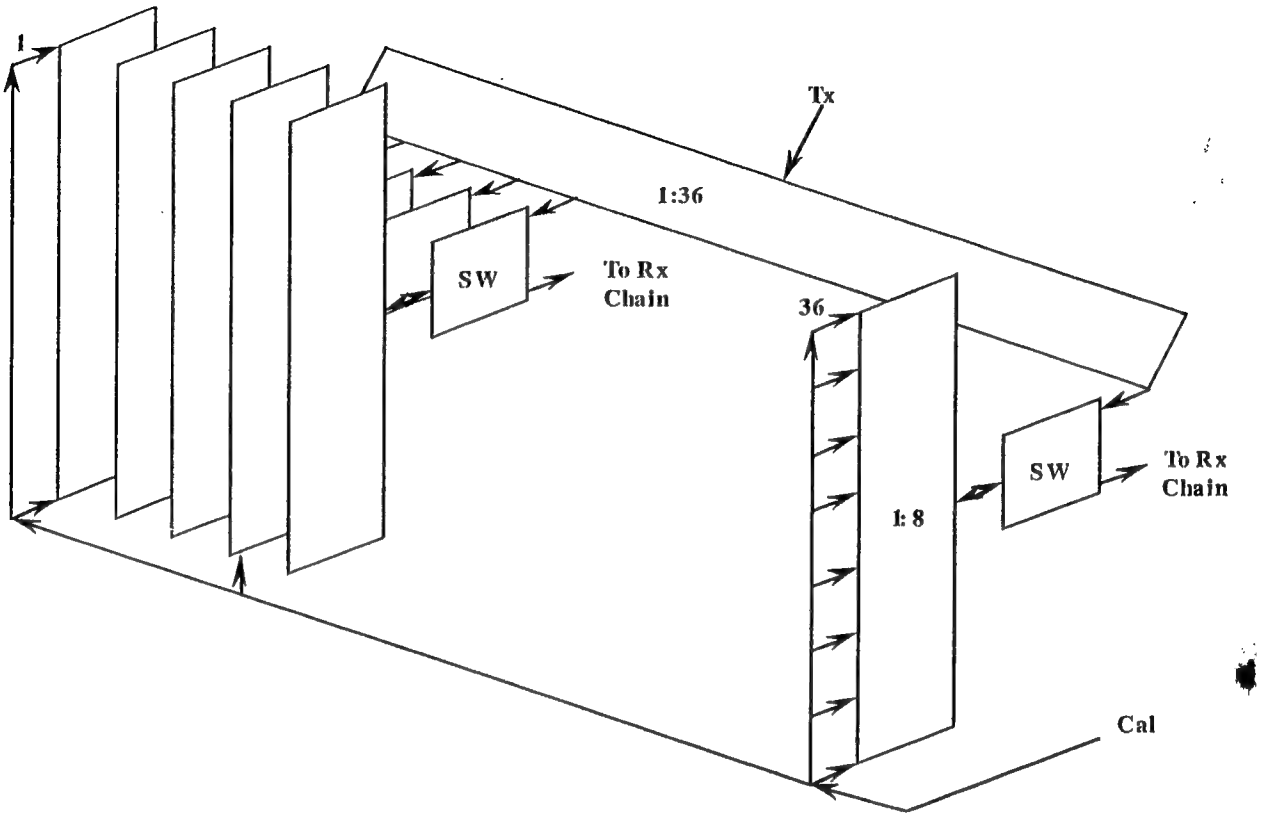

Figure 3.2-3 UHF Corporate Feed Manifold

The Band Select/STC (Figure 3.2-4) design is the same as the conventional beamformer described in Section 3.1. An STC section is included in the UHF path to reduce dynamic range requirements of that path. A common RF output is sent to the IF receiver. The IF Receiver (Figure 3.2-5) is comprised of one assembly with both first and second down converters and all associated filters and amplifiers. No bandwidth switch is used - only the 5 MHz bandwidth is processed through the A/D to reduce hardware. Instead, digital bandwidth reduction takes place in the DBF. IF filters will be lumped element and low order to allow easier matching between channels in the digital equalization process in the DBF. The digital beamforming preprocessor (Figure 3.2-6) first forms I & Q data from the real A/D samples, then equalizes all active channels - balances gain and phase to a reference channel so all channels look alike. The

equalization coefficient calculation is separate from equalization application (the former can be done in non-real-time). Block memory saves the data while adaptive beamforming weight computation is performed. Weight application and beam forming is done on the saved data (and on new data if appropriate) in real time to output Sum, Delta Azimuth, and Guard beams to the signal processor. The number of digital beams is purposely kept low to reduce the processing hardware and processing load.

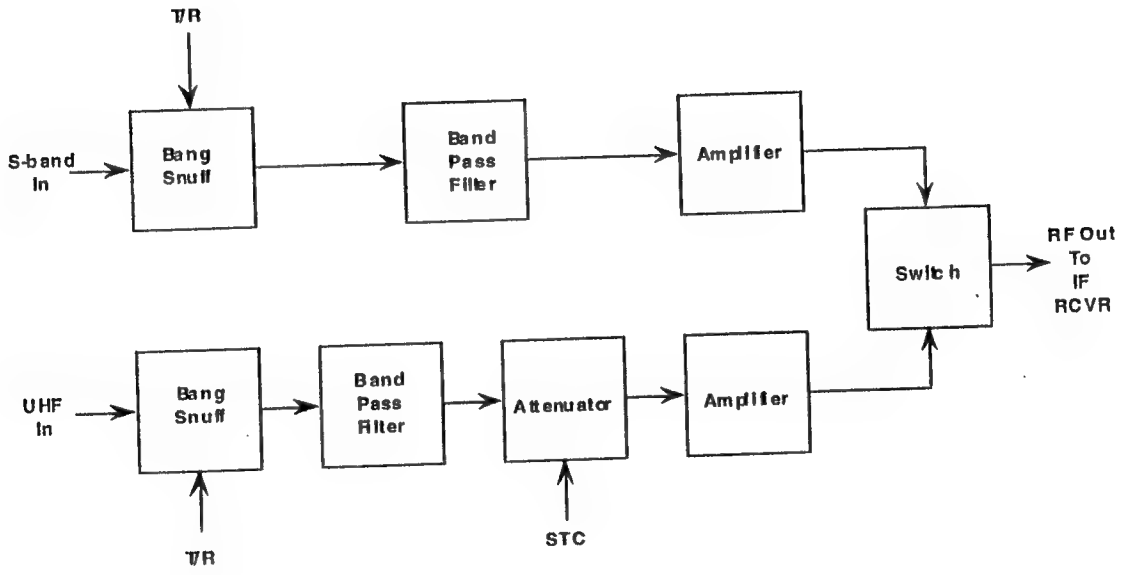

Figure 3.2-4 Band Select / STC

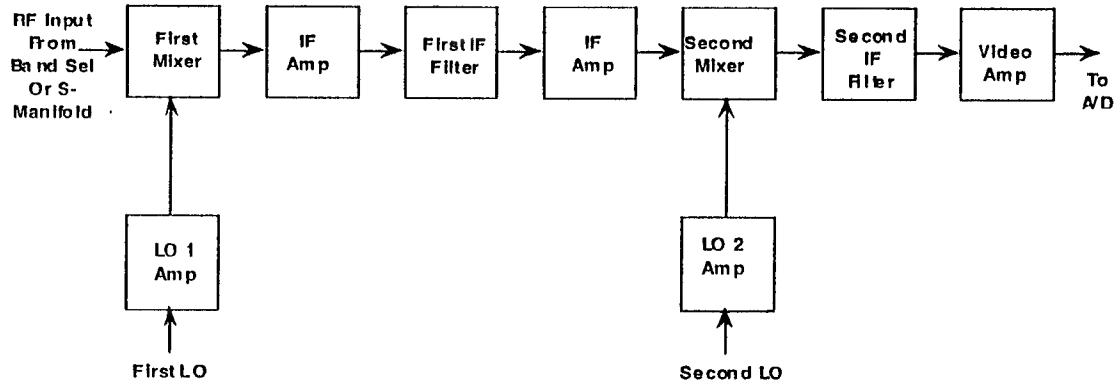

Figure 3.2-5 IF Receiver

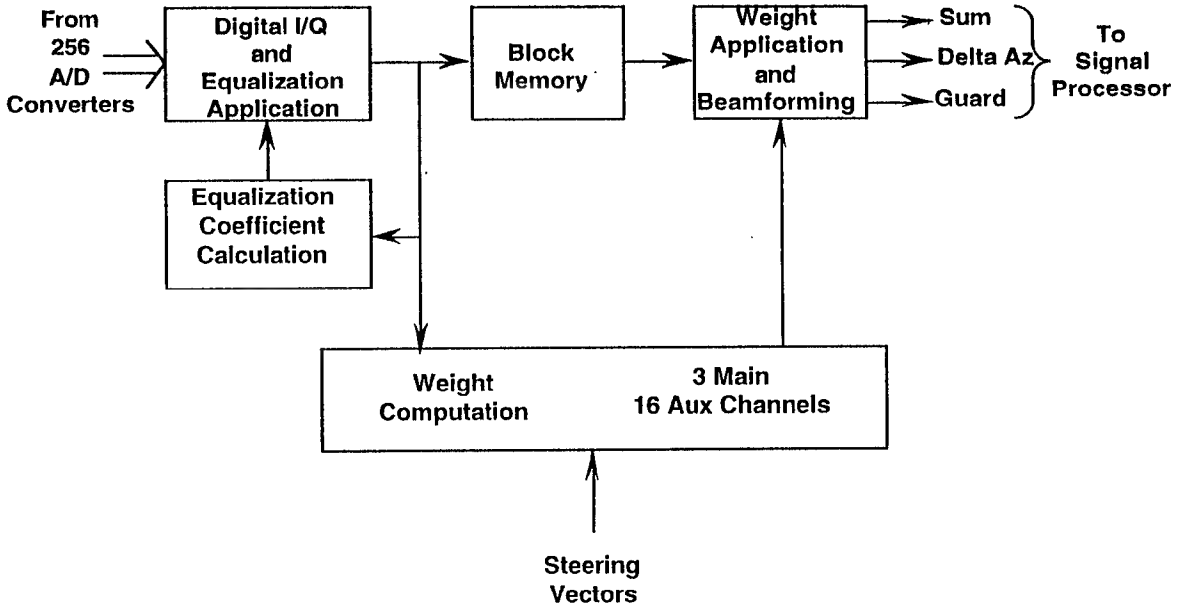

Figure 3.2-6 Digital Beamforming Preprocessor

3.2.3 Receive Channel Model

The receive channel model (Figures 3.2-7 and 3.2-8) is an analysis tool used to balance the overall receive design using individual stage inputs and overall system goals. The model of Figure 3.2-7 shows each stage as functionally combined in the receive chain. Figure 3.2-8 shows a printout of the spreadsheet calculations. Each stage is considered as a block for preliminary design. Given each stage gain, noise figure, and output intercept point, a spreadsheet analysis is performed, verifying the balance of design parameters to the overall system goals. This is only an initial design; further refinements must be made for the final detailed design. This is a good starting point for suballocating design requirements early in the design process - early detection of gross design imbalance is important. Fallout from this analysis is detection of stage contributions of intermods and maximum signal levels on a stage by stage basis. Noise figure buildup usually points out the slight jump in the noise figure caused by the A/D, which is often overlooked by system engineers.

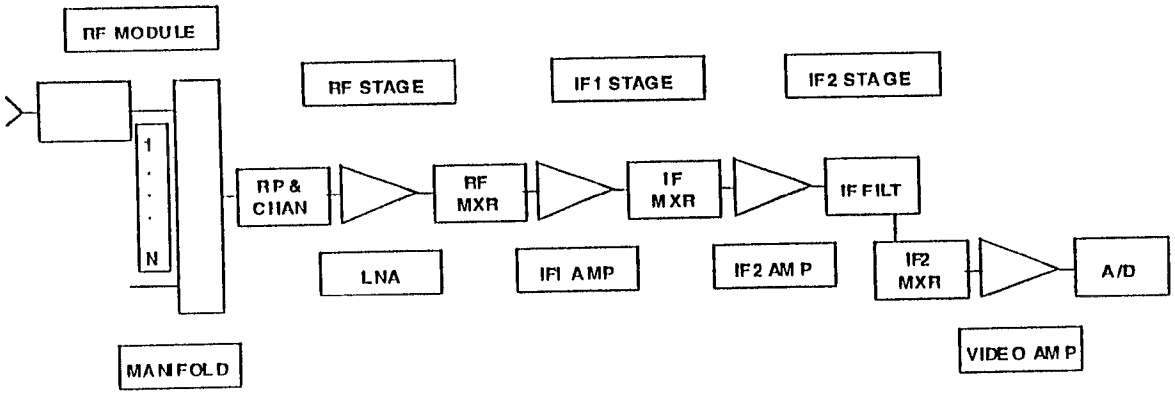

Figure 3.2-7 Receive Channel Model

28 -June-93 9:08 AM	Stage Gain	Stage NF	Stage OTOI	Cum Gain (nol)	CUM NF	REV CUM NF	REV CUM Ngain	REV CUM Noise	CUM Gain (coh)	Equiv OTOI	Equiv IOTOI	Max Sig TT dBm	Stage MP dBc	Cum IMP dBc	Signal dBm
rf module	20	3	20	20.0	3.0	3.6	47.0	1.38	20.0	20.0	0.0	-61.0	-162.0	-162.0	-55.0
manifold (noncoherent	-2	2		18.0	3.0	14.5	27.0	0.49							
manifold (coherent	36		80						56.0	54.5	-1.5	-25.0	-170.0	-159.1	-19.0
rp+Chan+ lna+sw	10	6	25	28.0	3.1	12.5	29.0	0.49	66.0	25.0	-41.0	-15.0	-80.0	-80.0	-9.0
mixer1+ ifamp1+filt	4	10	30	32.0	3.1	21.4	19.0	0.43	70.0	26.5	43.5	-11.0	-82.0	-74.9	-5.0
ifamp2+ mixer2+flit	3	5	32	35.0	3.1	25.1	15.0	0.41	73.0	27.5	45.5	-8.0	-80.0	-71.1	-2.0
video amp	12	10	50	47.0	3.2	28.1	12.0	0.41	85.0	39.2	45.8	4.0	-92.0	-70.3	10.0
ADC	0	40	50	47.0	3.6	40.0	0.0	0.40	85.0	38.8	46.2	4.0	-92.0	-69.6	10.0

1.4 QRMS set level
0.4 QRMS Internal
10 dBnFS
13 Bits
5 MHz Noise BW
40 NF dB
47.1 dB Noise Gain Reqd

-59.26 sBm (1 qrms)
6.9897 dB (Noise BW)

66.9 dB Dynamic Range (Noise BW)

Figure 3.2-8 Receive Channel Calculations

3.2.4 Digital Beamformer Conclusions

A digital beamformer for a dual frequency radar has been designed at the functional level. To keep the number of receiver channels to a reasonable number, only azimuth has full degrees of freedom, i.e. one channel per column. Each column has been combined in elevation by an analog manifold. Transmit manifolding is analog in both azimuth and elevation; there is no digital beamforming on transmit. Even with the limitations accepted for azimuth-only digital beamforming, there are 256 channels required. Hardware per channel was kept to a minimum and hardware was shared between S-band and UHF wherever possible. The number of output beams to be formed was kept low to be reasonable to build and to be comparable with the other types of beamformers so tradeoff comparisons among the three types of beamformers could be made.

Unique analog RF manifolds were required because of the spread between the two bands of operation; a single wideband design is not practical. Calibration is input through separate RF ports. STC is used only for the UHF band. The IF receivers are of a single common design, sharing local oscillators and the same hardware channels. A/D converters use offset baseband

architecture to keep the numbers to one half of conventional analog I/Q systems. Digital I/Q, equalization, and adaptive beamforming are all done in a digital preprocessor. A STALO (or exciter) is a common design with the Conventional Beamformer. A preliminary receiver analysis has been done to initially verify the balance of design parameters and insure that individual receive subsystems have reasonably suballocated specifications. The resulting digital beamformer physical characteristics are given in Figure 3.2-9.

		Each			Total		
Assembly	Qty	Size (cu.in.)	Weight (lbs)	Power (W)	Size cu.in.	Weight (lbs)	Power (W)
IF Receiver (Assy)*	256	2x6x.5=6	.5	15x.6=9	1536	128	2304
A/D Converty (assy)* 13 bit/20 Mhz	256	2x6x.5=6	.5	10	1536	128	2560
LO Distribution* (Assy)	16	16x16x3.9=1,000	10	15x.4=6	16000	160	96
DBF Preprocessor (Bds)	104	10x8x.75=60	3	5x6A=30	6240	312	3120
Exciter (Subassy)	6	14x20x2=560	10	15x2=30	3360	60	180
* For these assemblies, the size, weight and power estimates derived for the conventional design were used in the comparison spreadsheets.							

Figure 3.2-9 Digital Beamformer Physical Characteristics

3.3 Optical Beamformer

3.3.1. Introduction To Optical (Photonic) Manifolds

Fiber optic (FO) technology is an excellent candidate for lightweight and small volume RF manifolds for array antennas. This is because fiber is physically small, lightweight and flexible. For example, the mass of buffered fiber is about 0.07 gr/m and that of space-qualified fiber is about 0.8 gr/m (these figures of mass should be compared with the mass of a typical microwave coaxial cable which is about 40 gr/m). In addition, the fiber offers several other unique advantages including: (1) extremely low loss and dispersion (attenuation of <0.6 dB/Km @ 1300 nm and bandwidth-distance product of 100 GHz-Km), (2) excellent transmission stability by virtue of the small ratio of RF signal bandwidth to optical carrier frequency, (3) it is a non conductive dielectric and so does not disturb the RF field, is secure and is immune from EMI and RF crosstalk, (4) it allows the utilization of optical wavelength division multiplexing to minimize the number of lines in the phased array antenna (PAA) feed link, and (5) the phase variation with temperature for microwave signals on an optical carrier in the fiber is almost an order of magnitude lower than the corresponding phase variation of a coaxial line.

The overall structure of a typical FO manifold is shown schematically in Figure 3.3-1. This manifold consists of two independent FO manifolds, one for the transmit (Tx) and one for the receive (Rx) modes. Each T/R module (or subarray) requires a laser diode (LD), a detector (DET), and a 1x2 bi-directional electronic switch (1x2 SW). In the Tx mode, the RF signal to be transmitted modulates the intensity of a LD (or the output of a CW laser with an external optical modulator). The LD output is fed into a FO 1:N divider that splits the optical signal into N channels and directs the light from each channel into a separate fiber. These N fibers carry the optically encoded RF signal to each of the N antenna elements. The DET before the T/R module converts the optical modulation back into an electronic signal which is then directed to the T/R module through the properly configured 1x2 SW. Next the RF signals are amplified and fed to the PAA radiators for transmission. In the Rx mode, the RF signal received by each PAA radiator is amplified (in the T/R module) and fed via the 1x2 SW to a LD and modulates its intensity. (Alternatively, the received RF signal modulates the intensity of a CW laser through an external integrated optical Mach-Zehnder modulator or MZ.) The resulting N optical signals from the N LDs are then carried to the receiver site through N separate fibers, where they are coherently added by a hybrid N:1 FO-electronic combiner. This hybrid combiner may perform part of the coherent additions in the optical domain and part in the electronic domain.

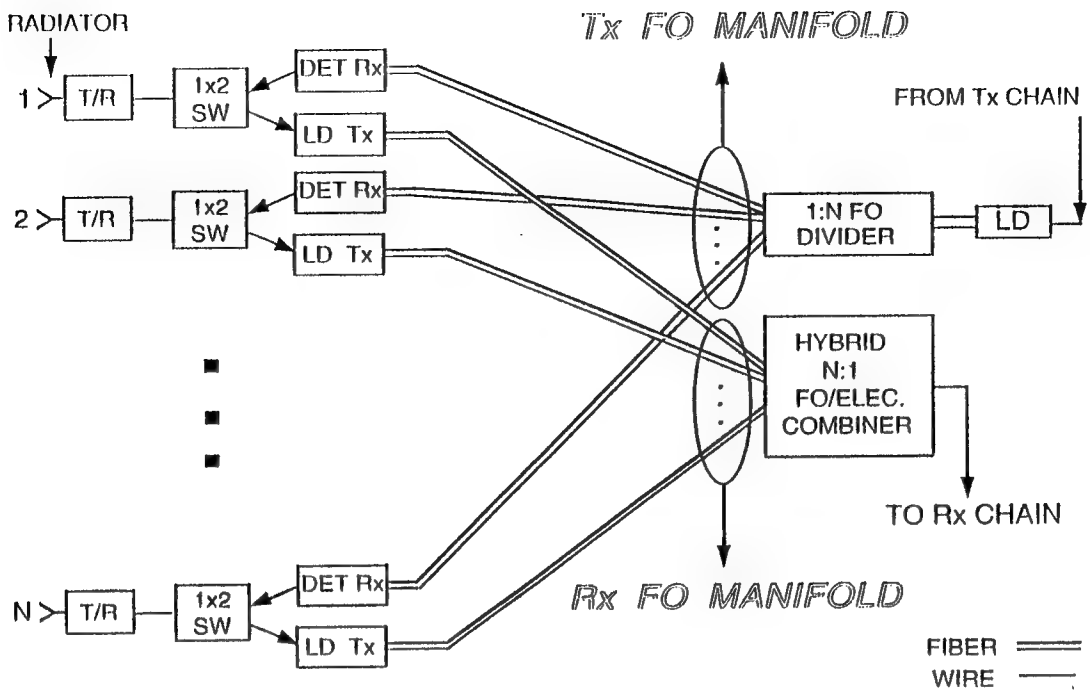

Figure 3.3-1 Schematic of a Generalized Fiberoptic Manifold

There are two main reasons for using two separate FO manifolds for Tx and Rx:

(1) Since each T/R module must be able to both transmit and receive RF signals, a LD and a DET, located in the T/R module, must be used for the Rx and Tx PAA modes respectively. Both devices are fiber pigtailed, and therefore if a single FO manifold was to be used, an optical 1x2 switch would be required per T/R module. The state-of the-art of 1x2 optical switches is not good enough for this application, i.e., fast (e.g., <10 μs switching time), low loss (<0.5 dB optical), small size (<1 cm^3), and low cost (a few 100s of $) optical switches simply do not exist. However, even if good optical switches were available, the added cost and increased system complexity and volume would not be offset by the elimination of a passive, lightweight FO network.

(2) A single FO manifold is not reversible; it can be optimized for either Rx or Tx, but unlike its electronic counterpart, not for both. This is because commercially available, single mode, N:1 FO combiners/dividers are "symmetric" devices and thus their combination loss is equal to their splitting loss. This is due to inherent mismatches in the mode field diameters (or alternatively to numerical aperture mismatches) between the input and output fibers. Therefore if a single N:1 FO combiner/divider is used in conjunction with a single FO manifold, excessive losses in the Rx mode would occur. Note that these losses may be severe since they increase as the square of the number of

combined channels because of the square-law relation between optical intensity and RF signal power (i.e., the dB-expressed loss in the optical domain doubles in the electronic domain). For example, a 32:1 single-mode FO combiner used for the Rx mode will exhibit minimum combination losses of 15 dB optical or 30 dB electrical. Losses of this magnitude are unacceptable for any PAA-based radar or communication system because they result in a high noise figure (NF); to overcome such losses a good NF amplifier with high gain is required before the FO link. This is not the case for electrical combiners where the combining loss is approximately equal to the excess loss, usually of the order of 2-4 dB. This problem forces the use of many small FO combiners followed by RF combiners, i.e., it results in hybrid FO-electronic combiners in the dedicated Rx FO manifold (see Figure 3.3-1).

3.3.2. UHF Photonic Transmit Manifolds

3.3.2.1 Discussion

Several UHF 8x36 photonic Tx manifold configurations were studied in order to identify the best, most efficient configuration. From these studies the following conclusions emerged:

(1) The photonic manifold must deliver 20.5 dBm of average RF power and 28.5 dBm of peak RF power. A straightforward approach would require the use of a single very powerful optical source (several tens of optical watts), so that in conjunction with a 8x36 manifold, enough gain would be available to recover the ~ 26 dB of insertion loss due to 24.6 dB of optical splitting loss (SL) and 1.4 dB of excess loss (EL). Note that the use of an optical amplifier does not help because most optical amplifiers deliver relatively small amounts of optical power, e.g., +10 to +15 dBm or 10 to 32 mW, (to be compared with readily available LDs at 830 nm with up to several watts of optical power).

For a directly modulated LD the RF signal obtained at the output of a FO link is given by[1]:

$$P_S = 0.5\, R_D\, (g\, r_D\, m\, P_O)^2, \qquad (3.3.1)$$

where: R_D is the DET termination resistor, g is the optical loss due to coupling etc., r_D is the detector responsivity in A/W and P_O is the optical bias power, typically 1/2 of the max LD power. For our application we will use m=0.4 for "average power " transmission and m=1.0 for "peak power" transmission. This is because from Equation 3.3.1 we see that the ratio $1^2/0.4^2$ is about 8 dB which is the difference between the required average and peak power output levels of the manifold. Thus by

assigning m=1.0 for peak power transmission and m=0.4 for average power transmission we ensure that we are in the linear modulation range of the LD for both cases (i.e., if we were to use m>.4 for average power transmission then we would saturate the LD for peak power transmission). The DET responsivity r_D depends on the operating optical wavelength, which for the UHF manifold, is 830 nm due to the availability of powerful LDs. For 830 nm a good r_D value is 0.5 A/W. The optical loss factor g depends on the splitting ratio, e.g., 1:8x36 or 1:288 or -24.6 dB, and the coupling efficiency is about 72% or -1.4 dB, for a total of -26 dB or $g=2.51\times10^{-3}$. Detectors that can operate at 20.5 dBm (112 mW) of average RF power have relatively large areas (~250 μm in diameter) and therefore large capacitance. For such detectors a typical R_D value of 50Ω would allow operation up to 450 MHz. Using this value and Equation 3.3.1 we find:

$$P_S = 25\,(2.51\times10^{-3} \times 0.5 \times 0.4 \times P_O)^2 = (0.00251 \times P_O)^2 \qquad (3.3.2)$$

or

$$P_O = P_S^{0.5} / 0.00251. \qquad (3.3.3)$$

Thus for an average signal power (P_S) of 20.5 dBm or 0.112 W the bias optical power P_O required is ~133 W and the peak optical power is ~266 W. LDs with such optical powers and the capability for direct modulation at UHF are not currently available, and furthermore, they are not expected to be available within the next 2 years (note that currently available LDs have peak optical power of about 5 W).

(2) The alternative would be to use several 5 W LDs, e.g., one LD per 18 elements for a total of 16 LDs (or g=0.72/18=0.04). Using the 5 W LDs biased at P_O=2.5 W we find that the average power of the output signal is:

$$P_S=25(0.04 \times 0.4 \times 0.5 \times 2.5)^2=10 \text{ mW or } 10 \text{ dBm}. \qquad (3.3.4)$$

The above shows that each output detector must drive a 20.5-10=10.5 dB gain amplifier (one per UHF element). However, the front end will now require an amplifier which must be able to drive the 16

LDs. It is worthwhile to calculate the average RF power required to drive one of the 16 LDs. This can be easily calculated from the gain of the directly modulated link, G_d, given by[2]:

$$G_d = (r_{LD} \times g \times r_D)^2 (R_D/R_L), \qquad (3.3.5)$$

where r_{LD} is the LD efficiency in W/A and R_L is the LD load resistor, typically 1 Ω for powerful LDs. Using the typical value of r_{LD}~0.8 W/A and g=0.04 we find that $G_d=(0.8x0.04x0.5)^2x50/1=0.0128$ or -18.9 dB. Therefore the average input RF power of the LD must be 18.9+10=28.9 dBm. To calculate the power required to drive the 16 LDs we must add to the 28.9 dBm value about 13 dBm required to cover the 13 dB of loss (12 dB SL and 1 dB of EL) due to the necessary 1:16 splitter (each of its 16 ports drives one of the LDs), for a total of 41.9 dBm. This means that since the input to the manifold is 0 dBm, a 41.9 dB gain amplifier capable of providing +41.9 dBm of average power and +49.9 dBm of peak power must be used to drive the 16 LDs. Such an amplifier however is undesirable for obvious reasons of power, volume, and weight.

(3) A more efficient Tx manifold is obtained if we use a single, medium power LD and take advantage of the fact that the output DET is a true current source. This means that a transimpedance amplifier (TAMP) can be used after the DET to provide very efficient gain to recover the majority of the loss. This is the most efficient solution and is discussed in detail in the following section.

3.3.2.2 Recommended UHF Photonic Tx Manifold

Figure 3.3-2 shows a schematic of the recommended manifold along with details of the gain and power requirements at various stages. A single moderate power (500 mW peak or P_O=250 mW bias power) LD is used (e.g., model SDL-2350 of Spectra Diode Labs) with its output coupled in a 1:8 FO divider with 100/125 μm input fiber and 50/125 μm output fiber. Each of the output 8 fibers drives a 1:36 FO divider. Each of the 288 resulting fibers are terminated in a DET followed by a TAMP and a voltage AMP. As Figure 3.3-2 shows, the single input amplifier has very moderate gain and peak power requirements. Next we will work backwards from the TAMP to the front and we will calculate the various gain and power figures shown in Figure 3.3-2.

A TAMP is a high-gain high-impedance amplifier with feedback provided to the amplifier input through a feedback resistor, and this yields both low noise and large dynamic range. TAMPs are

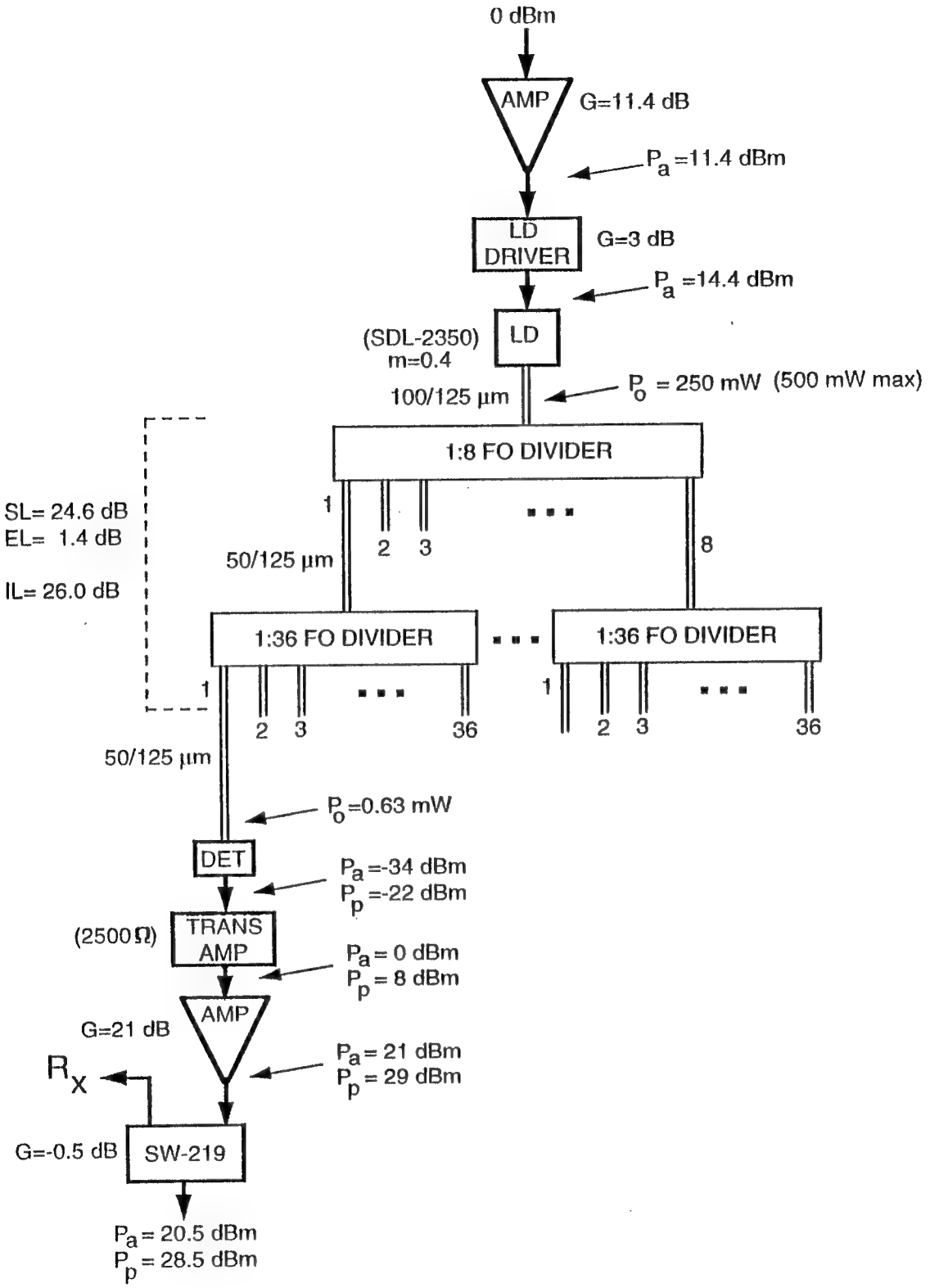

Figure 3.3-2 Schematic of the Recommended UHF Tx Manifold

available from several manufacturers and operate at frequencies in excess of 4.5 GHz with transimpedances in the range of 250-4000Ω thereby providing gain (relative to 50Ω) of 20log(200/50)=12 dB to 20log(4000/50)=38 dB. Westinghouse has had "good" experience with TAMPs, e.g., up to 36 dB of gain has been achieved with +4 dBm average powers at 500 MHz using commercially available devices. Figure 3.3-3 shows a photograph of a receiver board that uses a PIN DET and a 20 dB TAMP chip which weighs about 1 gr.

To design the Tx manifold, we first estimate the 1 dB-compression output power (P_1) from the TAMP. This varies from device to device, and is typically in the +4 dBm to +8 dBm range. For example, the AVANTEK ITA-12300900 MHz device has a typical P_1 value of +5.5 dBm with a 37 dB gain (relative to 50 Ω), the ATT HG1210AXA 3.5 GHz device has a P_1 value of +7 to +8 dBm and a gain of 29.5 dB, and the ANADIGICS ATA30011 2.5 GHz 1500Ω , P_1=+8 dBm device. Assigning P_1 to the peak power (P_p) we find that the average power (P_a) at the output of the TAMP is P_1-8 dB or 0 dBm for a TAMP with P_1=8 dBm. This means that the TAMP must be followed (see figure 3.3-2) by a conventional voltage AMP with gain of 21 dB which can provide the required +21 dBm of P_a or +29 dBm of P_p. When the loss (0.5 dB) of the SW-219 switch used to switch the Rx and Tx photonic manifolds is taken into account, the above values reduce to the manifold specification values of +20.5 dBm and +28.5 dBm for P_a and P_p respectively. The SW-219 has a P_1 value of +33 dBm and thus it can easily withstand the required peak power levels.

Let us now calculate the gain and the transimpedance of the TAMP. This can be accomplished by first calculating the P_a at the output of the DET using a 50 Ω load. Let us assume that we use a 500 mW LD (such as the SDL-2350) which we modulate directly around the optical bias power of P_o=250 mW. Note that the SDL-2350 delivers 500 mW with 0.8 W/A efficiency (r_{LD}) and it can be modulated up to 2 GHz (-3 dB bandwidth). Using Equation (3.2.1) with $g=2.51\times10^{-3}$ (or -26 dB total optical insertion loss), m=0.4, r_D=0.5 A/W, R_D=50 Ω and P_o=250 mW we find that P_s=-34 dBm which means that the gain of the TAMP (with respect to 50 Ω) must be G=34 dB. This gain corresponds to a transimpedance of about 2500 Ω. TAMPs with G=34 dB or R_{trans}=2500 Ω are commercially available from various vendors.

Now we must calculate the input RF power required by the LD. This can be accomplished by using equation 3.3.5 if we know R_L. Spectra Diode Labs indicates that the forward voltage of the SDL-2350 is given by:

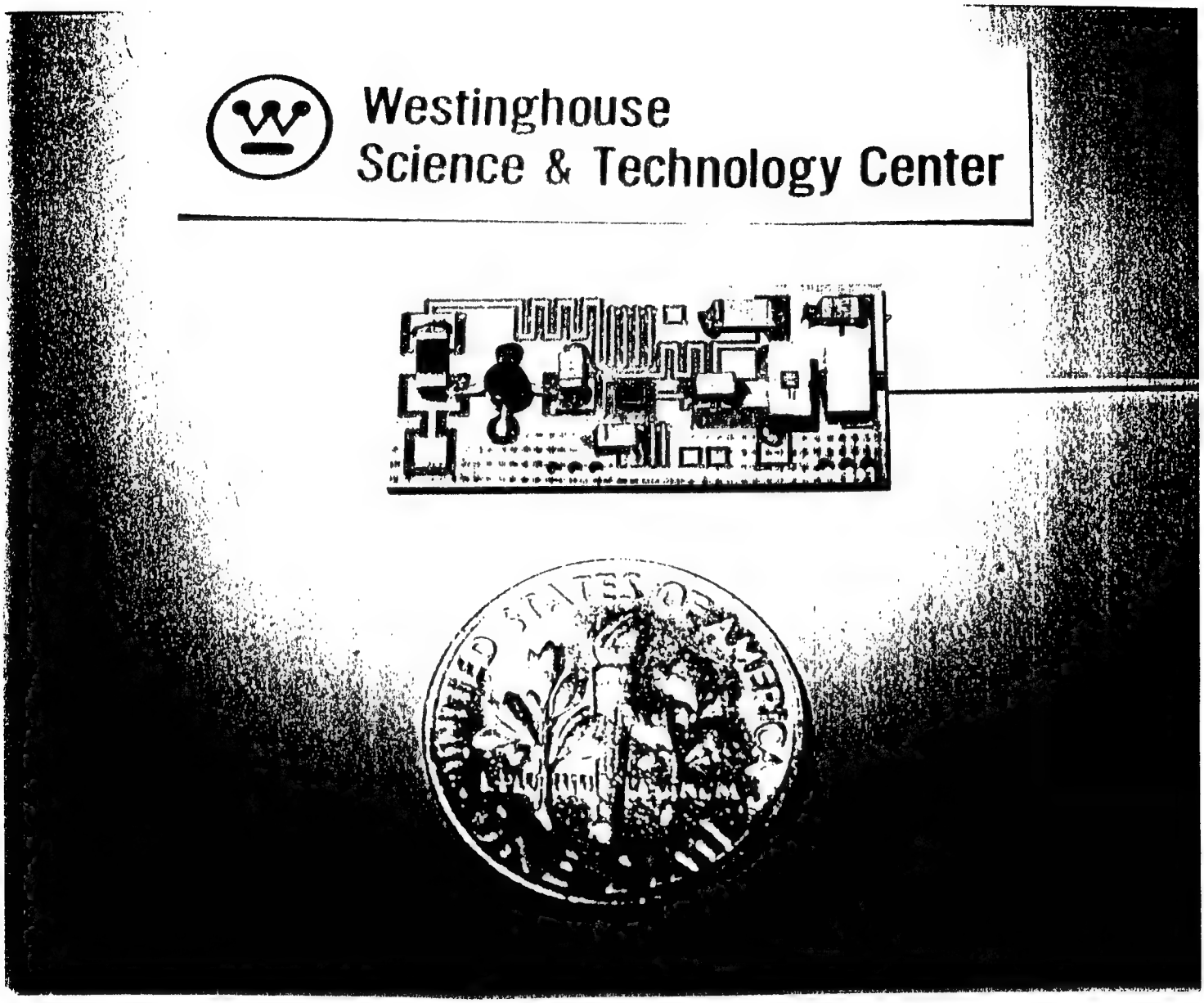

Figure 3.3-3 Photograph Showing a Miniaturized DET-TAMP Receiver

$$V_f = 1.5V + I_{op} x\, R_S, \qquad (3.3.6)$$

where: I_{op} is the current at P_o and R_S is the series resistance for the SDL-2350 which is 0.5 Ω. From Equation 3.3.6 with I_{op}=0.5 A (i.e., @ P_o=250 mW) we find that

V_f=1.5 V+ 0.5x0.5V=1.75 V. This means that the effective R_{LD} @ I_{op} is 1.75/0.5=3.5 Ω. Using Equation 3.3.5 with r_{LD}=0.8 W/A, g=2.51x10^{-3}, r_D=0.5 A/W, R_D=50 Ω and R_{LD}=3.5 Ω we find that G_d=-48.4 dB. Using G_d=-48.4 dB and P_s=-34 dBm prior to the TAMP we find that the average input RF power to the LD with modulation index of 0.4 is about +14.4 dBm. Out of the +14.4 dB required gain, we can get about 3 dB by cleverly designing the LD current driver and thus only 11.4 dB must be provided by the input AMP (see Figure 3.3-2).

It is worthwhile noting that the requirement for the input AMP is now reduced from G=41.9 dB and P_1=+49.9 dBm (16 LD design) to G=11.4 dB and P_1=+19.4 dBm (single LD design). Furthermore we now require only one 0.5 W LD (which is commercially available) versus sixteen 5 W LDs. The penalty paid was: (1) the use a chip TAMP per element and (2) the increased gain of the output AMP that follows the TAMP (from 6.8 dB including the SW-219 loss to 21 dB). It is the opinion of the author that this is a small price to pay given that 21 dB AMPs can be easily implemented using 2 commercially available transistors in a C-class amplifier design. Such transistors have been developed by various manufacturers for applications such as mobile telephones, etc., (see for example the Motorola MRF555 with 1.5 W output and 13 dB gain over the 425-450 MHz range). Note that UHF C-class amplifiers are commercially available from several vendors. For example, Motorola's MHW703 C-class AMP has a P_1=2.3 W output power capability over the 450-460 MHz with gain of 31 dB, and comes in a package of dimensions 4.5x1.4x0.6 cm^3.

3.3.2.3 Signal-to-Noise Performance of UHF Transmit Manifold

The easiest way to calculate the SNR at the output is via calculation of the currents induced at the output of the detector (and prior to the TAMP) by the signal and the various noise components. The average signal current (i.e., for m=0.4) can be calculated via the following equation which gives the output current for a directly modulated LD:

$$I(t) = g r_D P_O (1 + m \cos(2\pi\, ft)). \qquad (3.3.7)$$

From Equation 3.3.7 we find that the peak-to-peak current induced by the full swing of the modulation is:

$$I_{pp}=gr_DP_o[1+m-(1-m)]=2mgr_DP_o, \quad (3.3.8)$$

and therefore the rms modulation-induced current is:

$$I_{rs}=0.35x2mgr_DP_o=0.35x2x0.4x0.5x630\ \mu W=\underline{88.2\ \mu A}. \quad (3.3.9)$$

The LD relative intensity noise (RIN) generates a current given by:

$$I_{RIN}=gr_DP_o\sqrt{(RINxBW)}. \quad (3.3.10)$$

Assuming an LD with poor RIN performance, e.g., -130 dB/Hz, we find from Equation 3.3.10 that over 5 MHz of noise bandwidth (BW) the I_{RIN} is equal to:

$$I_{RIN}=0.5x630x10^{-6}\sqrt{[10^{-(13-6.7)}]}\ A=\underline{0.223\ \mu A}. \quad (3.3.11)$$

(Note that in Equation 3.3.11 the $10^{-(13-6.7)}$ comes from the calculation of the RIN (130 dB-67 dB) over 5 MHz of noise BW.

The shot noise and dark current contributions are given by:

$$I_{SD}=\sqrt{(2e[I(t)+I_D]BW)}=$$
$$=\sqrt{(2x1.6x10^{-19}x[(0.5x630x10^{-6}+10^{-9})]x5x10^6)}=\underline{0.0245\ \mu A}, \quad (3.3.12)$$

where $e=1.6x10^{-19}$ is the electron charge, I(t) is the average current generated at the photodetector ($\sim gr_DP_o$), and I_D is the dark current of the DET which is typically 1 nA.

Next we must calculate the equivalent input noise current (EINC) of the TAMP. Using the 4 pA/$\sqrt{}$Hz current noise figure of the 34 dB AVANTEK ITA-06300 we find that the EINC is:

$$EINC=(4\ pA/\sqrt{Hz})\ x\ \sqrt{(5\ MHz)}=\underline{0.0089\ \mu A}. \quad (3.3.13)$$

From Equations 3.3.11, 3.3.12 and 3.3.13 we find that the RIN-induced noise dominates (as expected) and alone results in an SNR of 20log(88.2/0.223)=51.94 dB @ noise BW of 5 MHz. Note that this can also be calculated directly from the SNR formula applicable to "large" optical signals :

$$SNR=0.5xm^2/RINxBW= 10log(0.5x0.4^2)-(-63\ dB)=52\ dB. \quad (3.3.14)$$

The actual SNR at the output of the TAMP is given by:

$$SNR=20log[88.2/ (0.223+ 0.0245+ 0.0089)]=\underline{50.73\ dB\ @\ BW=5\ MHz}. \quad (3.3.15)$$

Therefore since the power of the "average" signal at the output of the TAMP is P_a=0 dBm, the noise power at the TAMP output is P_n=(0-50.73) dBm=-50.73 dBm.

Let us now assume the use of a AMP (that follows the TAMP) with a noise figure (NF) of 5 dB. Then with G=21 dB the output noise power due to the AMP is:

$$P_{n\text{-}amp}=-(174\ -67-5-21)\ dBm = -81\ dBm, \quad (3.3.16)$$

whereas the link-TAMP noise is (-50.73 +21) dBm = -29.73 dBm. From the above we conclude that the RIN-induced noise is the limiting factor of the system SNR performance. Note however, that even though we used a LD with a poor RIN (i.e., -130 dB/Hz), the resulting SNR is quite high, especially for the Tx mode.

We can now calculate the manifold NF as follows:

$$NF=SNR_I/SNR_O=(174-67-50.7)\ dB=56.3\ dB. \quad (3.3.17)$$

It is of interest to calculate the performance improvement if a LD with good (not exceptional) RIN figure is used. For example, let us assume that RIN=-145 dB/Hz which is the RIN value of moderately priced commercially available LDs. From Equation 3.3.11 we find:

$$I_{RIN}=0.5x630x10^{-6}\sqrt{[10^{-(14.5-6.7)}]}\ A=\underline{0.0397\ \mu A}, \quad (3.3.18)$$

which shows that the RIN-induced noise component is now compatible with the shot noise component. The SNR prior to the voltage AMP is:

$$SNR=20\log[88.2/(0.0397+0.0245+0.0089)]=\underline{61.6\ dB\ @\ BW=5\ MHz},\qquad (3.3.19)$$

and thus a significant (>10 dB) improvement can be achieved in the SNR by careful selection of the LD used. Note that the link-TAMP noise (21-61.6=-40.6 dBm/5 MHz) still dominates the noise of the output voltage AMP (-81 dBm/5 MHz), and thus the NF of the manifold is:

$$NF=SNR_I/SNR_O=(174-67-61.6)\ dB=45.4\ dB.\qquad (3.3.20)$$

In conclusion, the SNR and NF of the proposed manifold are satisfactory and can easily be as high as 61.6 dB and 45.4 dB respectively. Note that if necessary, an optical switch can be used between the LD and the input fiber to the 1:8 FO divider (see Figure 3.3-2) to disconnect the LD from the antenna when the radar is at the Rx mode. This way most of the noise will be eliminated, thereby eliminating the rather unlikely possibility of noise crosstalk with the Rx electronics. With this technique the output noise will be mostly due to the TAMP noise, and will be about -79.9+21=-58.9 dBm over 5 MHz of noise BW.

3.3.2.4 Weight, Volume, and Power Consumption of UHF Tx Manifold

To calculate the weight of the UHF photonic Tx manifold we use the following reference values: (1) 1 m of buffered fiber weighs 0.07 gr and thus the total weight of 8x36 fibers each 10 m long is: 0.07x10x8x36=202 gr, (2) the DET receiver with a TAMP is about 1 gr or a total of 288 gr for all 8x36 required, (3) the LD with the driver, cooling electronics and feedback control is about 200 gr (this is the actual weight of a similar structure built at Westinghouse STC with vintage 1985 technology), (4) the input AMP (prior to the LD) is 85 gr (this is the actual weight of the Mini-Circuits ZHL-1HAD 10-500 MHz AMP with G=11 dB and P_1=+20 dBm), and (5) the weight of the output voltage AMP is about 10 gr or 10x288=2.88 kg for all 8x36 AMPs required. The overall weight of the UHF photonic manifold can be now be calculated as:

$$WEIGHT = (0.202+0.288+0.2+0.085+2.88)\ kg=\underline{3.7\ kg\ or\ 7.9\ lbs}.\qquad (3.3.21)$$

To estimate the UHF manifold volume we use the following reference values: (1) the volume of 8x36 buffered fibers, each 10 m long and 250 μm in diameter is $8x36x1x\pi\ x(125x10^{-6})^2\ m^3$ or 0.0005 ft^3, (2) the volume of the LD with the drivers, etc., is 10x10x3 cm^3 or 0.01 ft^3, (3) the actual volume of the Mini-Circuits ZHL-1HAD 10-500 MHz AMP is 3.175x3.962x3.962 cm^3 or 0.0018 ft^3, (4) the volume of the DET-TAMP assembly is about 1x0.5x0.3 cm^3 or 0.0015 ft^3 for all 8x36 required, (5) the dimensions of the Motorola MHW703 are 4.5x1.4x0.6 cm^3 or 0.000133 ft^3 or 0.038 ft^3 for all 8x36 required. Allowing a packaging factor of 2, the estimated volume of the UHF manifold is:

$$\text{VOLUME} = 2(0.0005+ 0.01+ 0.0018+ 0.0015+ 0.038)\ ft^3 = \underline{.1ft^3}. \qquad (3.3.22)$$

To estimate the power consumption of the manifold we use the following values: (1) DET receiver with TAMP about 180 mW, i.e., 10 mW for the DET and 170 mW for the TAMP (170 mW is the actual power consumption of the AVANTEK ITA-06300 TAMP), (2) LD with driver etc., requires about 15 watts, (3) the input AMP requires 1.75 W (this is the actual value for ZHL-1HAD), and (4) the power consumption of the output voltage AMP can be calculated as follows: (i) using the 42% efficiency of the MOTOROLA MHW703 and similar products, and since we require P_p=29 dBm (0.794 W) we find that P_{AMP}=0.794 W/0.42=1.9 W, (ii) since the MHW703 has a 31 dB gain, whereas we require 21 dB of gain, we can reduce the 1.9 W figure by about 1/3 and arrive at an estimate of average power consumption of about 1.3 W. The total power consumption can now be calculated as:

$$\text{POWER CONSUMPTION} = (8x36x(1.3 +0.18)+15 +1.75)\ W = \underline{443\ W} \qquad (3.3.23)$$

3.3.3 S-Band Photonic Transmit Manifold

3.3.3.1 Discussion

For the S-band Tx manifold, and unlike the UHF case, there are not many implementation options. This is because:

(1) High power (e.g., 1 W), high frequency (3-3.5 GHz) LDs do not exist and therefore a "one-to-many" all-fiber manifold similar to the UHF recommended manifold cannot be efficiently

implemented. For example, if we use a 20 mW 3-3.5 GHz DFB LD (expected to be commercially available in 2-3 years) in order to drive 256 elements (i.e., 64 LDs total) and the following "realistic" parameters: P_O=10 mW, -27 dB insertion loss of the 1:256 FO divider (i.e., g=0.5/256), r_D=1 A/W, and m=0.4, we find, via Equation 3.3.1, that the average output signal power is P_S=-58.16 dBm. Assuming about 25 dB of TAMP gain, we find that each output element would require an extra 46.6 dB of voltage gain which implies a dramatic increase in both the size and volume of the output T/R modules.

(2) Use of an optical amplifier does not help because most optical amplifiers deliver relatively small amounts of optical power, e.g., +10 to +15 dBm or 10 to 32 mW which is compatible with the power available from 3-3.5 GHz DFB LDs.

Fortunately, there exist both high frequency optical modulators and high power CW optical sources which will allow us to efficiently implement the S-band Tx manifold. This type of manifold is described next.

3.3.3.2 Recommended S-Band Photonic Tx Manifold

Figure 3.3-4 shows a schematic of the recommended S-band manifold along with details of the gain and power requirements at various stages. A single moderate power (38 dBm peak power) RF amplifier drives a 1:64 RF divider. Each divider output (with P_a=10 dBm and P_p=18 dBm) drives a MZ modulator. The MZ modulates the intensity of a 1 W CW solid state miniature laser. The output of the fiber-coupled MZ is then divided into 256 channels via a 1:256 FO divider made out of one 1:8 FO divider and thirty-two 1:32 FO dividers. Each of the 256 FO outputs drives a DET which is followed by aTAMP, an AMP, and a 1x2 switch (SW-228). Since we have a 64x256 element antenna, we require 64 independent 256-element manifolds. Each consists one CW laser, one MZ, one single mode1:256 FO divider, 256 DETs, 256 TAMPs, 256 AMPs, and 256 1x2 switches.

For a FO link with an external modulator, the link gain (G_e in dB) is given by[4]

$$G_e = 10 \log(g\, Po\, \pi /2\ V_\pi)^2\, r_D^2\, R_M\, R_D, \qquad (3.3.24)$$

where: g is the optical loss factor, P_O is the optical power at the input of the modulator, $V\pi$ is the voltage of the modulator for 100% modulation, r_D is the detector responsivity and R_M, R_D are the input impedance of the MZ and the output impedance of the DET respectively. Observe from Equation 3.3.24, that contrary to the gain of the directly modulated link (Equation 3.3.5), the gain of the externally modulated link is proportional to the square of the optical input power and thus by increasing the power

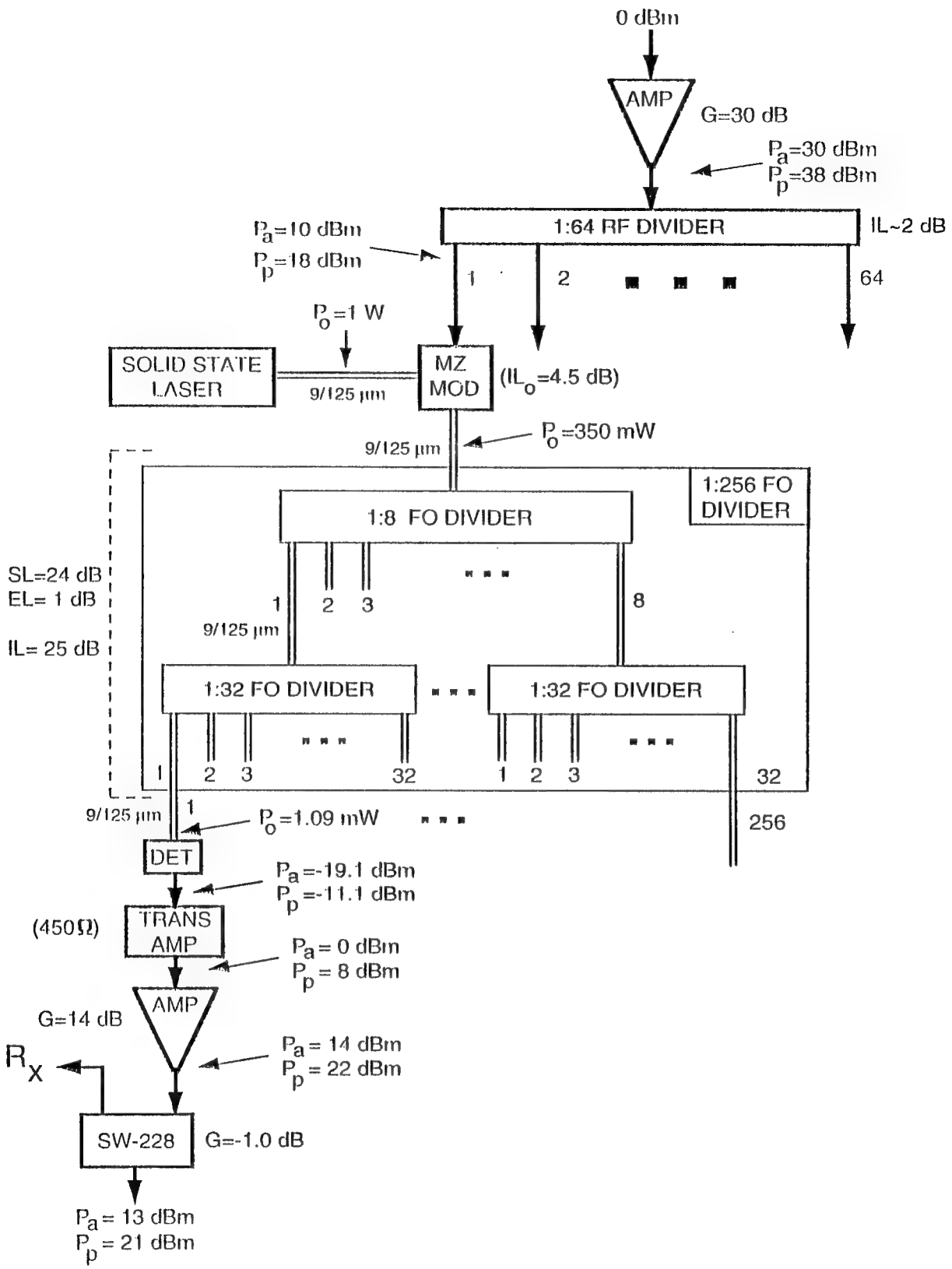

Figure 3.3-4 Schematic of the Recommended S-Band Tx Manifold

of the CW laser we increase the link gain. Unfortunately, commercially available MZs operating at 1300 nm can withstand no more than 200-400 mW of optical power in order to avoid optical damage. For example, almost all of the United Technologies MZs have a conservative specification of 200 mW. However, by taking into account the historical optical damage improvements as well as the basic physics of the MZ and the optical materials used, we expect that within the next 2-3 years this conservative limit will increase to at least 1 W.

To calculate the gain between the input of the MZ and the output DET (assuming a R_D of 50 Ω) we use Equation 3.3.24 and the following parameters: $g=1.12 \times 10^{-3}$ or 29.5 dB consisting of: 4.5 dB of MZ loss, 24 dB of 1:256 splitting loss (SL) and 1 dB of 1:256 excess loss (EL), $P_O=1$ W, $V_\pi=2.5$, $r_D=1$ A/W, and $R_{MZ}=R_D=50\Omega$. Regarding these values we note the following: (1) the 4.5 dB MZ loss and the $R_M=50$ Ω are typical values of commercially available MZs such as those made by United Technologies, (2) the 1 dB of EL for the 1:256 FO divider is possible with customized, commercially available FO dividers (see for example the Gould Inc. FO divider products), (3) the V_π is the figure of the 3 GHz MZ by United Technologies, (4) solid state miniature lasers with 1 W CW power already exist[5], and (5) the r_D figure is possible with currently available but custom selected DETs (Westinghouse STC has acquired such DETs from EPITAX). Using Equation 3.3.24 and the above values we find:

$$G_e=10\log[(1.12 \times 10^{-3} \times 1 \times 3.14/2 \times 2.5)^2 \times 1 \times 50 \times 50] = -29.1 \text{ dB}. \qquad (3.3.25)$$

The maximum input power of a 3 GHz MZ (i.e., the power that corresponds to the 1 dB compression point) with a $V_\pi \sim 2.5$ V is about 18 dBm and thus for $P_p=18$ dBm the DET's peak output will be $P_p=-11.1$ dBm. Similarly, for an input average power of $P_a=10$ dBm the DET average output will be $P_a=-19.1$ dBm. Use of a TAMP with a transimpedance of 450 Ω will provide a gain of $20\log(450/50)=+19.1$ dB and thus the DET outputs will be: $P_p=+8$ dBm and $P_a=0$ dBm, which are possible with today's commercially available devices such as the ATT's 3.5 GHz HG1210AXA. Furthermore, in order to provide the required $P_p=21$ dBm and $P_a=13$ dBm we use a voltage AMP with a gain of G=14 dB and a $P_1=22$ dBm. The extra 1 dB of gain is used in order to offset the loss of the Rx/Tx manifold switch which for the case of the SW-228 is 1 dB. By the way, the P_1 of the SW-228 is +33 dBm and thus the $P_p=21$ dBm presents no problem.

3.3.3.3 Signal-to-Noise Performance of S-Band Tx Manifold

To calculate the available SNR and NF of the S-band manifold, we will proceed in a manner similar to that used for the UHF manifold. Thus, we first calculate the input currents to the TAMP which are due to the signal and the various noise sources.

The rms signal current produced at the output of the DET can be calculated by Equation 3.3.9 and is found to be

$$I_{rs}=0.35x2mr_D(gP_o)=0.35\ x2\ x0.4x1x(1.09x10^{-3})=\underline{305.2\ \mu A}, \quad (3.3.26)$$

where m=0.4 corresponds to the "average" signal case, r_D is assumed to be 1 A/W, and gP_o=1.09 mW (see Figure 3.3-4). Assuming that the CW laser has a RIN value of -160 dB/Hz (which is available with commercially available CW lasers), we find using Equation 3.3.10 that over 500 MHz the I_{RIN} is equal to:

$$I_{RIN}=1x1.09x10^{-3}\ \sqrt{[10^{-(16-8.7)}]}\ A=\underline{0.244\ \mu A}. \quad (3.3.27)$$

Note that in Equation 3.3.27 the $10^{-(16-8.7)}$ comes from the calculation of the RIN (i.e., 160 dB-87 dB) over 500 MHz of noise BW.

The shot noise and dark current contributions are:

$$I_{SD}=\sqrt{(2x1.6x10^{-19}x[1.09x10^{-3}+10^{-9})]x5x10^{8}}=\underline{0.417\ \mu A}. \quad (3.3.28)$$

To calculate the equivalent input noise current (EINC) of the TAMP we use the 8 pA/$\sqrt{Hz}$ current noise figure of the 2 kW ATT HG1210AXA and we find that the EINC is:

$$EINC=(8\ pA\ /\sqrt{Hz})\ x\ \sqrt{(500\ MHz)}=\underline{0.179\ \mu A}. \quad (3.3.29)$$

From Equations 3.3.27, 3.3.28, and 3.3.29 we find that the three noise components are compatible, and result to an SNR at the output of the TAMP of:

$$SNR=20log[305.2/\ (0.244+0.417+0.179)]=\underline{51.2\ dB\ @\ BW=500\ MHz}. \quad (3.3.30)$$

Therefore since the power of the "average" signal at the output of the TAMP is P_a=0 dBm (see Figure 3.3-4), the noise power at the TAMP output is

$$P_n=(0-51.2)\ \text{dBm}=-51.2\ \text{dBm}. \quad (3.3.31)$$

Assuming the use of a voltage AMP with G=14 dB and NF=5 dB we find that the AMP-due noise power at the output of the AMP over a 500 MHz BW is:

$$P_{n\text{-}amp}=-(174-87-5-14)\ \text{dBm}=-68\ \text{dBm}, \quad (3.3.32)$$

which should be compared with the link noise contribution of (-51.2+14) dBm=-37.2 dBm. Therefore once again the FO link determines the overall noise performance.

Finally, we can calculate the NF of the system as:

$$NF=SNR_I/SNR_O=(174-87-51.2)\ \text{dB}=35.8\ \text{dB}, \quad (3.3.33)$$

which is lower than that of the UHF link. The reasons for this improved performance are: (1) higher optical power at each output DET and thus more signal, and (2) the much lower RIN level of the CW laser.

Finally, note that if an optical switch is used between the MZ and the 1:256 FO divider during Rx, the output noise will be due to the TAMP and it will be lower by 20log[(0.244+0.417+0.179)/0.179]=13.42 dB to (-37.2-13.4) dBm =-50.6 dBm.

3.3.3.4 Weight, Volume, and Power Consumption of S-Band Tx Manifold

To calculate the weight of the S-band photonic manifold we use the following reference values: (1) the input AMP and the 1:64 divider weigh 2.42 lbs (or 1.1 kg) (data from the statement of work), (2) the weight of an actual MZ is about 20 gr and thus the weight for 64 MZs is 1.28 kg, (3) the weight of each of the CW lasers (such as the MICRALASE) is estimate to be about 100 gr and thus for 64 lasers the weight is 6.4 kg, (4) 1 m of buffered fiber is 0.07 gr and thus the total weight of 64x256 fibers each 3 m long is 0.07x3x64x256= 3.44 kg (note: the 3 m value comes from the assumption that the 1:256 FO

dividers are located at the antenna, whereas the UHF FO divider is located at the LD and thus the UHF fibers need to be about 3x longer), (5) the DET receiver with a TAMP is about 1 gr and thus the weight of all 64x256 TAMPs is 16.3 kg, and (6) the weight of the output voltage AMP is about 3 gr (this is the actual weight of the WJ-RA46 1-4 GHz AMP with G=25 dB and P_1~21 dBm @ 3 GHz) and thus for 64x256 AMPs the weight is 49 kg. The overall weight of the S-band photonic Tx manifold can be now be calculated as:

$$\text{WEIGHT} = (1.1 + 1.2 + 6.4 + 3.44 + 16.3 + 49)\ \text{kg} = \underline{77.44\ \text{kg or} \sim 171\ \text{lbs}}. \qquad (3.3.34)$$

To estimate the volume of the S-band FO Tx manifold we use the following reference values: (1) the volume of the front AMP is assumed to be $4.5\text{x}10^{-3}$ ft^3, (2) the volume of the 64 MZ is 64x(10x2.3x1.1 cm^3) or 0.057 ft^3, (3) the volume of the 65 CW lasers is 64x (12x7x7 cm^3) or 1.33 ft^3 , (3) the volume of 64x256 buffered fibers, each 3 m long and 250 μm in diameter is 64x256x3mx'x$(125\text{x}10^{-6})^2$ m^3 or 0.085 ft^3, (4) the volume of the 64x256 DET-TAMP assembly is about 64x256x(1x0.5x0.3) cm^3 or 0.087 ft^3, and (5) the volume of the WJ-RA46 1-4 GHz AMP with G=25 dB and P_1~21 dBm @ 3 GHz is about 1 cm^3 and thus for 64x256 is 0.58 ft^3. Allowing a packaging factor of 2, the estimated volume of the S-Band Tx manifold is:

$$\text{VOLUME} = 2(0.45\text{x}10^{-3} + 0.057 + 1.33 + 0.085 + 0.087 + 0.58)\ \text{ft}^3 = \underline{4.28\ \text{ft}^3} \qquad (3.3.35)$$

To estimate the power consumption of the S-band Tx manifold we use the following reference values: (1) the power consumption of the DET receiver with the TAMP is about 100 mW, i.e., 10 mW for the DET and 90 mW for the TAMP for a total of 64x256x0.1=1,638 W, (2) there is negligible power consumption by the MZs, (3) assuming a 30% efficiency for each CW laser, we find that the total power consumption for all 64 lasers is 64/0.3= 213 W, (3) a 42% efficiency for the output voltage AMP results in a 25 mW/0.42=60 mW power consumption for a total of 983 W, and (4) about 6.6 W for the input AMP. The total power consumption can now be calculated as:

$$\text{POWER CONSUMPTION} = (1{,}638 + 213 + 983 + 6.6)\ \text{W} = \underline{2.8\ \text{kW.}} \qquad (3.3.36)$$

3.3.4. Receive Manifolds

Both UHF and S-band photonic FO manifolds require the use of FO combiners. The UHF manifold requires thirty-six 8:1 and one 36:1 FO combiners whereas the S-band manifold requires two-hundred and fifty-six 64:1 and one 256:1 FO combiners. As we discussed in Section 3.3.1, single-mode FO combiners are symmetric devices and thus their "combining" optical loss is equal to the splitting loss plus the excess loss. Since in most cases we use a square-law optical detector to convert light into RF signal, the overall loss doubles, e.g., a 10 dB optical loss for a 8:1 combiner is translated to 20 dB RF loss at the output of the optical detector. In FO communications and networking applications, this loss is recovered via the use of an optical amplifier which can easily provide 35 dB of optical gain thereby eliminating the loss and providing some gain. We can not employ this technique, however, because for the Rx mode we require multiple independent combiners (i.e., one per column), and thus we need as many optical amplifiers as the number of antenna columns. Unfortunately, this will result in unacceptably high cost. The obvious alternative would be to use an RF amplifier to recover the additional loss, however, this may result in reduction of the output SNR (this may be the case for the 64:1 combiner). Fortunately, there are at least two other alternatives that minimize the degradation of the output SNR. These alternatives are: (1) the use of RF combiners after detection of the RF signal from each individual fiber (in which case we will be subjected to the typical RF combining loss) and (2) the use of nearly lossless asymmetric N:1 FO combiners which use proprietary FO techniques developed at Westinghouse STC. These alternatives are discussed next.

3.3.4.1. RF Summation After Detection

This approach uses conventional microwave RF combiners in conjunction with individual FO links. Thus, each antenna element will have its own dedicated FO link, i.e., for the 8-element UHF column we will use 8 individual links. Prior to the RF combiner, a DET is used to detect the RF signal from each link. The outputs of the DETs are then be combined electrically via the use of a RF combiner. This technique eliminates the high optical combination loss at the expense of hardware. Fortunately the cost of the extra hardware is low, e.g., DETs in quantities of 100s operating in either the 830 nm or the 1300 nm optical bands with BWs sufficient for both UHF and S bands cost a few tens of $.

3.3.4.2 Asymmetric FO Combiners

Most commercially available FO combiners come in configurations of 4:1, 8:1, 16:1, and 32:1, with typical "incoherent" RF loss of 14.4 dB, 21.2 dB, 28 dB, and 35 dB respectively. These combiners

use single mode optical fiber at both the input and the output ends, and they are intended for long distance communication networks for which the use of a single mode fiber at both ends is necessary. However this is not the case for our application for which all distances are of the order of a tens of feet. For these kinds of distances the modal noise of multi-mode fibers is virtually absent for frequencies of up to 6 GHz (Westinghouse STC personnel have proved this experimentally by propagating a 6 GHz signal for over 100 m using multimode 50/125 μm fiber).

We can take advantage of the short distances involved and make a special kind of assymetric FO combiner which is nearly lossless. The basic idea is: use single mode fibers to bring the signals from each antenna element without any excess noise, bundle these fibers together and couple them into a wider diameter short piece (e.g., 1-2 meters) of multi-mode fiber, and use a single optical detector at the end of the short fiber piece to convert the combined optical signals into a single RF output. This technique has been pioneered by personnel at the Westinghouse STC, who have fabricated low-cost (<10$) prototypes for various N:1 configurations, and who have proved the above principle.

In general, there are two problems associated with fiber coupling:

(1) Lens-coupling a fiber bundle to a wider fiber in order to form a lossless combiner, may have constraints on the numerical aperture and the image size that cannot be satisfied simultaneously. For minimum losses, we require:

$$2 f u \tan\vartheta' / (u - f) \geq D \geq 2 u \tan\vartheta, \tag{3.3.37}$$

$$a \geq d_a f / (u - f), \tag{3.3.38}$$

where D and f are the diameter and focal length of the lens, respectively, u is the fiber-lens separation, d_a is the active diameter of the fiber bundle, a is the
aperture of the output fiber, ϑ is the divergence angle from each of the boundle fibers, and ϑ' is the acceptance angle of the output fiber.

(2) Butt-coupling a fiber bundle to a single output fiber, where the cross sectional areas of the active areas on either side of the coupling are not matched. For minimum losses, we require:

$$\vartheta' \geq \vartheta, \tag{3.3.39a}$$

$$a \geq d_a. \tag{3.3.39b}$$

Both of these problems are most severe with multi-mode fiber where the divergence of the light emitted from such fiber is largest. Westinghouse STC has developed a method of controlling the active cross sectional area of the fiber bundle to maximize the power transfer through the coupling, i.e., to control d_a to satisfy the relative fiber bundle active diameter and fiber aperture constraints given in Equations 3.3.37, 3.3.38 and 3.3.39. In general, the usual fiber arrangement involved in a fiber bundle which maximizes the active/ total area ratio is asymmetric. This particular arrangement is the lowest order member of the family whose total diameter (d_t), active diameter (d_a), active/total area ratio (R), and number (N) of fibers in the bundle are given by

$$\begin{aligned} d_t &= (2k + 1)\, d_{cl}, \\ d_a &= (2k + d_{co}/d_{cl})\, d_{cl}, \\ R &= \{[1 + 3k(k + 1)]/(2k + 1)^2\}\, (d_{co}/d_{cl})^2, \\ N &= 1 + 3k(k + 1), \end{aligned} \tag{3.3.40}$$

where k = 1, 2, 3, ..., and d_{co} and d_{cl} are the core and cladding diameters, respectively, of each of the fibers comprising the bundle. Evidently, the ratio R is a maximum when the ratio d_{co}/d_{cl} is a maximum, and in the limit when $d_{cl} = d_{co}$ (i.e., when the cladding is completely removed), $d_t = d_a$ and $R = [1 + 3k(k + 1)]/(2k + 1)^2$ (which varies between 0.78 for k = 1 and the limiting value 0.75 for infinite k).

In practice one can implement a lossless combiner for virtually any N value up to a practical limit of about 256 (at STC we have implemented lossless bundles having N values of up to 128). In these combiners, no output fiber was used, and the fibers were simply fit in a single ferrule which had been enlarged to accommodate the appropriate number of fibers. The output of the ferrule was connected to a single DET whose area was large enough to "read" all the fibers. For example, for N=7,19, 37, and 61 the corresponding active diameters of the bundles are 380, 660., 940, and 1220 μm. This illustrates the fact that despite the compact design of the splitter/combiner, the active diameter d_a of the bundle becomes inconveniently large for appreciable N, particularly for coupling in high speed systems where, for example, the active area of detectors is deliberately small to minimize capacitance.

For our application, where we need to couple a bundle of single-mode fibers to one multi-mode fiber, it is mandatory to reduce the diameter of the single mode fibers of the bundle, so that the end active areas of the coupling partners are matched. The degree of the reduction depends on the core of the multi-mode fiber used. This in turn depends on the particular design we are implementing. For any

design however, the method adopted for controlling the cross sectional area of a fiber is that of wet chemical etching by hydrofluoric acid (HF). Before etching, the fiber is first prepared by stripping several cm of the buffer coating from the fiber, cleaving the stripped portion of the fiber, and finally scrupulously cleaning the stripped portion with acetone. The fiber is then mounted vertically in a fixture attached to a micrometer drive such that the fiber can be mechanically lowered into a beaker containing concentrated HF (49% solution). During the etching process, the stripped, cleaned end of the fiber is lowered several cm below the surface of the HF solution. The fiber mounting fixture is designed so that several fibers may be etched simultaneously. After etching, the fiber is thoroughly washed in water to remove all traces of HF. In order to calibrate the process, a series of measurements is taken of the diameter of the etched fiber as a function of etch time at 5 min intervals up to 30 min. In this sequence, a few fresh fiber samples are etched simultaneously in fresh etchant solution for each predetermined etch time. The diameters of the fiber samples are etched simultaneously for a given etch time, and usually they are within 1%, which shows that the etching process is very reproducible. In general, there is a linear dependence of the fiber diameter and the etch time, and its slope determines the etch rate (i.e., rate of decrease of fiber diameter) which is usually about 3.5 μm/min. The diameter of the etched portion of the fiber is uniform over the length that the fiber had been immersed in the HF solution. At the cleaved end of the fiber, the etching is found to occur non uniformly and this is attributed to a variation in the etch rate with the amount of doping in the fiber, where the etch rate increases with increasing doping level. This small, non uniformly-etched region must be removed before the fiber can be used and this is normally achieved during polishing of the fiber after mounting in a ferrule connector.

Upon completion of the etching process, the reduced fibers are bundled together via the use of a thin layer of glue which is applied along the fiber axis, about 1 cm away from the etched fiber ends. Next, the fiber bundle is fine-polished via the use of standard FO polishing equipment. Polishing assures that all fiber ends are at the same plane and that no differential lengths or gaps exist between the various members of the bundle.

Next, the polished fiber bundle must be attached to the output fiber. This can be accomplished with a variety of techniques which include: (1) direct fusion via the use of a slightly modified commercially-available fiber fusion equipment (such equipment is available at STC), (2) butt-coupling in conjunction with the use of UV-cement, (3) lens coupling in conjunction with miniaturized SELFOC lenses, etc. In general, all above techniques work well, with the simplest being direct fusion which is fast, reliable, and low cost.

In the next section, we discuss the specifics of the UHF and S-band manifolds, and we identify where and how the lossless combiners can be used.

3.3.4.3 UHF Receive Photonic Manifold Design

The UHF receive manifold requires thirty-six 8:1 FO combiners. For this manifold virtually any fiber can be used in conjunction with low-cost, e.g., <$100 LDs. For example, the LDs can be coupled into either single-mode 5/125 μm, multi-mode 9/125 μm or 50/125 μm fibers all of which can provide nodal-noise free operation over the 0.42-0.45 GHz band for hundreds of meters of fiber. The cheapest and easiest technique is to use graded-index 50/125 μm fiber. To construct a lossless FO combiner (see Figure 3.3-5), 9 fibers are used in a 3x3 format (8 fibers for the combiner and 1 spare), in conjunction with a short piece (1-2 m) of 220/250 μm multi-mode fiber (alternatively, we can use 250/300 μm fiber and reduce the core to 220 μm). To fit the 3x3 format without loss over the 220 μm core of the 220/250 μm fiber, each of the 9 fibers must be reduced to about 52 μm which can be handled easily via the etching technique we described in the previous section. To ensure lossless operation, we must ensure that the full 220 μm diameter core can be "read-out" by a single detector who is fast enough to respond to the 0.45 GHz frequency. This condition can be easily satisfied with commercially available detectors, e.g., with the 240 μm-diameter NEC NDL2102 Si PIN which has a rise time 0.5 ns @ 40 V reverse bias and a 3-dB BW of 700 MHz.

To calculate the RF gain for each FO channel, we can use Equation 3.3.5. Let us assume the use of low-cost (e.g., <$100) 830 nm optoelectronic technology, and thus assume: r_{LD} in the 0.25-0.45 W/A range (e.g., for the Mitsubishi ML2701 LD r_{LD}=0.35 W/A with R_{LD} of about 10 Ω), and r_D of about 0.5 A/W with an effective impedance of 250Ω which allows for RF BWs of at least 500 MHz. Using r_{LD}=0.35 W/A, R_{LD}=10Ω, r_D=0.5 A/W, R_D=0.45 W/A, and assuming about 0.5 dB optical loss for the FO combiner, we find from Equation 3.3.5 that the RF loss per channel is about 5 dB. The worse-case NF value for all-passive FO links of this type is about 40 dB, and are associated with third order intersept points of about 27 dBm.

Given the high NF of the link we are forced to use an LNA prior to the LD to set the overall NF. A good choice is the WJ-RA89 with a 25 dB of gain and a 4 dB of NF. Using the above LNA, the ML2701 LD, the 8:1 FO combiner, and the NDL2102 DET, (which can tolerate up to 30 mW of optical power) we arrive at a FO Rx column manifold the schematic of which is shown in Figure 3.3-6. Thirty-six such manifolds are required for the full UHF antenna, one per column. In Figure 3.3-6 we also show the block diagrams of the T/R module AMP, the 1x2 switch, along with input and output signal values,

UHF FIBER-OPTIC COMBINER

(One per column, 36 total)

- Largest diameter detector available: 240 μm NEC NDL2102 (700 MHz, 3-dB BW)
- Fiber-optic combiner: 3x3 fiber format (8 used, 1 spare)

  50/125 μm fiber etched to 50/52 μm

  nearly-lossless combining

COMBINER CROSS-SECTION

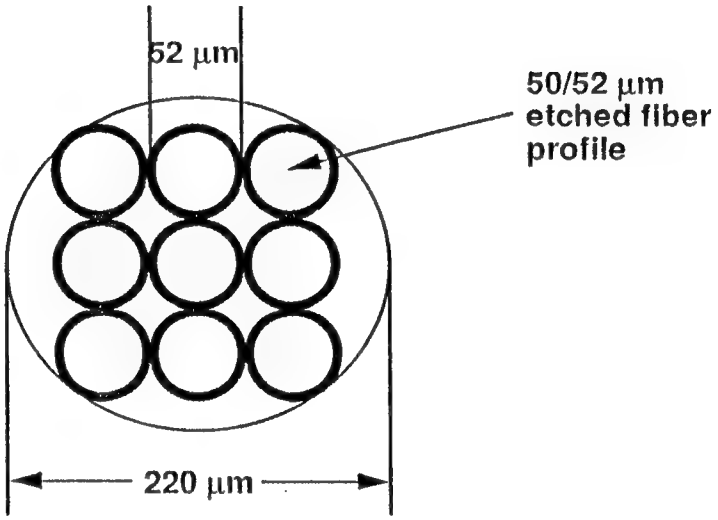

COMBINER SIDE VIEW

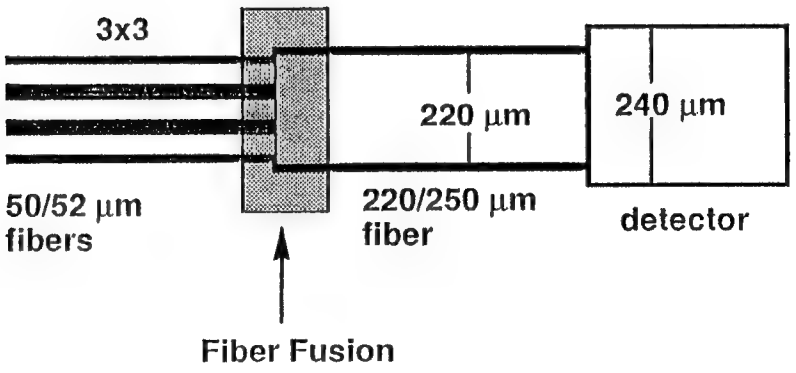

Figure 3.3-5 Schematic of the UHF Fiberoptic 9:1 Combiner

SNRs (SN), etc. At each block level we show the actual maximum signal (S) as well as the resulting SNR (SN). We used the following data: -40.5 dBm maximum received signal by the radiator[6], a T/R module AMP with 30 dB of gain and 3 dB of NF, the SW219 Anzac 1x2 switch with 0.5 dB of loss and 0.5 dB of NF, and a 3-dB attenuator prior to the LNA (used in order to optimize the spurious-free dynamic range (SFDR)). The signal levels, SNR values and DR figures have been calculated using the HP AppCAD software package, an output of which is shown in Figure 3.3-7. Note that the final signal level of 6 dBm corresponds to a single channel prior to coherent signal addition. Also note that the SNR available at each channel of the 8:1 combiner is 63.4 dB to be compared with the 63.5 dB value available at the output of the T/R module's amplifier, i.e., only 0.1 dB of SNR was lost by the photonic manifold. With coherent addition, the signal power will increase by 20log8=18.06 dB to 24.06 dBm and will support a SNR of 72 dB. From Figure 3.3-7 we find that the SFDR is about 55.4 dB per channel @ noise BW of 5 MHz.

3.3.4.4 Weight, Volume, and Power Consumption of the UHF Rx Manifold

To calculate the weight of the UHF photonic Rx manifold we start with the 0.2 kg reference value (see Section3.3.2.4) for the total weight of 8x36 fibers each 10 m long. Each 1x2 RF chip switch weighs 0.3 gr for a total of 8x36x0.3=0.08 kg, each LD transmitter weighs 11 gr for a total of 8x36x11=3.2 kg, whereas the DET assembly weighs about 1 gr. Therefore the overall weight of the UHF photonic manifold can be now be calculated as:

$$\text{WEIGHT} = (0.2+0.08+3.2)\ \text{kg}=\underline{3.5\ \text{kg or}\ 7.7\ \text{lbs}}. \tag{3.3.41}$$

To estimate the UHF Rx manifold volume we use the following data: (1) the volume of 8x36 buffered fibers, each 10 m long and 250 μm in diameter is $8x36x1mx\pi x(125x10^{-6})^2$ m^3 or 0.0005 ft^3, (2) the volume of the LD with the AMP and 1x2 switch is about 3x4x1 cm^3 or 0.0004 ft^3 for a total of $8x36x0.0004=0.12$ ft^3, and (3) the volume of the DET assembly is about 1x0.5x0.3 cm^3 or 0.00005 ft^3. Thus the estimated volume of the UHF Rx manifold is:

$$\text{VOLUME} = (0.0005+ 0.12)\ ft^3=\underline{0.12\ ft^3}. \tag{3.3.42}$$

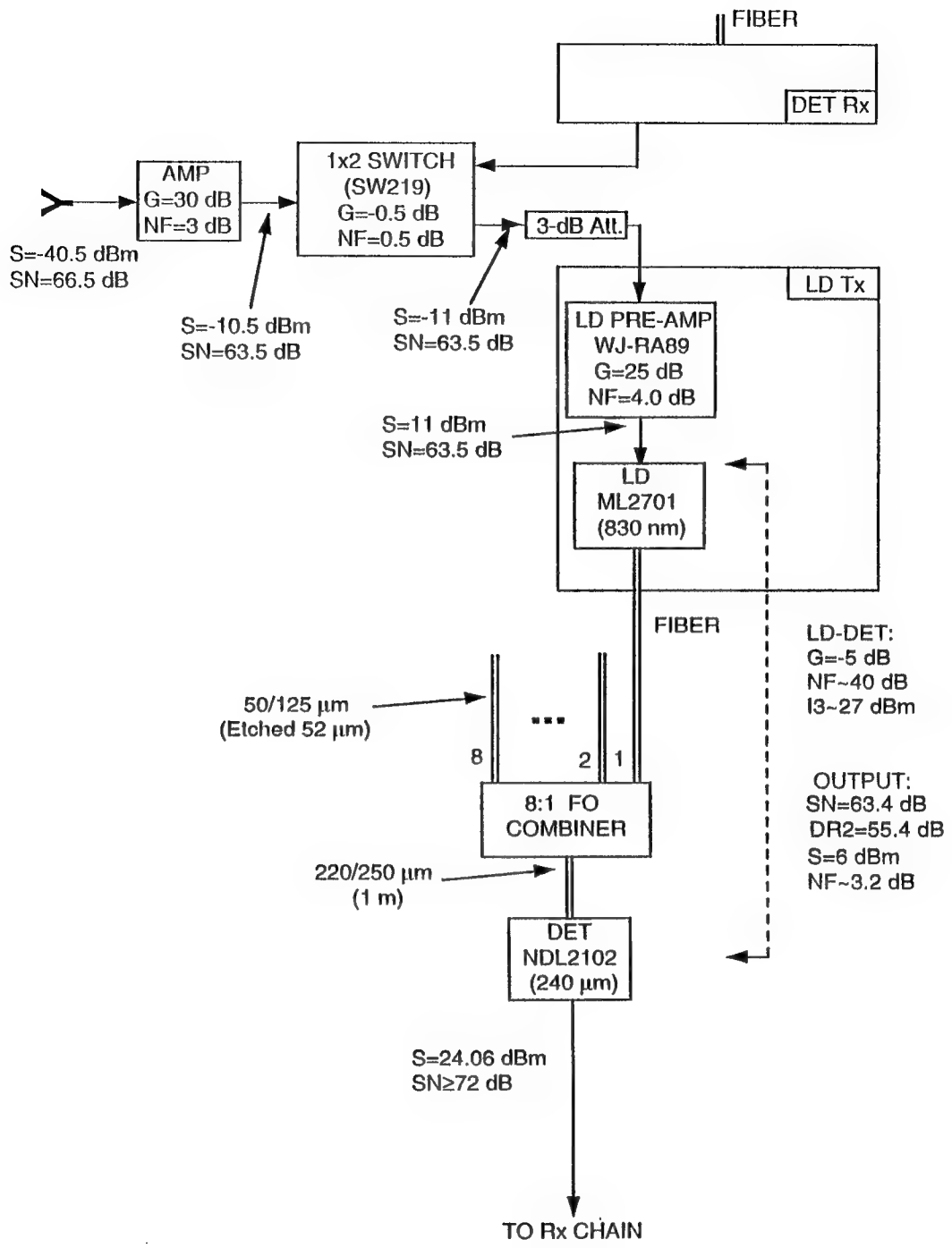

Figure 3.3-6 Detailed Schematic of the column UHF FO Manifold for Rx (36 such manifolds are required for the full UHF antenna)

Hewlett-Packard
AppCAD

12 - 12 - 1993
NoiseCalc (v1.02

Stage:	1	2	3	4	5
Noise Figure (dB)	3.00	0.50	0.00	4.00	40.00
Gain (dB)	30.00	-0.50	-3.00	25.00	-5.00
IP3 (dBm)	25.00	46.00	100.00	37.00	27.00
dNF/dT (dB/deg C)	0.000	0.000	0.000	0.000	0.000
dG/dT (dB/deg C)	0.000	0.000	0.000	0.000	0.000

Sys. Temp (deg C)	25.00	Reference Temp.(deg C)	25.00
Input Power (dBm)	-40.5	Noise Bandwidth (MHz)	5.000

Pout (dBm)	-10.5	-11.0	-14.0	11.0	6.0
dF/dFI (dB/dB)	0.97	0.00	0.00	0.00	0.04
dF/dGI (dB/dB)	-0.03	-0.03	-0.03	-0.03	0.00

Cascade Noise Figure (dB)	3.16	Cascade Gain (dB)	46.50
Noise Temperature (deg K)	310.2	Input IP3 (dBm)	-20.8
Signal-to-Noise ratio (dB)	63.4	Output IP3 (dB)	25.69
Spur Free Dynamic Range (dB)	55.4	IM3 O/P Level (dB)	-33.38
Nominal Detectable Sig. (dB)	%-103.9		

Figure 3.3-7 Output of the HP AppCAD Noise Calc Program for the Block Diagram of Figure3.3-6 (Note that the output values correspond to a single manifold channel)

The power consumption of the manifold is dominated by the power consumption of the LD assembly including the LNA (the DET assembly power consumption is no higher than 100 mW). At STC we recently developed UHF LD-modules with LNAs, which require a total current of about 50 mA @ 4 V, i.e., the power consumption is 200 mW. Using these values as guidelines we find that the total power consumption is about 8x36x0.2 W=57.6 W.

3.3.4.5 S-Band Receive Photonic Manifold Design

This manifold operates over the 3.0-3.5 GHz band and it must be configured in 256 individual 64:1 manifolds. To design the lossless FO combiner we start backwards from the detector whose area will determine the overall frequency response. Due to the higher RF frequencies involved, we will use 1.3 μm optoelectronic components and 9/125 μm single mode fiber (at 1.3 μm LDs and DETs with response up to 20 GHz are readily available). At this band, the typical pin or avalanche DET areas which will allow RF operation up to 3.5 GHz are in the 50-60 μm range. Let us use a conservative 50 μm value which is specified by several manufacturers, e.g., the Mitsubishi InGaAs PD805A2 DET. With a 50 μm detector area, and in order to eliminate optical losses, we must use an output fiber with core no larger than 50 μm. In this case the largest possible N:1 format is determined by the core of the input 9/125 μm single mode fiber, i.e., the smallest etched diameter for the input fiber that can still result in a lossless FO combiner is 9 μm. This means that the largest input fiber format will be 4x4 which corresponds to a lossless FO combiner of 16:1 (see Figure 3.3-8). Therefore to implement a single 64:1 FO manifold we will need four 16:1 lossless FO combiners as well as one 4:1 combiner that is needed in order to combine the outputs of the four 16:1 FO combiners. To eliminate unnecessary optical combination losses, we will add the four outputs in the electrical domain, i.e., a DET will be used at the output of each of the four 16:1 combiners, and the outputs of the 4 DETs will be combined via a conventional 4:1 RF combiner (see Figure 3.3-9). For the above 64:1 hybrid addition scheme, the total combining loss is equal to that of the 4:1 RF combiner, e.g., 1-2 dB.

For a low cost implementation of this manifold we should use low cost (<$100) 1.3 μm LDs such as the BTD ALS1100, which operates up to 3.5 GHz with r_{LD}~0.06 W/A and R_L of 10Ω. We have used this LD before, and have found that it is reliable and it can provide a SNR of about 144 dB @ 3.5 GHz with a NF of 42 dB assuming the use of all-passive components for matching the LD and DET. Similarly, we can use the Mitsubishi PD805A2 DET which has a r_D value of 0.85 A/W and a R_D of 90Ω

(it is determined by the RC constant with C=0.5 pF @ 40 V). Using Equation 3.3.5 and the above values, we find that the link gain for each channel of the 16:1 combiner is $(0.06x0.85)^2$ x 90/10=-16.3dB.

Given the high NF of the links, we will use an LNA prior to each LD in order to set the NF. This is shown in Figure 3.3-9 which shows a complete block diagram of the 64:1 manifold. For the LNA we use the NEC UPG105B/P which has gain of 27 dB and a NF of 1.7 dB. Using the HP AppCAD program we calculated the signal power and SNR values shown next to each block of Figure 3.3-9. The actual output of the AppCAD is shown in Figure 3.3-10. Note that the output values of Figure 3.3-10 correspond to a single FO channel, i.e., prior to coherent detection. Figures 3.3-9 and 3.3-10 show that the SNR at each output of the 16:1 combiner is 28.2 dB, which should be compared with the 29 dB value available at the output of the T/R module's amplifier. This means that only 0.8 dB of SNR was lost by the photonic manifold. The SNR available at the output of the 16:1 combiner is 40.24 dB, the difference being the 16 channel coherent detection. Similarly, at the output of the 4:1 RF combiner the available SNR increases to 46.24 because of the 4 channel coherent addition.

3.3.4.6 Weight, Volume, and Power Consumption of the S-Band Rx Manifold

To calculate the weight of the S-band photonic Rx manifold we start with the 3.44 kg reference value (see Section 3.3.3.4) which is the weight of the 256x64 fibers. Each 1x2 switch weighs 0.3 gr for a total of 256x64x0.3=4.9 kg, each LD transmitter weighs 11 gr for a total of 256x64x0.011=180 kg, whereas the four DET assemblies weigh about 4 gr for a total of 64x0.004= 1 kg. Therefore the overall weight of the manifold can be now be calculated as:

$$\text{WEIGHT} = (3.44 + 4.9 + 180 + 1)\ \text{kg} = \underline{189\ \text{kg or } 417\ \text{lbs}}. \qquad (3.3.43)$$

To estimate the S-band Rx manifold volume we use the following data: (1) the volume of fibers is 0.085 ft^3, (2) the volume of the LD with the AMP and switch is about 3x4x1 cm^3 or 0.0004 ft^3 for a total of 256x64x0.0004=6.6 ft^3, and (3) the volume of the DET assembly is about 1x0.5x0.3 cm^3 or 0.00005 ft^3 for a total of 256x0.00005=0.012 ft^3. Thus the volume of the S-band Rx manifold is dominated by the volume of the LD modules and is of the order $\underline{6.6\ ft^3}$.

Once again, the power consumption of the manifold is dominated by the power consumption of the LD assembly including the LNA (the DET assembly power consumption is no higher than 100 mW). The BTD LD can provide about 1 mW of optical power with ~25 mA of current at about 2 V for a total

S - FIBER-OPTIC COMBINER

(Four per column, 256 total)

- Largest diameter detector available: 50 μm, Mitsubishi PD805A2 (3.5-4 GHz, 3-dB BW)
- Fiber-optic combiner: Four 16:1 FO combiners, one 4:1 RF adder

  each 16:1 has a 4x4 fiber format (all used)

  9/125 μm fiber etched to core , i.e., 9/9 μm

  nearly-lossless combining

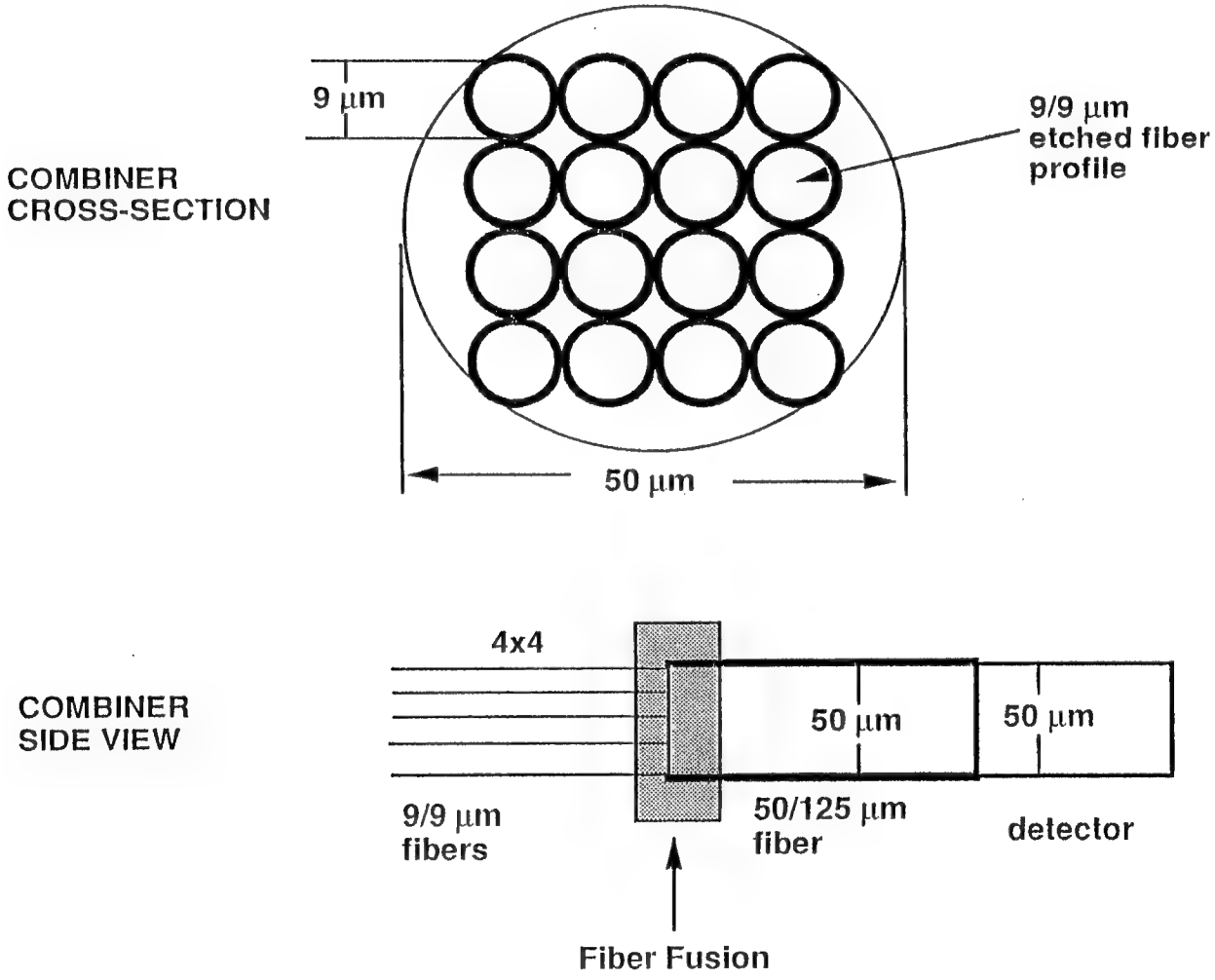

Figure 3.3-8 Schematic of the S-Band Fiberoptic 16:1 Combiner

S-BAND PHOTONIC RECEIVE MANIFOLD: BLOCK DIAGRAM

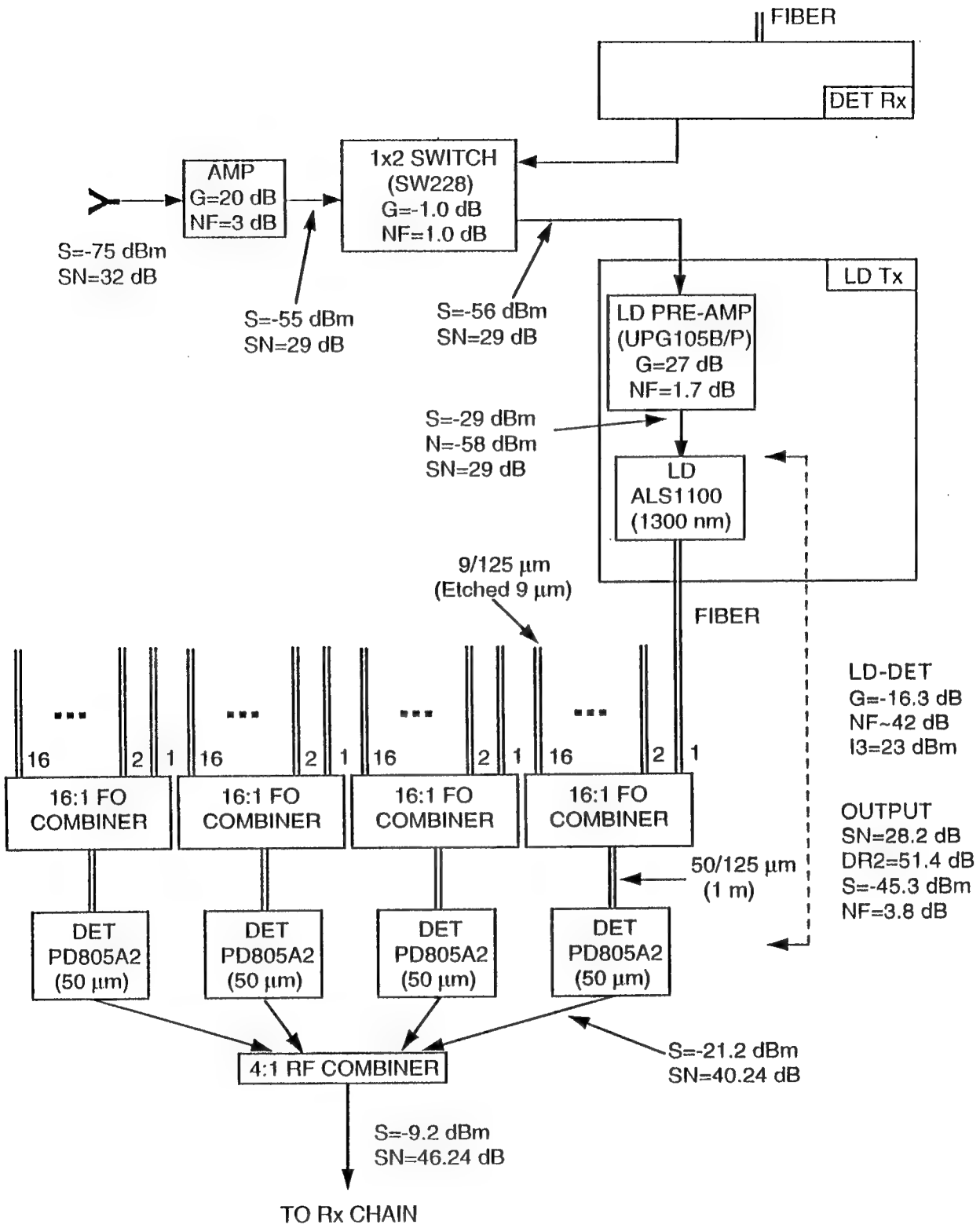

Figure 3.3-9 Detailed Schematic of the Column S-Band FO Manifold for Rx (256 such manifolds are required for the full S-band antenna)

Hewlett-Packard
AppCAD

8 - 10 - 1993
NoiseCalc (v1.02

Stage:	1	2	3	4
Noise Figure (dB)	3.00	1.00	1.70	42.00
Gain (dB)	20.00	-1.00	27.00	-16.30
IP3 (dBm)	25.00	46.00	20.00	23.00
dNF/dT (dB/deg C)	0.000	0.000	0.000	0.000
dG/dT (dB/deg C)	0.000	0.000	0.000	0.000

Sys. Temp (deg C)	25.00	Reference Temp.(deg C)	25.00
Input Power (dBm)	-75.0	Noise Bandwidth (MHz)	5.000

Pout (dBm)	-55.0	-56.0	-29.0	-45.3
dF/dFI (dB/dB)	0.85	0.01	0.01	0.18
dF/dGI (dB/dB)	-0.15	-0.15	-0.15	0.00

Cascade Noise Figure (dB)	3.81	Cascade Gain (dB)	29.70
Noise Temperature (deg K)	406.6	Input IP3 (dBm)	-26.1
Signal-to-Noise ratio (dB)	28.2	Output IP3 (dB)	3.65
Spur Free Dynamic Range (dB)	51.4	IM3 O/P Level (dB)	%-143.19
Nominal Detectable Sig. (dB)	%-103.2		

Figure 3.3-10 Output of the HP AppCAD Noise Calc Program for the Block Diagram of Figure 3.3-10 (Note that the output values correspond to a single manifold channel)

power consumption of 50 mW. To this we must add the power consumption of the LNA which for the case of the UPG105B is 35 mA x 4.5 V=0.16 W. Therefore using the total LD assembly power consumption of 0.16+0.05= 0.21 W we find that the manifold power consumption is 256x64x0.21 W=3.3 kW. Once again we see that the total power consumption is dominated by the LD assembly.

REFERENCES

1. A. Goutzoulis et al, "Prototype binary fiber optic delay line", Westinghouse R&D Report No. 88-1S41-ORFVD-R1, Dec. 7, 1988.
2. C. H. Cox, "Analog FO links with intrinsic gain", Microwave Journal, Sept. 1992, pg.20
3. Spectra Diode Labs, Laser diode product catalog, Note-3, pg 3 for SDL-2350, 1993.
4. See Ref.2 and United Technology technical notes.
5. For example the MICRALASE semiconductor laserd by MICRACOR Inc.
6. Communication with D. Speir of Westinghouse, Electronic Systems Group.

3.4 Weight, Volume and Power Consumption Data

Based upon the hardware implementations described in the preceding sections, an extensive data base of weight, volume and power consumption estimates were derived. This data is summarized in the spreadsheet tables provided on the following pages.

Included are the following:

Table 3.5-1 Monostatic Weight Data - Conventional, 'Digital', 'Optical'

Table 3.5-2 Monostatic Volume Data - Conventional, 'Digital', 'Optical'

Table 3.5-3 Monostatic Power Consumption Data - Conventional, 'Digital', 'Optical'

Table 3.5-4 Monostatic Weight Data - Conventional, 'Digital', Optical/Conventional
(Conventional and 'Digital' Data is Identical to Table 3.5-3)

Table 3.5-5 Monostatic Pwr Consumption Data - Conventional, 'Digital', Optical/Conventional
(Conventional and 'Digital' Data is Identical to Table 3.5-3)

Table 3.5-6 Bistatic Weight Data - Conventional, 'Digital', 'Optical'

Table 3.5-7 Bistatic Volume Data - Conventional, 'Digital', 'Optical'

Table 3.5-8 Bistatic Power Consumption Data - Conventional, 'Digital', 'Optical'

Table 3.5-1 Monostatic Weight (lbs)

			Conventional				'Digital'				'Optical'			
S Band														
Rad. Elements	(inc.Cal.M'fold)					306				306				306
T/R Modules						4096				4096				4096
Power Cnvtr (Array)						733				733				733
Beam Controller						109				109				109
		Manifold	Tx Sum	Rx Sum	Rx Del		Tx Sum	Rx Sum	Rx Del		Tx Sum	Rx Sum	Rx Del	
		Elevation	1348	[Tx Sum]	[Tx Sum]		1348	[TxSum]	[TxSum]		19	417	[Rx Sum]	
		Azimuth	24	[Tx Sum]	24		24	-	-		152	-	-	
		M'fold Subtotal	1372	0	24		1372		0		171	417	0	
		Total S Manifolds				**1396**				**1372**				**588**
	S	Band Sel/STC	(18 Rcv Channels)			12	(36 Shared Rcv Channels)			24	(36 Shared Rcv Channels)			24
	Beamformer	Dn Cnvtr, A/D	(18 Rcv Channels)			14	(256 Rcv Channels; 36 Shared)			200	(256 Rcv Channels; 36 Shared)			200
		Exciter				60				60				60
		LO Distribution	(18 Rcv Channels)			3	(256 Rcv Channels; 36 Shared)			43	(256 Rcv Channels; 36 Shared)			43
		Tx Driver Amp				40				40	(included in Tx Sum Manifold)			0
		Preprocessor	(Demod / SLC)			2	(Demod / SLC / Digital Beamfmr)			312	(Demod / SLC / Digital Beamformer)			312
		Power Convrter	(for Beamformer only)			12	(for Beamformer only)			64	(for Beamformer only)			77
		Total S Beamformer				**1539**				**2115**				**1304**
		Total S-Band Aperture				**6783**				**7359**				**6548**
UHF														
Rad. Elements	(inc.Cal.M'fold)					567				567				567
T/R Modules						2304				2304				2304
Power Cnvtr (Array)					733	Shared			733	Shared			733	Shared
Beam Controller					109	Shared			109	Shared			109	Shared
		Manifold	Tx Sum	Rx Sum	Rx Del		Tx Sum	Rx Sum	Rx Del		Tx Sum	Rx Sum	Rx Del	
		Elevation	56	[Tx Sum]	[Tx Sum]		56	[TxSum]	[TxSum]		1	8	[Rx Sum]	
		Azimuth	7	[Tx Sum]	7		7	-	-		7	-	-	
		M'fold Subtotal	63	0	7		63	0	0		8	8	0	
		Total UHF Manifolds				**70**				**63**				**16**
	UHF	Band Sel/STC	(18 Rcv Channels)			5	(36 Shared Rcv Channels)			10	(36 Shared Rcv Channels)			10
	Beamformer	Dn Cnvtr, A/D	(18 Rcv Channels)		14	Shared	(36 Rcv Channels)		28	Shared	(36 Rcv Channels)		28	Shared
		Exciter			60	Shared			60	Shared			60	Shared
		LO Distribution	(18 Rcv Channels)		3	Shared	(36 Rcv Channels)		6	Shared	(36 Rcv Channels)		6	Shared
		Tx Driver Amp				40				40	(included in Tx Sum Manifold)			0
		Preprocessor	Demod / SLC		2	Shared	(Demod/SLC/DBF)		44	Shared	(Demod / SLC / DBF)		44	Shared
		Power Convrter	(for Bmfmr only)		12	Shared	(for Beamformer only)		10	Shared	(for Beamformer only)		10	Shared
		Total UHF Beamformer				**115**				**113**				**26**
		Total UHF Aperture				**2986**				**2984**				**2897**
Total Dual Band Beamformer (20 + 40)						**1654**				**2228**				**1330**
Shared Portion of Beamformer					**91**	**6%**			**148**	**7%**			**148**	**11%**
Total Dual Band Aperture (21 + 41)						**9769**				**10343**				**9445**
Shared Portion of Aperture					**933**	**10%**			**990**	**10%**			**990**	**10%**

[ ] *means there is no allocation for this function, either because the hardware is shared, or it occupies the same volume as the referenced assembly.*

Table 3.5-2 Monostatic Volume (cubic feet)

			Conventional				Digital				Optical			
S Band														
Rad. Elements	(inc.Cal.M'fold)					13.8				13.8				13.8
T/R Modules						109.6				109.6				109.6
Power Cnvtr (Array)						11.7				11.7				11.7
Beam Controller						1.7				1.7				1.7
	Manifold	Tx Sum	Rx Sum	Rx Del		Tx Sum	Rx Sum	Rx Del		Tx Sum	Rx Sum	Rx Del		
	Elevation	577	[Tx Sum]	[Tx Sum]		577	[TxSum]	[TxSum]		4.28	6.6	[RxSum]		
	Azimuth	[UHF]	[UHF]	[UHF]		[UHF]	-	-		incl'd w/El	-	-		
	M'fold Subtotal	577	0	0		577	0	0		4.28	6.6	0		
	Total S Manifolds				**577**				**577**					**10.88**
S	Band Sel/STC	(18 Rcv Channels)			0.12	(36 Shared Rcv Channels)			0.24	(36 Shared Rcv Channels)				0.24
Beamformer	Dn Cnvtr, A/D	(18 Rcv Channels)			0.14	(256 Rcv Channels; 36 Shared)			2.02	(256 Rcv Channels; 36 Shared)				2.02
	Exciter				0.61				0.61					0.61
	LO Distribution	(18 Rcv Channels)			0.03	(256 Rcv Channels; 36 Shared)			0.44	(256 Rcv Channels; 36 Shared)				0.44
	Tx Driver Amp				0.41				0.41	(included in Tx Sum Manifold)				0
	Preprocessor	(Demod / SLC)			0.02	(Demod / SLC / Digital Bmfr)			3.16	(Demod / SLC / Digital Beamformer)				3.16
	Power Convrter	(for Beamformer only)			0.12	(for Beamformer only)			0.65	(for Beamformer only)				0.65
	Total S Beamformer				**578.45**				**584.53**					**18**
	Total S-Band Aperture				**715.25**				**721.33**					**154.8**
UHF														
Rad. Elements	(inc.Cal.M'fold)				170.8				170.8					170.8
T/R Modules					61.7				61.7					61.7
Power Cnvtr (Array)				11.7	Shared			11.7	Shared			11.7	Shared	
Beam Controller				1.7	Shared			1.7	Shared			1.7	Shared	
	Manifold	Tx Sum	Rx Sum	Rx Del		Tx Sum	Rx Sum	Rx Del		Tx Sum	Rx Sum	Rx Del		
	Elevation	2.5	[Tx Sum]	[Tx Sum]		2.5	[TxSum]	[TxSum]		0.1	0.12	[Rx Sum]		
	Azimuth	3.3	[Tx Sum]	3.3		3.3	-	-		incl'd w/El	-	-		
	M'fold Subtotal	5.8	0	3.3		5.8	0	0		0.1	0.12	0		
	Total UHF Manifolds				**9.1**				**5.8**					**0.22**
UHF	Band Sel/STC	(18 Rcv Channels)			0.05	(for 36 Shared Rcv Channels)			0.1	(for 36 Shared Rcv Channels)				0.1
Beamformer	Dn Cnvtr, A/D	(18 Rcv Channels)		0.14	Shared	(36 Rcv Channels)		0.28	Shared	(36 Rcv Channels)		0.28	Shared	
	Exciter			0.61	Shared			0.61	Shared			1.22	Shared	
	LO Distribution	(18 Rcv Channels)		0.03	Shared	(36 Rcv Channels)		0.06	Shared	(for 36 Rcv Channels)		0.06	Shared	
	Tx Driver Amp				0.41				0.41	(included in Tx Sum Manifold)				0
	Preprocessor	Demod / SLC		0.02	Shared	(Demod/SLC/DBF)		0.44	Shared	(Demod / SLC / DBF)		0.44	Shared	
	Power Convrter	(for Beamfmr only)		0.12	Shared	(for Beamformer only)		0.09	Shared	(for Beamformer only)		0.09	Shared	
	Total UHF Beamformer				**9.56**				**6.31**					**0.32**
	Total UHF Aperture				**242.06**				**238.81**					**232.82**
Total Dual Band Beamformer (20 + 40)					**588.01**				**590.84**					**18.32**
Shared Portion of Beamformer				1	**0%**			1.48	**0%**			2.09		**11%**
Total Dual Band Aperture (21 + 41)					**957.31**				**960.14**					**387.62**
Shared Portion of Aperture				14.32	**1%**			14.88	**2%**			15.49		**4%**

[ ] *means there is no allocation for this function, either because the hardware is shared, or it occupies the same volume as the referenced assembly.*

1						Table 3.5-3 Monostatic Power Consumption (watts)									
2				Conventional				Digital				Optical			
3	**S Band**														
4	Rad. Elements	(inc.Cal.M'fold)				0				0					0
5	T/R Modules					110000				110000					110000
6	Power Cnvtr (Array)					19411				19411					19411
7	Beam Controller					16384				16384					16384
8		Manifold	Tx Sum	Rx Sum	Rx Del		Tx Sum	Rx Sum	Rx Del		Tx Sum	Rx Sum	Rx Del		
9		Elevation	0	(Tx Sum)	(Tx Sum)		0	(TxSum)	(TxSum)		2800	3300	(Rx Sum)		
10		Azimuth	0	(Tx Sum)	0		0	-	-			-	-		
11		M'fold Subtotal	0	0	0		0	0	0		2800	3300	0		
12		**Total S Manifolds**				**0**				**0**					**6100**
13	**S**	Band Sel/STC	(18 Rcv Channels)			36	(36 Shared Rcv Channels)			72	(36 Shared Rcv Channels)				72
14	**Beamformer**	Dn Cnvtr, A/D	(18 Rcv Channels)			360	(256 Rcv Channels; 36 Shared)			5120	(256 Rcv Channels; 36 Shared)				5120
15		Exciter				150				150					150
16		LO Distribution	(18 Rcv Channels)			0	(256 Rcv Channels; 36 Shared)			0	(256 Rcv Channels; 36 Shared)				0
17		Tx Driver Amp				1300				1300	(included in Tx Sum Manifold)				0
18		Preprocessor	(Demod / SLC)			20	(Demod / SLC / Digital Bmfr)			3120	(Demod / SLC / Digital Beamformer)				3120
19		Power Convrter	(for Beamformer only)			373	(for Beamformer only)			1952	(for Beamformer only)				1692
20		**Total S Beamformer**				**2239**				**11714**					**16254**
21		**Total S-Band Aperture**				**148034**				**157509**					**162049**
22															
23	**UHF**														
24	Rad. Elements	(inc.Cal.M'fold)				0				0					0
25	T/R Modules					70300				70300					70300
26	Power Cnvtr (Array)					12406				12406					12406
27	Beam Controller					288				288					288
28		Manifold	Tx Sum	Rx Sum	Rx Del		Tx Sum	Rx Sum	Rx Del		Tx Sum	Rx Sum	Rx Del		
29		Elevation	0	(Tx Sum)	(Tx Sum)		0	(TxSum)	(TxSum)		443	58	(Rx Sum)		
30		Azimuth	0	(Tx Sum)	0		0	-	-			-	-		
31		M'fold Subtotal	0	0	0		0	0	0		443	58	0		
32		**Total UHF Manifolds**				**0**				**0**					**501**
33	**UHF**	Band Sel/STC	(18 Rcv Channels)			36	(for 36 Shared Rcv Channels)			72	(for 36 Shared Rcv Channels)				72
34	**Beamformer**	Dn Cnvrtr, A/D	(18 Rcv Channels)			360	(36 Rcv Channels)			720	(36 Rcv Channels)				720
35		Exciter				150				150					150
36		LO Distribution	(18 Rcv Channels)			0	(36 Rcv Channels)			0	(for 36 Rcv Channels)				0
37		Tx Driver Amp				1300				1300	(included in Tx Sum Manifold)				0
38		Preprocessor	Demod/SLC			20	(Demod/SLC/DBF)			439	(Demod / SLC / DBF)				439
39		Power Convrter	(for Bmfmr only)			373	(for Beamformer only)			536	(for Beamformer only)				276
40		**Total UHF Beamformer**				**2239**				**3217**					**2158**
41		**Total UHF Aperture**				**85233**				**86211**					**85152**

Table 3.5-4 Monostatic Weight for Optical/Conventional (lbs)

			Conventional				'Digital'				Optical/Conventional			
S Band														
Rad. Elements	(inc.Cal.M'fold)				306				306				306
T/R Modules					4096				4096				4096
Power Cnvtr (Array)					733				733				733
Beam Controller					109				109				109
	Manifold	Tx Sum	Rx Sum	Rx Del		Tx Sum	Rx Sum	Rx Del		Tx Sum	Rx Sum	Rx Del	
	Elevation	1348	(Tx Sum)	(Tx Sum)		1348	(TxSum)	(TxSum)		19	417	(Rx Sum)	
	Azimuth	24	(Tx Sum)	24		24	-	-		152	48	-	
	M'fold Subtotal	1372	0	24		1372		0		171	465	0	
	Total S Manifolds				1396				1372				636
S	Band Sel/STC	(18 Rcv Channels)			12	(36 Shared Rcv Channels)			24	(18 Receive Channels)			12
Beamformer	Dn Cnvtr, A/D	(18 Rcv Channels)			14	(256 Rcv Channels; 36 Shared)			200	(18 Receive Channels)			14
	Exciter				60				60				60
	LO Distribution	(18 Rcv Channels)			3	(256 Rcv Channels; 36 Shared)			43	(18 Receive Channels)			3
	Tx Driver Amp				40				40	(included in Tx Sum Manifold)			0
	Preprocessor	(Demod / SLC)			2	(Demod / SLC / Digital Beamfmr)			312	(Demod / SLC)			2
	Power Convrter	(for Beamformer only)			12	(for Beamformer only)			64	(for Beamformer only)			44
	Total S Beamformer				1539				2115				771
	Total S-Band Aperture				6783				7359				6015
UHF													
Rad. Elements	(inc.Cal.M'fold)				567				567				567
T/R Modules					2304				2304				2304
Power Cnvtr (Array)				733	Shared			733	Shared			733	Shared
Beam Controller				109	Shared			109	Shared			109	Shared
	Manifold	Tx Sum	Rx Sum	Rx Del		Tx Sum	Rx Sum	Rx Del		Tx Sum	Rx Sum	Rx Del	
	Elevation	56	(Tx Sum)	(Tx Sum)		56	(TxSum)	(TxSum)		1	8	(Rx Sum)	
	Azimuth	7	(Tx Sum)	7		7	-	-		7	14	-	
	M'fold Subtotal	63	0	7		63	0	0		8	22	0	
	Total UHF Manifolds				70				63				30
UHF	Band Sel/STC	(18 Rcv Channels)			5	(36 Shared Rcv Channels)			10	(18 Receive Channels)			5
Beamformer	Dn Cnvrtr, A/D	(18 Rcv Channels)		14	Shared	(36 Rcv Channels)		28	Shared	(18 Receive Channels)		14	Shared
	Exciter			60	Shared			60	Shared			60	Shared
	LO Distribution	(18 Rcv Channels)		3	Shared	(36 Rcv Channels)		6	Shared	(18 Receive Channels)		3	Shared
	Tx Driver Amp				40				40	(included in Tx Sum Manifold)			0
	Preprocessor	Demod / SLC		2	Shared	(Demod/SLC/DBF)		44	Shared	(Demod / SLC)		2	Shared
	Power Convrter	(for Bmfmr only)		12	Shared	(for Beamformer only)		10	Shared	(for Beamformer only)		7	Shared
	Total UHF Beamformer				115				113				35
	Total UHF Aperture				2986				2984				2906
Total Dual Band Beamformer (20 + 40)					1654				2228				806
Shared Portion of Beamformer				91	6%			148	7%			86	11%
Total Dual Band Aperture (21 + 41)					9769				10343				8921
Shared Portion of Aperture				933	10%			990	10%			928	10%

1						Table 3.5-5 Monostatic Power Consumption for Optical/Conventional (watts)									
2				Conventional				'Digital'				Optical/Conventional			
3	**S Band**														
4	Rad. Elements	(inc.Cal.M'fold)				0				0					0
5	T/R Modules					110000				110000					110000
6	Power Cnvtr (Array)					19411				19411					19411
7	Beam Controller					16384				16384					16384
8		Manifold	Tx Sum	Rx Sum	Rx Del		Tx Sum	Rx Sum	Rx Del		Tx Sum	Rx Sum	Rx Del		
9		Elevation	0	(Tx Sum)	(Tx Sum)		0	(TxSum)	(TxSum)		2800	3300	(Rx Sum)		
10		Azimuth	0	(Tx Sum)	0		0	-	-			-	-		
11		M'fold Subtotal	0	0	0		0	0	0		2800	3300	0		
12		**Total S Manifolds**				0				0					6100
13	**S**	Band Sel/STC	(18 Rcv Channels)			36	(36 Shared Rcv Channels)			72	(18 Rcv Channels)				36
14	**Beamformer**	Dn Cnvtr, A/D	(18 Rcv Channels)			360	(256 Rcv Channels; 36 Shared)			5120	(18 Rcv Channels)				360
15		Exciter				150				150					150
16		LO Distribution	(18 Rcv Channels)			0	(256 Rcv Channels; 36 Shared)			0	(18 Rcv Channels)				0
17		Tx Driver Amp				1300				1300	(included in Tx Sum Manifold)				0
18		Preprocessor	(Demod / SLC)			20	(Demod / SLC / Digital Bmfr)			3120	(Demod / SLC)				20
19		Power Convrter	(for Beamformer only)			373	(for Beamformer only)			1952	(for Beamformer only)				1667
20		**Total S Beamformer**				2239				11714					8333
21		**Total S-Band Aperture**				148034				157509					154128
22															
23	**UHF**														
24	Rad. Elements	(inc.Cal.M'fold)				0				0					0
25	T/R Modules					70300				70300					70300
26	Power Cnvtr (Array)					12406				12406					12406
27	Beam Controller					288				288					288
28		Manifold	Tx Sum	Rx Sum	Rx Del		Tx Sum	Rx Sum	Rx Del		Tx Sum	Rx Sum	Rx Del		
29		Elevation	0	(Tx Sum)	(Tx Sum)		0	(TxSum)	(TxSum)		443	58	(Rx Sum)		
30		Azimuth	0	(Tx Sum)	0		0	-	-			-	-		
31		M'fold Subtotal	0	0	0		0	0	0		443	58	0		
32		**Total UHF Manifolds**				0				0					501
33	**UHF**	Band Sel/STC	(18 Rcv Channels)			36	(for 36 Shared Rcv Channels)			72	(18 Rcv Channels)				36
34	**Beamformer**	Dn Cnvrtr, A/D	(18 Rcv Channels)			360	(36 Rcv Channels)			720	(18 Rcv Channels)				360
35		Exciter				150				150					150
36		LO Distribution	(18 Rcv Channels)			0	(36 Rcv Channels)			0	(18 Rcv Channels)				0
37		Tx Driver Amp				1300				1300	(included in Tx Sum Manifold)				0
38		Preprocessor	Demod/SLC			20	(Demod/SLC/DBF)			439	(Demod / SLC)				20
39		Power Convrter	(for Bmfmr only)			373	(for Beamformer only)			536	(for Beamformer only)				267
40		**Total UHF Beamformer**				2239				3217					1334
41		**Total UHF Aperture**				85233				86211					84328

Table 3.5-6 Bistatic Weight (lbs)

			Conventional				'Digital'				'Optical'			
S Band														
Rad. Elements	(inc.Cal.M'fold)					306				306				306
Receive Modules						1229				1229				1229
Power Cnvtr (Array)						328				328				328
Beam Controller						109				109				109
	Manifold	Tx Sum	Rx Sum	Rx Del			Tx Sum	Rx Sum	Rx Del		Tx Sum	Rx Sum	Rx Del	
	Elevation	-	2193	(Rx Sum)			-	1348	(RxSum)		-	417	(Rx Sum)	
	Azimuth	-	960	960			-	-	-		-	-	-	
	M'fold Subtotal	0	3153	960			0	1348	0		0	417	0	
	Total S Manifolds					4113				1348				417
S	Band Sel/STC	(18 Rcv Channels)				12	(36 Shared Rcv Channels)			24	(36 Shared Rcv Channels)			24
Beamformer	Dn Cnvtr, A/D	(80 Rcv Channels)				62	(256 Rcv Channels; 36 Shared)			200	(256 Rcv Channels; 36 Shared)			200
	Exciter					60				60				60
	LO Distribution	(80 Rcv Channels)				13	(256 Rcv Channels; 36 Shared)			43	(256 Rcv Channels; 36 Shared)			43
	Tx Driver Amp	(not applicable)				0				0	(included in Tx Sum Manifold)			0
	Preprocessor	(Demod / SLC)				160	(Demod / SLC / Digital Beamfmr)			2049	(Demod / SLC / Digital Beamformer)			2049
	Power Convrter	(for Beamformer only)				17	(for Beamformer only)			71	(for Beamformer only)			93
	Total S Beamformer					4437				3795				2886
	Total S-Band Aperture					6409				5767				4858
UHF														
Rad. Elements	(inc.Cal.M'fold)					567				567				567
Receive Modules						230				230				230
Power Cnvtr (Array)				328	Shared				328	Shared			328	Shared
Beam Controller				109	Shared				109	Shared			109	Shared
	Manifold	Tx Sum	Rx Sum	Rx Del			Tx Sum	Rx Sum	Rx Del		Tx Sum	Rx Sum	Rx Del	
	Elevation	-	56	(Rx Sum)			-	56	(RxSum)		-	8	(Rx Sum)	
	Azimuth	-	7	7			-	-	-		-	-	-	
	M'fold Subtotal	0	63	7			0	56	0		0	8	0	
	Total UHF Manifolds					70				56				8
UHF	Band Sel/STC	(18 Rcv Channels)				5	(36 Shared Rcv Channels)			10	(36 Shared Rcv Channels)			10
Beamformer	Dn Cnvtr, A/D	(18 Rcv Channels)		14	Shared		(36 Rcv Channels)		28	Shared	(36 Rcv Channels)		28	Shared
	Exciter			60	Shared				60	Shared			60	Shared
	LO Distribution	(18 Rcv Channels)		3	Shared		(36 Rcv Channels)		6	Shared	(36 Rcv Channels)		6	Shared
	Tx Driver Amp	(not applicable)				0				0	(included in Tx Sum Manifold)			0
	Preprocessor	Demod / SLC		2	Shared		(Demod/SLC/DBF)		44	Shared	(Demod / SLC / DBF)		44	Shared
	Power Convrter	(for Bmfmr only)		12	Shared		(for Beamformer only)		10	Shared	(for Beamformer only)		10	Shared
	Total UHF Beamformer					75				66				18
	Total UHF Aperture					872				863				815
Total Dual Band Beamformer (20 + 40)						4512				3861				2904
Shared Portion of Beamformer				91	2%				148	4%			148	5%
Total Dual Band Aperture (21 + 41)						7281				6630				5673
Shared Portion of Aperture				528	7%				585	9%			585	10%

[ ] *means there is no allocation for this function, either because the hardware is shared, or it occupies the same volume as the referenced assembly.*

Table 3.5-7 Bistatic Volume (cubic feet)

			Conventional				Digital				Optical			
S Band														
Rad. Elements	(inc.Cal.M'fold)					13.8				13.8				13.8
Receive Modules						9.5				9.5				9.5
Power Cnvtr (Array)						5.2				5.2				5.2
Beam Controller						1.7				1.7				1.7
	Manifold	Tx Sum	Rx Sum	Rx Del			Tx Sum	Rx Sum	Rx Del		Tx Sum	Rx Sum	Rx Del	
	Elevation	-	587	[Rx Sum]			-	577	[RxSum]		-	6.6	[RxSum]	
	Azimuth	-	[UHF]	[UHF]			-	-	-		-	-	-	
	M'fold Subtotal	0	587	0			0	577	0		0	6.6	0	
	Total S Manifolds					587				577				6.6
S	Band Sel/STC	(18 Rcv Channels)				0.12	(36 Shared Rcv Channels)			0.24	(36 Shared Rcv Channels)			0.24
Beamformer	Dn Cnvtr, A/D	(80 Rcv Channels)				0.62	(256 Rcv Channels; 36 Shared)			2.02	(256 Rcv Channels; 36 Shared)			2.02
	Exciter					0.61				0.61				0.61
	LO Distribution	(80 Rcv Channels)				0.03	(256 Rcv Channels; 36 Shared)			0.44	(256 Rcv Channels; 36 Shared)			0.44
	Tx Driver Amp	(not applicable)				0	(not applicable)			0	(not applicable)			0
	Preprocessor	(Demod / SLC)				1.6	(Demod / SLC / Digital Bmfr)			20.7	(Demod / SLC / Digital Beamformer)			20.7
	Power Convrter	(for Beamformer only)				0.17	(for Beamformer only)			0.72	(for Beamformer only)			0.72
	Total S Beamformer					590.15				601.73				31.33
	Total S-Band Aperture					620.35				631.93				61.53
UHF														
Rad. Elements	(inc.Cal.M'fold)					170.8				170.8				170.8
Receive Modules						5.3				5.3				5.3
Power Cnvtr (Array)				5.2	Shared				5.2	Shared			5.2	Shared
Beam Controller				1.7	Shared				1.7	Shared			1.7	Shared
	Manifold	Tx Sum	Rx Sum	Rx Del			Tx Sum	Rx Sum	Rx Del		Tx Sum	Rx Sum	Rx Del	
	Elevation	-	2.5	[Rx Sum]			-	2.5	[Rx Sum]		-	0.12	[Rx Sum]	
	Azimuth	-	3.3	3.3			-	-	-		-	-	-	
	M'fold Subtotal	0	5.8	3.3			0	2.5	0		0	0.12	0	
	Total UHF Manifolds					9.1				2.5				0.12
UHF	Band Sel/STC	(18 Rcv Channels)				0.05	(for 36 Shared Rcv Channels)			0.1	(for 36 Shared Rcv Channels)			0.1
Beamformer	Dn Cnvrtr, A/D	(18 Rcv Channels)		0.14	Shared		(36 Rcv Channels)		0.28	Shared	(36 Rcv Channels)		0.28	Shared
	Exciter			0.61	Shared				0.61	Shared			1.22	Shared
	LO Distribution	(18 Rcv Channels)		0.03	Shared		(36 Rcv Channels)		0.06	Shared	(for 36 Rcv Channels)		0.06	Shared
	Tx Driver Amp	(not applicable)				0	(not applicable)			0	(not applicable)			0
	Preprocessor	Demod / SLC		0.02	Shared		(Demod/SLC/DBF)		0.44	Shared	(Demod / SLC / DBF)		0.44	Shared
	Power Convrter	(for Beamfmr only)		0.12	Shared		(for Beamformer only)		0.09	Shared	(for Beamformer only)		0.09	Shared
	Total UHF Beamformer					9.15				2.6				0.22
	Total UHF Aperture					185.25				178.7				176.32
Total Dual Band Beamformer (20 + 40)						599.3				604.33				31.55
Shared Portion of Beamformer				1	0%				1.48	0%			2.09	7%
Total Dual Band Aperture (21 + 41)						805.6				810.63				237.85
Shared Portion of Aperture				7.82	1%				8.38	1%			8.99	4%

[ ] *means there is no allocation for this function, either because the hardware is shared, or it occupies the same volume as the referenced assembly.*

1						Table 3.5-8 Bistatic Power Consumption (watts)								
2				Conventional				'Digital'				'Optical'		
3	**S Band**													
4	Rad. Elements	(inc.Cal.M'fold)				0				0				0
5	Receive Modules					49152				49152				49152
6	Power Cnvtr (Array)					8674				8674				8674
7	Beam Controller					16384				16384				16384
8		Manifold	Tx Sum	Rx Sum	Rx Del		Tx Sum	Rx Sum	Rx Del		Tx Sum	Rx Sum	Rx Del	
9		Elevation	-	0	(Rx Sum)		-	0	(RxSum)		-	3300	(Rx Sum)	
10		Azimuth	-	0	0		-	-	-		-	-	-	
11		M'fold Subtotal	0	0	0		0	0	0		0	3300	0	
12		**Total S Manifolds**				0				0				3300
13	**S**	Band Sel/STC	(18 Rcv Channels)			36	(36 Shared Rcv Channels)			72	(36 Shared Rcv Channels)			72
14	**Beamformer**	Dn Cnvtr, A/D	(80 Rcv Channels)			1600	(256 Rcv Channels; 36 Shared)			5120	(256 Rcv Channels; 36 Shared)			5120
15		Exciter				150				150				150
16		LO Distribution	(80 Rcv Channels)			0	(256 Rcv Channels; 36 Shared)			0	(256 Rcv Channels; 36 Shared)			0
17		Tx Driver Amp	(not applicable)			0	(not applicable)			0	(not applicable)			0
18		Preprocessor	(Demod / SLC)			1600	(Demod / SLC / Digital Bmfr)			20490	(Demod / SLC / Digital Beamformer)			20490
19		Power Convrter	(for Beamformer only)			677	(for Beamformer only)			5172	(for Beamformer only)			5832
20		**Total S Beamformer**				4063				31004				34964
21		**Total S-Band Aperture**				78273				105214				109174
22														
23	**UHF**													
24	Rad. Elements	(inc.Cal.M'fold)				0				0				0
25	Receive Modules					864				864				864
26	Power Cnvtr (Array)					152				152				152
27	Beam Controller					288				288				288
28		Manifold	Tx Sum	Rx Sum	Rx Del		Tx Sum	Rx Sum	Rx Del		Tx Sum	Rx Sum	Rx Del	
29		Elevation	-	0	(Rx Sum)		-	(TxSum)	(TxSum)		-	58	(Rx Sum)	
30		Azimuth	-	0	0		-	-	-		-	-	-	
31		M'fold Subtotal	0	0	0		0	0	0		0	58	0	
32		**Total UHF Manifolds**				0				0				58
33	**UHF**	Band Sel/STC	(18 Rcv Channels)			36	(for 36 Shared Rcv Channels)			72	(for 36 Shared Rcv Channels)			72
34	**Beamformer**	Dn Cnvrtr, A/D	(18 Rcv Channels)			360	(36 Rcv Channels)			720	(36 Rcv Channels)			720
35		Exciter				150				150				150
36		LO Distribution	(18 Rcv Channels)			0	(36 Rcv Channels)			0	(for 36 Rcv Channels)			0
37		Tx Driver Amp	(not applicable)			0	(not applicable)			0	(included in Tx Sum Manifold)			0
38		Preprocessor	Demod/SLC			20	(Demod/SLC/DBF)			439	(Demod / SLC / DBF)			439
39		Power Convrter	(for Bmfmr only)			188	(for Beamformer only)			276	(for Beamformer only)			288
40		**Total UHF Beamformer**				754				1657				1727
41		**Total UHF Aperture**				2058				2961				3031

APPENDIX A

AVERAGE SIDELOBE LEVELS IN CORPORATE FEED ARRAYS

A.1 INTRODUCTION

Simple relations for the average sidelobe level associated with random, independent amplitude and phase errors in the excitation of an array antenna have been widely published.[1] Typically, the net error corresponding to each element is assumed to be independent and not account for the origin of the errors in the feed network. Errors occurring early in the division of a multilevel feed network such as a corporate-type structure, however, will result in highly correlated errors at the array level. In fact, the errors at the array level will, in general, contain both correlated and uncorrelated components even though the sources of the errors throughout the feed network are independent. Correlated errors will tend to both raise sidelobes and constrain their impact nearer to broadside.

A simple model of average sidelobe level is presented here that accounts for the variation of average sidelobe level throughout the radiation sphere, not just in the principal planes, arising from amplitude and phase errors originating at different levels in a corporate combiner feed network. The expressions are most accurate for high aperture efficiency weighting, $\eta \approx 1$, but, as will be discussed later, are likely to be reasonably accurate for smaller η as well.

A.2 AVERAGE SIDELOBES

The average sidelobe gain associated with random errors at the i^{th} combiner level (higher values of i corresponding to combiner levels nearer the radiating elements) and normalized to the broadside gain can be expressed as:

$$S_{r,i}(t_{az},t_{el})\frac{\sigma_i^{\,2} g_i(t_{az},t_{el})}{n_i \eta_i g_i(0,0)} \qquad \text{(A-1)}$$

---

[1] See, for example, T.C. Cheston, "Effects of Random Errors on Sidelobes of Phased Arrays," Antenna Designer's Notebook, IEEE Antennas and Propagation Society Newsletter, April 1985.

where t_{az} and t_{el} are the azimuth and elevation sine space coordinates of a field point normalized, respectively, by the full array azimuth and elevation plane beamwidths. Also, σ_i^2 = sum of variances of radian phase error and fractional amplitude error associated with the i^{th} level, n_i = number of "subarrays" associated with the i^{th} level, η_i = weighting efficiency corresponding to the distribution of power between these subarrays, and $g_i(t_{az}, t_{el})$ is the gain of each of these subarrays. The number and size of subarrays associated with a combiner level is illustrated by the 48 element linear array of Figure A-1(a). The feed network is composed of four levels of combiners: one 2:1 combiner at Level 1, two 3:1 combiners at Level 2, six 2:1 combiners at Level 3, and 12 4:1 combiners at Level 4. Errors introduced at Level 3, therefore, are associated with 6 x 2 = 12 subarrays, each of 48/12 = 4 elements (Figure A-1(b)). The decorrelation length of corresponding errors at the array element level is four elements. Similarly, there are 2 x 3 = 6 subarrays, each of 48/6 = 8 elements, associated with Level 2 errors (Figure A-1(c)). The decorrelation length for Level 2 errors is eight elements. Finally, Level 1 errors are associated with two 24 element subarrays, and Level 4 errors are simply the array level independent errors, one per radiating element.

Returning to the planar case, if the i^{th} combiner level combines only along one axis (azimuth or elevation), then $\eta = \eta_{az}$ or $\eta_1 = \eta_{el}$, respectively, where η_{az} is the efficiency associated with the azimuth plane weight taper and η_{el} is that for the elevation plane. Otherwise, $\eta_i \approx \eta_{az} \; x \; \eta_{el} = \eta$. If the random error average sidelobe level is to be assessed only within the mainbeam region of the subarray pattern, $g_i(t_{az}, t_{el}) \approx g_i(0,0)$ and (1) reduces to a more commonly found form. The sidelobe levels associated with a multilevel feed network, such as a corporate feed, however, is best treated by retaining the subarray gain dependence. A simplification is obtained by approximating $g_i(t_{az}, t_{el}) / g_i(0,0)$ by a two-level pattern, and since there are $n_i = n_{az,i} \; x \; n_{el,i}$ subarrays corresponding to the i^{th} level where $n_{az,i}$ = number of azimuth plane "columns" and $n_{el,i}$ = number of elevation plane "rows" of total number of ports on the radiator side of the i^{th} level combiners, it follows that

$$g_i(t_{az} t_{el}) / g_i(0,0) = \begin{cases} 1 & |t_{az}| < \frac{n_{az,i}}{2} \quad and \quad |t_{el}| < \frac{n_{el,i}}{2} \\ 0 & otherwise \end{cases} \qquad \text{(A-2)}$$

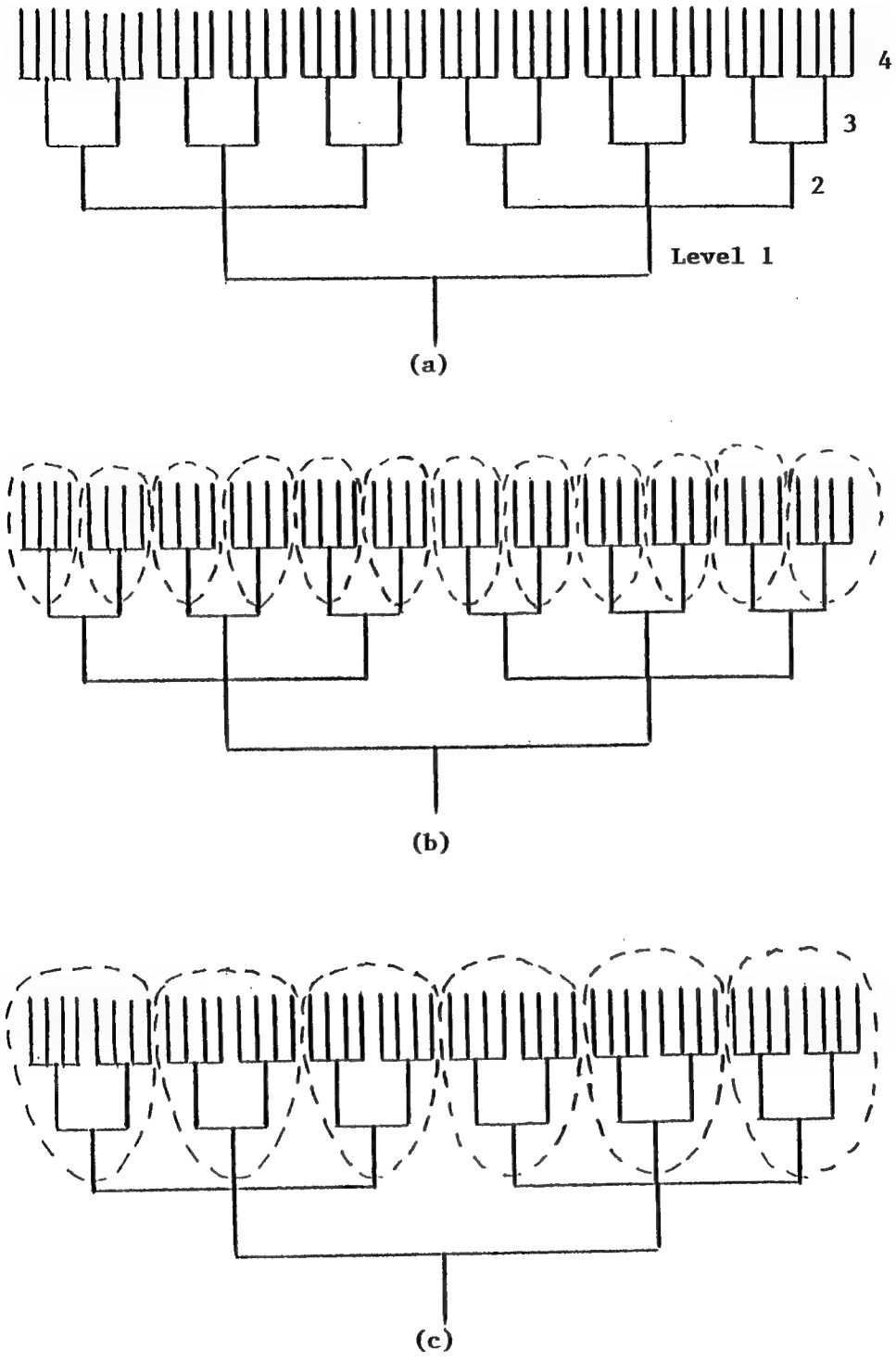

Figure A-1. 48 Element Linear Array (a), Level 3 Subarrays (b), Level 2 Subarrays (c)

The sidelobe level within Region i, that identified by the inequalities in (2), arises from errors in levels i,i+1.., m for an m level corporate feed. Since the errors between levels are independent, the average relative sidelobe level (with respect to the broadside gain) is given by

$$S_r(t_{az},t_{el}) = \sum_{i=1}^{m} S_{r,i}(t_{az},t_{el}) \tag{A-3}$$

By combining (A-1), (A-2), and (A-3), and recognizing the nesting feature of successive level subarray patterns, there results

$$S_r(t_{az},t_{el}) = \begin{cases} \dfrac{\sigma_m^2}{n_m \eta_m} & \dfrac{n_{az,m-1}}{2} < |t_{az}| < \dfrac{n_{az,m}}{2} \text{ and } \dfrac{n_{el,m-1}}{2} < |t_{el}| < \dfrac{n_{el,m}}{2} \\ \dfrac{\sigma_m^2}{n_m \eta_m} + \dfrac{\sigma_{m-1}^2}{n_{m-1}\eta_{m-1}} & \dfrac{n_{az,m-2}}{2} < |t_{az}| < \dfrac{n_{az,m-1}}{2} \text{ and } \dfrac{n_{el,m-2}}{2} < |t_{el}| < \dfrac{n_{el,m-1}}{2} \\ \bullet & \\ \bullet & \\ \bullet & \\ \sum_{j=1}^{m} + \dfrac{\sigma_j^2}{n_j \eta_j} & |t_{az}| < \dfrac{n_{az,1}}{2} \text{ and } |t_{el}| < \dfrac{n_{el,1}}{2} \end{cases} \tag{A-4}$$

The average sidelobe level with respect to isotropic is given by

$$S_{iso}(t_{az},t_{el}) = m\eta S_r(t_{az},t_{el})\, g_m(t_{az},t_{el}) \tag{A-5}$$

where the m^{th} level element pattern is, of course, that of a radiating element which has a peak value $\approx \pi$.

These expressions assume equal subarray patterns corresponding to a combiner level. A weighted aperture, however, implies that the subarray patterns corresponding to a lower level of combining are, in general, not equal, and, therefore, that the pattern multiplication implied in (A-1) is not strictly correct. That the subarray patterns are likely to be quite similar, however, can be demonstrated by considering a cosine weighted aperture, unity at center and zero at opposing edges. Let the aperture be divided into 32 subarrays along one dimension.. The normalized subarray radiation patterns are shown in Figure A-2. The patterns are reasonably close, especially in sidelobe structure.

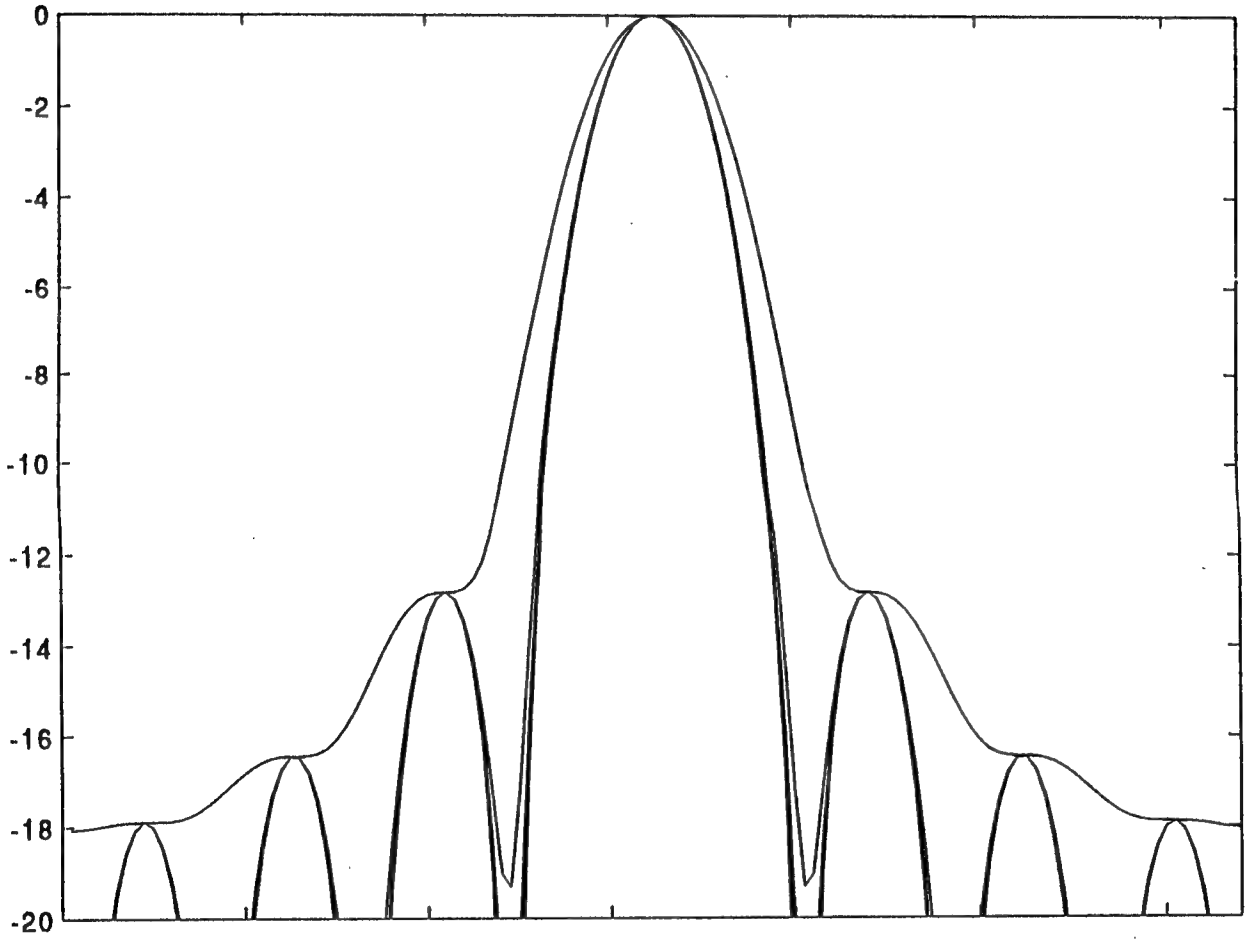

Figure A-2. Normalized Subarray Radiation Patterns

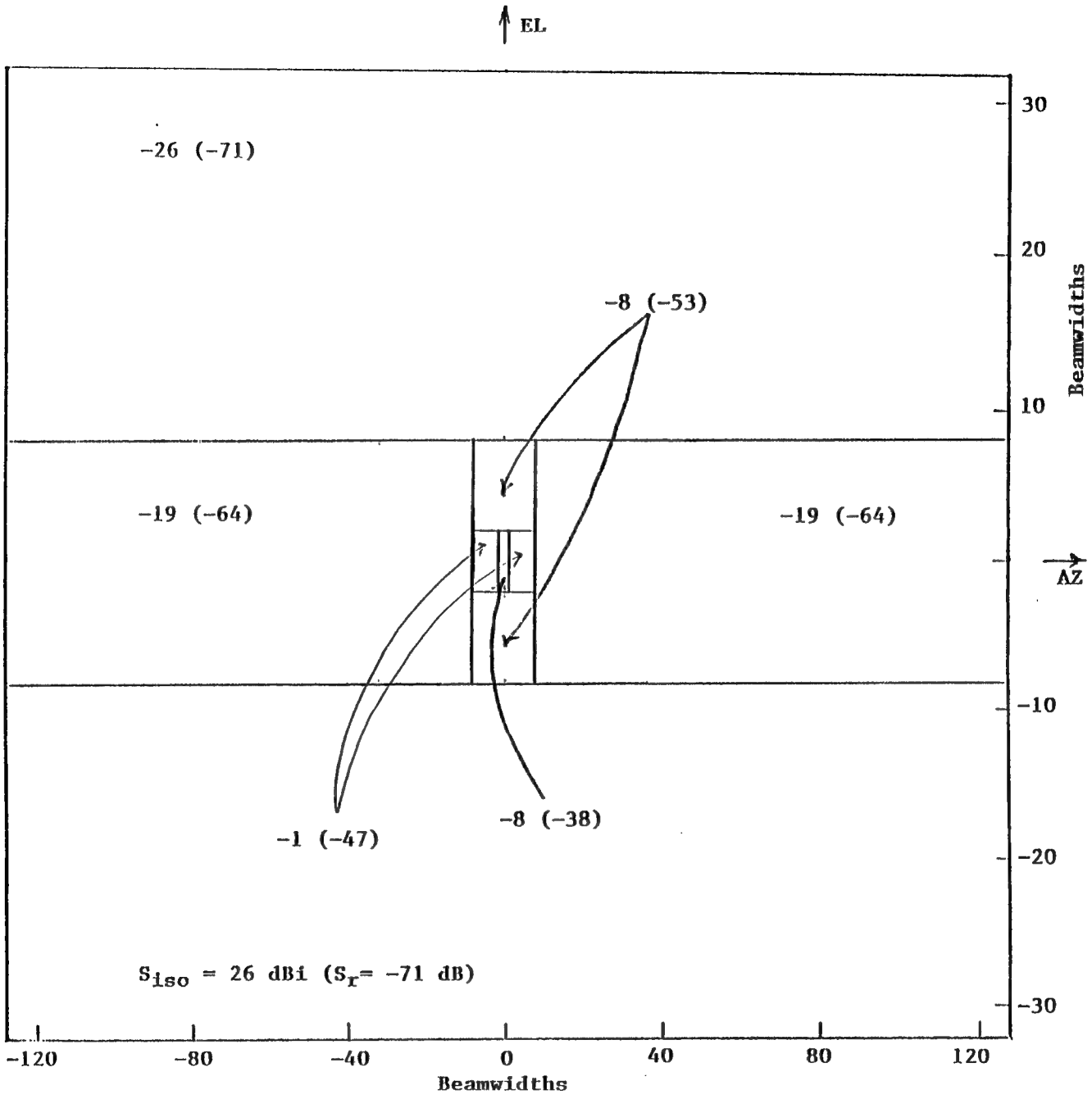

Figure A-3 Average Sidelobe Error Due to Random Errors in Interleaved Az/El Combiner

A.1 EXAMPLE

As an example of the application of (A-4) and (A-5), consider an array of 16,384 elements positioned in 64 rows and 256 columns. Consider a row as parallel to the azimuth plane and a column as parallel to the elevation plane. Consider two candidate corporate feed networks, an "interleaved azimuth/elevation combiner level" network (Figure 3-1) and a "sequential azimuth/elevation combiner level" network (Figure 3-3). Each network has six combiner levels. Assume that the channels (complete paths from transmitter/receiver to radiating elements) can be matched with six-bit phase shifters and eight-bit attenuators to within 3.9×10^{-3} of phase error variance (one percent of a wavelength RMS) and 10^{-4} of fractional amplitude error variance (one percent RMS) in addition to the quantization phase and amplitude error variances of 8.0×10^{-4} and 1.3×10^{-6} respectively. The total channel error variance is $\sigma^2 \approx 4.8 \times 10^{-3}$. Assume, for simplicity, that the error variances imparted at each combiner level are equal and given by $\sigma_i^2 = \sigma^2 / 6 = 8 \times 10^{-4}$. Assume also equal amplitude tapers in azimuth and elevation corresponding to $\eta_{az} = \eta_{el} = .82$ (≈-35dB near in diffraction sidelobes).

Figures A-3 and 3-5 show the sidelobe levels computed from (4) associated with random amplitude and phase errors in the interleaved feed network and sequential feed network respectively. Perhaps the major difference between the two networks is that the interleaved design results in reasonably high sidelobes (> -7.7 dBi) confined to a region near broadside, whereas with the sequential design the high sidelobes (>-7.2 dBi) exist in a narrow elevation region for nearly all azimuth angles.

APPENDIX B

ARRAY SIDELOBE LEVEL ANALYSIS

B.1 INTRODUCTION

It has been shown that the ability to detect targets in clutter, over a wide spread in target Dopplers, is dependent on the low antenna sidelobe levels in the intercardinal plane region. In addition, target minimum discernible velocity (mdv) is dependent upon the azimuth principle plane sidelobe levels. Based on detection and mdv requirements, the desired antenna sidelobe levels can be specified. The specification sidelobe requirements must also consider the current state of the art in fabrication of distribution networks and associated tolerances, these tolerances translate to random amplitude and phase errors. This appendix investigates the impact of random beamforming errors on the resultant 3-D antenna patterns. The analysis will be performed for the dual bands, S and UHF.

B.2 BEAMFORMER ARCHITECTURE

The beamformer size and aperture weighting are given in the following tables B1 and B2.

Table B1. S Band Architecture

	No.	Receive Taper	Transmit Taper
Row	64	Taylor (25 dB)	Uniform
Columns	256	Taylor (35 dB)	Taylor (35 dB)

Table B2. UHF Band Architecture

	No.	Receive Taper	Transmit Taper
Row	8	Taylor (25 dB)	Uniform
Columns	36	Taylor (30 dB)	Taylor (30 dB)

To investigate random error affects, the beamformer is modeled as shown in Figure B1. It represents a corporate feed architecture, where columns of elements are combined to form vertical subarrays and the subarrays are combined to produce the array output. The elements are assumed to have half wavelength spacing, at both S and UHF bands. Weighting applied vertically, within a subarray, is referred to as elevation weighting and suppresses the elevation sidelobes of the antenna pattern. Weighting applied horizontally , across subarrays, is referred to as azimuth weighting and suppresses the azimuth sidelobes of the antenna pattern. An error is

associated with each antenna element. This error is the product of errors in the row and column feeds.

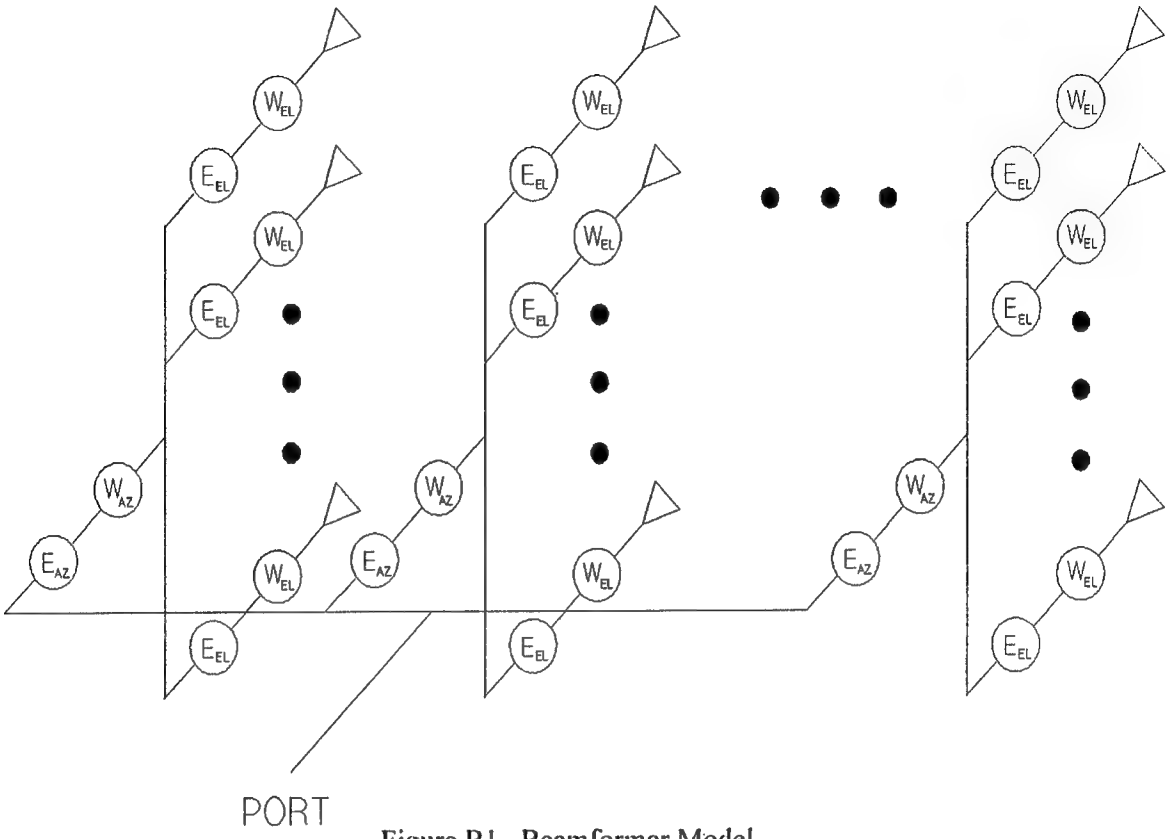

Figure B1. Beamformer Model

B.3 BEAMFORMING ERROR DEFINITION

Each error term is modeled as a complex error, having both an amplitude and phase error, as shown in equation (B-1). The random variables δ and ϕ represent the amplitude and phase errors.

$$E = (1+\delta)e^{j\phi} \qquad \text{(B-1)}$$

It is assumed that the phase error in both the azimuth and elevation beamformers has a Gaussian pdf with $\sigma = 4°$. The amplitude error in both the azimuth and elevation beamformers is assumed to be approximately zero. These assumptions reflect current tolerances in fabrication technology.

B.4 ANTENNA PATTERN CALCULATION

The antenna pattern calculation is based on the Fourier transform relation between the aperture illumination or excitation and its beampattern. The aperture excitation is the product of three terms, the desired excitation, weighting and error. The aperture excitation for a 2-D array can be viewed as a element wise product of matrices, where the number of rows and columns in the matrices represent the number elements in rows and columns of the array, as shown in Equation (B-2). The matrix D is the desired excitation matrix, W is the weighting matrix and E is the error matrix.

$$S = D \cdot W \cdot E \qquad \text{(B-2)}$$

The antenna pattern is calculated by computing the 2-D FFT of the aperture excitation matrix (S). The resultant matrix represents the beampattern as the azimuth and elevation are varied from -90 to 90 degrees from boresight, sampled at the matrix size. To examine the finer structure of the beampattern the aperture excitation matrix was zero padded prior to the Fourier transform. For beampattern calculations, Kaiser weighting was substituted for Taylor weighting.

B.5 S BAND ANTENNA PATTERNS

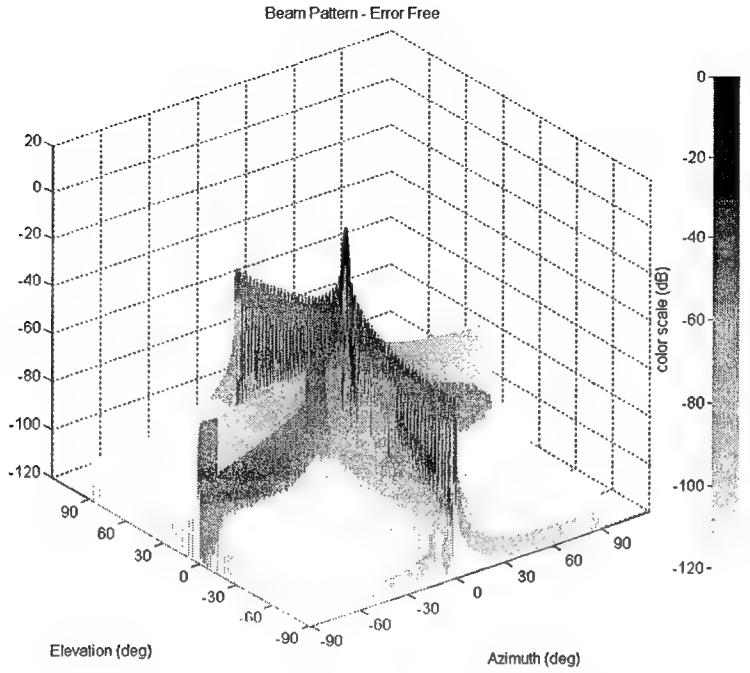

Figure B2. S Band, Beampattern - Error Free

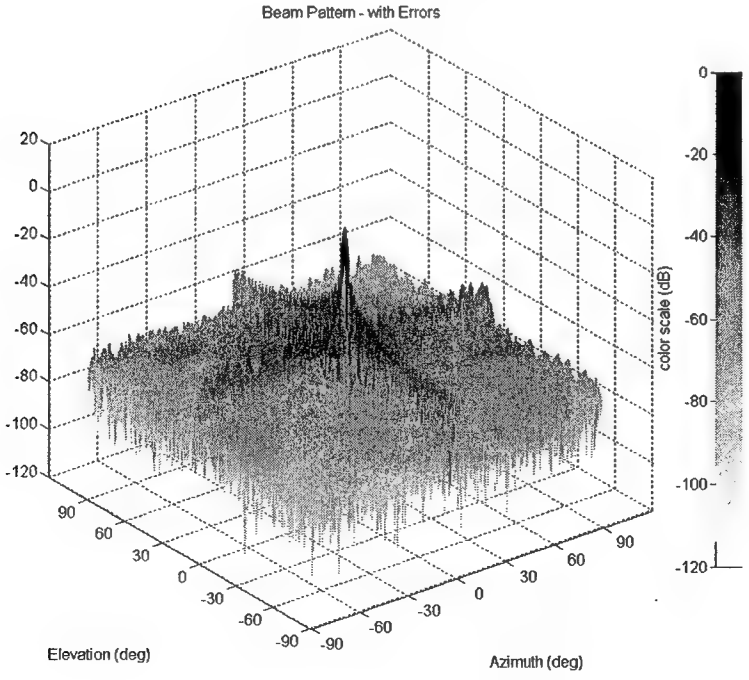

Figure B3. S Band, Beampattern with Errors

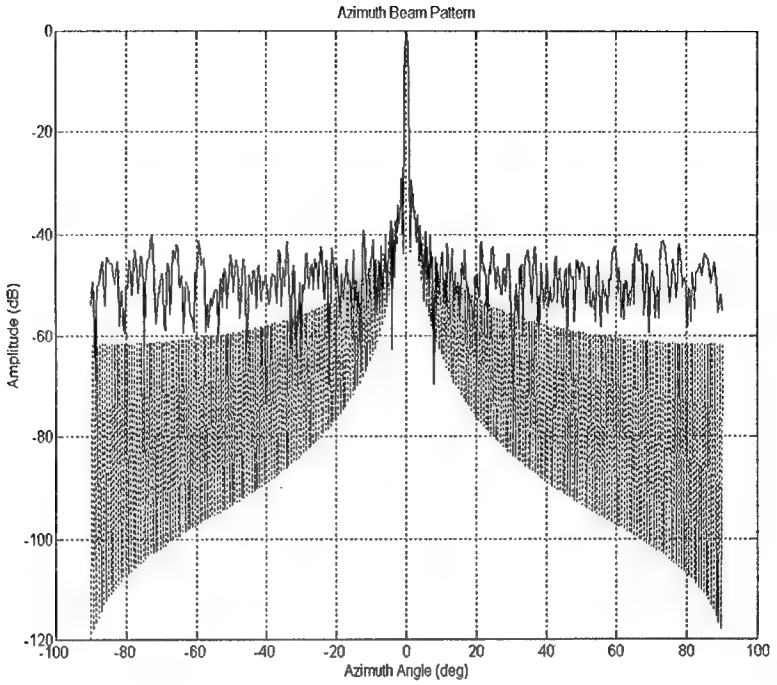

Figure B4. S Band, Azimuth Principle Plane with and without Errors

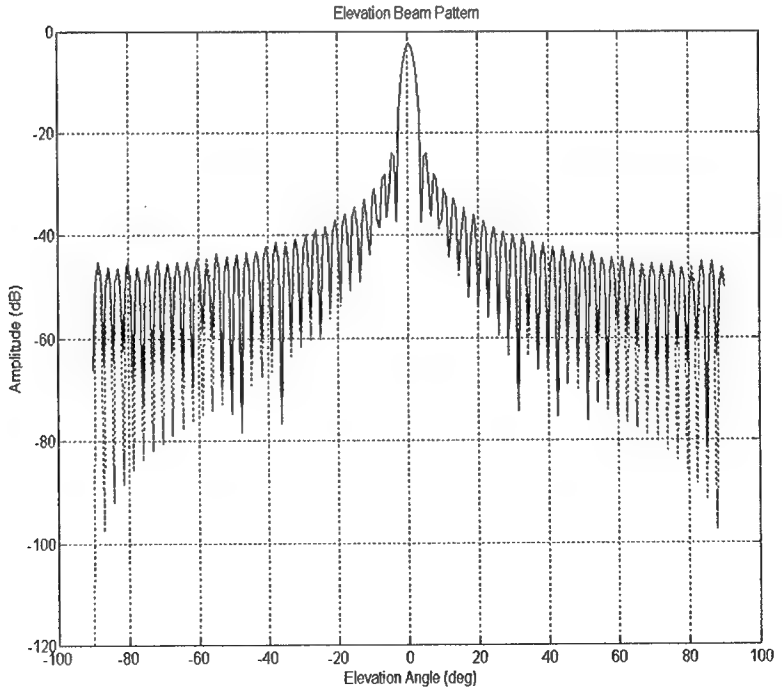

Figure B5. S Band, Elevation Principle Plane with and without Errors

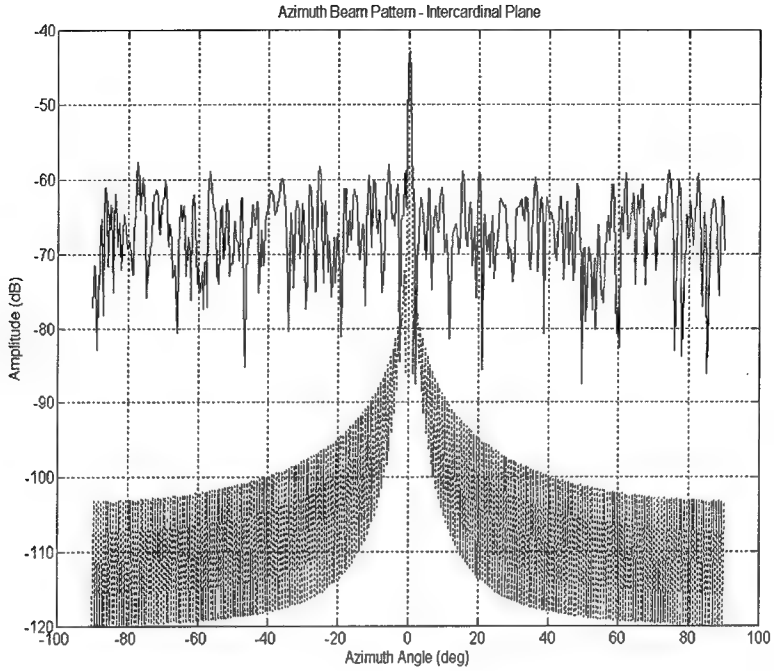

Figure B6. S Band, Intercardinal Plane with and without Errors

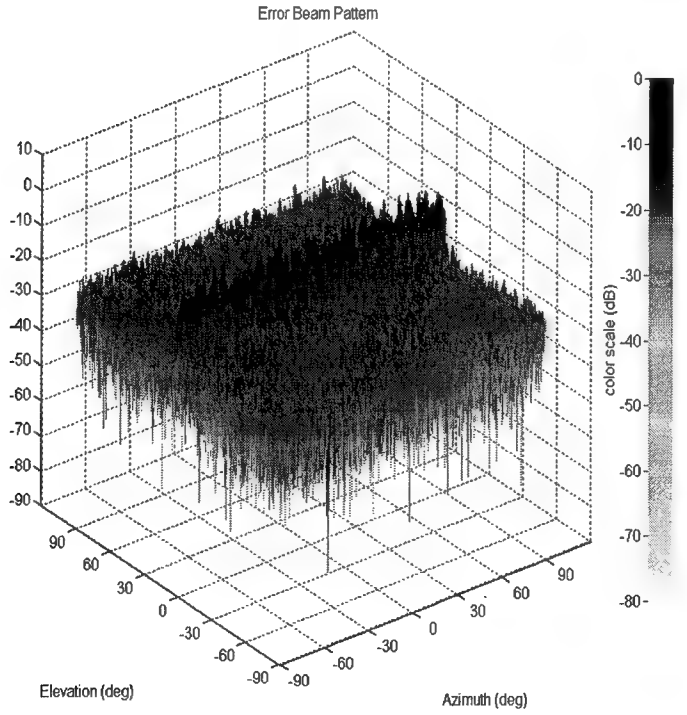

Figure B7. S Band, Beampattern - Error Only

B.6 UHF BAND ANTENNA PATTERNS

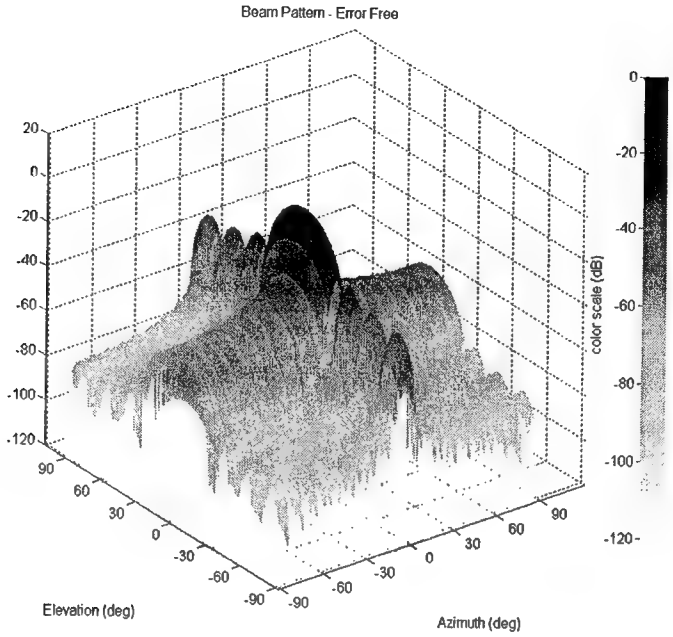

Figure B8. UHF Band, Beampattern - Error Free

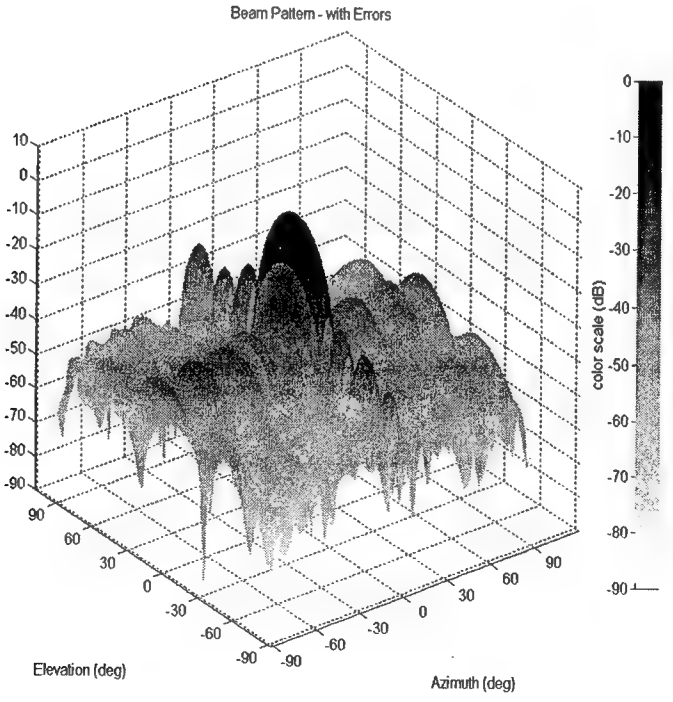

Figure B9. UHF Band, Beampattern with Errors

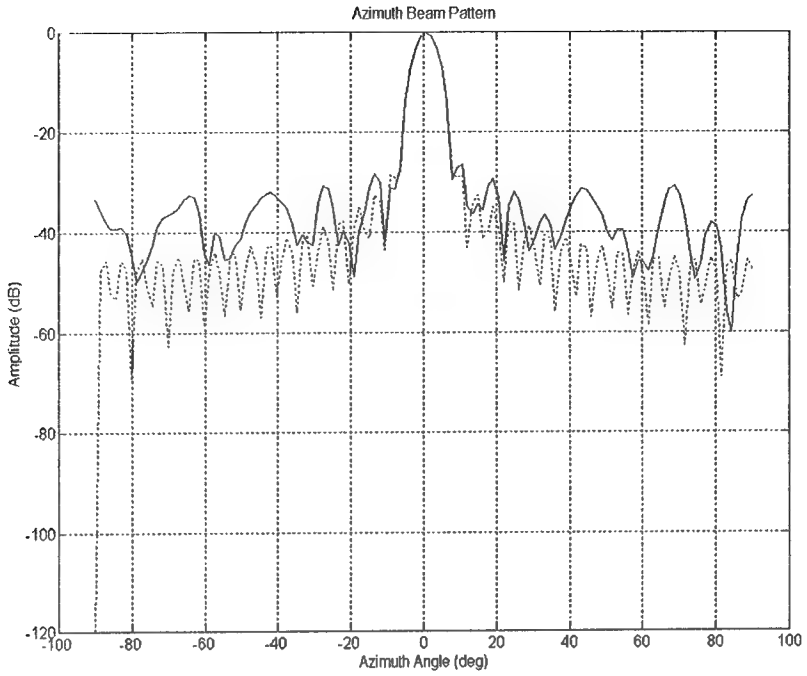

Figure B10. UHF Band, Azimuth Principle Plane with and without Errors

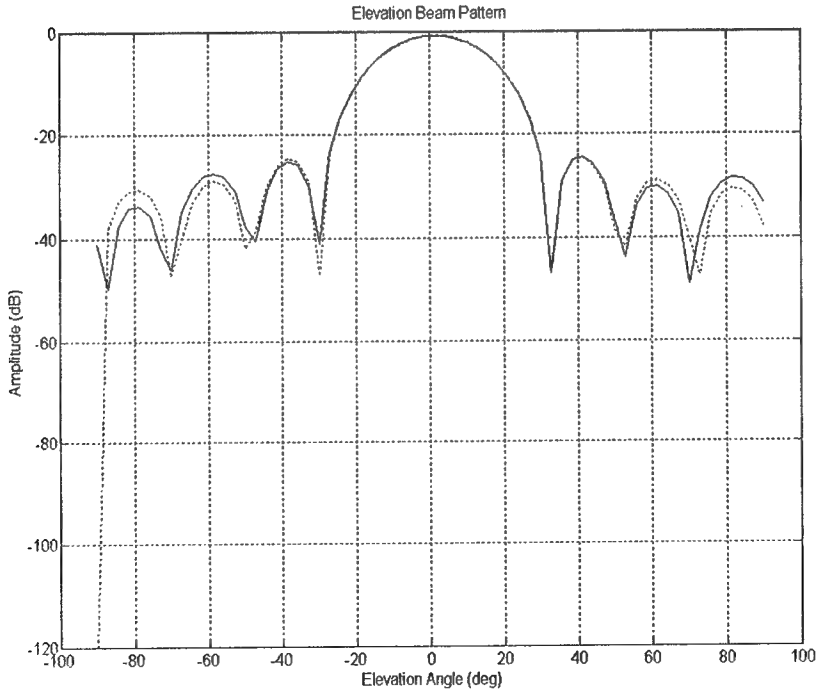

Figure B11. UHF Band, Elevation Principle Plane with and without Errors

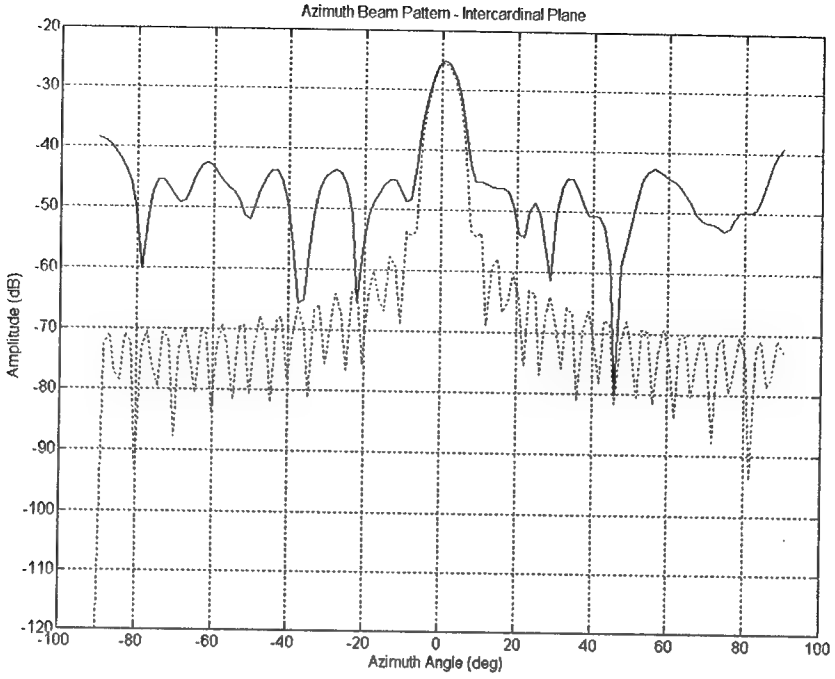

Figure B12. UHF Band, Intercardinal Plane with and without Errors

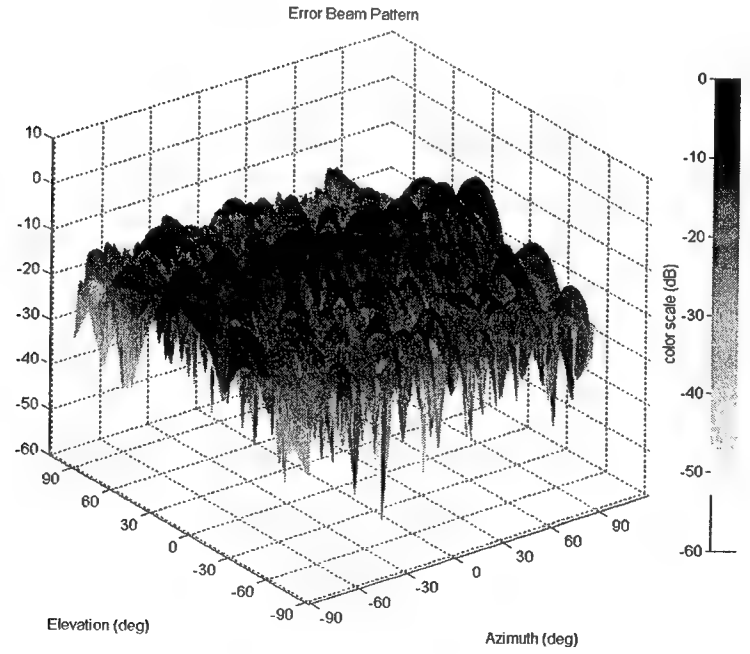

Figure B13. UHF Band, Beampattern - Error Only

B.7 CONCLUSION

The beampatterns with errors were statistically evaluated for the mean sidelobe level in the intercardinal plane region. This mean sidelobe level was then converted to dBi, to assess the antenna's performance. This is summarized in table B3.

Table B3. Sidelobe Level Analysis

	S Band	UHF Band
mean SLL (intercardinal Plane, normalized pattern)	-66.6 dB	-47.5 dB
Gain (10*log(M*N))	42.1 dB	24.6 dB
mean SLL (intercardinal Plane)	-24.5 dBi	-22.9 dBi

With mean sidelobe levels less than -20 dBi, these antennas can be categorized as ULSA in performance. This performance is attributable to the low beamformer errors due to small fabrication tolerances.

APPENDIX C

AN ALTERNATE DUAL BAND (L,X) APERTURE APPROACH

Data applicable to the Radar Resource Sharing study can be derived from work done on another integrated dual band system, specifically L and X band. This design is capable of radiating vertically polarized signals in the 1.0 to 1.4 GHz band simultaneously with dual polarized signals at 9.0 to 10.0 GHz. The design can be scaled to the S and UHF bands (X/L = 9800/1300 = 7.5, S/UHF = 3250/435 = 7.5). VSWR is less than 2:1 across the L band with a scan volume of ±45 in azimuth and ±30 in elevation. The dual polarized X band radiator scans ±60° in azimuth and ±30° in elevation. This configuration is shown in Figure B.1. This type of configuration is preferred to that suggested in the RRSS work statement because the UHF dipoles in front of the S band radiators create intolerable grating lobes at S band due to a periodic distortion across the aperture. The "low band" radiator is integrated with and placed behind the "high band" radiators in order to eliminate this problem.

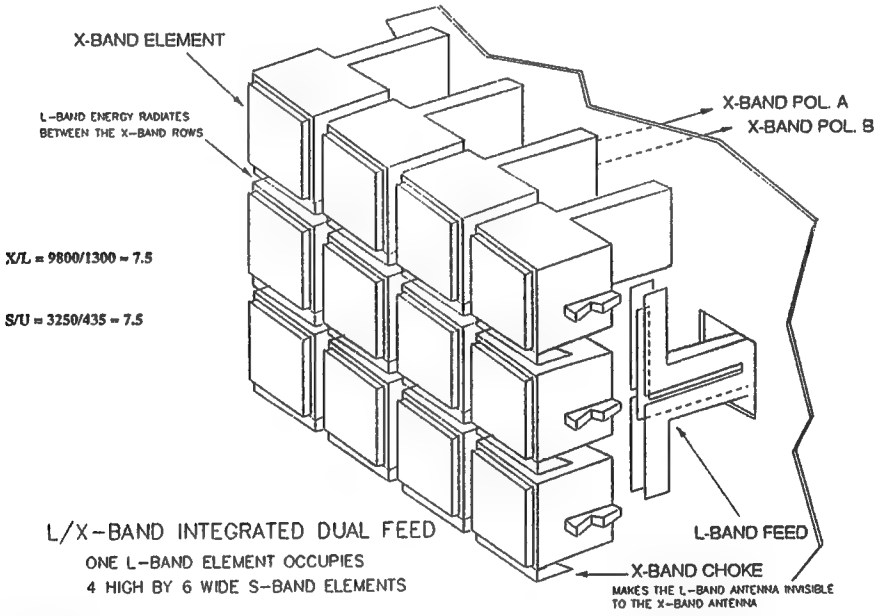

Figure C-1 An X band element configuration scaleable to S band.

The X band element in the L/X band integrated antenna is a rectangular waveguide fed by a dual polarized patch radiator. See Figure C-2. The patch is dimensioned to a half wavelength of the midband frequency in the given dielectric material. Figure C-3 shows the tested design.

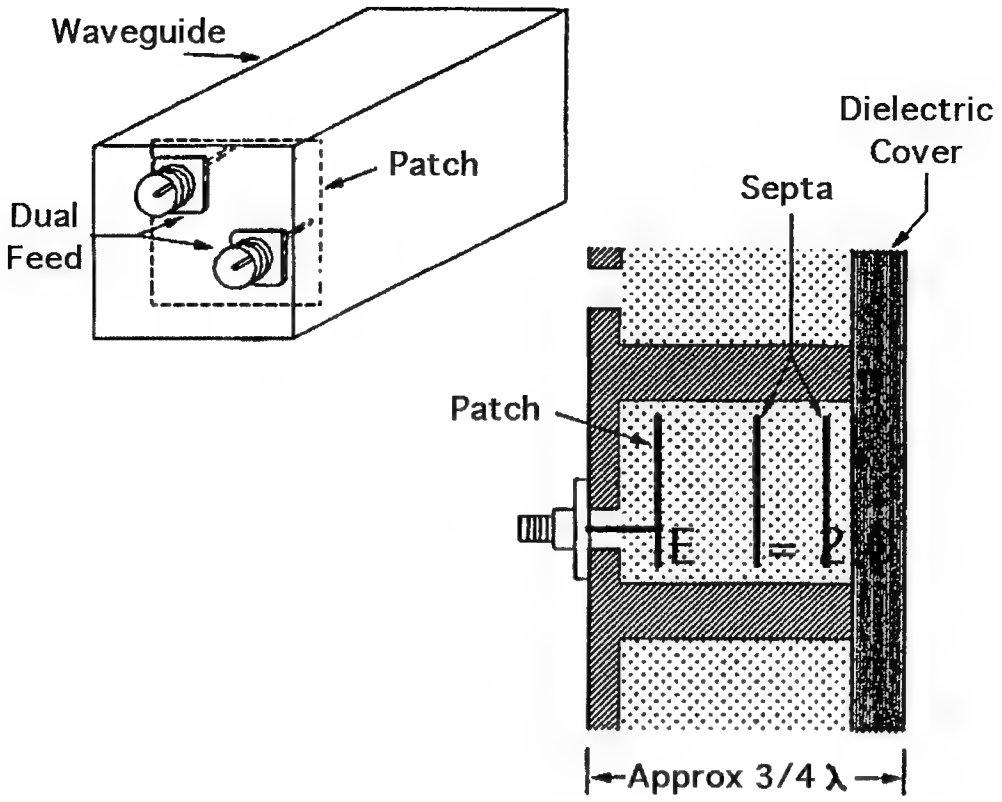

Figure C-2 X band radiator feed.

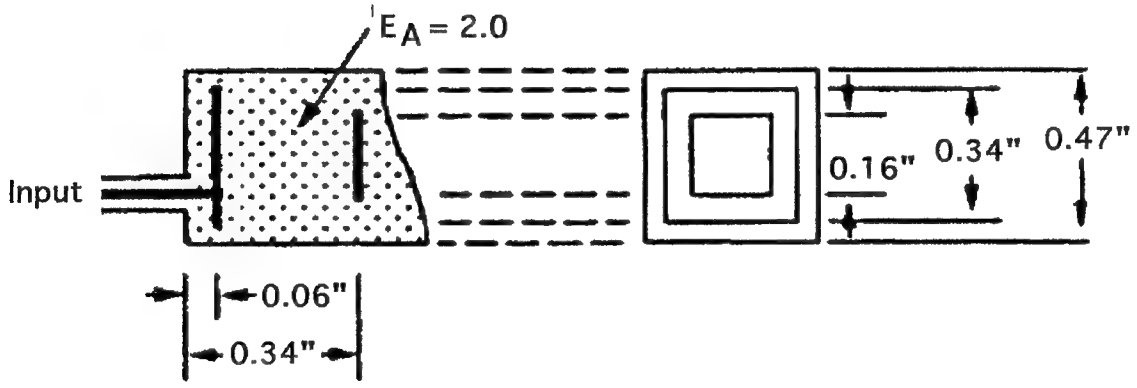

Figure C-3 A Proven X band element design scaleable to S band.

The X band form factor drives the L band element design. This is shown in Figure C-4. The L band elements are driven by a tuned feed which provides VSWR better than 1.32:1 at boresight and less than 2:1 over the full scan range of ±45° in azimuth and ±30° in elevation.

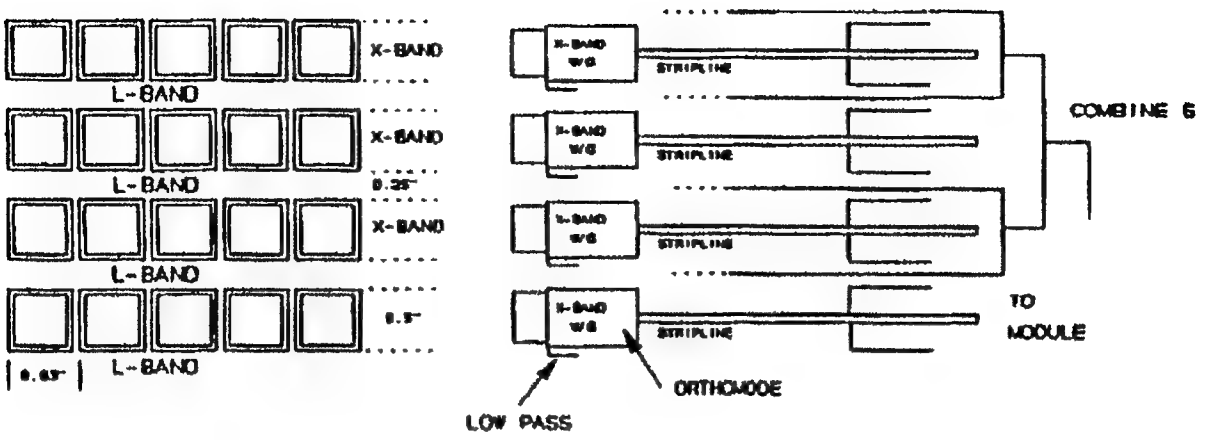

Figure C-4The Proven L band radiator configuration scaleable to UHF.

"High band leakage into the "low band" is a key consideration in this design, particularly since the "high band" signal could be co-polarized with the "low band". Isolation of the bands is provided by X band chokes. See Figure C-5. The integrated L and X band feed is shown in Figure C-6.

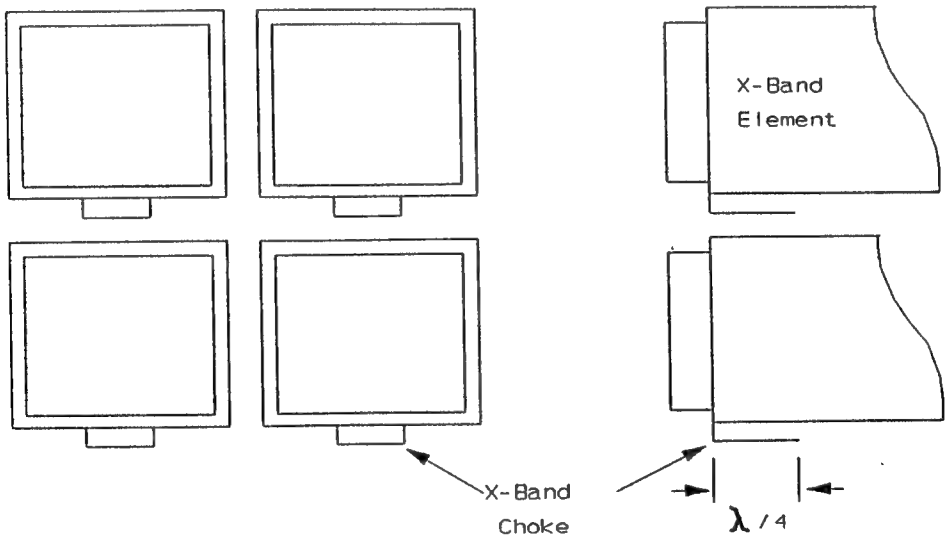

Figure C-.5 X band choke design.

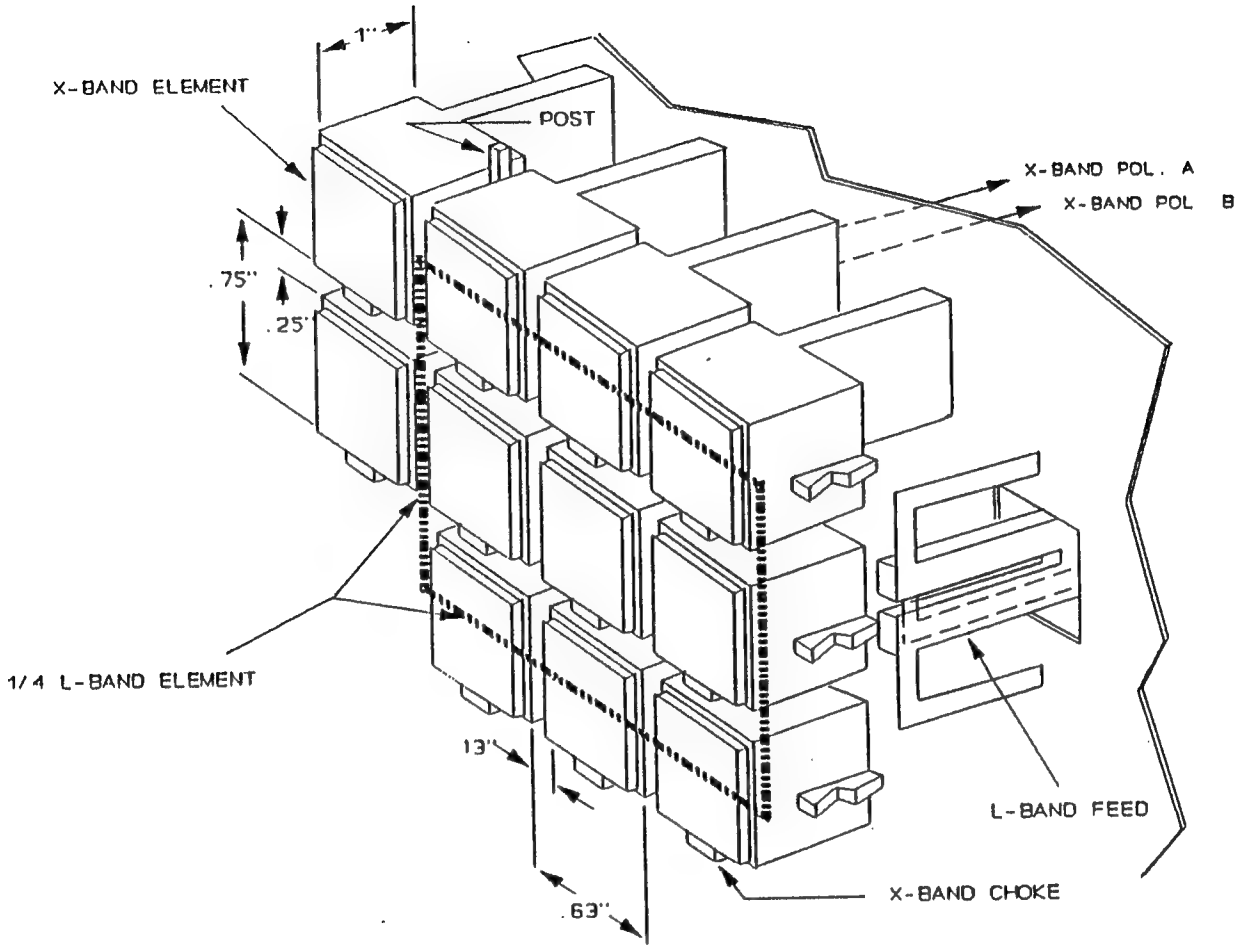

Figure C-6 The Tested Integrated L/X band dual feed scaleable to UHF/S band.

The integrated dual band aperture study was done assuming a flat array face, but the results are adaptable to a conformal array geometry, and improvements in element match and L band scan are achievable. Adapting the work done at L and X band to the RRSS frequencies warrants further investigation.

APPENDIX D

CYLINDRICAL APERTURE CONSTRAINTS

The RRSS statement of work defined the aperture as a cylindrical surface with a radius of curvature of 120 inches. With this much curvature, it is possible that the required sidelobe levels cannot be maintained unless the amplitude taper is varied with scan angle. Since variable amplitude control could substantially complicate the beamformer, it was necessary to determine if amplitude control was required. Nominal system operating parameters are shown in Table D-1.

Table D-1 Nominal System Operating Parameters

Frequency	420 MHz - 450 MHz	3.0 GHz - 3.5 GHz
Polarization	Vertical	Horizontal
Radiator	Dipole	Patch
Gain (nominal)	30 dBi	45 dBi
Number of Elements	288 (8x36)	16384 (64x256)
Azimuth Scan	60 degrees	60 degrees
Elevation Scan	30 degrees	35 degrees
Average Power Radiated	100 W/ft^2	100 W/ft^2
Duty Cycle	15% max.	15% max.
PRF	600 Hz max.	10 kHz max.
Pulse Width	300 μs max.	50 μs max.
Transmit Illumination	Uniform	Uniform
Rx Azimuth Sidelobe Level	-45 dB rms	-60 dB rms
Rx Elevation Sidelobe Level	-30 dB rms	-45 dB rms

The dual band array shown in Figure D-1 consists of UHF elements with a grid spacing of 11.9 inches and S band radiators with a grid spacing of 1.7 inches. Cylindrical arrays pose problems not associated with planar arrays. Due to the curvature of the array, total area is reduced compared to a planar array with the same spacing and number of elements. Scanning in the plane of curvature is more limited than in the linear plane without using amplitude control on the elements. Without correction, skewing of the main beam and degraded sidelobes are caused which increase with scan angle. If each element has amplitude and phase control, this problem can be corrected with a modification to the aperture

amplitude and phase control, this problem can be corrected with a modification to the aperture distribution. With fixed divider feeds, beam sharing techniques can partially, but not completely, remedy the problem.

Azimuth patterns are not affected by the curvature in this configuration. Sidelobes are controlled by phasing the system accurately and controling manufacturing tolerances. Typical scanned patterns are shown in Figure D-2.

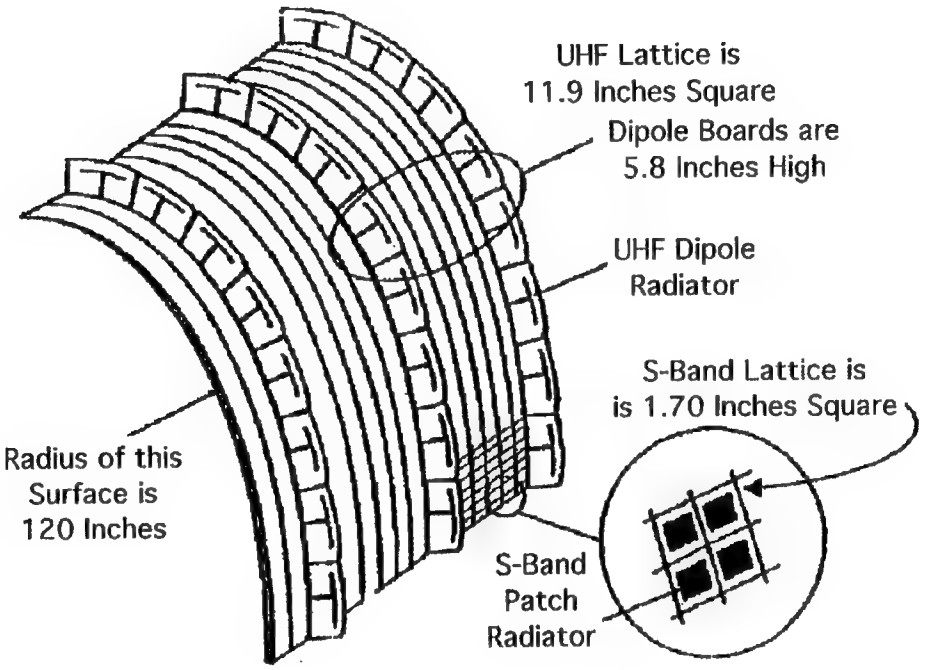

Figure D-1 Cylindrical Array Configuration.

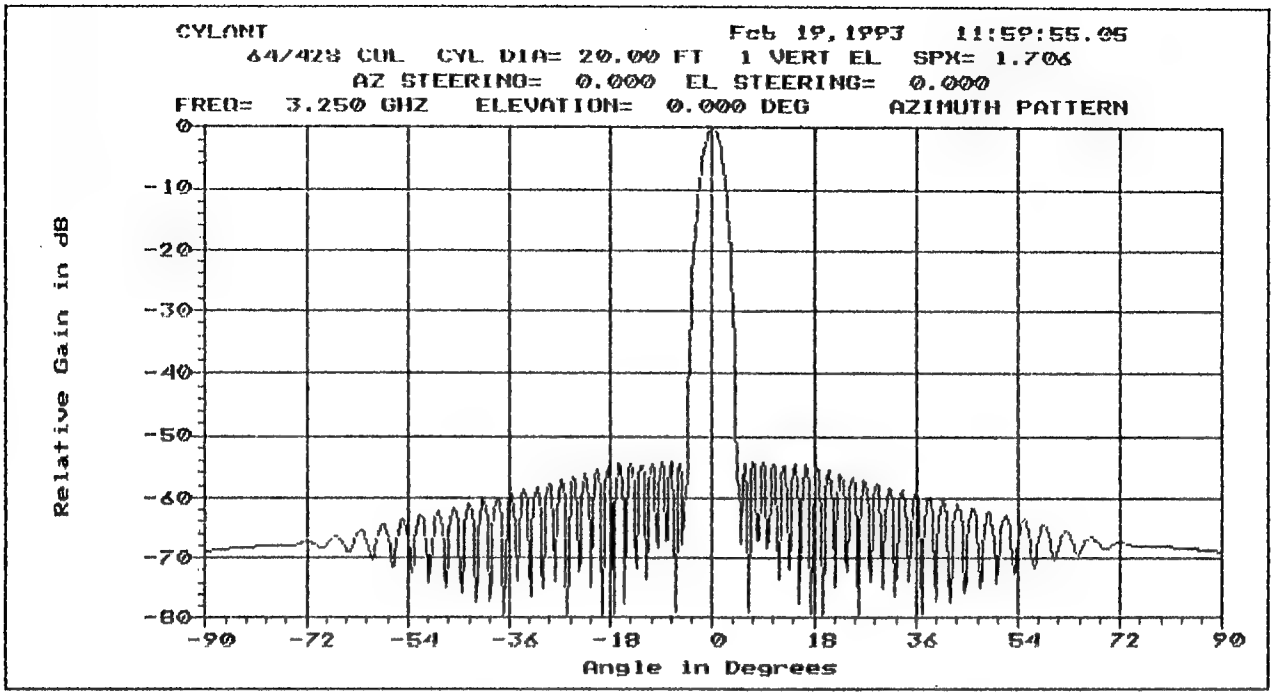

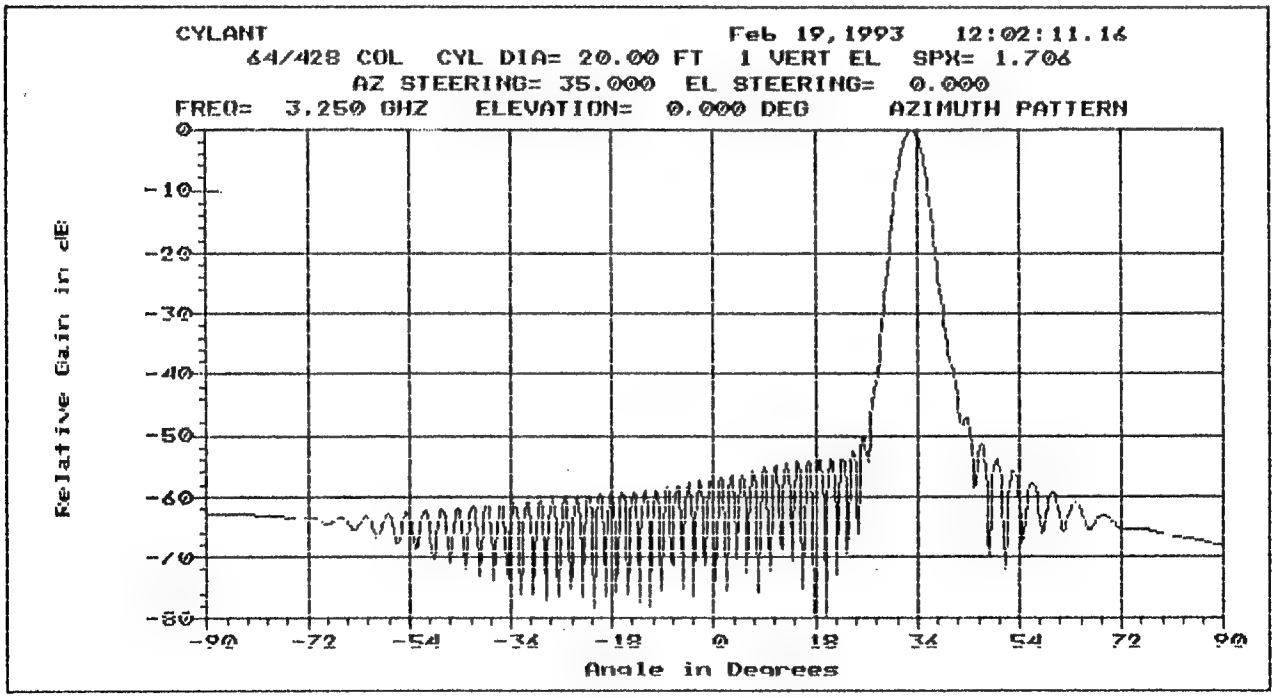

Figure D-2 Typical Cylindrical Array Patterns. Beam at 0 Elevation and 0 Azimuth and 35 Azimuth.

APPENDIX E

BISTATIC RADAR SIDELOBE REQUIREMENTS

The sidelobe requirements for dual band bistatic radar operation were established using a similar procedure as that used for the monostatic radar analysis. Baseline receive antenna sidelobe parameters for an S band and a UHF band bistatic mode of operation were derived after doing a parametric analysis of performance in clutter for various array sidelobe parameters. For the S Band bistatic radar, the results of a performance analysis done for the Bistatic Adjunct Surveillance System (BASS) study are used to set the sidelobe requirements. In this study the performance of a10 by 1 meter S Band receive antenna was analyzed using the E3A as the illuminator. For the UHF case this analysis was extended to a UHF receive array which hosts off the E2C as a source of illumination.

The sidelobe requirements listed in Table E-1, were selected after performing an analysis of radar performance in urban clutter using deterministic ultra low sidelobe antenna patterns in a sidelooking radar installation. The urban clutter model was selected as it is most stressing for radar operations.

	S Band	**UHF**
Antenna Size	length 10 m height 1 m	length 10 m height 1 m
Transmit		
azimuth taper	E3A	E2C
elevation taper	"	"
intercardinal sidelobes	"	"
Receive		
azimuth taper	55 dB Taylor	30 dB Taylor
elevation taper	40 dB Taylor	20 dB Taylor
intercardinal sidelobes	- 20 dBi	- 20 dBi

Table E-1 Bistatic Radar Sidelobe Requirements

E.1 ANALYSIS OF S BAND BISTATIC SIDELOBE REQUIREMENTS

The BRADS simulation program was used to analyze the performance of the S Band radar in clutter. The radar analysis was done for the BASS receive array configuration which is a 10 by 1 meter array on a high flyer. The BRADS simulation modeled radar performance of matched pulse Doppler operation using the E3/RSIP waveform. A plot of the BARE clutter spectrum is shown in Figure E-2, for baseline S Band array sidelobe parameters, at a range of 200 nmi from the transmitter. BARE clutter is calculated in range and Doppler bins but does not include the effect of Doppler filter or range sidelobes from the pulse compression process These BARE clutter plots are useful in visualizing the effect that various antenna sidelobes have on radar performance.

As shown in the coverage pictorial insert, the clutter to noise plot is for the case where the transmit beam is illuminating point 5 in the coverage pictorial, which is located 100 degrees from the E3 velocity vector. A single receive beam of the ensemble of BASS antenna beams, which points in this same direction, is modeled on the high altitude receive platform.

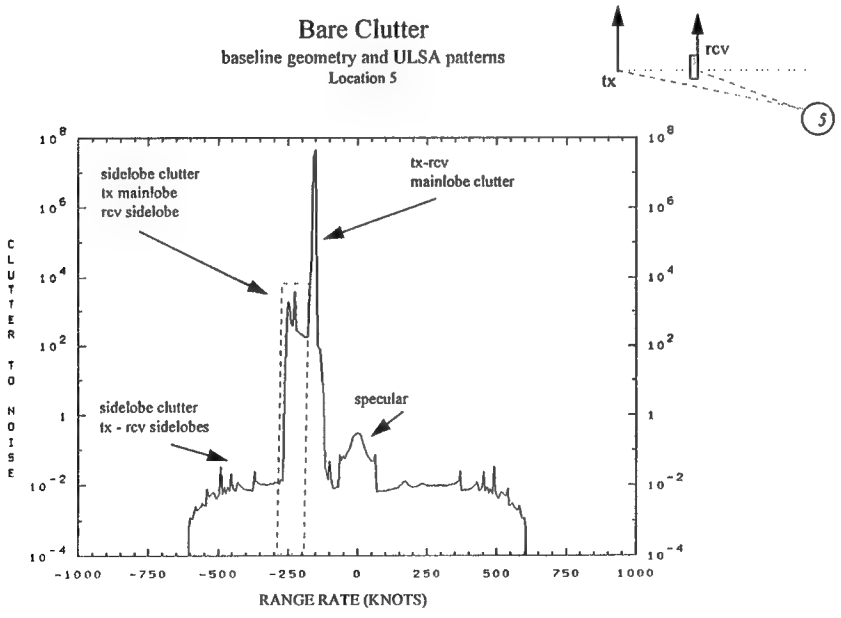

Figure E-2 BARE Clutter Plot for Location 5

The plot shows 1) a main beam clutter region which is associated with that illuminated by both the E-3 transmit beam and the BASS receive beam, 2) a far out sidelobe region

illuminated by the transmit and receive beam sidelobes, and 3) most importantly a third region which is illuminated by a mainbeam of one and the sidelobe of the other pattern. The level of sidelobe clutter from this third region is strong with a clutter to noise ratio equal to 40 dB. Detection of weak targets is not possible in this region which is a unique problem associated with the high PRF waveform and the bistatic geometry.

In order to test the sensitivity of this clutter spectrum to variations in antenna sidelobes, the BRADS simulation program was rerun for different values of elevation taper, azimuth taper and intercardinal region sidelobes. The results are shown in FigureE-3.

Bare Clutter

baseline geometry - Location 5

Parametric ULSA patterns

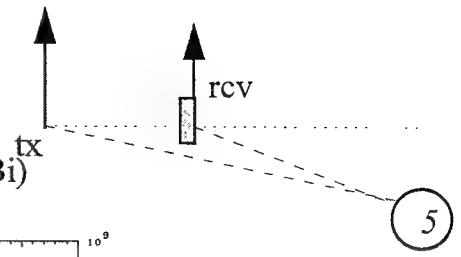

a) (az = - 55 dB, el = - 40 dB, ic = - 20 dBi)

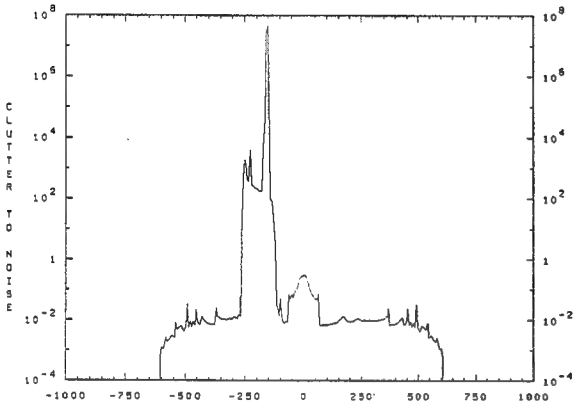

b) (*az = - 45 dB*, el = - 40 dB, ic = - 20 dBi)

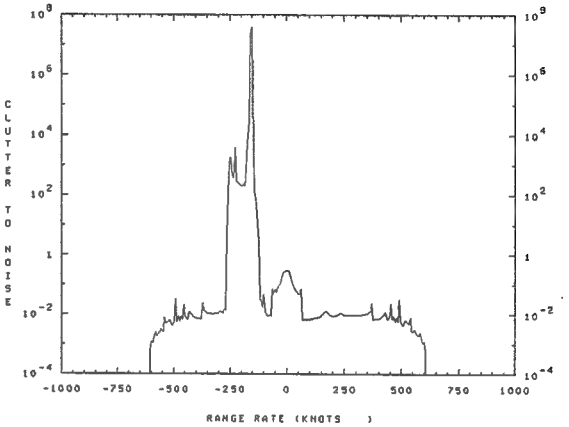

c) (*az = - 45 dB, el = - 30 dB, ic =* - 20 dBi)

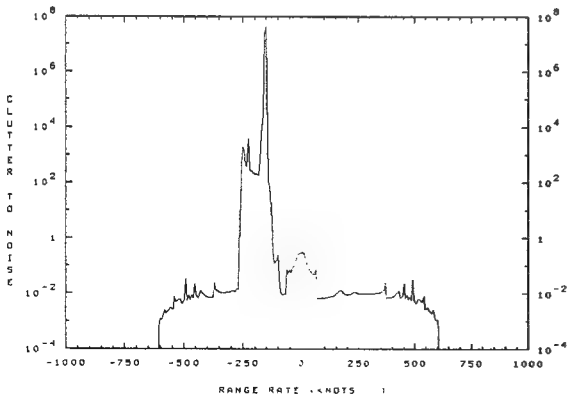

d) (*az = - 45 dB, el = - 30 dB, ic = - 5 dBi*)

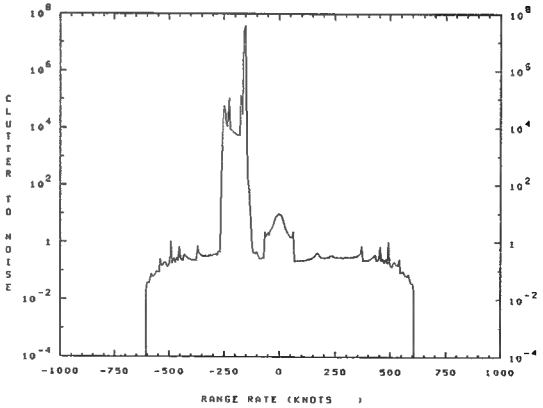

Figure E-3 Bare Clutter Plots with Parametric ULSA Patterns

Figure E-3(a) is a repeat of the clutter spectrum for location 5 with the baseline parameters. Figure E-3(b), is for the case of a 10 dB increase in the azimuth principal plane. The bare clutter spectrum for this case is identical with that of the ULSA pattern case. In Figure E-3(c), the elevation principal plane sidelobes were also increased 10 dB, and again no effect on the clutter spectrum was noted. In Figure E-3(d), the far out sidelobes of the antenna were increased and the clutter levels show an increase in C/N for range rates. The far out sidelobes of the receive antenna are thus again seen to have a direct impact on the performance of the bistatic radar in clutter, as was the case in the monostatic radar.

The case shown is only one of many analyzed for the BASS radar, but is representative of the results observed from looking at many other cases. Thus the intercardinal region sidelobes are critical to the proper operation of the S Band bistatic radar. The region of high clutter to noise ratio which was observed over a portion of the clutter spectrum (transmit mainlobe to receive sidelobe) is a special problem which cannot totally be eliminated with ULSA sidelobe patterns alone, and is not therefore considered to be a primary driver in establishing receive antenna sidelobe specifications.

E.2 ANALYSIS OF BISTATIC UHF SIDELOBE REQUIREMENTS

A analysis of a UHF bistatic radar which exploits the E2C as the illuminator was evaluated using the BRADS simulation program. In Figure E-4 the BARE clutter spectrum for the UHF BASS radar is shown, where the transmit and receive beams are pointed to a target at 150 nmi from the E2C. The receive pattern in this example was an ULSA pattern with intercardinal sidelobes at -20 dBi. The principal plane sidelobes were set by a 30 dB Taylor azimuth taper and a 20 dB Taylor elevation taper.

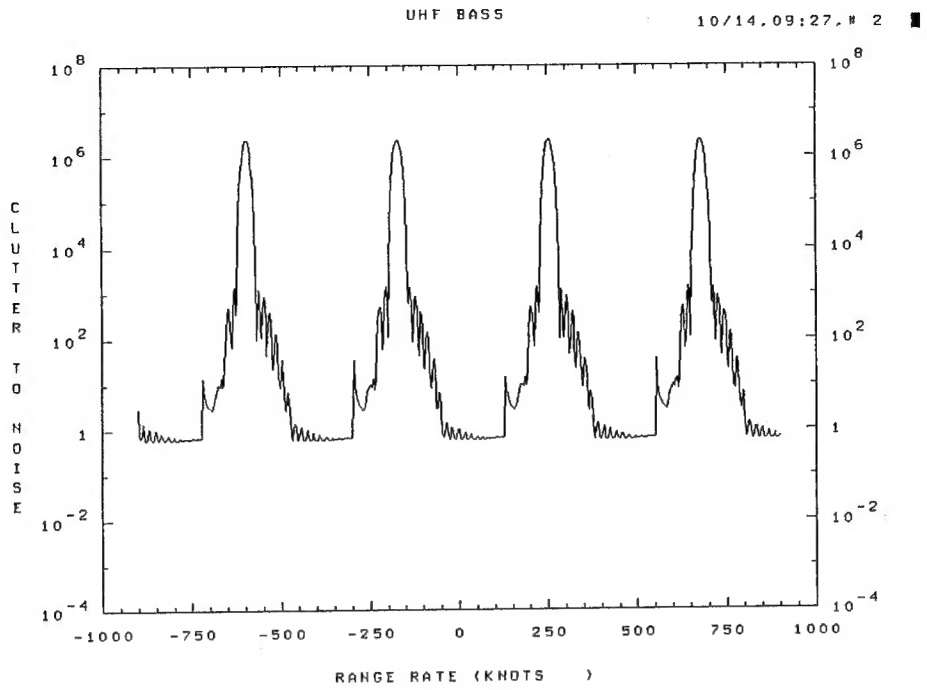

FigureE-4 BARE Clutter Spectrum for UHF Bistatic Radar

The clutter plot shows the effect of the Doppler ambiguities associated with the low prf of the E2C waveform. The region between these clutter peaks falls off in response to the antenna azimuth sidelobes along the azimuth principal plane, reaching an acceptable clutter to noise level. The far sidelobes of the baseline UHF antenna are thus sufficient for detection of targets. As is the case of the E2C radar, use of staggered prf's is necessary to eliminate the blind speeds associated

*U.S. GOVERNMENT PRINTING OFFICE: 1995-610-126-50192

Rome Laboratory

Customer Satisfaction Survey

RL-TR-_____

Please complete this survey, and mail to RL/IMPS, 26 Electronic Pky, Griffiss AFB NY 13441-4514. Your assessment and feedback regarding this technical report will allow Rome Laboratory to have a vehicle to continuously improve our methods of research, publication, and customer satisfaction. Your assistance is greatly appreciated.
Thank You

_____

_____

Organization Name:_____(Optional)

Organization POC: _____(Optional)

Address:_____

1. On a scale of 1 to 5 how would you rate the technology developed under this research?

5-Extremely Useful 1-Not Useful/Wasteful

Rating_____

Please use the space below to comment on your rating. Please suggest improvements. Use the back of this sheet if necessary.

2. Do any specific areas of the report stand out as exceptional?

Yes___ No_____

If yes, please identify the area(s), and comment on what aspects make them "stand out."

3. Do any specific areas of the report stand out as inferior?

Yes___ No___

If yes, please identify the area(s), and comment on what aspects make them "stand out."

4. Please utilize the space below to comment on any other aspects of the report. Comments on both technical content and reporting format are desired.

MISSION

OF

ROME LABORATORY

Mission. The mission of Rome Laboratory is to advance the science and technologies of command, control, communications and intelligence and to transition them into systems to meet customer needs. To achieve this, Rome Lab:

a. Conducts vigorous research, development and test programs in all applicable technologies;

b. Transitions technology to current and future systems to improve operational capability, readiness, and supportability;

c. Provides a full range of technical support to Air Force Materiel Command product centers and other Air Force organizations;

d. Promotes transfer of technology to the private sector;

e. Maintains leading edge technological expertise in the areas of surveillance, communications, command and control, intelligence, reliability science, electro-magnetic technology, photonics, signal processing, and computational science.

The thrust areas of technical competence include: Surveillance, Communications, Command and Control, Intelligence, Signal Processing, Computer Science and Technology, Electromagnetic Technology, Photonics and Reliability Sciences.